

STRENGTH CHARACTERISTICS OF GROUTED SANDY SOIL

IFFAT TARANNUM

MASTER OF SCIENCE IN CIVIL ENGINEERING
(GEOTECHNICAL)



DEPARTMENT OF CIVIL ENGINEERING
BANGLADESH UNIVERSITY OF ENGINEERING AND TECHNOLOGY
DHAKA, BANGLADESH

May, 2022

STRENGTH CHARACTERISTICS OF GROUTED SANDY SOIL

by

Iffat Tarannum

A Thesis Submitted to the
Department of Civil Engineering
in partial fulfillment for the degree of
MASTER OF SCIENCE IN CIVIL ENGINEERING
(GEOTECHNICAL)



Department of Civil Engineering
Bangladesh University of Engineering and Technology
Dhaka, Bangladesh

May, 2022

The thesis titled "Strength Characteristics of Grouted Sandy Soil", submitted by Iffat Tarannum, Student No.: 1017042206 has been accepted as satisfactory in partial fulfillment of the requirement for the degree of Masters of Science in Civil Engineering (Geotechnical) on the 14th May 2022.

BOARD OF EXAMINERS



Dr. Mohammad Shariful Islam
Professor
Department of Civil Engineering
BUET, Dhaka-1000

Chairman
(Supervisor)



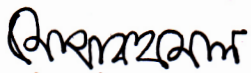
Dr. Md. Delwar Hossain
Professor and Head
Department of Civil Engineering
BUET, Dhaka-1000

Member
(Ex-officio)



Dr. Mehedi Ahmed Ansary
Professor
Department of Civil Engineering
BUET, Dhaka-1000

Member



Dr. Md. Aftabur Rahman
Associate Professor
Department of Civil Engineering
CUET, Chattogram-4349

Member
(External)

DECLARATION

It is hereby declared that this thesis and the studies embodied in it are the results of the investigation carried out by the author under the supervision of Dr. Mohammad Shariful Islam, Professor, Department of Civil Engineering, Bangladesh University of Engineering and Technology. Wherever contributions of others were involved, every effort has been made to indicate this clearly with due reference to the literature and acknowledgment of collaborative research and discussions. Neither thesis nor any part of it has been submitted to or is being submitted to for any other purposes (except for publications)



Iffat Tarannum

ACKNOWLEDGEMENT

I am grateful to the omnipotent for the blessings that gave me the ability to complete the thesis work successfully.

I wish to express my deepest gratitude to my supervisor Professor Dr. Mohammad Shariful Islam, Department of Civil Engineering, Bangladesh University of Engineering and Technology for his valuable suggestions, guidance, and supervision. I am enriched by the knowledge provided to me throughout my entire work. He was very kind enough to supply me with various references which helped me in many ways. His relentless efforts and skills in this regard were my sources of inspiration for this endeavor. My sincere appreciation also goes to the members of my board of examiners.

I would like to acknowledge the research grant received for this study from the Committee for Advanced Studies and Research (CASR) BUET, Dhaka.

I must also record my special gratitude to the Fosroc (construction company) and their team. My special thanks to all staffs and lab instructor of Geotechnical Engineering Laboratory in the Department of Civil Engineering for their help for successful completion of all lab experiments.

I am grateful to my parents, especially my mother who sacrificed her time during my pregnancy for the birth of the second child for which I was able to continue this study smoothly. My elder son Saifan Rahman co-operated with me and my newborn son Ifran Rahman without making much trouble.

Final but not least I am also thankful and indebted to my husband Mulikutur Rahman Samy for his full-fledged support.

ABSTRACT

Seepage control is a big concern for embankments, dams, and other hydraulic structures constructed with sandy soil. Grouting, especially permeation grouting is one of the appropriate solutions for controlling seepage. However, cement-based permeation grouting is still a trial and error-based process both in the laboratory and field. In this study, attempts have been made to determine the strength characteristics of permeation grouted sandy soil. The properties of sand is Fineness Modulus (F.M.) 1.12, Permeability 8.84×10^{-6} cm/sec, Cohesion (c) 4.24 kN/m² and Angle of internal friction (ϕ) 35°.

A simple method has been devised to prepare grouted samples with water-cement ratios (W:C) of 2:1, 3:1, 4:1, 5:1 and the percentage of cement is respectively 11%, 8%, 6.5% and 5.5%. It is found that compressive strength of the samples prepared with 2:1 W:C ratio varies in the range between 200 kPa and 250 kPa after 28 days of curing. After 120 days of curing, the strength of the same samples increases up to 1000 kPa. The samples show ductile behavior and the failure strain is 9%. For low cement contents, i.e., 5:1 and 4:1 (W:C), the compressive strength varies from 28 kPa to 40 kPa, after 7 to 14 days of curing period. A significant increase was noticed in the compressive strength after 28 days of curing and it reached its peak after 90 days. Dry density increases whereas moisture content and void ratio decrease with the increase of cement content and curing age. It is also observed that, cohesion and Young's modulus increase with the increase of cement content and curing age. Failure patterns of samples are column mode, collapse, axial split and shear for W:C of 5:1, 4:1, 3:1 and 2:1 respectively. However, failure pattern can change with increased curing age, e.g., for 2:1 (W:C) cured for 120, a failure pattern of slickenside was observed.

Consolidated Undrained (CU) triaxial tests were also performed on the grouted samples prepared with 11% (i.e., W:C of 2:1) cement cured for 7 days. It is observed that dilation occurred during the volume changes and pore pressure decreased with the increase of confining pressure. From the triaxial test, cohesion, c and angle of internal friction, ϕ are found to be 200kN/m² and 37.4° respectively. In the case of triaxial test, the failure pattern is different, i.e., bulging failure pattern.

The changes of microstructures and chemical composition during hydration reaction were observed by the Scanning Electron Microscope (SEM), and Energy Dispersive Spectroscopy (EDS) respectively. Ettringite needles, C-S-H gel, C₃S and C₂S (2 Cao.SiO₂) formation increases with the cement content and curing age, which means hydration and pozzolanic reaction increase as well. Ettringite is a needle-shaped crystal that contributes to the early strength development and works as the reinforcement, and C-S-H gel is like a glue binder that solidifies the samples. Particularly the cementitious products not only enhance the inter-cluster bonding strength but also fill the pore space. From these investigations, it is observed that the porosity decreases with the cement content and curing age, which means permeability decreases as well, without disturbing the soil microstructure. Permeation grouting is effective in increasing the strength and decreasing the permeability.

TABLE OF CONTENTS

ABSTRACT	v
TABLE OF CONTENTS	vi
LIST OF FIGURES	ix
LIST OF TABLES	xii
NOTATION AND ABBREVIATIONS	xiii
CHAPTER 1: INTRODUCTION	
1.1 General	1
1.2 Background	2
1.3 Objectives of the study	5
1.4 Organization of the Thesis	5
CHAPTER 2: LITERATURE REVIEW	
2.1 Introduction	7
2.2 Soil grouting	7
2.3 Application of Grouting	8
2.3.1 Types of Grouting Method	9
2.3.2 Permeation Grouting	9
2.3.3 Compaction Grouting	10
2.3.4 Fracture and Compensation Grouting	12
2.3.5 Jet Grouting	12
2.4 Purpose of Permeation Grouting and Its Scope	14
2.5 Basics Mechanism of the Research	15
2.5.1 Degree of Solidification	17
2.5.2 Injection Probe Layout	17
2.5.3 Required Grout Quantity	18
2.5.4 Injection Holes/Probe	18

2.5.5 Bottom- Up Staging	18
2.5.6 Sleeve Port Pipes	19
2.6. Permeability and the Characteristics of Soil	19
2.6.1 Permeability of Sands and Clays	20
2.6.2 Vertical and Horizontal Permeability	21
2.7 Grouting Technique	22
2.7.1 Groutibility	22
2.8 Past Researches and Research Gap	24
2.9 Summary	40
CHAPTER 3: EXPERIMENTAL PROGRAM	
3.1 Introduction	41
3.2 Materials	41
3.2.1 Sand	41
3.2.2 Cement	42
3.3 Laboratory Test Program	45
3.3.1 Index Properties of Sand Used for Grouting	45
3.3.2 Physical and Strength Properties of Grouted Samples	46
3.3.3 Permeability Test	47
3.3.2 Direct Shear Test	48
3.3.3 Unconfined Compression Test	50
3.3.4 Consolidated Undrained Triaxial Test	51
3.4 Flow Diagram of this Experiment	55
3.5 Experimental Design	56
3.6 pH Test of the Grouted Samples	63
3.7 Scanning Electron Microscopy of Grouted Samples	64

3.8 Summary	66
CHAPTER 4: RESULTS AND DISCUSSIONS	
4.1 Introduction	67
4.2 Groutability Check	67
4.3 Mix Design of Grouted Sand	68
4.3.1 Cementitious Suspensions	69
4.4 Shear Strength Parameter of Sand Used for Grouting	71
4.5 Strength Characteristics of Grouted Sand	72
4.5.1 Unconfined Compression Test Results	74
4.5.2 Triaxial Test Results	91
4.6 Failure Pattern of Grouted Samples	95
4.7 Microstructure Analysis	103
4.8 Energy Dispersive Spectroscopy (EDS)	119
4.9 Summary	123
CHAPTER 5: CONCLUSIONS AND FUTURE RECOMMENDATIONS	
5.1 Introduction	126
5.2 Conclusions	126
5.3 Future Recommendations	130
REFERENCES	132
APPENDIX A: Scanning Electron Microscopic Images of Grouted Samples with W:C ratio 5:1, 4:1, 3:1 and 2:1 Cured for 28 days	136
APPENDIX B: Scanning Electron Microscopic Images of Grouted Samples with W:C ratio 5:1, 4:1, 3:1 and 2:1 Cured for 90 days	162
APPENDIX C: Energy Dispersive Spectroscopy (EDS) Images of Grouted Samples with W:C ratio 5:1, 4:1, 3:1 and 2:1 Cured for 28 days	188
APPENDIX D: Energy Dispersive Spectroscopy (EDS) Images of Grouted Samples with W:C ratio 5:1, 4:1, 3:1 and 2:1 Cured for 90 days	201

LIST OF FIGURES

Figure 1.1	Failure patterns of earth embankment (a) cross-section of an embankment (b) failure of embankment due to channel formation (c) under seepage through pervious sand foundations (failure due to piping)	3
Figure 2.1	Various forms of improvement in soil and rock grouting: (a) permeation grouting (penetration) (b) compaction grouting (controlled displacement) and (c) hydro-fracturing (uncontrolled displacement) (Koerner, 1985)	9
Figure 2.2	Permeation grouting: conceptual diagram of soil solidification by permeation grouting (Ronald and Riley, 1995)	10
Figure 2.3	Permeation grouting in: (a) soil and (b) rock (Rahman, 2016)	11
Figure 2.4	(a) Compaction grouting and (b) permeation grouting (Gamil et al., 2017)	11
Figure 2.5	Fracture grouting (Geo grout, 2019)	13
Figure 2.6	Process of jet grouting (a) drilling with water, (b) start high-pressure grouting, (c) execution of jet-grout column, (d) repeating for the next column (Taehwa, 2020)	14
Figure 2.7	Formation of an impermeable curtain due to grouting under the dam	16
Figure 2.8	Process of permeation grouting in the cylinder: (a) inserted sleeve port pipe to inject grouting materials, (b) plan view after grouting	17
Figure 2.9	Four sleeve port pipe in a cylindrical mold to prepare grout sample	19
Figure 3.1	Particles size distribution curve of the sand	42
Figure 3.2	Schematic view of the laboratory setup for constant head test method	48
Figure 3.3	(a) Direct shear test device, (b) stress vs. displacement pattern (loose sand), (c) stress strain relationship of sand	49
Figure 3.4	Schematic view of the laboratory setup for the unconfined compression test	51
Figure 3.5	(a) Specimen under chamber confining pressure, (b) deviatoric stress application, (c) variation of pore water pressure with axial strain for dense sand	53
Figure 3.6	(a) Triaxial testing Machine, (b) grouted sample after 7 days of curing, (c) grouted sample at failure stage (CU condition), (d) grouted sample after triaxial test	54
Figure 3.7	Flow diagram of the experimental program	55
Figure 3.8	Arrangement for preparing horizontal grouting sample (all dimensions are in mm)	56
Figure 3.9	Irregular shaped sample from trial 1	57
Figure 3.10	Arrangement for preparing vertical grouting sample (all dimensions are in mm)	58
Figure 3.11	Irregular shaped sample from trial 2	58

Figure 3.12	Arrangement for preparing grouting sample (all dimensions are in mm)	59
Figure 3.13	Irregular shaped sample from trial 3	59
Figure 3.14	Schematic drawing for Step by step process of trial 4 : (a) filled the bottle with sand ,(b) inject grout slurry into the sand, (c) after curing cylindrical shaped sample is found	60
Figure 3.15	Grouted sample is retrieved from trial 4	61
Figure 3.16	Grouting samples from laboratories setup (Carter et al., 2019)	61
Figure 3.17	Grouting samples from field setup (Hashimoto et al., 2015)	62
Figure 3.18	Indication of pH value	63
Figure 3.19	Working principles of Energy Dispersive Spectroscopy	65
Figure 4.1	Comparison of suitable soil for different grouting methods	68
Figure 4.2	Direct shear test results of sand sample: (a) shear stress vs.shear displacement, (b) shear stress vs. normal stress	72
Figure 4.3	Axial stress vs. axial strain of the samples prepared with different W:C ratio after 7 days of curing: (a) W:C ratio 5:1, (b) W:C ratio 4:1, (c) W:C ratio 3:1, (d) W:C ratio 2:1.	78
Figure 4.4	Typical axial stress and axial strain curves of different sample cured for 7 days	79
Figure 4.5	Axial stress vs. axial strain of the samples prepared with different W:C ratio after 14 days of curing: (a) W:C ratio 5:1, (b) W:C ratio 4:1, (c) W:C ratio 3:1, (d) W:C ratio 2:1.	81
Figure 4.6	Typical axial stress and axial strain curves of different samples cured for 14 days	81
Figure 4.7	Axial stress vs. axial strain of the samples prepared with different W:C ratio after 28 days of curing: (a) W:C ratio 5:1, (b) W:C ratio 4:1, (c) W:C ratio 3:1, (d) W:C ratio 2:1.	83
Figure 4.8	Typical axial stress and axial strain curves of different samples cured for 28 days	84
Figure 4.9	Axial stress vs. axial strain of the samples prepared with different W:C ratio after 90 days of curing: (a) W:C ratio 5:1, (b) W:C ratio 4:1, (c) W:C ratio 3:1, (d) W:C ratio 2:1	86
Figure 4.10	Typical axial stress and axial strain curves of different samples cured for 90 days	86
Figure 4.11	Axial stress and axial strain curves of W:C ratio 2:1 sampled cured for 120 days	87
Figure 4.12	Bar chart of compressive strength and W:C ratio	88
Figure 4.13	Bar chart of comparison of compressive strength (MPa) for W:C ratio 2:1 of present study with other researches for different curing ages	88
Figure 4.14	Triaxial test results (deviatoric stress vs axial strain curves)	94
Figure 4.15	Pore pressure vs mean effective stress graph	94
Figure 4.16	Stress path of triaxial test (mean effective stress vs deviatoric stress)	95
Figure 4.17	Shear stress vs normal stress of grouted samples	96

Figure 4.18	Failure patterns of grouted samples: (a) shear failure, (b) axial split, (c) bulging (d) collapse, (e) column mode failure	96
Figure 4.19	Deformed shaped under perpendicular load (a) bulging effect of low modulus of elasticity sample and (b) stress condition of high modulus of elasticity sample (Warner, 2004)	97
Figure 4.20	Failure pattern of 2:1 proportionate grouted sand after 120 days	98
Figure 4.21	Sand compacted with grouting materials (Marchi et al., 2012)	99
Figure 4.22	Failure pattern of different proportionate grouted sand after 28 days of curing: (a) Multiple shear failure for W:C 2:1, (b) Axial split for W:C 3:1, (c) collapse failure for W:C 4:1, (d) column mode failure for W:C 5:1	100
Figure 4.23	Failure pattern of different proportionate grouted sand after 90 days of curing: (a) Multiple shear failure for W:C 2:1, (b) Axial split for W:C 3:1, (c) collapse failure for W:C 4:1, (d) column mode failure for W:C 5:1	101
Figure 4.24	Failure pattern of 2:1 proportionate grouted sand under Triaxial test	102
Figure 4.25	SEM Image of grouted sand (5:1) after 28 days of curing	107
Figure 4.26	SEM Image of grouted sand (4:1) after 28 days of curing	108
Figure 4.27	SEM Image of grouted sand (3:1) after 28 days of curing	109
Figure 4.28	SEM Image of grouted sand (2:1) after 28 days of curing	110
Figure 4.29	SEM Image of grouted sand (5:1) after 90 days of curing	111
Figure 4.30	SEM Image of grouted sand (4:1) after 90 days of curing	112
Figure 4.31	SEM Image of grouted sand (3:1) after 90 days of curing	113
Figure 4.32	SEM image of grouted sand (2:1) after 90 days of curing	114
Figure 4.33	SEM Image of grouted sand (3:1) after 14 days of curing (nonhomogeneous shaped sample)	115
Figure 4.34	SEM Image of grouted sand (2:1) after 120 days of curing (sample 1)	116
Figure 4.35	SEM Image of grouted sand (2:1) after 120 days of curing (sample 2)	117
Figure 4.36	SEM Image of grouted sand (2:1) after 120 days of curing (sample 3)	118
Figure 4.37	EDS analysis of grouted sand samples cured for 90 days: (a) W:C 2:1, (b) W:C 3:1, (c) W:C 4:1 and (d) W:C 5:1	121
Figure 4.38	EDS analysis of Grouted sample (2:1) after 120 days of curing: (a) sample 1, (b) sample 2 and (c) sample 3	123

LIST OF TABLES

Table 2.1	Dry unit weight and porosity of various granular soils (Warner, 2004)	18
Table 2.2	Permeability and drainage conditions of soils (Lambe and Whitman, 1969)	21
Table 2.3	Typical values of permeability for sands (Murthy, 2003)	21
Table 2.4	Grouting technique with relevant ground types (European Standard, 1996)	22
Table 2.5	Approximate relationship between hydraulic conductivity and groutability (Karol, 2003)	24
Table 2.6	Comparison of different research works with present study	30
Table 2.7	List of tests conducted in this study	39
Table 3.1	Location of collected soil sample	42
Table 3.2	Properties of sand	43
Table 3.3	Physical Properties of the cement	43
Table 3.4	Chemical Properties of the cement	44
Table 3.5	Test plan for finding the properties of the grouted and non-grouted sand	44
Table 3.6	Summary of samples and test conditions	63
Table 4.1	Properties of sand used for grouting	68
Table 4.2	Conversion of Mix proportion from volume to weight	70
Table 4.3	Sample designation	72
Table 4.4	List of samples for unconfined compression and triaxial tests	73
Table 4.5	Physical properties of the tested grouted samples	74
Table 4.6	Comparison of strength properties in grouted samples	89
Table 4.7	Comparison of compressive strength (MPa) for W:C ratio 2:1 of present study with other researches for different curing ages	90
Table 4.8	Summary of triaxial test results	91

NOTATIONS AND ABBREVIATIONS

Symbols	Description
Δu_d	Pore Water Pressure
$\Delta\sigma_d$	Deviatoric Stress
A	Cross Sectional Area of Soil
\bar{A}_f	Skemton's Pore Water Parameter at Failure
C_u	Co-efficient of Uniformity
CU	Consolidated Undrained
C_z	Co-efficient of Curvature
e	Void Ratio
EDS	Energy Dispersive Spectroscopy
F.M.	Fineness Modulus
I	Hydraulic Gradient
K	Permeability Coefficient
Q	Flow Rate
q_u	Unconfined Compressive Strength
SEM	Scanning Electron Microscope
S_u	Undrained Shear Strength
UC	Unconfined Compression
W: C	Water Cement Ratio
σ_1'	Major Effective Principal Stress
σ_3'	Minor Effective Stress

Chapter 1

INTRODUCTION

1.1 General

Grouting is commonly used to strengthen soil formations, either temporarily during construction or permanently for increasing strength and load-bearing capacity (Paul, 2009). There are four distinctly different mechanisms by which this is accomplished: densification, cohesion, reinforcement, and chemical exchange (Warner, 2004). Grouting is often performed in the soil to lower the permeability and inhibit the movement of water. Permeation grouting is the longest established and most widely used grouting technique, sometimes referred to as penetration grouting, it involves the filling of cracks, joints, or the pore spaces of soils, aggregates, or other porous media (Kainrath et al., 2015). The objective is to fill a void space without displacement of the formation or any change in the void configuration or volume. Grouting effectiveness is usually determined by the level of reduced permeability achieved, which is determined by water pressure tests often in successive grout holes that are injected. In soils, the procedure involves permeating and filling the soil pore spaces without any significant disturbance to, or movement of, the individual soil grains (Mainmark, 2013).

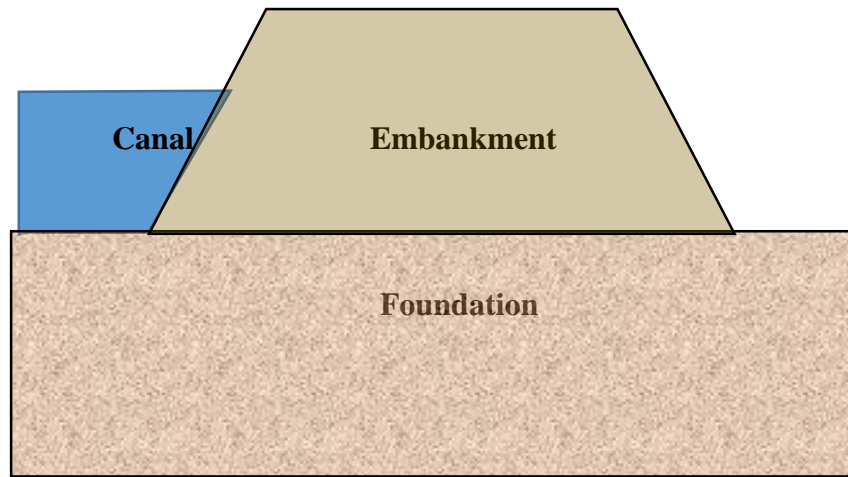
Grouting may also be used to reduce seepage and to fill voids beneath the canal lining and within the canal embankment and foundation. Grouting may be performed with the use of drill holes from the embankment surface or core holes through the canal lining. The selection of an acceptable drilling method is critical for any grouting project. For example, the use of pressurized air or water can damage the embankment and/or foundation and should not be used. Permeation grouting is environment friendly because the main characteristic of permeation grouting is not to disturb the adjacent soil or structure. Once the grout is injected below the ground surface or beneath the canal lining, it is difficult to monitor where the grout travels. Batch weights and flow measurement devices may be used to record the volume of grout

injected which can be an indicator of the degree of flaws in the embankment/foundation. Monitoring grout travel is usually done by monitoring adjacent grout holes and seepage locations. Grouting is considered to be successful once the seepage rate slows to an acceptable level (U.S. Department of the Interior Bureau of Reclamation, Canal operation and maintenance: Embankment, 2017).

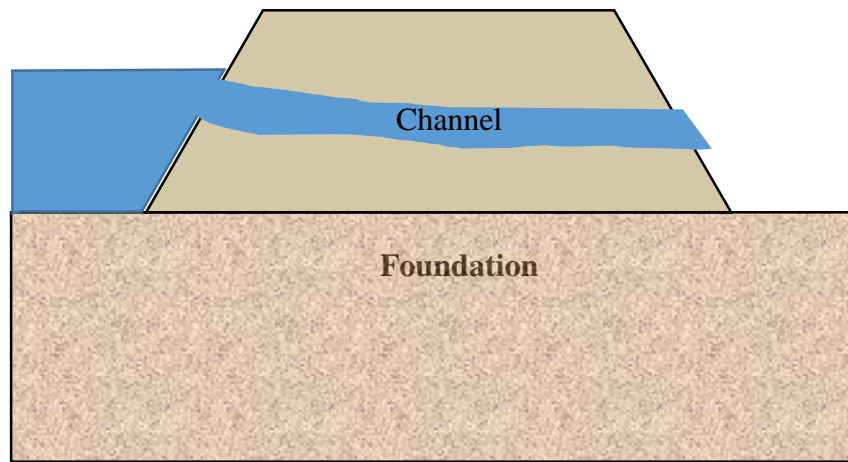
Nowadays, a large number of hydraulic structures like tunnels, embankments, and bridges are constructed in Bangladesh. In most of the areas of Bangladesh, the engineering geological condition is very complex. The surroundings structure of the newly constructed is in a vulnerable condition. In this case, permeation grouting can play an important role. The permeation grouting method can fill the loose deposited mass well and improve the overall strength of the surrounding structure efficiently. Permeation grouting with cement-based grout has become an effective method for water leakage treatment because of its convenient construction and friendliness to the environment. Permeation grouting is an effective method used for enhancing stabilization and reducing the permeability of granular soil deposits without disturbing the original soil structure.

1.2 Background

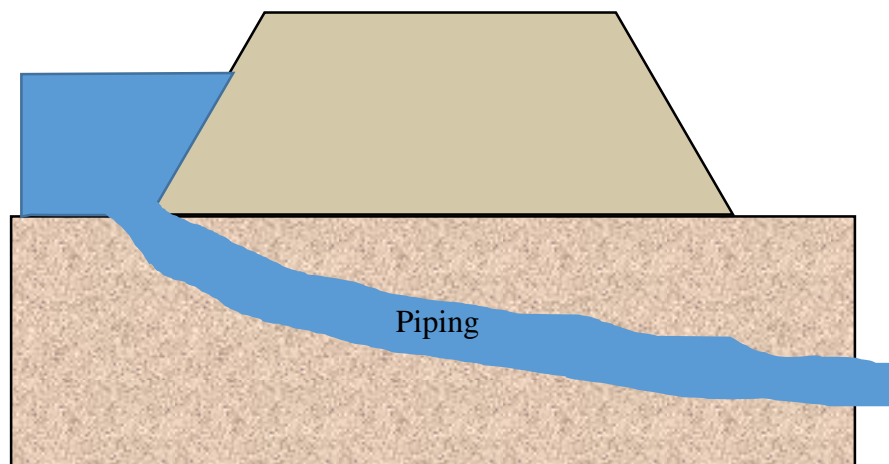
Seepage control of the earthen dam and embankment is one of the most challenging issues in Geotechnical Engineering. Grouting is widely used to stabilize weak soils, control seepage in tunnels, and mitigate failed dams by forming seepage barriers. In recent years, the levee breached by flood due to seepage has become an alarming problem in Bangladesh (Rahman, 2016) which has shown in Figure 1.1. The seepage phenomenon beneath the earthen embankments may be controlled by treating the underlying granular soil with grout suspensions delivered by permeation grouting, resulting in a less permeable deposit. Permeation grouting using cement grout is the most common ground treatment technique for granular soil (Jadid et al., 2016). It involves the injection of suitable suspension into soil pores to either reduce the permeability or increase the shear strength and thus the bearing capacity of the ground (Avci et al., 2017). It involves the free flow of grout into the soil voids with minimal effect. It fills a void space without displacement of the formation or any change in the void configuration or volume. This technique is generally used to reduce ground



(a)



(b)



(c)

Figure 1.1: Failure patterns of earth embankment (a) cross-section of an embankment (b) failure of embankment due to channel formation (c) under seepage through pervious sand foundations (failure due to piping)

permeability and control groundwater flow, but it can also be used to strengthen and stiffen the ground. It refers to the replacement of water in voids between soil particles with a grout fluid at a low injection pressure to prevent fracturing (Raman et al., 2012). Benzuijen (2007) stated that the injection process of the grouting will lead to the reduction in the permeability of the soil and form a thick bonding so that it reduces the bleeding in the sample. Tahia (2005) concluded that the measured ultimate bond capacity of grouted is linearly increasing with the surcharge pressure. The durability of soil against wetting drying cycles is of great importance for an embankment like monsoon country Bangladesh. Kampala et al. (2014) explored that the durability of soil was mainly related to its unconfined compressive strength. Eisazadeh et al. (2013) explored the influence of cement on alluvial sandy soil mechanical properties clearly, microstructure analysis had been conducted using a scanning electron microscope. Liquefaction is one of the most disastrous effects of the hydraulic structure. Hashimoto et al. (2015) stated that permeation grouting helped to mitigate the liquefaction. According to Bono et al. (2014), the presence of cement had a dramatic influence on the triaxial behavior of sand; for sand sheared at a given confining pressure, cementation generally causes an increase in stiffness, peak strength, and the amount and rate of dilation with these effects increasing with cement content. Keong et al. (2005) stated that permeation grouting, which is an example of grouting technics, in porous media depends on stability, filtration pressure, yield stress, and grain size distribution. Cementation also influenced the failure modes of sand; brittle failure with shear planes is often witnessed in cemented specimens. There had been many research activities based on laboratory tests like the unconfined compression test as well as the triaxial test aimed at examining the stability of sandy soil against liquefaction and seepage during the flood. Kamata et al. (2009) evaluated based on the undrained shear strength obtained from the undrained triaxial test on soil specimens. In recent years, due to the development of cities, there is a growing need for the construction of underground structures. That's why stabilization of loose sandy soil is very important when constructing such projects (Jafarpour et al., 2019).

Therefore, an effective measure to reduce and control the seepage in the context of alluvial soil characteristics in Bangladesh may be permeation grouting. Seepage occurs in both vertical and horizontal directions. Horizontal seepage is a most common phenomenon in an earthen dam, embankments, etc. than that vertical

seepage. So it will be a practical case to emphasize controlling seepage in the horizontal direction. So, laboratory tests on soil samples and other similar materials are relevant to comprehending soil behavior in this regard. In the prospect of Bangladesh, controlling seepage in dams, embankments, and other slope protection structures will work as a beneficial outcome.

Moreover, by permeation grouting, some other indirect advantages can also be obtained like soil strengthening and water tightness. The main job of permeation grouting is to permeate a concentrated suspension through the pores of granular soil. Permeation grouting with low pressure is an appropriate method for improving the loose sandy soil under the foundation of sensitive structures and bridge footings, due to the merits of no change in soil structure and no large displacement (Jafarpour et al., 2019).

1.3 Objectives of the Study

The main objectives of this research are as follows:

- (i) To characterize the shear strength properties of grouted and non-grouted sandy soil by preparing horizontally and vertically grouted samples.
- (ii) To determine the permeability properties of grouted and non-grouted sandy soil.
- (iii) To investigate the microstructural characteristics (topographical and compositional variation) of the grouted soils by Scanning Electron Microscope (SEM).

1.4 Organization of the Thesis

The contents of this research study have been arranged in five chapters. Chapter One is the introductory part of the thesis. This chapter includes the background, importance, and reasons for conducting this study and outlines the objectives and organization of the thesis work.

Chapter Two illustrates a literature review on different grouting techniques, grouting materials, the basics of this research, a summary of permeation grouting, characteristics and features of grouting on soil, and different influencing factors of grouting technique. Finally, the research gap has been included in this chapter.

Chapter Three describes the methodology of the research. This chapter includes relevant material properties, a test program, preparation of specimens, and a description of the experimental setup.

Chapter Four presents the results and findings of the study. This chapter incorporates the results of the test program as well as the detailed analysis of different parameters and observations obtained from the microstructural study, scanning electron microscope.

The conclusions of this study are presented in Chapter Five. Some recommendations for future study have also been reported in this chapter.

Chapter 2

LITERATURE REVIEW

2.1 Introduction

The introduction of a cementing agent into sand produces a material with two components of strength- that due to the cement itself and due to friction. Density, grain size distribution, grain shapes, and grain arrangements all have a significant effect on the behavior of cemented sand (Clough et al., 1981). The construction of underground structures on the soft ground often requires the soil to be improved to ensure the safety and stability of surrounding buildings. Grout permeation is an efficient technique for reducing permeability and increasing stiffness and strength of coarse-to-medium grained soils with low initial mechanical properties. This chapter presents a summary of research about permeation grouting and permeability to provide a satisfactory background for subsequent discussions. Also focused on the research gap of this topic.

2.2 Soil Grouting

The predominant reason for grouting is strengthening or inhibiting the flow of water through a mass. A grouted formation may be required to last for only a short period, such as temporary improvement to aid ground support during excavation or the control of water seepage during construction. Many applications, however, require permanent improvement, where long-term durability becomes important. Grouting is often used in remedial work to control seepage and strengthen soil or rock, concrete, or masonry. There are three classes of grouting materials (Sio-Keong, 2005):

- (i) Suspension type grouts: Small particles of solids are distributed in a liquid dispersion medium, e.g. cement and clay in water having Bingham's fluid characteristics.
- (ii) Emulsion type grouts: A two-phase system containing minute (colloidal) droplets of liquid in a disperse phase, e.g. bitumen and water that are evaluative Newtonian fluids in which viscosity increases with time.

- (iii) Solution type grouts: Liquid homogeneous molecular mixtures of two or more substances, e.g. sodium silicate, organic resins, and a wide variety of other so-called chemical grouts, non-evaluative Newtonian solutions in which the viscosity is constant until set within an adjustable period. The suspension type grouts include clay, cement, and lime, while the emulsion type grouts include bitumen, and the solution type grouts include a wide variety of chemicals. With various pressures and operations applied in the grouting process, the improvement can be achieved in various forms like permeation or penetration, compaction or controlled displacement, and hydro fracturing or uncontrolled displacement.

2.3 Application of Grouting

The use of grouting has become more popular in recent years due to the rapid development of sub-surface urban infrastructures (e.g. basement, subway, and metro rail transport system), underground facilities (e.g. common services duct and deep tunnel sewer system), and civil defense (e.g. shelter and storage). Grouting can be used to improve the condition of the site against possible construction problems, such as:

- (i) To reduce the permeability of soil for minimizing the seepage effect.
- (ii) To strengthen soils for improving their load-carrying capacity, excavation stability, and resistance against liquefaction effect.
- (iii) To improve the stability of existing structures and to adjust the profile of distorted structures.
- (iv) To stabilize the ground for facilitating tunneling or shaft excavation.
- (v) To form a barrier or cutoff to water or contaminant flow in the ground.
- (vi) To fill voids to prevent excessive settlement.
- (vii) To prevent loose to medium sand densification under adjacent structures (i.e., both for vertical and lateral movements) due to adjacent excavations, pile driving, etc.
- (viii) To attain foundation underpinning.
- (ix) To perform Slope stabilization works.
- (x) To control the volume changes of expansive soils through pressure injection of grout slurry (only for some expansive soils, not all).

2.3.1 Types of Grouting Method

The use of grouting is becoming increasingly important for dams and levees, and other aging infrastructure. Though there are various types of grouting, permeation grouting is the only kind of grouting for which design equations and relationships exist. All other kinds of grouting are follow-ups and they comprise a list of processes variously called compaction grouting, soil fracture grouting, compensation grouting, jet grouting, consolidation grouting, and seepage grouting which are not grouting at all but are soil mixing.

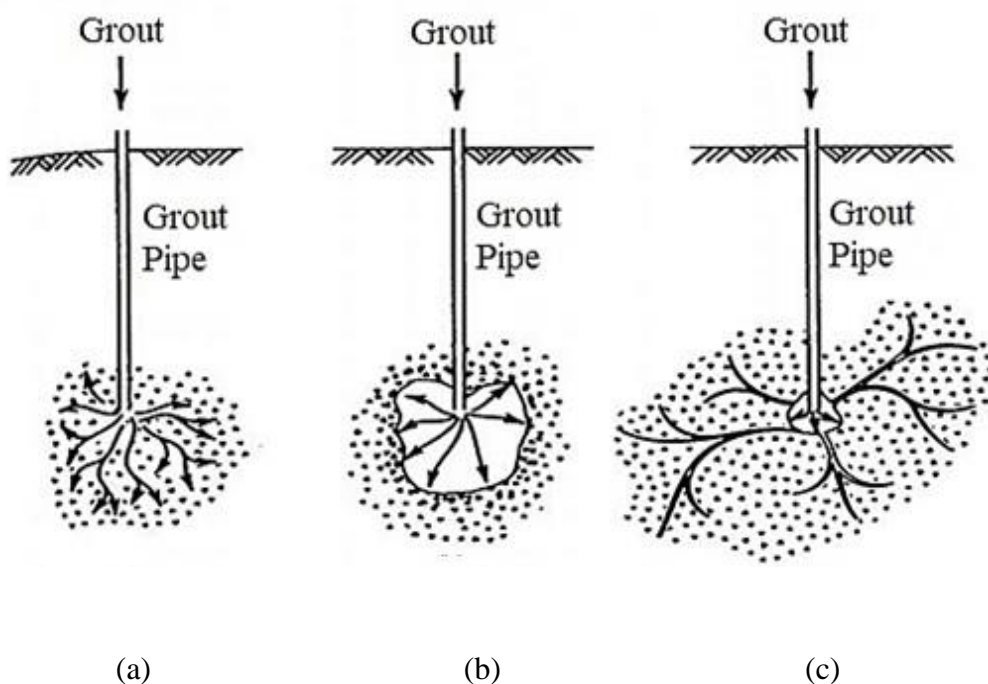


Figure 2.1: Various forms of improvement in soil and rock grouting: (a) permeation grouting (penetration), (b) compaction grouting (controlled displacement) and (c) hydro-fracturing (uncontrolled displacement) (Koerner, 1985)

2.3.2 Permeation Grouting

Permeation grouting is typically defined as the flow of a low-viscosity grout (bentonite, sodium silicate, microfine cement, acrylate, or polyurethane) into the pores of the soils, aggregates (or cracks, joints, or generally small defects in rock, concrete or masonry) without displacing or changing the original soil structure. It is also referred to as penetration grouting. It is the most common and oldest form of soil grouting. The conceptual diagrams of permeation grouting are shown in Figure 2.2, Figure 2.3(a), and 2.3 (b).

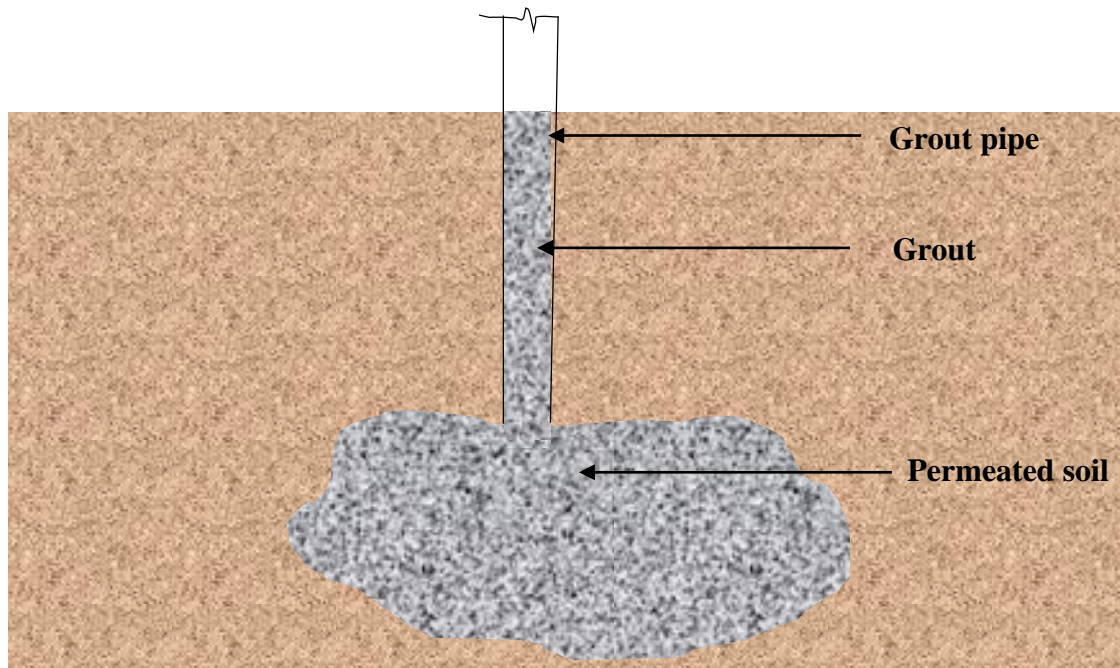


Figure 2.2: Permeation grouting: conceptual diagram of soil solidification by permeation grouting (Ronald and Riley, 1995)

2.3.3 Compaction Grouting

Compaction or low mobility grouting is the high-pressure injection of a thick immobile grout into subsurface soils, because of high viscosity the grout expands radially as a homogenous bulb from the injection point instead of permeating into the soil pores as shown in Figure 2.4(a). Compaction grouting is commonly used for increasing bearing capacity, arresting or reducing foundation settlements, reduction of liquefaction potential, and lifting and leveling structures. Compaction Grouting is also known as low mobility grouting. The slump of grouting slurry is less than 1” and the cementitious grout is injected into weak or soft soil to densify the soil. This type of grouting is used to reduce the settlement and give overall ground improvement. This grouting helps us to compensate of ground loss during the tunneling. In this case, high pressure is the main requirement to make it effective. The plan for Sequencing the injection points are the main task of compaction grouting.

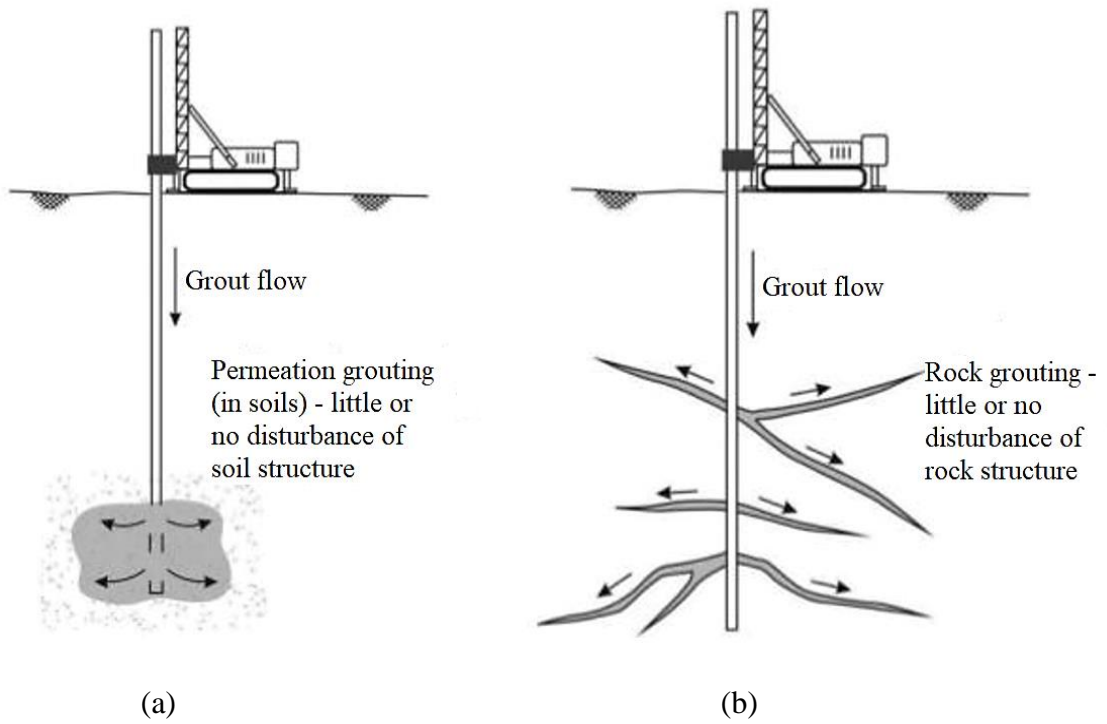


Figure 2.3: Permeation grouting in: (a) soil and (b) rock (Rahman, 2016)

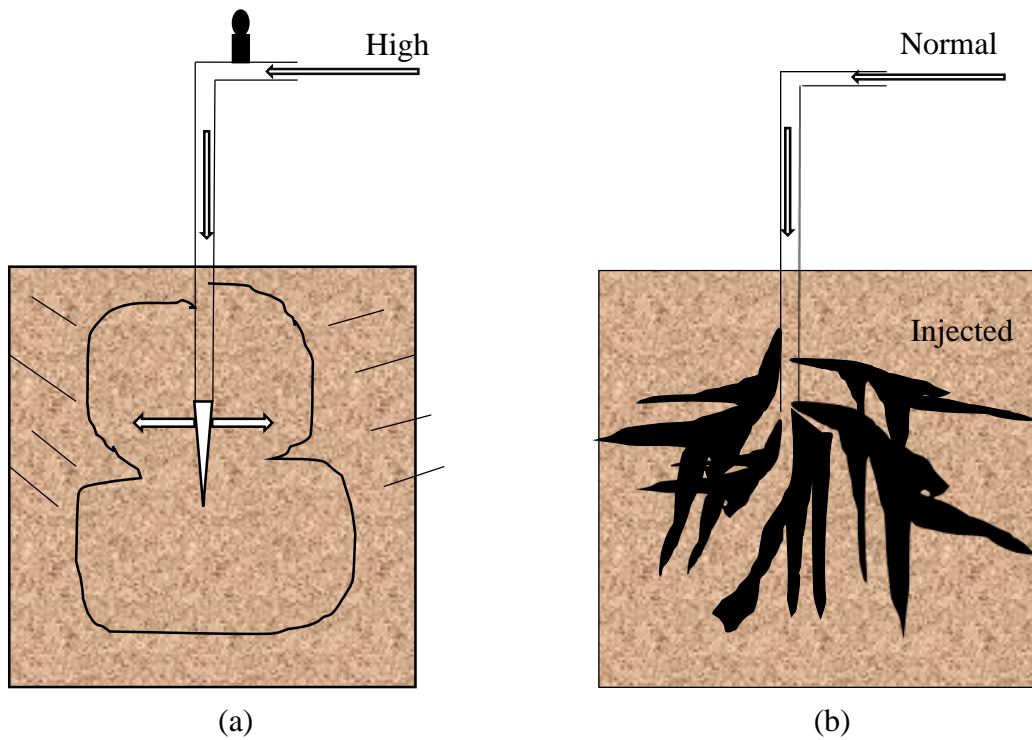


Figure 2.4: (a) Compaction grouting and (b) permeation grouting (Gamil et al., 2017)

2.3.4 Fracture and Compensation Grouting

Fracture grouting is the intentional fracturing of the ground by high-pressure injection of cement-based grout through sleeve port pipes to form intertwined lenses or veins of grout to provide reinforcement and even some consolidation of the soil. Grouting is typically performed in several phases with repeat injections at each port to ensure the formation of multiple fractures through the soil.

When performed concurrently with underground construction such as soft ground tunneling, fracture grouting of the soils between the tunnel and the overlying structures have specific design intent of providing a controlled ground heave to compensate for potential structural settlement. Such an application of fracture grouting is referred to as compensation grouting. Rock curtain grouting is the filling or partly filling by grout injection of fractures, fissures, and joints in a rock mass to reduce permeability, strengthen or stabilize the rock, or both as shown in Figure 2.3(b). The grout curtain is constructed by the drilling and grouting of closely-spaced drill holes oriented to optimize the intersection of rock joints. Its applications include:

- (i) Reduction of water seepage and pressure beneath a dam or other structure.
- (ii) Control of seepage beneath a cut-off wall for "bathtub" excavations.
- (iii) Pretreatment of permeable rock masses.
- (iv) Control of seepage under a frozen cut-off wall.
- (v) Grouting of a water-bearing zone to minimize the quantity of water to be handled within a shaft excavation.

2.3.5 Jet Grouting

Jet Grouting uses high-pressure, high-velocity jets to hydraulically erode, mix and partially replace the in situ soil or weak rock with cementitious grout slurry to create an engineered soil-cement product of high strength and low permeability, the process of jet grouting is shown in Figure 2.6.

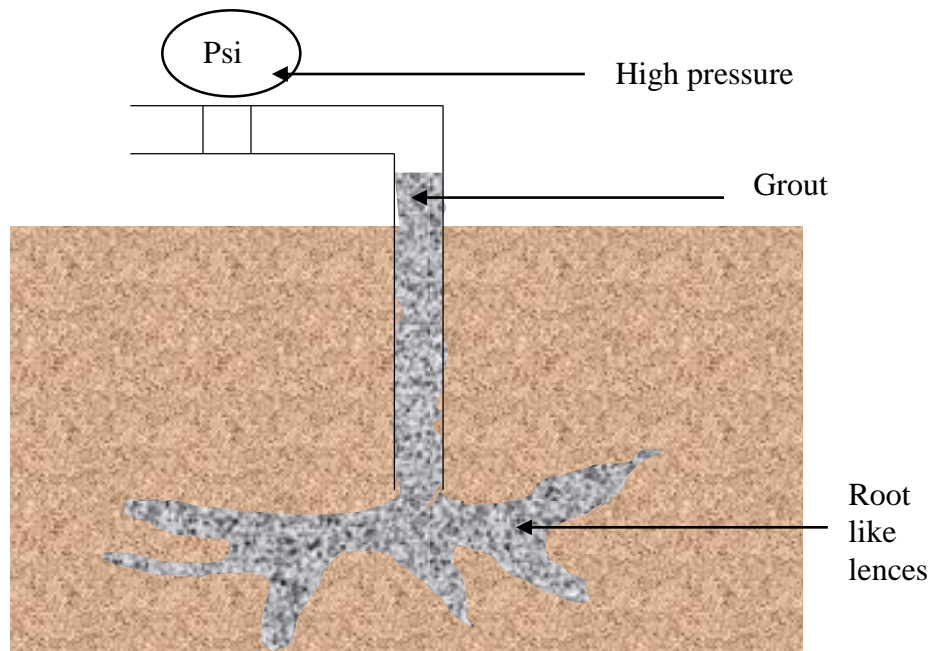


Figure 2.5: Fracture grouting (Geo grout, 2019)

Jet grouting can be performed above or below the water table and in most subsurface stratigraphy from cohesion-less soils to highly plastic clays. The three basic systems in general use are single-fluid, double-fluid, and triple-fluid jet grouting. The selection of the most appropriate system is dependent on the in situ soil characteristics and the application. Jet grouting has several construction-related applications, including Structural underpinning and excavation support.

- (i) Groundwater control or cut-off
- (ii) Utility support
- (iii) Temporary or permanent soft soil stabilization
- (iv) Slope stabilization
- (v) Hazardous waste containment

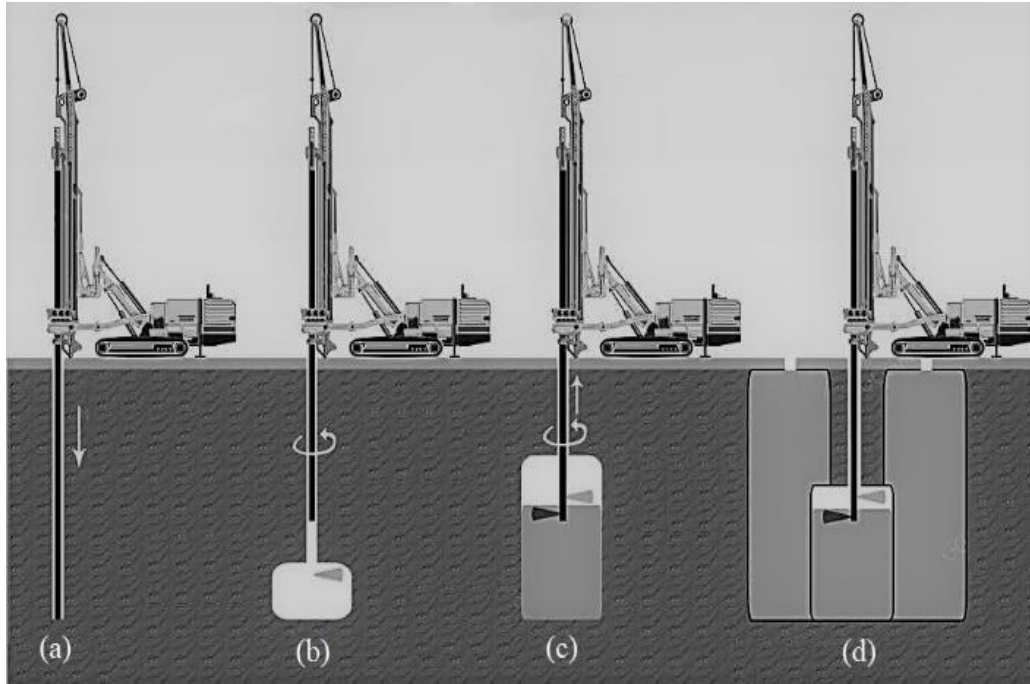


Figure 2.6: Process of jet grouting (a) drilling with water, (b) start high-pressure grouting, (c) execution of jet-grout column, (d) repeating for the next column (Taehwa, 2020)

2.4 Purpose of Permeation Grouting and Its Scope

The definition of permeation grouting has been presented under Section 2.3.2. It involves the injection of grout at low pressures into the soil matrix to permeate or encapsulate the individual soil grains without otherwise disturbing the natural state of the soil. This grouting is the longest established and most widely used grouting technique. The characteristics of the ground are modified with the hardening or gelling of the grout.

Depending on the requirements of the project and the grout materials can be temporary or permanent. Permeation grouting may serve two purposes:

- (i) To reduce soil permeability and provide water tightening and
- (ii) To increase the strength and cohesion of granular soils.

Permeation grouting can be a very cost-effective solution for significant infrastructure challenges and ground improvements. It is the only type of grouting that can be used in all of the different media into which grout may be pumped. Primary applications of Permeation grouting include:

- (i) Pre-excavation grouting for excavations in soil or poorly cemented sedimentary rock.
- (ii) Improvement of excavation conditions at portals, shallow shafts, or along alignments.
- (iii) Soil stabilization for excavation support.
- (iv) Ground modification.
- (v) Groundwater control on tunneling projects.
- (vi) Utility and footing support.
- (vii) Water cut-off.
- (viii) Exclusion or in situ containment of contamination on environmental projects
- (ix) Sealing off of high permeability backfill.

In this research permeation grouting has been carried out for the following reasons:

- (i) This type of grouting technique requires a less sophisticated equipment facility.
- (ii) It can be a very cost-effective solution for significant infrastructure challenges.
- (iii) Bangladesh is delta land. It is an appropriate and most effective method for the dams and embankments that are constructed with granular soils in Bangladesh.
- (iv) This method is the most ordinary methodology for larger-scale work like dams, embankment and excavation works, etc.

2.5 Basic Mechanism of the Research

In this research, cement-based grout is made of cement and water, which is added with sand. In the application, the grout is placed by using the injection method with hand pressure. Permeation grouting is an effective way to send the grout into the ground without disturbing the soil structure. Cement grout with different water-cement ratios 2:1, 3:1, 4:1, and 5:1 are injected into the sand. The grout materials which is injected into the sand, are capable of forming a gel and binding the soil particles. Where water control is required, the mechanism of improvement is the filling of all voids. In this application, the strength of the grout is of relatively little importance as long as it fills the soil pore space and does not deteriorate or escape from the area in which it has been deposited. To completely block the liquid flow, virtually 100 percent of all pore space must be filled. In strengthening operations, the primary mechanism of improvement is through adhesion, which is simply the gluing

of the soil grains together. This results in a substantial increase in the cohesion properties of the soil, which will also increase the bearing strength.

The degree of filling is relatively unimportant, however, as long as the grains are sufficiently bonded together. The degree of that bonding can vary widely, depending on the final strength requirement. Obviously, in the application that requires both strengthening and water control, the pore space must be filled, and the strength of grout becomes fundamental. Figure, 2.7, is shown the oldest uses of grouting. Badly jointed or fractured soil can be returned to a monolithic condition by grouting. This may be done for improvement of bearing capacity, but is more typically done to increase the capacity of embedded soil bolts, ground anchors, and such. It can also be used to strengthen weak soil under and around the tips of foundation piles. In many cases, the grouting intent is a combination of both water control and strengthening.

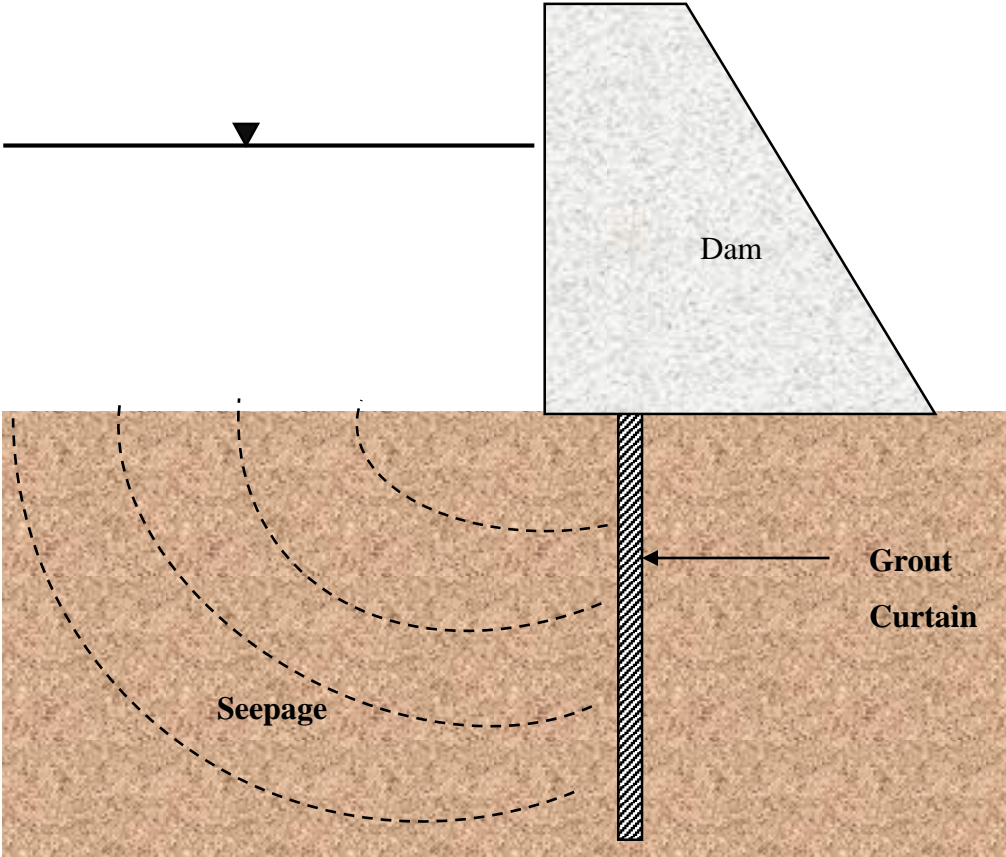


Figure 2.7: Formation of an impermeable curtain due to grouting under the dam (Warner, 2004)

2.5.1 Degree of Solidification

Soil solidification is relatively expensive, and it is thus usually preferable to minimize the amount of grout injected and thus the volume of soil solidified. For this reason, grouting is generally used only as part of an overall system where most of the load is supported by other means. Where the grouted mass is to serve as the sole support, a properly-designed gravity structure is required, and this, of course, will result in significantly more grouted ground (Warner, 2004)

2.5.2 Injection Probe layout

The solidification requirements, as discussed in the preceding paragraphs, will dictate both the probe layout and the amount of grout required. The probes can be spaced to provide solidified columns that just touch each other as shown in Figure 2.8. The spacing of the probes will also be dependent on the permeability of the soil and the penetrability of the particular grout to be used. Injection probe spacing usually fails within a range of 2 to 4 ft. (0.6 to 1.2m) or occasionally more. Experience shows, however, that closer spacing allows greater control of the work and generally results in a better-finished product. It can also provide a significant reduction in the quantity of grout required (Warner, 2004).

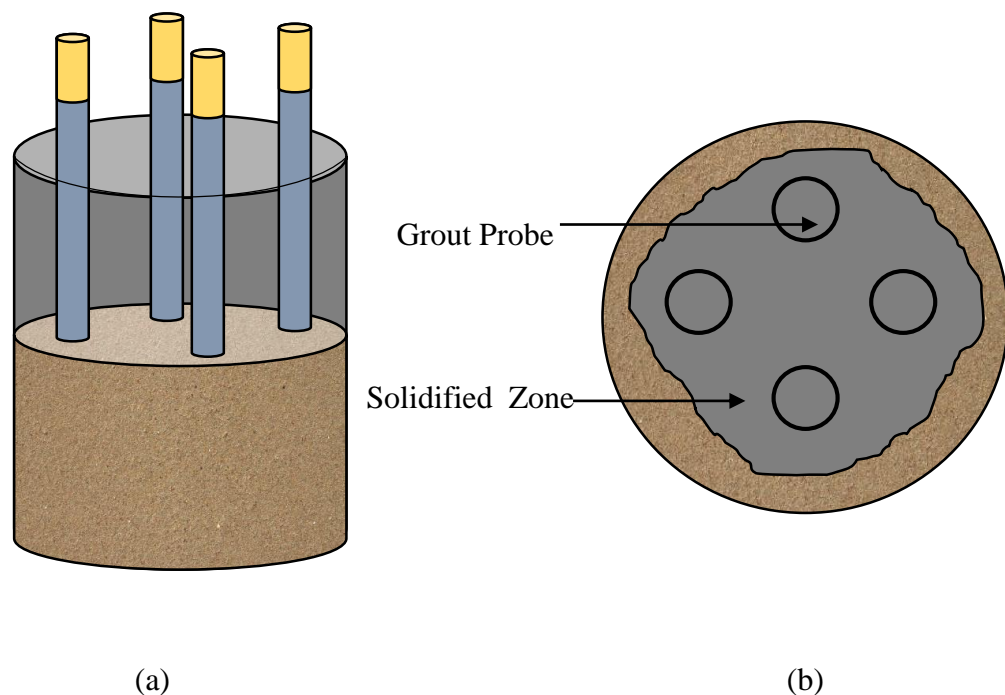


Figure 2.8: Process of permeation grouting in the cylinder: (a) inserted sleeve port pipe to inject grouting materials, (b) plan view after grouting

2.5.3 Required Grout Quantity

As discussed earlier, the quantity of grout used for a particular application depends on the thoroughness required of the work and the volume of the pore void system of the particular soil to be improved. The volume of the voids and porosity can vary greatly at a given density, depending on both the shape of the grains and their moisture content. Soil porosity is fundamental to determining the amount of grout that will be required to treat a given volume of it. However, porosity is dependent on the grain shape and structure of the deposit, so the following table serves as guidelines.

Table 2.1: Dry Unit Weight and Porosity of Various Granular Soils (Warner, 2004)

Soil Type	Porosity %		Dry unit weight (kg/m ³)	
	Loose	Dense	Minimum	Maximum
Uniform coarse sand	50	32	1312	1840
Uniform fine to medium sand	50	29	1328	1888
Well graded sand	49	17	1360	2208
Well graded sand and gravel	46	12	1421	2320

2.5.4: Injection Holes/ Probes

Permeation grouting can be performed from the top-down, from the bottom up, or at selected intervals, with the use of a sleeve port pipe. Where the soil permeability varies greatly, special care must be taken to ensure that the grout is deposited at the planned location. This can be accomplished by the use of a special drive needle that positively restricts the location of grout deposition, or through the use of sleeve port pipes whereby the locations of grout deposition can be selectively chosen (Warner, 2004).

2.5.5 Bottom-Up Staging

Bottom-up staging should be only used in deposits that decrease in permeability with depth. The reason is that even though the injection pipe has been raised, the grout can

continue to flow to the lower previously completed stages if they are in soil that takes the grout more readily (Warner, 2004).

2.5.6 Sleeve Port Pipes

By far the most accurate way to place grout is with the use of a sleeve port pipe. This is simply a tube that has small portholes drilled at regularly spaced intervals. In this research, in Figure 2.9, four PVC pipes of 20 mm diameter are used for the grouting. Then four rubber pipes of 10mm diameter are inserted at the top of the PVC pipe to maintain the pressure and avoid the pressure loss. These PVC pipes are acted as sleeve port pipes to inject grouting materials. (Warner, 2004)



Figure 2.9: Four sleeve port pipe in a cylindrical mold to prepare grout sample

2.6 Permeability and the Characteristics of Soil

Permeability is a measure of the ease with which a fluid (usually water) can flow through the soil. The permeability of a material is generally described by the coefficient of permeability (k), which is the average velocity of a fluid through a unit area driven by a unit hydraulic gradient within the material. In 1856, Henry Darcy derived an empirical formula for the behavior of flow through saturated soils under steady-state conditions. He determined that the flow rate (Q) through saturated soil was directly proportional to the cross-sectional area (A) of soil normal to the direction of flow under the hydraulic gradient (i) as expressed by the following formula:

$$Q = kiA \quad (2.1)$$

Here Q= Flow rate, cm³/sec

k= permeability coefficient, cm/sec

A= cross sectional area of soil, cm²

i= Hydraulic gradient, cm

The permeability characteristic of soil to grout is an important factor in the study of permeation grouting. This property is necessary for the calculation of seepage through earth dams or under sheet pile walls, the calculation of the seepage rate from waste storage facilities (landfills, ponds, etc.), and the calculation of the rate of settlement of clayey soil deposits. Moreover, the factors influencing the permeability of soil (Lambe, 1969) are also necessary. According to Lambe (1969), the following five factors influence the permeability of the soil to water:

- (i) Particle size
- (ii) Void ratio (with the linear relationship found between k value and void ratio)
- (iii) Composition (e.g. content of fines and coarse sand)
- (iv) Fabric and
- (v) Degree of saturation

All these influencing factors are also found applicable to the permeability of the soil to cement grout (Mitchell, 1981 and Perret et al., 2000). For the sandy soil adopted in the present study, the first three factors have a significant influence on the permeability characteristics of sand.

2.6.1 Permeability of Sands and Clays

Sands are granular with relatively large void spaces. So, sands have a high permeability. Sands are naturally occurring sedimentary materials with diameters ranging from 0.06mm to 2mm. Due to the high permeability of sands, they drain relatively quickly. Clays are also a naturally occurring material composed primarily of fine-grained minerals that develop plasticity with the addition of water. Clay is typically a fine flake-shaped particle with diameters less than 0.002mm. So, clays have low permeability. Due to the low permeability of clays, they drain very slowly. Table 2.1 and Table 2.2 show the ranges of permeability and drainage characteristics based on soil types.

2.6.2 Vertical and Horizontal Permeability

Natural soil deposits are almost always stratified or in layers. Soil stratification and discontinuities provide flow channels within the soil that are less resistive to flow. Due to the variability associated with geological formations of soils, the orientation of soil particles, and discontinuities, there is a high demand that a methodology is found that can measure permeability rapidly at multiple depths and locations. This variability associated with natural soil deposits contributes to soil's anisotropy. That is, the coefficients of permeability in the horizontal and vertical directions are different.

Table 2.2: Permeability and drainage conditions of soils (Lambe and Whitman, 1969)

Types of Soil	Coefficient of Permeability (cm/sec)
Clean gravel	10^1 to 10^2
Clean sand	10^1
Clean sand and gravel mixture	10^{-1} to 10^{-4}
Very fine sand	10^{-5}
Silt	10^{-6}
Clayey soils	10^{-7} to 10^{-9}

Table 2.3 Typical values of permeability for sands (Murthy, 2003)

Type of Sand (U.S. Army Engineer classification)	Coefficient of Permeability, ($k \times 10^{-4}$) (cm/sec)
Very fine sand	50
Fine sand	200
Fine to Medium sand	500
Medium sand	1000
Medium to coarse sand	1500
Gravel and coarse sand	3000

The orientation of particles in soils which have been consolidated vertically and discontinuities in layers ensure that the average permeability in the horizontal plane is greater than that of the vertical plane. Soil permeability in the horizontal and vertical directions is greatly affected by the sizes and orientation of soil particles as well as any discontinuities present. Soil permeability is an important parameter for any geotechnical design where the flow of water through soil is a matter of concern. Therefore, to ensure an efficient design, it is expected that the soil permeability in both the vertical and horizontal directions can be determined.

2.7 Grouting Technique

Permeation grouting is influenced mainly by the permeability of the ground. The significant variation in permeability found in natural soils and rocks required a range of grout and grouting techniques which for effective treatment. The different grouting techniques with relevant ground types have been shown in Table 2.4. In this table, the coefficient of permeability to water (W:C) does not take into consideration the influence of viscosity (i.e. ratio) on the Injectability of grout, and the method of measurement for k value is not reported, therefore, it can be used as a general guide only.

Table 2.4 Grouting technique with relevant ground types (European Standard, 1996)

Types of soil	Coefficient of permeability(k) range (cm/sec)	Type of Permeation
Gravel, coarse sand, and sandy gravel	> 500	Pure cement suspension, Cement based suspensions
Medium sand	500 to 100	Micro-fine suspensions
Fine sand, silt, silty clay	5×10^{-2} to 1×10^{-4}	Specific Chemicals

2.7.1 Groutability

Groutability of soil is of primary concern in field applications. The ability of the grout to reach the desired location in the soil mass is expressed by groutability. A groutable soil is one that under practical pumping pressure limitations, accepts the injection of

a chemical grout at a sufficient flow rate to make the project economically feasible (Baker, 1982). The initial permeability or the grain size distribution is used to determine the groutability of soil. Soils with fines content of more than 20% (particles smaller than #200 US sieve size) have been reported to be non-groutable (Baker, 1982). For being groutable, the grout should possess sufficiently high fluidity, and the suspended particles, if any, must be of a size that enables them to enter the void spaces in the soil mass (Gulhati and Datta, 2005). Burwell (1958) suggested the following simple equation for the particulate grouting.

$$N = \frac{D_{15}(\text{soil})}{D_{85}(\text{grout})} \quad (2.2)$$

Where N is the groutability (or groutibility ratio) of soil, D_{15} is the diameter of soil passing 15% of total soil mass, D_{85} is the diameter of grout passing 85% of total grout mass. By the equation, a soil is groutable when N is greater than 25, and ungroutable if N is less than 11. However, Burwell (1958) found that another criterion should be satisfied even with the soil has N greater than 25.

$$N = \frac{D_{10}(\text{soil})}{D_{95}(\text{grout})} \quad (2.3)$$

Burwell (1958) suggested that if N is greater than 11, soil can be successfully grouted, but soil cannot be grouted if N is less than 5. Baker (1982) has shown a graphical summary in Figure 2.8 of the range of gradation of soils which could be permeation grouted using suspensions and chemical solutions. He has come up with four major zones: zone groutable with suspensions, groutable with solutions, moderately groutable with solutions, and not groutable at all. According to him, the soil particle size (D_{10}) range is 0.4 mm~0.04 mm for permeation grouting using suspensions is practical.

Other criteria were suggested by Karol, (2003) based on the hydraulic conductivity of the base soils. Table 2.5 describes the approximated relationship between hydraulic conductivity and groutability. Based on this relationship, the suspension grouts require base soils having a hydraulic conductivity of greater than 0.1 cm/sec to become groutable. As the groutability is dependent on hydraulic conductivity and hydraulic conductivity is a function of grain size, so the distribution of grain size becomes a useful indicator of groutability.

Table 2.5 Approximate relationship between hydraulic conductivity and groutability (Karol, 2003)

Permeability (cm/sec)	Groutability
$\leq 10^{-6}$	UngROUTable
10^{-5} to 10^{-6}	Groutable with difficulty by grouts with viscosity < 5 MPa and ungroutable with grouts having viscosity >5 MPa
10^{-3} to 10^{-5}	Groutable with low viscosity grouts but difficult with grouts with a viscosity greater than 10 MPa
10^{-1} to 10^{-3}	Groutable with all commonly used chemical grouts
$\geq 10^{-1}$	Requires suspension grouts or chemical grouts containing a filler material

2.8 Past Researches and Research Gap

According to Zebovitz (1989) suspension grouting is more effective and environmentally friendly than chemical grouting. The use of very fine cement can extend the range of soils that can be injected with suspension grouts to fine sands; microfine cement grouts with a water-to cement ratio as low as two can permeate well-compacted fine sands with D_{15} in the range of 0.15 mm, at least for sands with lower coefficients of uniformity and negligible amounts of fines. The groutability ratio is larger or smaller than 25.

Dano et al. (2004) detected that grouted sand considers an intermediate material between soil and concrete. Based on the triaxial test, the friction angle is unchanged by the injection treatment. The Mohr–Coulomb cohesion varies between 0.1 and 0.5 MPa depending on the cement content of the grout and the relative density of the soil and increases in proportion with the cement-to-water ratio. The secant modulus, measured at an axial strain of 0.1%, is increased by a factor equal at least to 2, referring to the experimental data of this work. This ratio should be greater for a reinforcement ground treatment and can reach 4–5, depending on the mean effective stress. In the very small strain domain, the increase of real elastic properties leads to higher values of improvement ratios. The grouted sands show a contractive–dilatant response along a deviatoric stress path and Poisson’s ratio is between 0.15 and 0.3. The dilation angle of the grouted sand is at least equal to and usually higher than the dilation angle of the uncemented sand at the same dry density.

Schwarz et al. (2006) described that grouted gasoline-contaminated sands have higher permeability generally up to three orders of magnitude and lower strength typically 40% less than grouted non-contaminated sands; the degree of improvement is dependent on the pre and post grouting contaminant residual saturation. A microscopic examination of grouted contaminated sands shows that adhesion of the grout to the soil surface is influenced by the “wetness” of the sand and the residual contaminant layers.

Hicher et al. (2008) adapted a microstructural model developed for non-cohesive granular materials to the mechanical behavior of grouted sand. The introduction of grouting influence was made by introducing an adhesive force at each grain contact, the function of the nature, and concentration of the cement grout. Experimental results demonstrated that the intensity of these adhesive forces decreased during mechanical loading. Numerical simulations of triaxial tests demonstrated the ability of this new version of the model to reproduce the mechanical properties of grouted Fontainebleau sand with various cement grout concentrations.

Dayaker et al. (2012) initiated to determine the increase in the strength of the grouted sand, and the plate load test was conducted in the tank with grouted sand. The efficiency of grouting mainly depends upon the penetration of cement grout through the pores of sand. Then the plate load test determination assessed the increase in strength of the grouted soil mass. The conclusions of this research were drawn from the plate load tests. It had been seen that as the grout ratio decreases the ultimate load increases by 5 to 18 times for 3 days of curing and 15 to 30 times for 7 days of curing in case of a loose state of soil (void ratio 0.6). Whereas in the case of medium dense state (void ratio 0.55) the grout ratio decreases the ultimate load increases by 11 to 20 times for 3 days of curing and 18 to 50 times for 7 days of curing. Also, it had been concluded that as the void ratio and grout ratio decrease the ultimate load increases.

Satyano et al. (2014) tried to establish some empirical formula for grout mix design. The value of s/c (sand/cement) is not more than 2.0 and the grout compressive strength depends on the value of s/c was suggested here. Review of the literature shows that the mechanical behavior of grouted sand is one of the important investigations of calculating strength. Hamidi (2014) had been performed to

investigate the mechanical behavior of cemented sand, in which a series of triaxial compression tests were performed on coarse-grained alluvial soil. He concluded that the strain associated with the peak deviatoric stress decreases as the cementation increase. Also, it was indicated that the maximum rate of dilation and negative pore water pressure occurs after the maximum shear strength is obtained.

Ryan (2015) illustrated that the water-cement ratio decreased the unconfined compressive strength by a factor of ten. It was also found that sand was considered moderately groutable and grouted sand strength decreased as moisture increased. With greater proportions of grout to initial soil and water, an increase in strength was seen. As the initial suction increased from 50 to 1,000,000 kPa, the grouted sand strength increased by 150%.

Several studies have shown that the permeation grouting helps to increase the shearing strength of the soil. Bentonite suspension has the greatest influence on the shear strength performance of grouting materials (Rahman, 2016). A series of tests were carried out to determine the appropriate grout suspension for effective control of seepage through pores of granular soil medium. The optimum range of bentonite flow is 2.5% and the injection time of the grout sample decreases with the increase of grout concentration. The injected grout weight decreased with the increase of grout concentration and direct shear tests on the grouted soil sample give very little indicative results of increasing shear strength by grouting operation. Similar results were also found by Jadid et al. (2015). Other than that they have figured out that Bentonite consumption was found to be the minimum while used a 3% grout. Authors stated that based on the present market price, the estimated probable cost per unit area of sand column (for bentonite consumption only) is 1.85 USD.

Hashimoto et al. (2016) conducted a field test of permeation grouting of ultra-microfine cement to examine whether zones of improved soil of sufficient size can be created economically in sand deposits, which would be expected to contribute to improving ground conditions as a countermeasure against soil liquefaction. The application of permeation grouting of ultra-microfine cement was demonstrated in field tests and proved to be capable of creating columns of improved soil of an affordable size in sand deposits, which would be expected to contribute to improving ground conditions as a countermeasure against soil liquefaction.

Fransson et al. (2016) were investigating the grouting design and selection of grouting materials. The hydraulic aperture was a key parameter when describing grouting behavior and it was used to determine the extent to which the grout entered fractures, that is, the penetrability. The hydraulic aperture also determines the penetration length, and therefore the grout parameters (e.g. yield stress and viscosity) as well as the grouting pressure and time needed to be adopted to the hydraulic aperture. Once these parameters are chosen, a suitable grouting technique could be adopted.

Eyuvan et al. (2017) instigated an idea about the permeation grouting with super fine cement. It was launched that an increase in w/c ratio increased the penetrability of super fine cement suspension into various grading mediums to fine sand specimens. The groutability of super fine cement suspension decreased with the increasing content of fine particles as well as the relative density of the sand specimen. An increase in $W:C$ ratio increased the permeability of grouted sand samples and the permeability of grouted sand specimens reduced with curing time.

Introducing Zeolite (NZ) a new environmental-friendly pozzalonic material by Jafarpour et al. (2019) had been used as a cement additive to stabilize soil, and contains a large amount of SiO_2 and Al_2O_3 compounds, which are combined with $\text{Ca}(\text{OH})_2$ produced in cement hydration process, resulting in the production of C-A-H and C-S-H gels, which improve the microstructure of the cemented sand. From the tri-axial test, it was observed that the peak deviatoric stress (q_{\max}) increased significantly due to cement grouting. The effect of cementitious bonds is considerable up to the yield stress (q_y) and beyond that, the bond's effect dissipates gradually. While uncemented sand specimens show ductile behavior, cement grouting leads to more brittle behavior. Grouting with cement has an incremental effect on the peak friction angle of the grouted specimen. Increasing the zeolite content increases the friction angle values of the grouted sand specimens.

Cement production requires a lot of energy and is also one of the most important sources of carbon dioxide (CO_2) emissions. Consequently, the replacement of part of the cement with an environmentally friendly and cost-effective material, such as zeolite, is of great importance. Kordnaeijetal et al. (2019) involved conducting a series of laboratory tests on loose sand specimens grouted with cementitious

materials (cement and zeolite) to investigate the effect of different parameters on the unconfined compressive strength (UCS) of the grouted sand specimens. It was found that the UCS values of the grouted samples increased with an increase in the percentage of cement replaced with zeolite content (Z) up to 30% (Z_{opt}). Increasing the amount of zeolite from the Z_{opt} led to a reduction in the UCS of the grouted sand samples. The UCS of the grouted sand specimens decreased with an increase in the W:C of the grouting suspensions. This can be explained by the fact that by decreasing the W:C more pores of sand were occupied by cementitious materials; and subsequently, strong bonds between sand particles were formed. By decreasing the W:C in the grout, more pores of sand were occupied by cement and zeolite particles; and subsequently, strong bonds between sand particles were formed. By reducing the W:C in the suspension containing zeolite close to Z_{opt} , more C-S-H and C-A-H gels were synthesized in the grouted samples. By applying active compounds (AC), the simultaneous effect of both Z and W:C on the UCS of the grouted sand specimens were considered. For each grouted sand sample (D_{11} , D_1 , and D_2), the UCS increased with an increase in its corresponding AC. However, the trend is not unique for grouted sands with different grain sizes and it is sand specific. Celik F (2019) investigated the features of cement-based permeation grout, based on some important grout parameters such as rheological properties (yield stress and viscosity), coefficient of permeability to grout, and the inject ability of cement grout which govern the performance of cement-based permeation grouting in porous media.

Eyubhan (2021) was investigated the effects of different curing temperatures and curing conditions on the unconfined compressive strength of microfine cement injected into sand samples. In this experiment, the unconfined compressive strengths of the grouted sand samples were increased with time and the rate of increase started to slow down after a certain value. Due to the increase of temperature, the grouted sand samples were gained faster strength. The unconfined compressive strength values of the injected samples increased with increasing temperature. The unconfined compressive strength of the sand samples that were grouted and kept in the air-dried environment was higher than the unconfined compressive strength of the sand samples that were injected and kept in the wet-curing conditions.

Zhu et al. (2021) were discussed the effects of the grout flow velocity and the water/cement ratio of the grout on the diffusion mechanism in their research paper. Experimental results showed that there were dramatic variations in rheological parameters and porosity along the diffusion distance.

Recent years, Permeation grouting is very popular among the building contractors as a cheap, simple and untrusive form of ground improvement was stated by Lee (2021). According to him, this grouting system is effective for underpinning structure, hydraulic structure, beneath retaining wall, embankment, and for the containmnet for contaminated ground. In sydney, many projects like Alexgnder post office, Umina woolworths etc, benefisary by using of permeation grouting. Researcher concluded that, permeation grouting can limit despersion of contaminated ground water. It is used to limit the consolidation of soil due to vibration, and stabilize ground for excavation. When good quality permeation can be performed, CPT test has been used to indentify the ground improvement.

Several case studies have shown that grouting especially suspension grouting helps to control the seepage in the practical field. The application of cement-based permeation grouting is a trial and error method in the current practice. Since studying previous research works, each researcher has performed this work in the laboratory not in the practical field. Different researchers developed different types of devices but all of them were struggling to make homogeneous samples. After getting the homogeneous sample, many researchers gave attention to the Rheological properties (yield stress and viscosity) of the grouted sample. Most of the research works are designed in a common laboratory test which is given in Table 2.6. From the review of different studies and discussion of research work, it has been concluded that huge patronage is needed for the permeation grouting. In this study, a general methodology has been applied to alluvial sandy soil to help gain real field experience and then perform the laboratory test to get information about the strength and bearing capacities.

Table 2.6 Comparison of different research works with present study

Author	Type of grouting	Soil Type	Device developed	Index properties	Permeability test	Direct Shear test	Unconfined compression test	Tri axial Test	Scanning Electron Microscope	Grout cost	Improvement
Zebovit et al. (1989)	Permeation grouting	D ₁₅ = 0.15mm	×	√	√	×	√	×	×	×	Very fine cement grouts with a water-to-cement ratio as low as two can permeate several feet into well-compacted fine sands with D ₁₅ in the range of 0.15 mm.
Dano et al. (2004)	Permeation grouting	FS (D ₅₀ = 2 × 10 ⁻⁴ mm), SRS (D ₅₀ =5.3 × 10 ⁻⁴ mm), ADM (D ₅₀ =4.1 × 10 ⁻⁴ mm), ADC (D ₅₀ =0.0013mm), DS (D ₅₀ = 0.0024 mm)	√	√	√	×	√	×	×	×	The Poisson's ratio, for uncemented and grouted sands, is between 0.15 and 0.30, the friction angle was hardly changed by permeation grouting.

Table 2.6 Comparison of different research works with present study

Author	Type of grouting	Soil Type	Device developed	Index properties	Permeability test	Direct Shear test	Unconfined compression test	Tri axial Test	Scanning Electron Microscope	Grout cost	Improvement
Schwarz et al. (2006)	Permeation grouting	Ottawa 20-30 sand (D_{50} =0.71 mm), Ottawa F-62 (D_{50} =0.12 mm),	√	√	√	×	√	×	√	×	The leaching tests and gas chromatography ; results were typically 50% greater in cases where gasoline saturated initially dry sand.
Keong (2005)	Permeation Grouting	Coarse sand 2 mm to 6 mm	√	√	√	×	×	√	×	×	Permeability coefficient taking into consideration of the injection pressure through the nonlinear relationship between hydraulic gradient and viscosity established.

Table 2.6 Comparison of different research works with present study

Author	Type of grouting	Soil Type	Device developed	Index properties	Permeability test	Direct Shear test	Unconfined compression test	Tri axial Test	Scanning Electron Microscope	Grout cost	Improvement
Hicher et al. (2008)	Cement grouting	Fontaine bleau sand (0.1mm)	√	√	√	×	√	√	×	×	The intensity of adhesive forces is a function of nature and the amount of grout present inside the material can be reduced due to a damage mechanism at the grain contact during loading.
Dayakar et al. (2012)	Permeation grouting	D ₆₀ = 0.9mm D ₃₀ = 0.6mm and D ₁₀ = 0.47	√	√	√	×	×	×	×	×	The increases load-carrying capacity of the sandy soil
Satyarn et al. (2014)	Cement grouting	Not mentioned	×	×	×	×	×	×	×	×	An empirical formula was developed.

Table 2.6 Comparison of different research works with present study

Author	Type of grouting	Soil Type	Device developed	Index properties	Permeability test	Direct Shear test	Unconfined compression test	Tri axial Test	Scanning Electron Microscope	Grout cost	Improvement
Bono et al. (2014)	Cemented sand	D ₁₀ = 4 mm E ₁₀ =0.75	×	×	×	×	×	√	×	×	In the cemented materials, an increase in the degree of crushing was observed with increasing cement content and failure from ductility to brittle.
Ryan (2015)	Ultrafine cement grout	D ₁₀ = 0.18mm to 0.28mm	√	√	√	×	×	×	×	×	Increased initial moisture decreased the grouted soil strength, with decreases in strength exceeding 50 percent was studied.

Table 2.6 Comparison of different research works with present study

Author	Type of grouting	Soil Type	Device developed	Index properties	Permeability test	Direct Shear test	Unconfined compression test	Tri axial Test	Scanning Electron Microscope	Grout cost	Improvement
Hamidi et al. (2015)	Permeation grouting	Sand, D ₁₀ = 0.15, Gravel, D ₁₀ = 9.82, Sand+ gravel, D ₁₀ = 0.17mm	×	√	√	×	√	√	×	×	Cement content, cement type, relative density, and grain size distribution, can influence the mechanical behaviors of cemented soils. well graded gravely sands indicated more dilation or negative pore pressure in poorly graded samples
Jadid et al. (2015)	Permeation grouting	River sand F.M. 1.02	√	√	√	×	×	×	×	√	Grout concentration was proposed considering cost and other factors like penetration distance and injection time.

Table 2.6 Comparison of different research works with present study

Author	Type of grouting	Soil Type	Device developed	Index properties	Permeability test	Direct Shear test	Unconfined compression test	Tri axial Test	Scanning Electron Microscope	Grout cost	Improvement
Kainath et al. (2015)	Permeation Grouting	Sand, $C_c= 0.9$, $C_u= 1.72$	×	√	×	×	√	√	×	×	Higher cementation increases the stiffness and strength of grouted soil. The cohesion and the angle of internal friction are increasing with higher cement content. Grouted soil with lower cement content behaves like soil, while higher cement content behaves more like concrete.

Table 2.6 Comparison of different research works with present study

Author	Type of grouting	Soil Type	Device developed	Index properties	Permeability test	Direct Shear test	Unconfined compression test	Tri axial Test	Scanning Electron Microscope	Grout cost	Improvement
Hashimoto et al. (2016)	Permeation grouting	Field condition SPT N values less than 5	×	×	×	×	×	×	×	×	Capable of creating columns of improved soil of an affordable size in sand deposits, which helps improve ground conditions as a countermeasure against soil liquefaction.
Rahman (2016)	Permeation grouting	Sand F.M. 1.02	√	√	√	√	×	×	×	√	Injection time to stop grout flow, injected grout weight, and penetration distance for various bentonite concentrations are measured.

Table 2.6 Comparison of different research works with present study

Author	Type of grouting	Soil Type	Device developed	Index properties	Permeability test	Direct Shear test	Unconfined compression test	Tri axial Test	Scanning Electron Microscope	Grout cost	Improvement
Eyuvan et al. (2017)	Permeation grouting	Sp. Gravity = 2.61	√	√	√	×	×	×	√	×	The coefficient of permeability increased as the W:C increased but decreased as the relative density.
Jin et al. (2018)	Chemical Grout	D ₁₁ = 0.21 mm	√	√	√	×	√	√	√	×	Bearing capacity, effect of frictional angle, effect of the cohesion increased,
Jafarpour et al. (2019)	Permeation grouting	Uniform silica sand (D ₁₀ = 0.29 mm)	×	√	√	×	×	√	√	×	The effect of cohesion on the shear strength reduced gradually while the frictional angle increased.

Table 2.6 Comparison of different research works with present study

Author	Type of grouting	Soil Type	Device developed	Index properties	Permeability test	Direct Shear test	Unconfined compression test	Tri axial Test	Scanning Electron Microscope	Grout cost	Improvement
Kordnaeij et al. (2019)	Permeation grouting	Uniform sand (D ₅₀ = 2.65 mm)	√	√	√	×	√	×	√	×	The results indicate when Z is increased from zero zeolites (Z0), the UCS initially increases. Then, after reaching an optimal amount (Z30), it decreases.
Eyubhan (2021)	Permeation grouting	Fine and medium sand	√	√	×	×	√	×	×	×	Curing temperature and condition affect the strength of grouted samples.

Table 2.6 Comparison of different research works with present study

Author	Type of grouting	Soil Type	Device developed	Index properties	Permeability test	Direct Shear test	Unconfined compression test	Tri axial Test	Scanning Electron Microscope	Grout cost	Improvement
Zhu et al. (2021)	Permeation grouting	Medium sand	√	√	×	×	×	×	×	×	The smaller water cement ratio, the diffusion distance is 1.2m

According to the Table 2.7, this research paper has been worked out in this manner:

Table 2.7 List of tests conducted in this study

Type of grouting	Soil Type	Grout Pushing method	Index Properties	Permeability test	Direct Shear test	Unconfined Compression test	Triaxial test	Scanning Electron Microscope	Energy Dispersive Spectroscopy
Permeation	Alluvial sandy soil	Injection	√	√	√	√	√	√	√

2.9 Summary

All the knowledge and topics including substantive findings of past research related to this research, as well as theoretical and methodological description have been discussed in this chapter which can be summarized as follows: Different types of grouting, their methodology, and techniques are briefly discussed here. Along with this, it proved that permeation grouting with low pressure is one of the oldest and safe methods to improve the subsoil strength of an existing embankment or any hydraulic structures without disturbing the existing soil condition. In this research, sandy soil especially alluvial soil is the subject of discussion. A review of the literature showed that most research works only focus on one or two laboratory tests to evaluate the mechanical properties of the sample soil. So, rarely does any study completely comprehend all the mechanical aspects of grouted alluvial sand. Therefore, the present research is to investigate the mechanical behavior of an alluvial sandy soil treated by permeation grouting through various conventional laboratory test methods.

Chapter 3

EXPERIMENTAL PROGRAM

3.1 Introduction

This chapter discussed in detail the materials used, the layout and design of the experimental setup and the testing procedures to be followed for grouting operations for horizontal and vertical access. Materials collection, physical properties, and chemical composition of the collected materials are also briefly described here. The permeation grouting tests with different concentrations of grout suspension have been performed through the sand sample. To comprehend the strength of the samples, unconfined compression tests and triaxial tests were performed on the grouted samples. To investigate the microstructure of grouted samples Scanning Electron Microscope test was performed.

3.2 Materials

The selection of proper grouting materials depends upon the type of granular medium and the purpose of grouting. In this research cement was used as grouting material and sand was used as granular medium. The type of grout material involved in this study belongs to the suspension type of grout according to the definition as discussed in Section 2.2 of Chapter 2.

3.2.1 Sand

Selected sand sample was used as a grouting medium in this study. The sand sample was collected from the riverbank of Turag (Table 3.1). The grain size distribution of the sand were performed as per ASTM (D-422) which is shown in Figure 3.1 and the properties of sand are presented in Table 3.2.

Table 3.1 Location of the collected sand sample

Sand Type	Location	Latitude	Longitude
Dredged sand	Mirpur Beribadh, Part of Turag river	23.854	90.342

The sand used was river dredged sand. Index properties of the sand samples were obtained from laboratory tests. The specific gravity of the soil is 2.89. From the grain size distribution curve, it has been found that the coefficient of uniformity $C_u=1.375$ and coefficient of curvature $C_z = 0.207$. Fineness modulus of the soil found was 1.12704.

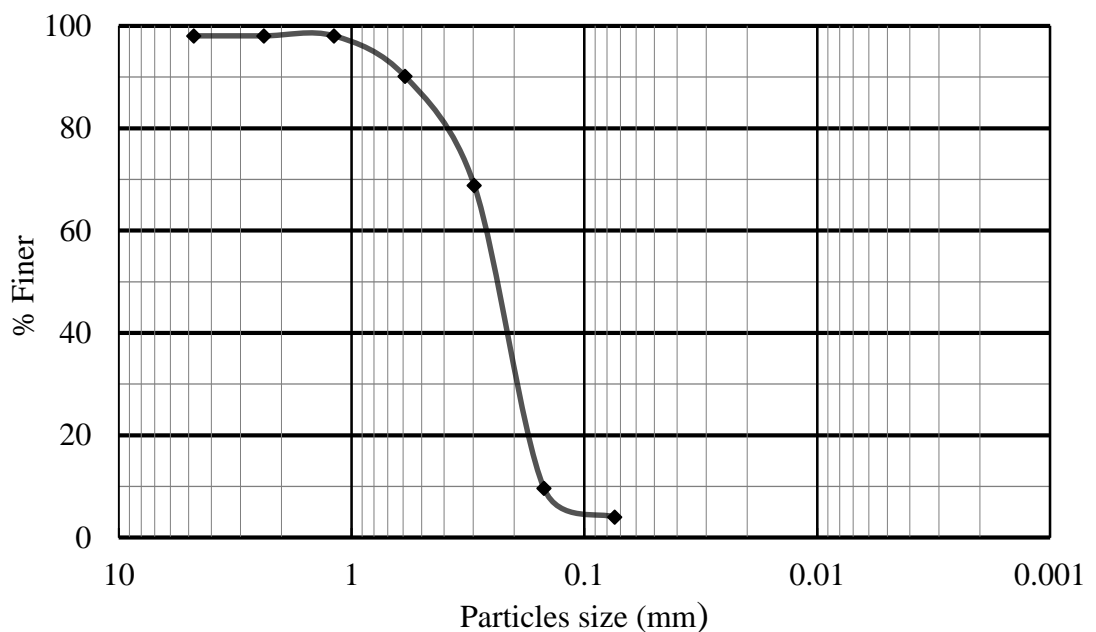


Figure 3.1: Particles size distribution curve of the sand

3.2.2 Cement

Portland Composite Cement, type CEM II/B was added with water to make grout slurry. Physical properties of cement are presented in Table 3.3 and chemical properties are presented in Table 3.4.

There are two types of materials are used for grouting. One is cementitious materials, different types of ultrafine cement are included in this types. Other is non-cementitious materials. In this group, chemical solutions such as sodium silicate, polymers, polyurethane, etc, resinous materials such as epoxies, urethanes, phenolic

foams, polyesters, etc., and miscellaneous materials such as bitumen, asphalt emulsion are included. Among all these materials Portland Composite Cement, type CEM II/B was selected for its availability and cost-effectiveness.

Table 3.2 Properties of sand

Parameter	Unit	Value
Bulk Specific Gravity, G_b	-	2.89
SSD Specific Gravity	-	2.9
Apparent Specific Gravity	-	2.91
Uniformity Co-efficient, C_u	-	1.375
Co-efficient of Gradation, C_c	-	0.061
Effective Size, D_{10}	mm	0.424
Fineness Modulus, F.M.	-	1.2
Void Ratio, e	-	0.85
Dry Unit weight, γ_d	g/cm^3	1.41
Permeability	cm/sec	8.89×10^{-3}

Table 3.3 Physical Properties of the Cement

Property	Unit	Value
Standard Consistency (ASTM C187)	%	30.00
Initial Setting Time (ASTM C191)	min	235.00
Final Setting Time (ASTM C191)	min	340.00
Fineness (ASTM C204)	m^2/kg	468.00
Soundness (By Autoclave method)	%	0.24
Compressive Strength (ASTM C109)		
7 days	MPa	28.25
28days	MPa	41.92

Table 3.4 Chemical Properties of the Cement

Property	Value (%)
C ₃ S	55.0
C ₂ S	20.0
C ₃ A	<6.0
C ₄ AF	8.0
MgO	2.9
SO ₃	2.5
Ignition loss	0.8
Free CaO	1.0

Table 3.5 Test plan for finding the properties of the grouted and non-grouted sand

Type of Test	Name of Test	ASTM	Test Condition
Index Properties	Particles size distribution	ASTM D422-63	-
	Specific gravity	ASTM D854-92	
Permeability	Permeability of soil by constant head permeameter	ASTM D2434-68	
Compression Test	Direct Shear test	ASTM D3080-98	Undrained
	Unconfined Compression test	ASTM D7012-14	Undrained
	Triaxial Test	ASTM D9767-95	Consolidated undrained
Microstructure analysis	Scanning Electron Microscope (SEM)	ASTM C1723-16	-
	Energy-dispersive Detector (EDS)		

3.3 Laboratory Test Program

The permeability of soil can be reduced by the application of grout. If the grout is applied for a certain period, the grouting medium will be impervious gradually i.e. the pore spaces of the medium will be clogged by grouting materials. In this research work, a testing program was conducted to investigate the horizontal and vertical infiltration of cement suspension into a granular sandy soil medium. Tests were performed with a specified soil specimen with different grouting concentrations. Moreover, the strength characteristics of the grouted soil sample were examined and the microstructure was investigated. Accordingly, the test program of this research work consists of two parts. At first, ready the test sample by infiltration of grout material through the granular medium in suspension form. Secondly, tests such as Permeability (constant head), Direct Shear test, Unconfined Compression test, Triaxial test and Scanning Electron Microscope were done to determine the strength and microstructure of the grouted sample.

3.3.1 Index Properties of Sand Used for Grouting

Index properties like specific gravity, permeability, dry density and fineness modulus will be discuss here.

Specific gravity, G_s

This test is conducted according to the ASTM D854. Water temperature was noted since water density varies with temperature. The specific gravity of the soil is calculated by Equation 3.1.

$$G_s = \frac{G_T W_s}{W_s - W_1 + W_2} \quad (3.1)$$

Where, W_1 = weight of pycnometer + water + soil,

W_2 = weight of pycnometer + water,

G_T = G_s at water temperature $T^\circ\text{C}$.

Density index, I_d

The ratio expressed as percentage, of the difference between any given dry density and the minimum dry density of a cohesionless soil to the difference between its maximum and minimum dry densities. The equation is:

$$I_d = \frac{\gamma_d - \gamma_{dmin}}{\gamma_{dmax} - \gamma_{dmin}} \times 100. \quad (3.2)$$

Fineness modulus, F.M.

To define the characteristics of *soils*, grain size analysis was done using #4, #8, #16, #30, #50, #100 and #200 sieves on samples to determine the Fineness Modulus (F.M.) and the percentage of the fines. The F.M. was determined using Equation is 3.4.

$$F.M. = \frac{\% \text{ of the sample of aggregate retained on each series of sieves}}{100}. \quad (3.3)$$

3.3.2 Physical and Strength Properties of Grouted Samples

To determine physical properties following equations are used:

Moisture content

It is an indicator of the amount of water present in soil.

$$W(\%) = \frac{M_w}{M_s} \times 100 \quad (3.4)$$

Here, M_w = Mass of water

M_s = Mass of solids.

Void ratio

The ratio of the volume of voids to the volume occupied by soil.

$$e = \frac{V_v}{V_s} \quad (3.5)$$

Here, V_v = Volume of voids.

V_s = Volume of solids.

The data of physical properties of grouted sand are given in Table 4.4.

Now for determining strength properties, graph 4.3 to 4.11 are used to determine highest pick points which is called UCS, q (kPa) and cohesion is the half of the axial stress.

Young's modulus

It is the slope of the linear part of the stress-strain curve for a material under tension or compression. For determining graph 4.3 to 4.11 are used.

3.3.3 Permeability Test

Two general types of permeability test methods are routinely performed in the laboratory: (a) constant head test and (b) falling head test method. The constant head test method is used for permeable soils ($k > 10^{-4}$ cm/s) and the falling head test is mainly used for less permeable soils ($k < 10^{-4}$ cm/s).

Constant Head Test: The constant head method is suggested for soils with a coefficient of permeability not less than 10^{-3} cm/sec (Terzaghi and Peck, 1940). For very fine soils, with low permeability values the constant head test may be considered unsatisfactory because of the length of time needed for as sufficient quantity of water to flow through the sample and the possibility of evaporation losses of this water (Davidson, 2002). ASTM D 2434 is the standard test method for determining permeability of granular soils using the constant head. The purpose of this test is to determine the permeability (hydraulic conductivity) of sandy soil by the constant head test method. A schematic diagram of the constant head permeability apparatus is shown in Figure 3.2 which consists of a vertical cylindrical tube containing the soil specimen. The sample length (L) and cross-sectional area (A) is subjected to a constant head (H) of water flow. Under steady-state and fully saturated conditions, the volume of water (Q) collected in a given time (t) is measured. The value of the coefficient of permeability (k) can then be calculated.

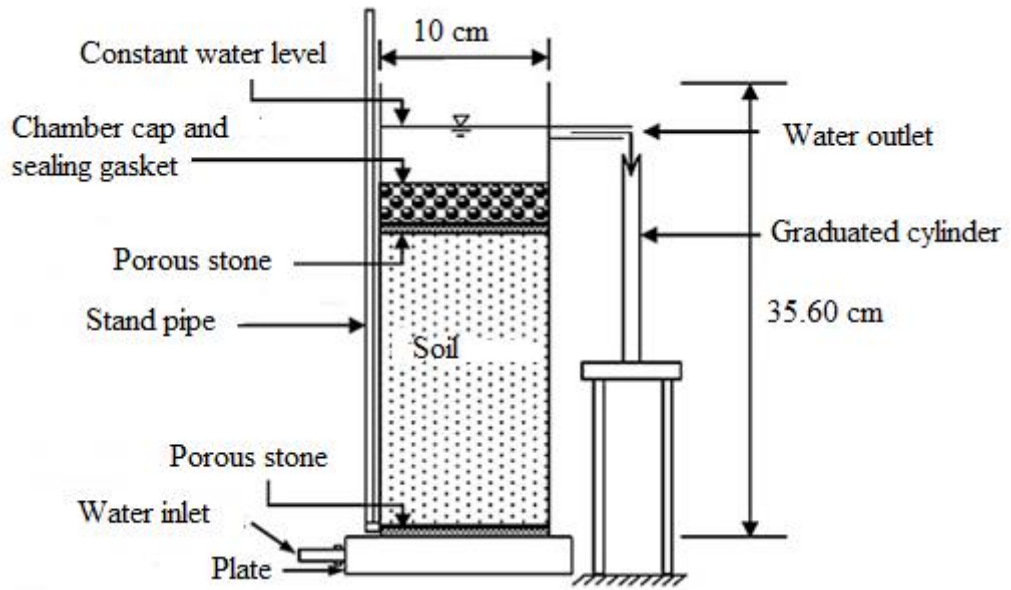


Figure 3.2: Schematic view of the laboratory setup for the constant head test method

Here constant head permeability method is used because of cohesionless soil. The flow is very low at the beginning, gradually increases, and then stands constant. Permeability of sample sand is calculated in Equation 3.6

$$k = \frac{2.3 \times a \times L \times (\log_{10} h_1 / h_2)}{A \times t} \quad (3.6)$$

Here, t= time (sec)

a = area of stand pipe (cm²)

A= area of specimen (cm²)

L= length of the specimen (cm)

h_1 / h_2 = constant head causing flow (cm).

k = coefficient of permeability at 27⁰ cm/sec

3.3.2 Direct Shear Test

Unconfined undrained (UU) direct shear test was performed on the ungrouted sandy soil. In the laboratory, a direct shear device will be used to determine the shear strength of a cohesionless soil (i.e. angle of internal friction, ϕ). From the plot of the shear stress versus the horizontal displacement, the maximum shear stress is obtained for a specific vertical confining stress. After the experiment is run several times for

various vertical-confining stresses, a plot of the maximum shear stresses versus the vertical (normal) confining stresses for each of the tests is produced. From the plot a straight-line approximation of the Mohr-Coulomb failure envelope curve can be drawn (Figure 3.3), and for cohesionless soils ($c = 0$), the shear strength can be computed from the equation:

$$\tau = \delta \tan \phi \quad (3.5)$$

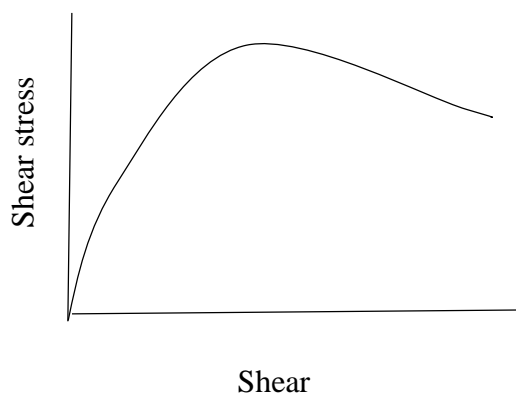
Here τ = Shear strength

δ = Normal stress

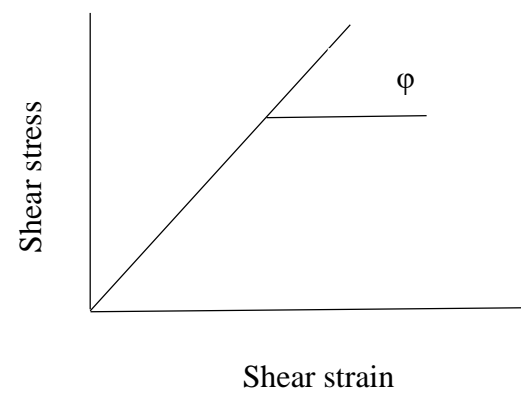
ϕ = Angle of internal friction



(a)



(b)



(c)

Figure 3.3: (a) Direct shear test device, (b) stress vs. displacement pattern (loose sand), (c) stress strain relationship of sand

3.3.3 Unconfined Compression Test

The primary purpose of this test is to determine the unconfined compressive strength, which is then used to calculate the unconsolidated undrained shear strength of the clay under unconfined conditions. According to the ASTM standard, the unconfined compressive strength (q_u) is defined as the compressive stress at which an unconfined cylindrical specimen of soil will fail in a simple compression test. Besides, in this test method, the unconfined compressive strength is taken as the maximum load attained per unit area, or the load per unit area at 15% axial strain, whichever occurs first during the performance of a test. After grouting sandy soil with cement, the confining stresses in the triaxial compressive tests may destroy the cementation or bonding between weakly cemented soil particles (Saxena et al., 1978). Under such triaxial testing conditions, the cement is not as effective as observed under unconfined conditions (Maher et al., 1993). The unconfined compressive strength (UCS) obtained from unconfined compression tests is often used as an index for assessing the quality of the soil improvement due to stabilization. An unconfined compression test can determine the strength of cemented soils without the need to apply the confining stress while maintaining the soil cementation or bonding before shearing. An increase in UCS of more than 345 kPa must be achieved for a treatment to be considered effective (ASTM D 4609, 2008). Figure 3.4 showed the schematic view of the device.

For soils, the undrained shear strength (s_u) is necessary for the determination of the bearing capacity of foundations, dams, etc. The undrained shear strength (s_u) of grouted sample is commonly determined from an unconfined compression test. The undrained shear strength (s_u) of the cohesive sample is equal to one-half the unconfined compressive strength (q_u) when the soil is under the $f = 0$ condition ($\phi =$ the angle of internal friction).

The uniaxial compressive strength (UCS) is the maximum axial compressive stress that a right-cylindrical sample of material can withstand before failing. It is also known as the unconfined compressive strength of a material because confining stress is set to zero. This test is suitable for clay because the dry sand and crumbly clay fall apart without any lateral confinement (Fig 3.4). In this experiment, dry sand is used when it gets solidified by grouting slurry and behaves like clay.

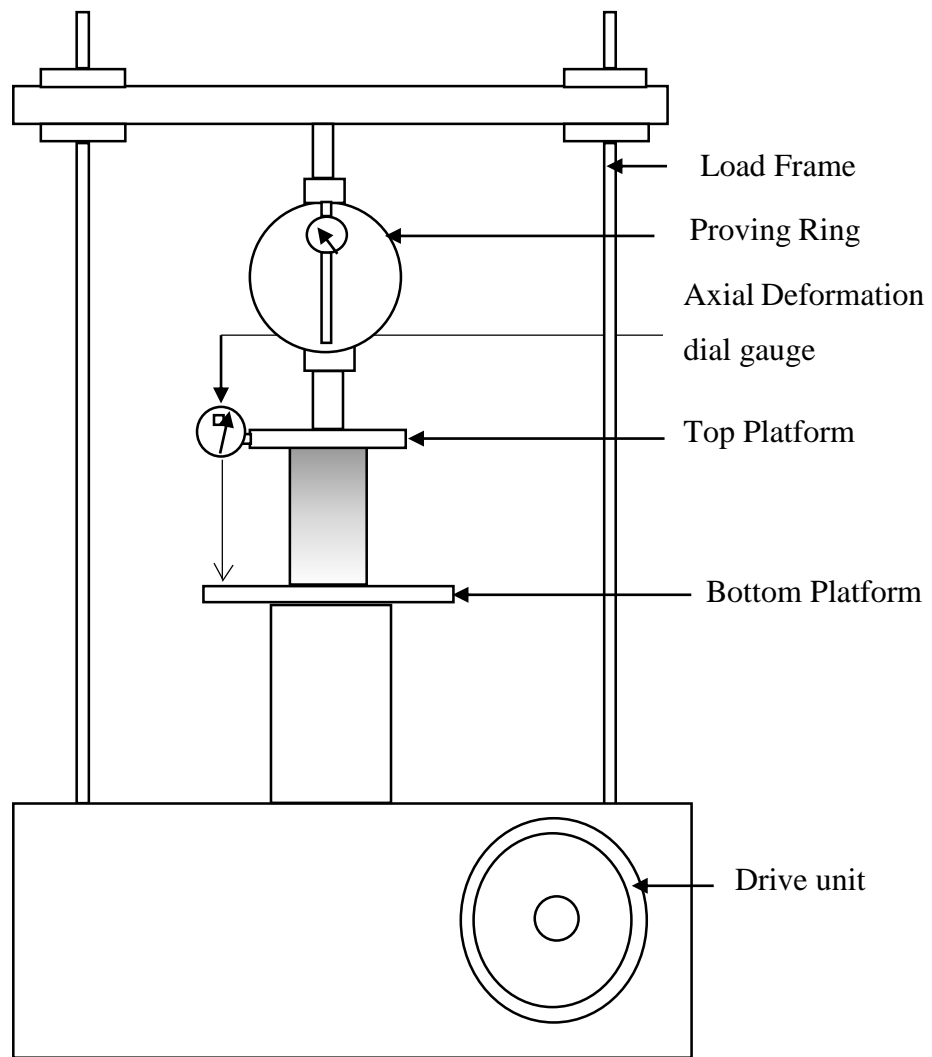


Figure 3.4: Schematic view of the laboratory setup for the unconfined compression test

3.3.4 Consolidated Undrained Triaxial Test

The automated triaxial test setup was used to conduct the consolidated undrained (CU) tests. Volume change was measured through drain lines connected to the porous stones at the top and bottom of the sample. The measured volume change was used to determine the radial strain of the sample which indicates the volumetric change of sample. The specimens were saturated with water with a pressure of 20 kPa. To fasten the saturation of sample and ensuring 100% saturation, CO₂ was incorporated in the saturation process at initial stage as a back pressure. Throughout the tests, the total confining pressure was kept constant whereas the vertical stress was 47 kPa increased by increasing the vertical compressional load. This is strain controlled test and the

strain rate was 0.03040mm/min. Compressive strength test was performed with three effective confining stress $\sigma_3' = 50, 100, \text{ and } 200 \text{ kPa}$. The axial strain, axial stress and pore water pressure were measured during the shearing process. The whole triaxial process was grouped in three phases that is a) Saturation stage, b) Consolidation stage, and c) Shearing stage. In saturation phase, CO_2 is introduced to accelerate the saturation phase by decreasing the pore. When the Skempton's pore pressure value B value was achieved 0.97, the sample was taken as fully saturated. After the saturation stage, samples were consolidated. Consolidation stage was taken to be completed when no volume change in cell pressure reading was showing. For test samples, they were consolidated approximately 24 hours. After consolidation, samples were prepared for shear test. Loads are applied on the sample vertically in a strain controlled situation. In deflection meter when desired deflection is shown, in load display panel, the load was recorded. From that display panel, load deflection, pore pressure values were recorded. This test is used to determine the soil properties of a clay samples. Typically, Triaxial Testing is used to solve stability problems by determining the shear strength and stiffness of soil when retaining reservoirs of water. The soil is set to be consolidated by allowing the drainage through the sample. The volume of the soil reduces without the air replacement. This consolidation is done under the confining pressure. In case of undrained conditions, the pore water is not allowed to drain out of soil. Compressive strength, failure strain, and ultimate failure point were determined from the stress-strain relationships. From the stress strain diagram the deviatoric stress at failure was obtained. This test has been chosen from other triaxial test to get clear picture of what happens when the embankment is fully and partially saturated. During the test, simultaneous measurements of deviatoric stress, $\Delta\sigma_d$ and Δu_d are made.

Unlike the consolidated- drained test, the total and effective principal stresses are not the same in the consolidated undrained test (Figure 3.5), because the pore water pressure at failure is measured in this test, the principal stresses may be analyzed as follows:

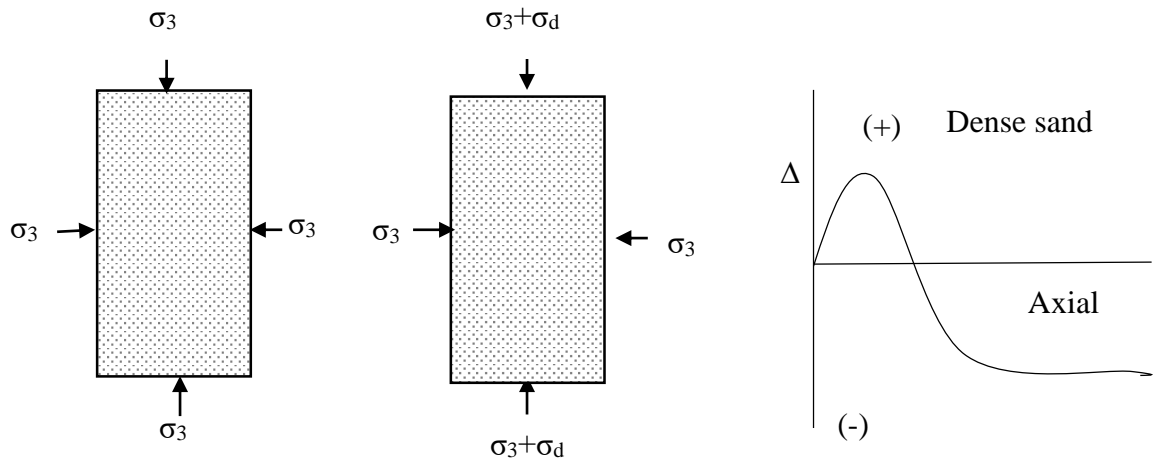


Figure 3.5: (a) Specimen under chamber confining pressure, (b) deviator stress application, (c) variation of pore water pressure with axial strain for dense sand

Major principal stress at failure (total): $\sigma_3 + (\Delta\sigma_d)_f = \sigma_1$

Major principal stress at failure (effective): $\sigma_1 - (\Delta u_d)_f = \sigma'_1$

Minor principal Stress at failure (total): σ_3

Minor principal stresses at failure (effective): $\sigma_3 - (\Delta u_d)_f = \sigma'_3$

Where $(\Delta u_d)_f$ = pore water pressure at failure. The preceding derivations show that

$$\sigma_1 - \sigma_3 = \sigma'_1 - \sigma'_3.$$

Consolidated undrained tests can be conducted on such soils with pore pressure measurements to obtain the drained shear strength parameters. Because drainage is not allowed in these tests during the application of deviator stress, they can be performed quickly.

Skempton's pore water pressure parameter $\bar{A} = \Delta u_d / \Delta\sigma_d$

And at failure, the parameter $\bar{A} = \bar{A}_f = (\Delta u_d)_f / (\Delta\sigma_d)_f$

The general range of \bar{A}_f in most clay soil is as follows:

Normally consolidated clay: 0.50 to 1 and overconsolidated clays: -0.5 to 0.

Figure 3.6 present the laboratory setup of triaxial test.



(a)



(b)



(c)



(d)

Figure 3.6: (a) Triaxial testing Machine, (b) Grouted sample after 7 days of curing, (c) grouted sample at failure stage (CU condition), (d) grouted sample after triaxial test

3.4 Flow Diagram of this Experiment

The steps of this experiment are tried to explain through the flow diagram which is presented in Figure 3.7.

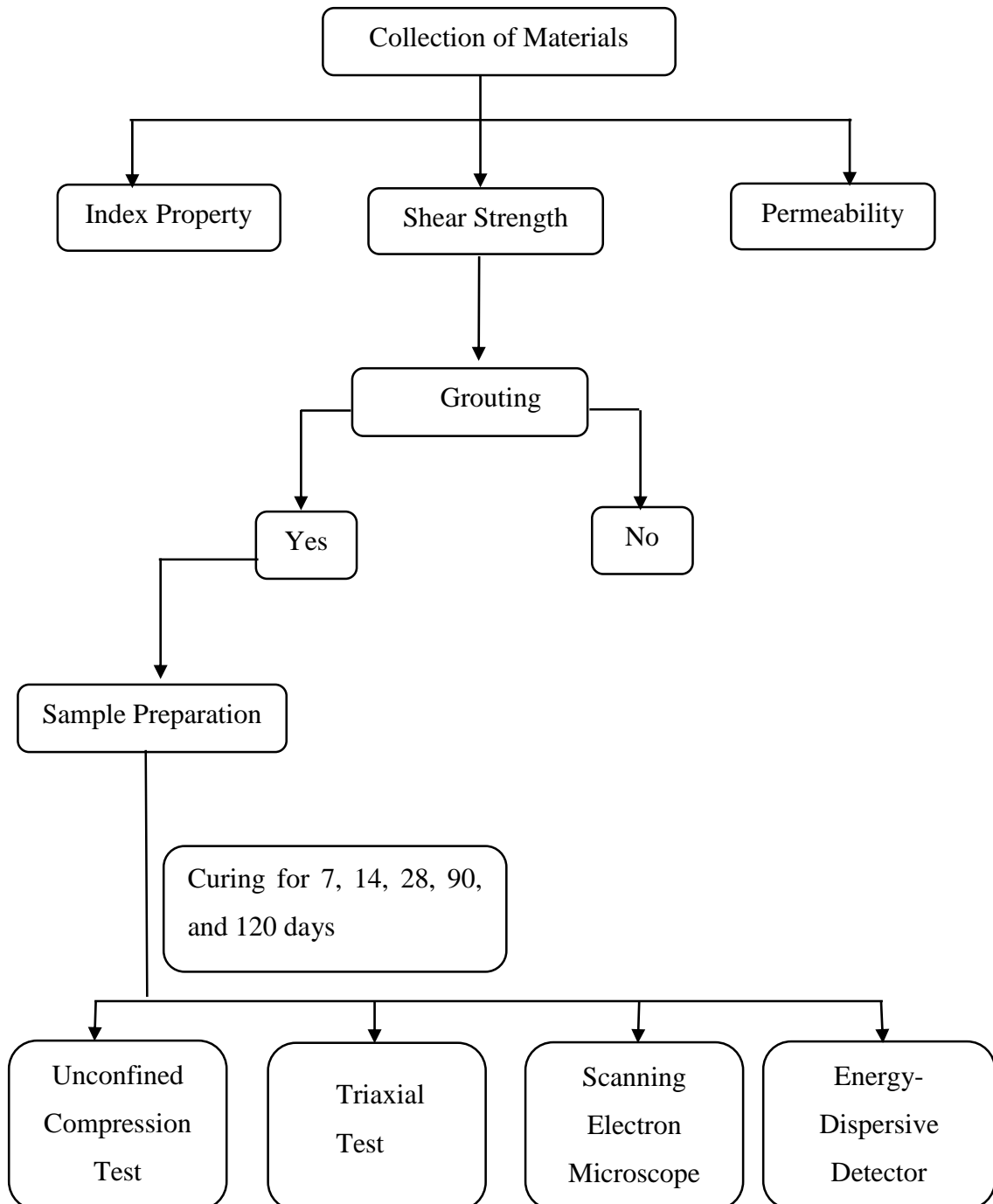


Figure 3.7: Flow diagram of the experimental program

3.5 Experimental Design

Making homogeneous grouted samples is a trial and error method. In this study, four experiments were performed to create a homogeneous grouted sample. Attempts have been made to create sample sizes from (300mm × 300mm) to (300mm × 100mm) as described in trial 1 to trial 3. Later, according to Lombardi (1985), to develop cohesion, it was intended to limit the travel of the grout. By creating shapes 40 mm in diameter and 78 mm in height, it was possible to limit the travel of grout and created the integrated pattern that is presented in Trial 4.

Trial 1: One of the experimental setups used in this research work consisted of setting up the permeameter and mixing the soil mixture. A schematic line diagram of the modified permeability testing setup is presented in Figure 3.8. A 1.5m long

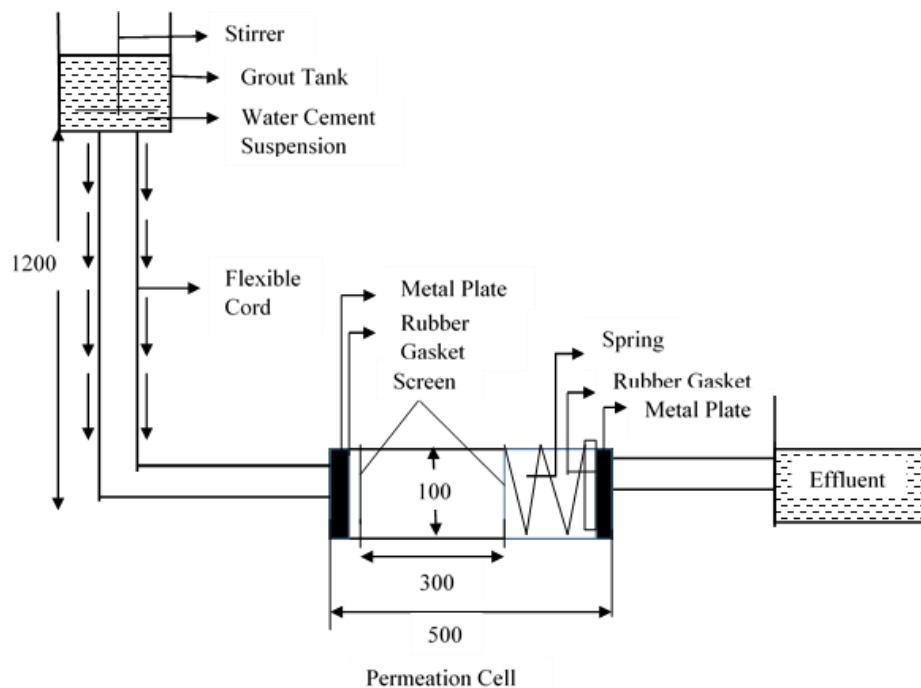


Figure 3.8: Arrangement for preparing horizontal grouting sample (all dimensions are in mm)

Vertical sand was provided to clamp the grout tank. Grout suspension was kept in the grout tank. The height of the tank can be changed to apply different pressures to the soil specimen. A stirrer was attached to the tank to do the stirring operation manually to keep the grout at suspension condition during the whole testing operation. A transparent flexible cord was connected from the bottom of the grout tank to the permeation cell. The permeation cell was made of a transparent cylinder and had a

100 mm outside diameter and 95 mm inside diameter. The length of the permeation cell was 500 mm and the length of the sand column within the permeation cell was 300 mm. Two rubber gaskets of 100 mm outside diameter were placed at the two side joints of the permeation cell with the metal plate to prevent water leakage. Moreover, two screens (aperture size 0.1 mm) were placed at the left and right sides of the sand column to help in providing uniform distribution of suspension throughout cross-section of the sand column and prevent sand washing into the tubes. Each of the screens was supported by a metal plate having many circular slits at the outlet end and above the top screen, a 150 mm long and 90 mm diameter. Spring was placed to keep sand column in stable condition during the testing operation. A graduated plastic or glass beaker was provided at the outlet to collect the effluents during testing operation. The irregular shaped sample in Figure 3.9 have been retrieved from the preparation after 28 days.



Figure 3.9: Irregular shaped sample from trial 1

Trial 2: For preparing permeation grouted samples vertically, a steel cylinder (diameter: 250mm, height: 300mm) will be used. The sand to be grouted will be filled in the cylinders at the loosest state and four PVC pipes (diameter 20mm) will be set up for the grouting process. Then four rubber pipes (diameter 10mm) will be inserted of the PVC pipe to maintain the pressure and avoid pressure loss. After the installation of this pipe these pipes in the sand-filled cylinder, grout slurry will be injected into the sand through permeameter. Figure 3.10 showed the set up of trial 2.

The irregular shaped sample (Figure 3.11) has been extracted from trial 2 after 28 days.

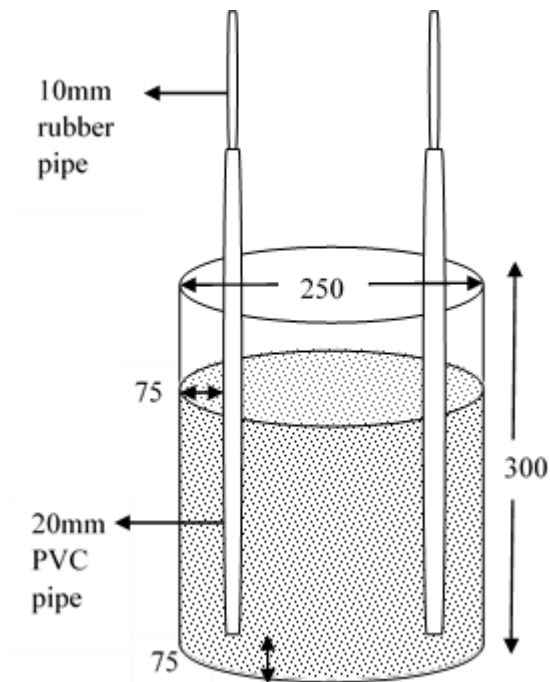


Figure 3.10: Arrangement for preparing vertical grouting sample (all dimensions are in mm)



Figure 3.11: Irregular shaped sample from trial 2

Trial 3: For preparing permeation grouted samples, a glass tank of the size of 300mm× 300mm × 300mm is surrounded with wooden sheet. The sand to be grouted is filled in the tank at the loosest state and pipe setup for grouting process. PVC Pipes

of 20 mm diameter are used for the grouting, with perforations in surface of the pipe with 3mm diameter which are 36 number for each pipe. The bottom of the PVC pipe is plugged so as to disperse the grout circumferentially and make the grouting more effective. At this stage rubber pipes of 10mm diameter will be inserted at the top of the PVC pipe to maintain the pressure and avoid the pressure loss and the grouting slurry are injected with permeameter (Figure 3.12). Irregular shaped grouted sample obtained from trial 3 is presented in Figure 3.13.

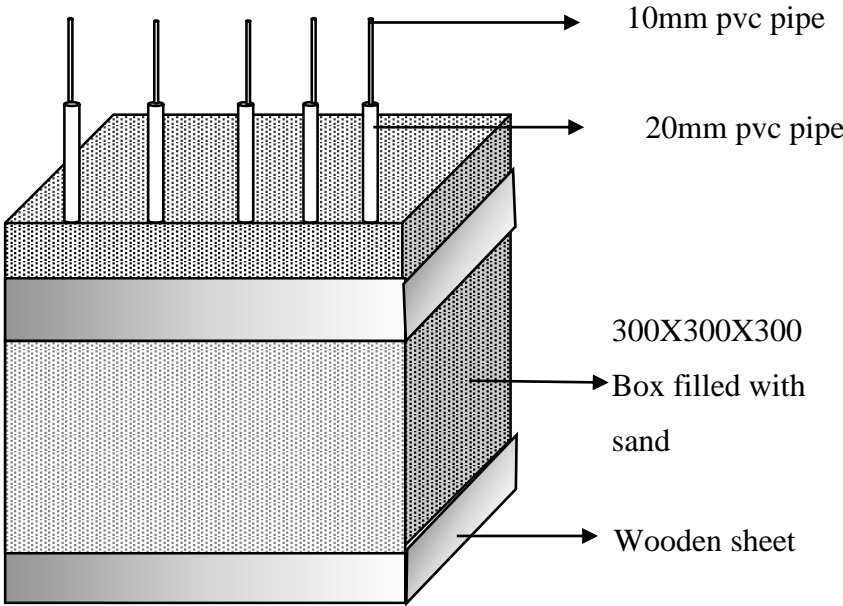


Figure 3.12: Arrangement for preparing grouting sample (all dimensions are in mm)



Figure 3.13: Irregular shaped sample from trial 3

Trial 4: For making a cylindrical-shaped sample, 40mm dia and 78mm height plastic bottles are filled with sand at the loosest condition then fill up the 30mm dia and

height 105mm injection with grout slurry and inject it into the sand with a low speed of about 15 to 20 minutes. When the sand of the plastic bottle is wetted with the grout slurry then the bottle is placed under wet towel for curing. After 7, 14, 28, and 90 days the cylindrical regular-shaped sample is achieved. Figure 3.14 showed the step-by-step procedure of trial 4. The grouted sample obtained from trial 4 which is shown in Figure 3.15.

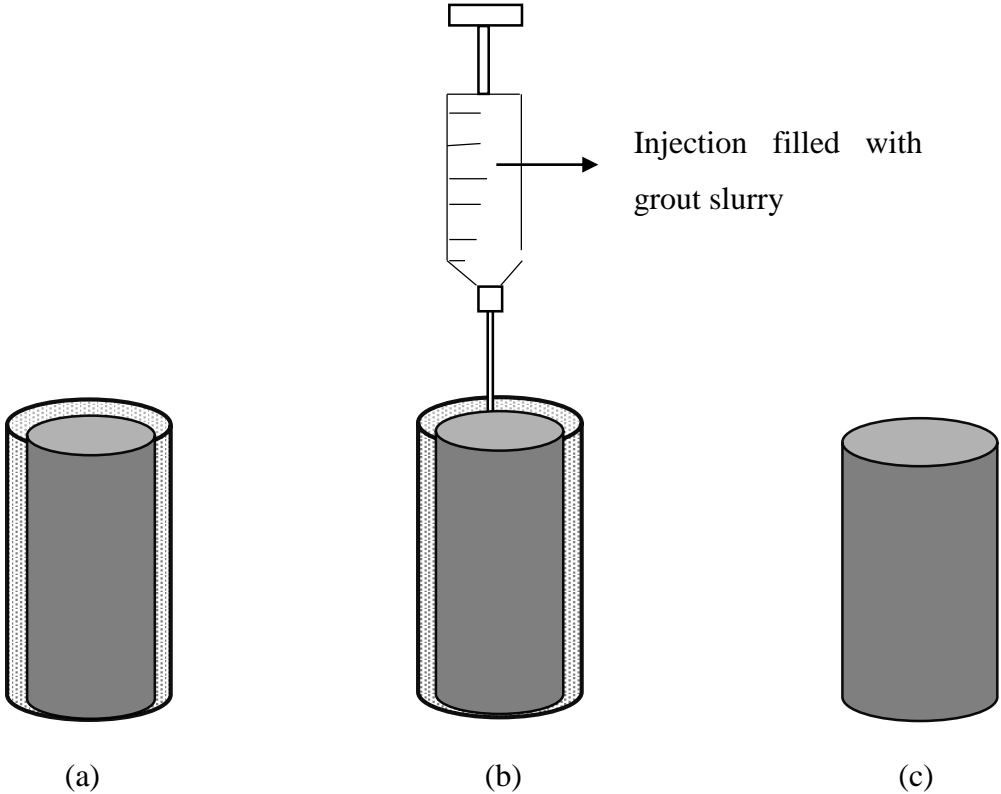


Figure 3.14: Schematic drawing for Step by step process of trial 4: (a) filled the bottle with sand, (b) inject grout slurry into the sand, (c) after curing cylindrical shaped sample is found



Figure 3.15: Grouted sample is retrieved from trial 4

The sample making for permeation grouting is always a tough job. According to Carter et al. (2019), “Effects of grout injection techniques in pressure grouted soil nail system”, they newly developed pressure grouted soil nail system where a latex membrane was used as a liner around the grouting outlet to form a Tube a Manchette (TAM) for direct injection of grout into the sand. In this system, volume-controlled injection system was used to inject the cement grout into the sand for a specified flow rate and the interaction of injected grouted with the soil mass was monitored by the installed total Earth Pressure Cell (EPC) around the grout outlet. Even after adopting modern methods, homogeneous samples were not found which is seen from Figure 3.16. For this reason we have been sampling the small ones in a simple way.



Figure 3.16: Grouting samples from laboratories setup (Carter et al., 2019)

In Figure 3.17, the grouting samples from field testing of permeation grouting using micro fine cement. Hashimoto et al. (2015) were doing a series of field tests at a location close to some of the other boreholes used for injection of cement solution, a borehole was set up, from which groundwater was pumped up, and a flow of groundwater was induced around in the periphery. These boreholes were known as “pumping up borehole and those boreholes were known as “injection boreholes”, at which cement soluting were introduced. At these injection boreholes, polyvinyl pipes of 5cm in diameter were penetrated down to a depth of 5m. After two and a half months of curing period, some excavation was carried out around the location of improved soil and the top surface of improved soil, dome-shaped external appearance was found at depth of 2.4 to 2.7 m below the original ground surface. From two of these Figures, it is clear that the sample preparation is troublesome work.



Figure 3.17: Grouting samples from field setup (Hashimoto et al., 2015)

After all the trial and error procedures, the samples were finally recovered from the trial 4 methods, and the following tests were performed under the defined condition.

Table 3.6 Summary of samples and test condition

Type of tests	Testing condition	Sample size	Cement content	Curing condition	Total number of tests
Unconfined compression test	Constant rate of 0.3 mm/min	40mm dia and 78mm height	5.5%, 6.5%, 8% and 11%	7, 28, 90 and 120 days	51
Triaxial Compression test	Confining pressure of 50 kPa, 100kPa, and 200kPa, strain rates of 0.03040 mm/min for undrained test on saturated samples	38mm dia and 76mm height	11%	7days	3



Figure 3.18: Indication of pH value

3.6 pH Test of the Grouted Samples

The pH of Portland composite Cement is usually 12.5 to 13.5 but the pH of the water is around 7. So, the pH decrease with increasing W/C ratio due to the dilution effect. pH is an approximate measure of acidity or alkalinity of a solution and is defined as the negative logarithm of the hydrogen ion (H⁺) concentration. Decreasing pH may cause to decrease in calcium carbonate and decreasing that may decrease the reaction

rate of producing of C-S-H gel as hardening and strengthening element in concrete. So it is clear that there is an obvious impact on strength due to pH but not w/c ratio. The color of the litmus paper indicates that the pH value of the grouted sample is more than 12 which indicates the formation of calcium hydroxyl in the grouted sample. Figure 3.18 is showed pH test in laboratory.

3.7 Scanning Electron Microscopy of Grouted Samples

The compressive strength and microstructure of grouted sample comprised of Portland Composite Cement (PCC). Scanning Electron Microscopy (SEM) with a Solid-state and Energy Dispersive X-ray (EDX) analysis is employed to obtain a view of the microstructure and to conduct an analysis of the morphology and composition of grouted samples, after 28 days of moist curing. The analytical results together with the physical observations have shown the formation of Calcium Silicate Hydrate (C-S-H) gel and additional pozzolanic (C-S-H) gel. The quantification of the compound content of the sample showed the presence of Calcite (CaCO_3), Quartz (SiO_2), and Alumina (Al_2O_3) crystals.

When sand is stabilized with a calcium-based binder (such as lime) in the presence of water, the reaction of calcium (from lime), alumina, and any sulfate present in the system produce calcium aluminate sulfate hydrate (C-A-S-H) minerals. These minerals have a very large expansive potential. One of these minerals is ettringite, which absorbs very large quantities of water within its structure. During its formation, very high swelling pressure can develop with disruptive increases in volume. The ettringite occupies a greater volume than the original constituent reactants and grows as rod or needle-shaped crystals that generate high internal stresses in the stabilized system and can cause it to crack and disintegrate. The matrix of the stabilized soil showed fewer large capillary pores resulting in a more stable microstructure. Thus, the formation of ettringite in the sample will be of benefit to the stabilized system. In such a case, less water will be available for ettringite formation, accounting for the reduced quantity of rod and plate-like particles in the system. This phenomenon will make the surface structure look more compact, which can only come from the stronger bonds between grains, formed during the hydration process, and the possibility of additional pozzolanic C-S-H gel.

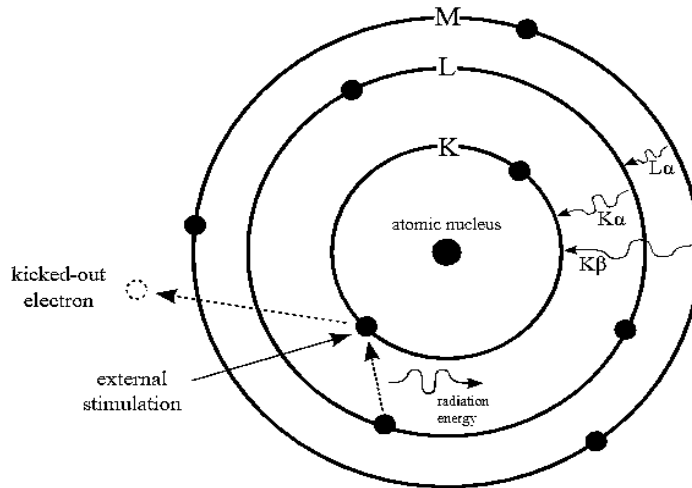


Figure 3.19: Working principles of Energy Dispersive Spectroscopy

EDS also helps to measure multi-layer coating thickness of metallic coatings and analysis of various alloys. The accuracy of this quantitative analysis of sample composition is affected by various factors. Many elements will have overlapping X-ray emission peaks (e.g., Ti K_{β} and V K_{α} , Mn K_{β} and Fe K_{α}). The accuracy of the measured composition is also affected by the nature of the sample. X-rays are generated by any atom in the sample that is sufficiently excited by the incoming beam. These X-rays are emitted in all directions (isotropically), and so they may not all escape the sample. The likelihood of an X-ray escaping the specimen, and thus being available to detect and measure, depends on the energy of the X-ray and the composition, amount, and density of material it has to pass through to reach the detector. Because of this X-ray absorption effect and similar effects, accurate estimation of the sample composition from the measured X-ray emission spectrum requires the application of quantitative correction procedures, which are sometimes referred to as matrix corrections. Figure 3.19 is an example of how EDS works. The letters K, L, and M refer to the n value that electrons in that shell have (K electrons, closest to the nucleus, are $n=1$ electrons), while α and β indicate the size of the transition. The relaxation from M to L or L to K are therefore described as L_{α} or K_{α} , while going from M to K would be a K_{β} transition.

3.8 Summary

In this chapter, a brief description of selected soil collection, sample preparation, testing procedure, and laboratory tests were given. After collecting soil samples, groutability check was done and the index and chemical properties of both soil samples and grouting materials were searched here. Creating grouted samples is not easy which has been proven through discussion of trial and error methods. Here briefly discussed the test and test plan on the grouted samples. Then the absolute idea about the chemical reaction was found from the Scanning Electron microscope examination.

Chapter 4

RESULTS AND DISCUSSIONS

4.1 Introduction

This research aims at analyzing the strength and microstructure of grouted sand with different water-cement (W:C) ratios and curing times. Here used cement-based grout, is made of mixed water and cement, which is also added with sand. It is commonly used for soil improvement, for repairing the damages to concrete and masonry, or for the construction of preplaced aggregate concrete. In this application, the grout is placed by using injection methods, with pressure, or by its weight only. Therefore, in this chapter, the first discussed subject is to check the groutability and index properties of the sample sand and then discuss the mix design to make grouted samples. Then relevant discussions on interpretations of graphs, which will be found by unconfined compression and triaxial tests. Afterward, in this chapter vivid discussion on microstructure analysis like scanning electron microscope (SEM) and energy dispersive spectroscopy (EDS) to get a clear picture of stabilization after injecting grouting materials.

4.2 Groutability Check

The successful permeation of particulate grouts into a geological formation primarily depends on the relative sizes of the voids being grouted and the solid particles in the grout. Experiments have shown that the depth of permeation of a particulate grout in a soil formation is strongly controlled by the size of the smaller voids in the formation and the larger particles in the grout (Mitchell et al.,1970), and these have led to the development of pertinent design criteria. On the other hand, it can be checked according to the graph which was modified by Elias et.al. (2006) that is presented in Figure 4.1 which is defined that the sample sand is suitable for grouting. It is shown that the suitability range of permeation grouting is from 2mm particle size to 0.06mm particle size for sand, and the sample sand is fallen in that range also. The properties of sand used for grouting are given in Table 4.1 by using the equations from 3.1 - 3.4.

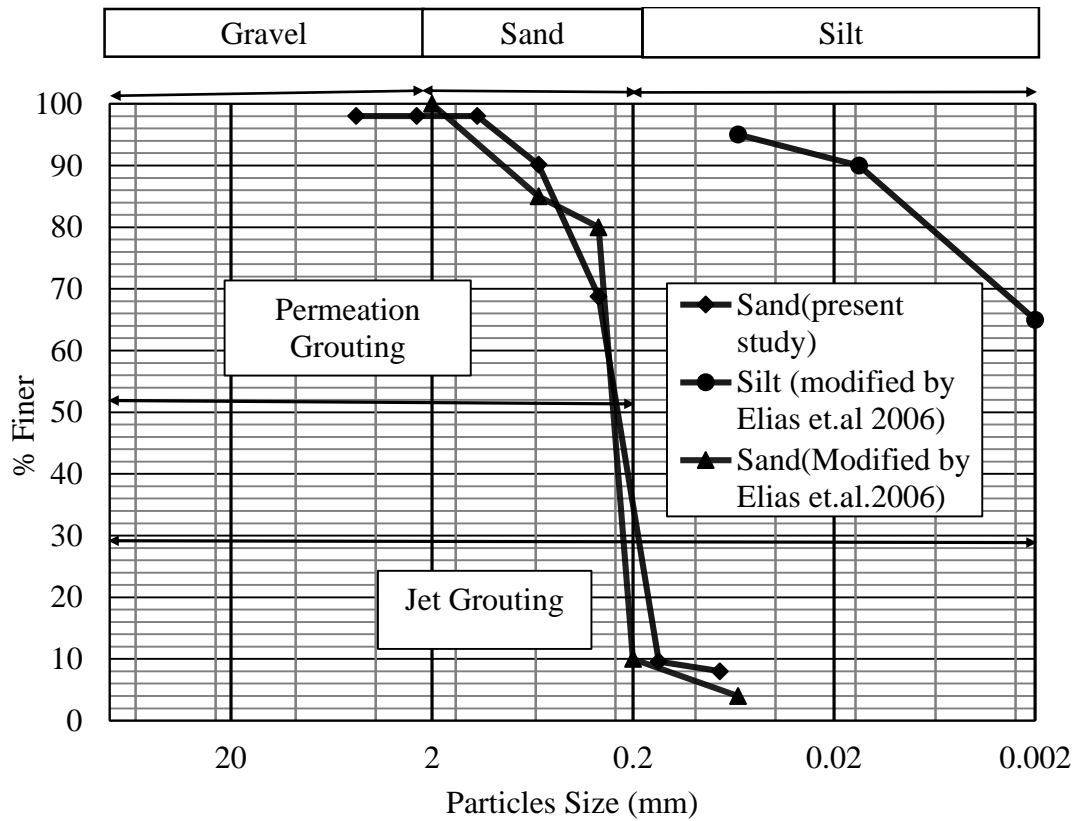


Figure 4.1: Comparison of suitable soil for different grouting methods

Table 4.1 Properties of sand used for grouting

Specific gravity	Permeability (cm/sec)	Density Index	F.M.
2.89	8.84×10^{-6}	4.921%	1.12

4.3 Mix Design of Grouted Sand

Cementitious grouts can be formulated to provide an endless range of different properties and are conveniently placed in the following categories:

- (i) Suspensions
- (ii) Pourable paste or slurry
- (iii) Plastic consistency
- (iv) Low-density cellular paste or slurry
- (v) No-slump mortar-like low mobility

Most grouts is simply composed of cement and water, whereas innumerable admixtures, supplementary cementing materials, and fillers are used also. Grouting has traditionally been dominated by simple mixtures with few ingredients, the tendency now is toward the use of much more sophisticated mix designs containing many components (Warner, 2004).

4.3.1 Cementitious Suspensions

Cementitious suspensions were the very first grouts used and are still widely employed. They are mixtures of cement and water only without any other ingredients. Water cement ratios are about 0.3:1 by weight, which is the thickest, and 10:1 is the thinnest. For this reason a W:C ratio greater and smaller than 3:1, is both questionable. From the tests and observations of actual grout performance in curtains at several dams, Houlsby (1982) concluded that a water-cement ratio of 3 can provide the most complete filling of cracks which is less than 1.5mm thick. He also concluded that grouts with a water-cement ratio of 3:1 by volume were good quality, whereas those with a water: cement ratio of 5:1 by volume or greater are of questionable effectiveness.

The workability of the grout mixture and its injectibility depend on the proportion of the water to dry cement ratio (W: C). The W:C ratio is the fundamental property in all cementitious mixtures. This important parameter dictates the consistency of the final mixture. More important on its achievable strength and long-term durability. Standard of the W:C ratio of concrete is well established and widely recognized. However, it is not established for grout application which is a complex issue. This ratio can be calculated either on a weight or volume basis. Typical calculation for a particular W:C ratio has been presented below:

Conversion of W:C ratio (Practical Handbook of Grouting):

Weight to Volume multiplied by 1.5

Volume to weight multiplied by 0.66

Water

1gallon=8.3 lbs. =3.8L

1ft³=7.5 gallon=62.4 lbs. =28.4 L

Cement:

Weight of 1 bag cement =94 lbs. =42.7 kg =28.4L (blucked).

Table 4.2 showed the conversion of mixproportion from volumn to weight.

Table 4.2 Conversion of Mix proportion from volume to weight

Water Cement ratio by volume	Water Cement ratio by weight
0.4:1	0.26:1
0.5:1	0.33:1
0.6:1	0.40:1
0.8:1	0.53:1
1:1	0.66:1
2:1	1.32:1
3:1	1.98:1
4:1	2.64:1
5:1	3.30:1

In this study, equation 4.5 is used to calculate the volume of cement

$$\frac{v_c \rho_c}{d_c \rho_w} + \frac{av_c \rho_s}{d_s \rho_w} + \frac{w/c.v_c \rho_c}{\rho_w} = 1 \quad (4.5)$$

Here, V_c = the necessary volume of cement per cubic meter grout

ρ_c = bulk density of cement

ρ_s = bulk density of sand

ρ_w = density of water

a = volumetric portion of sand

b = volumetric portion of water

d_c = relative density of cement

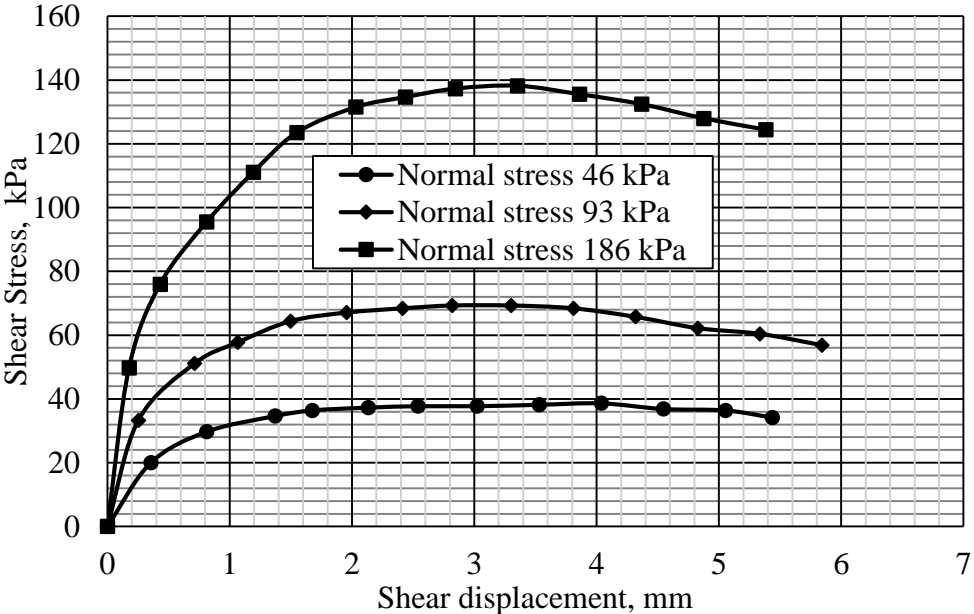
d_s = relative density of sand

This equation established by Satyarno et al. (2014) is based on the well-known absolute volumes of each material principle, but with some minor modifications, based on their mass or volume ratios. That equation easily determines the necessary volume of cement per m^3 of grout (V_c) because it is the only unknown in the equations.

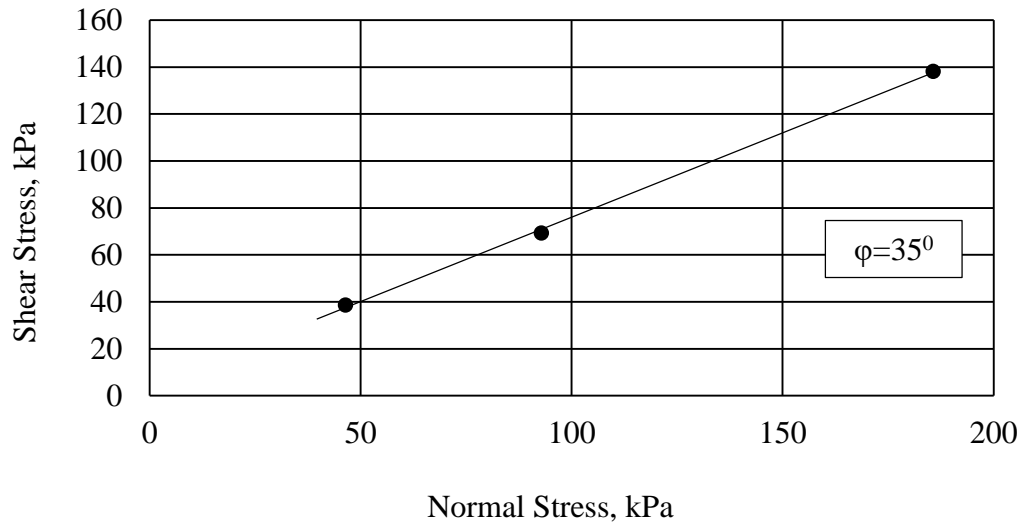
4.4 Shear Strength Parameter of Sand Used for Grouting

A direct shear test was performed on sand samples with normal loads of 46kPa, 93kpa and 186 kPa. Figure 4.2 (a) presents the shear stress and shear displacement graph for the sand sample.

Figure 4.2 (b) represented shear stress vs normal stress under the unconsolidated undrained condition of direct shear stress. From the graph the value of cohesion is very negligible only $c= 4.2437$ where the angle of internal friction is much high $\phi=35^\circ$.



(a)



(b)

Figure 4.2: Direct shear test results of sand sample: (a) shear stress vs. shear displacement, (b) shear stress vs. normal stress

4.5 Strength Characteristics of Grouted Sand

Unconfined compression tests and triaxial tests were performed on the grouted samples to analyze their strength characteristics. The samples were loaded with a constant strain rate of 0.01% per minute and triaxial tests were conducted as consolidated undrained with a different cell pressure. All tests were carried out on the grouted samples according to ASTM standards. For carrying out the tests, fifty one samples were prepared. Four types of W:C ratios that is 2:1,3:1,4:1 and 5:1 were selected for four different curing ages (7, 14, 28, and 90 days). However in case of W:C ratio 2:1 some samples were cured 120 days. To check the repeatability of the test results 3 samples were tested in each case.

The designation of samples and list of samples are given in Table 4.3 and Table 4.4, respectively.

Table 4.3: Sample designation

Notation	Abbreviation
UC	Unconfined compression test
21	Grouting mix ratios (W:C)
7	Curing time
(1)	Sample one

Table 4.4: List of samples for unconfined compression and triaxial tests

W:C ratio	Sample No.	Curing age (day)	Samples designation
2:1	1	7	UC21-7(1)
	2		UC21-7(2)
	3		UC21-7(3)
	1	14	UC21-14(1)
	2		UC21-14(2)
	3		UC21-14(3)
	1	28	UC21-28(1)
	2		UC21-28(2)
	3		UC21-28(3)
	1	90	UC21-90(1)
	2		UC21-90(2)
	3		UC21-90(3)
	1	120	UC21-120(1)
	2		UC21-120(2)
	3		UC21-120(3)
3:1	1	7	UC31-7(1)
	2		UC31-7(2)
	3		UC31-7(3)
	1	14	UC31-14(1)
	2		UC31-14(2)
	3		UC31-14(3)
	1	28	UC31-28(1)
	2		UC31-28(2)
	3		UC31-28(3)
	1	90	UC31-90(1)
	2		UC31-90(2)
	3		UC31-90(3)
4:1	1	7	UC41-7(1)
	2		UC41-7(2)
	3		UC41-7(3)
	1	14	UC41-14(1)
	2		UC41-14(2)
	3		UC41-14(3)
	1	28	UC41-28(1)
	2		UC41-28(2)
	3		UC41-28(3)
	1	90	UC41-90(1)
	2		UC41-90(2)
	3		UC41-90(3)
5:1	1	7	UC51-7(1)
	2		UC51-7(2)
	3		UC51-7(3)
	1	14	UC51-14(1)
	2		UC51-14(2)
	3		UC51-14(3)
	1	28	UC51-28(1)
	2		UC51-28(2)
	3		UC51-28(3)
	1	90	UC51-90(1)
	2		UC51-90(2)
	3		UC51-90(3)

Table 4.5 Physical properties of the tested grouted samples

Mix Ratio	Curing age (day)	7 Days	14 Days	28 Days	90 Days	120 Days
5:1	Dry density (gm/cm ³)	9.3	9.8	8.9	9.89	-
	Moisture content (%)	32.6	30.4	23.5	8.7	-
	Void ratio, e	0.33	0.31	0.23	0.11	-
4:1	Dry density (gm/cm ³)	10.36	10.27	10.01	9.6	-
	Moisture content (%)	30.5	29.2	19.6	4.5	-
	Void ratio, e	0.31	0.29	0.19	0.14	-
3:1	Dry density (gm/cm ³)	10.42	10.05	9.99	9.3	-
	Moisture content (%)	30.2	30.2	15.1	3.9	-
	Void ratio,e	0.37	0.3	0.15	0.15	-
2:1	Dry density (gm/cm ³)	10.46	9.74	9.6	8.4	8.0
	Moisture content (%)	29.0	31.0	19.3	3.5	4.5
	Void ratio,e	0.4	0.31	0.19	0.12	0.1

4.5.1 Unconfined Compression Test Results

Reconstituted samples were prepared by mixing sand with cement and water. For the experimental purpose, 2:1, 3:1, 4:1, and 5:1 W:C ratios are used for making grouted sand. In the experiment, Unconfined Compression tests (UC) were conducted on the

samples then plotted graphs to make the comparison of the compressive strength of different W:C ratios and different curing times.

Axial stress vs. axial strain of the samples prepared with different W:C ratio 2:1,3:1,4:1, and 5:1 for different curing times 7,14,28 and 90 days have been presented in Figures 4.3 to 4.11. Graphs showed the compressive strength of different proportioned grouted sand after different curing periods. From the figures, it was seen that axial strength increases with curing time. For 7 days cured samples, it was observed that the strength of samples prepared with W:C ratio of 2:1 is 120 kPa while it is 40 kPa for the samples prepared with W:C ratio of 5:1 and 4:1. Particularly, compressive strength depended on the cement content and curing time. For that reason, the compressive strength reached 400 kPa of 2:1 water-cement ratio after 90 days of curing (Figure 4.9d)

In the case of the samples prepared with W:C ratio 5:1 in Figures 4.3 (a), 4.5 (a), 4.7 (a), and 4.9 (a) with different curing times, it was seen that axial stress increased slightly from 35kPa to 40kPa after cured 7days to 28 days. However, it increased abruptly to about 70kPa after 90 days of curing. Similarly, the samples prepared with W:C ratio 4:1 were presented in Figures 4.3 (b), 4.5 (b), 4.7 (b), and 4.9 (b), it was also investigated that the axial stress increased from 28 kPa to 30 kPa from 7 to 14 days of curing where it increased more than 55 kPa after 28 days to 90 days.

Afterward from the presented graph, there was a massive increase in strength from the ratio 3:1 to 2:1 at every curing period. The compressive strength of the 3:1 sample went high up to 120 kPa in Figure 4.3 (c), 4.5 (c), 4.7 (c), and 4.9 (c) from 7 to 90 days of curing. Overall 3:1 samples represented ductile materials.

The compressive strength of 2:1 grouted sand was always at the highest vertex for whole the curing period. Though it showed the highest crown the sample represented the brittle materials. In figure 4.11, the compressive strength was more than 1000 kPa where the strain was about 9%, with the comparison of other samples, showing the axial strain was less than 9%. These samples showed more ductility than other samples.

The axial stress was increased with the increase of curing time. From the discussed graphs it is seen that the axial strains are about 6% for W:C ratios 2:1, 3:1, 4:1, and

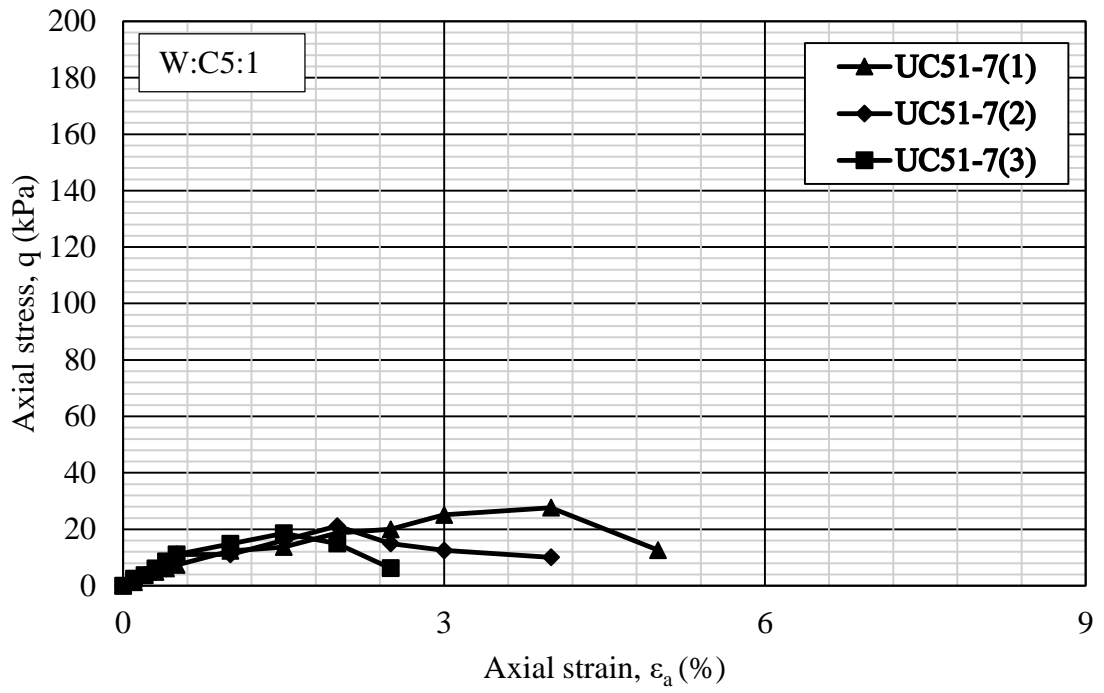
5:1 for every curing age. For 120 days of curing and W:C ratio 2:1 showed the highest strain about 9% which is clear from Figure 4.11.

It was observed that ductility and brittleness were changed with the change of curing time and cement content. Though the axial stress of 5:1 and 4:1 was not so high but curves showed ductility from the curing ages 7 days to 90 days whereas for 3:1 and 2:1 grouted samples were showing slight ductility from 7 days to 14 days but they showed high brittleness from 28 days to 90 days of curing.

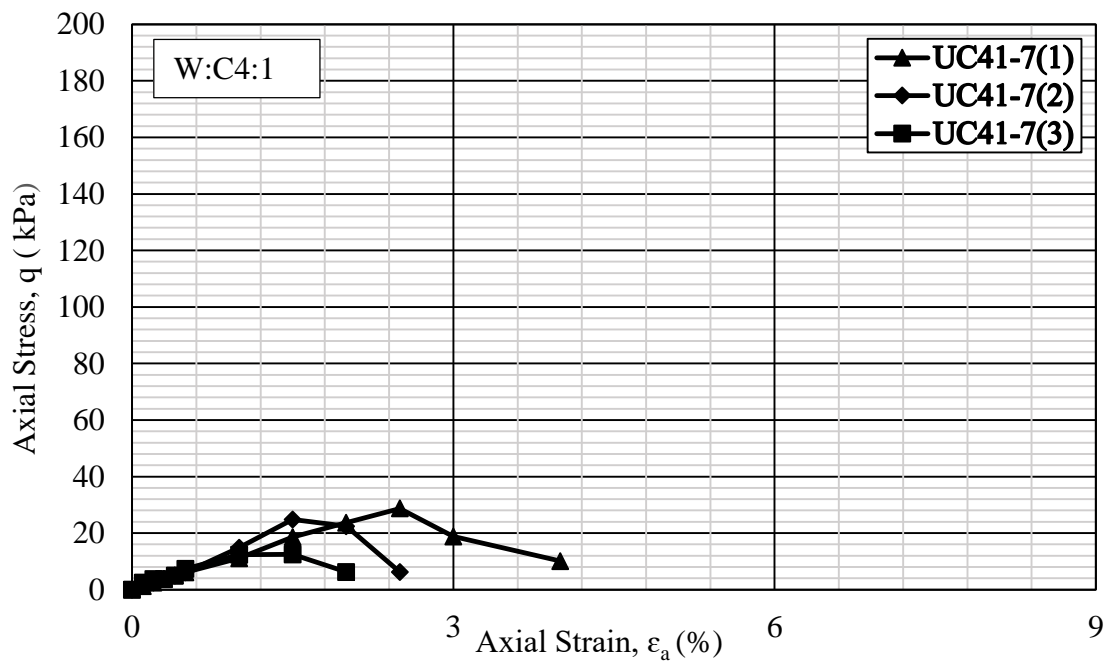
Table 4.5 was presented the physical properties like dry density, moisture content, and void ratio of grouted samples W:C ratio 2:1, 3:1, 4:1, and 5:1 with curing ages 7,14,28, and 90 days. From Table 4.5, dry density decrease with an increase in curing ages. It was also observed that the moisture content and void ratio decreased with the increase of cement content.

Table 4.6 portrays the samples based on compressive strength. This table represents the unconfined compression strength, cohesion, young's modulus, and failure pattern of different proportionate grouted samples with different curing times. It is observed that cohesion and young modulus are increasing with the increase of compressive strength. These parameters are increasing with cement content and curing ages. From Figure 4.13, the barchart represents that compressive strength increasing with the increase of cement content.

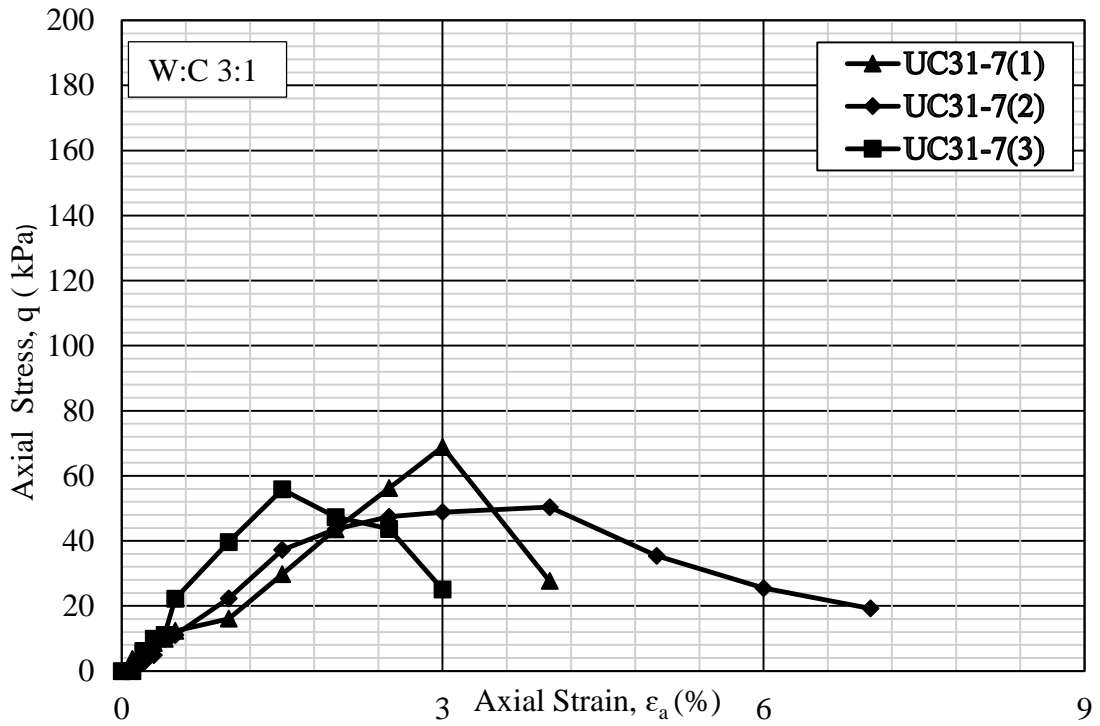
The barchart in Figure 4.13 is the comparison of compressive strength in MPa for W:C ratio 2:1 of present study with other researches for different curing ages like 7,14, 28, 90 and 120 days. The compressive strength of present study is very low than others. From table 4.7 it has seen that different researchers developed their devices according to their suitability and some of the researcher mixed admixture to increase the strength. In the present study the simple injection methodology is used for making samples without using any strength increasing admixture.



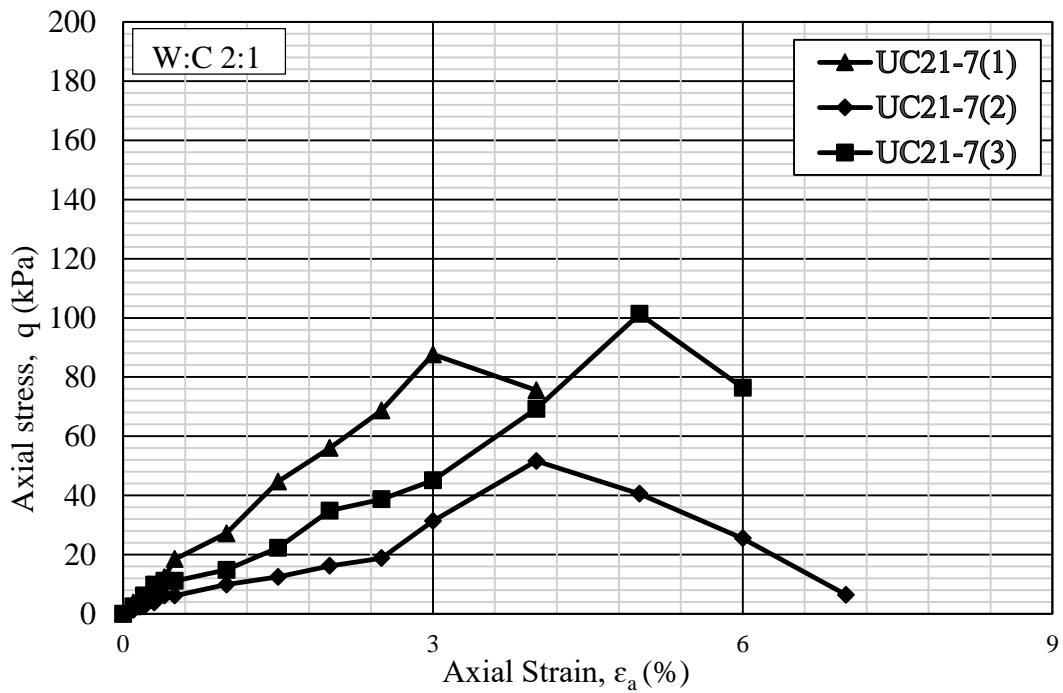
(a)



(b)



(c)



(d)

Figure 4.3: Axial stress vs. axial strain of the samples prepared with different W:C ratio after 7 days of curing: (a) W:C ratio 5:1, (b) W:C ratio 4:1, (c) W:C ratio 3:1, (d) W:C ratio 2:1

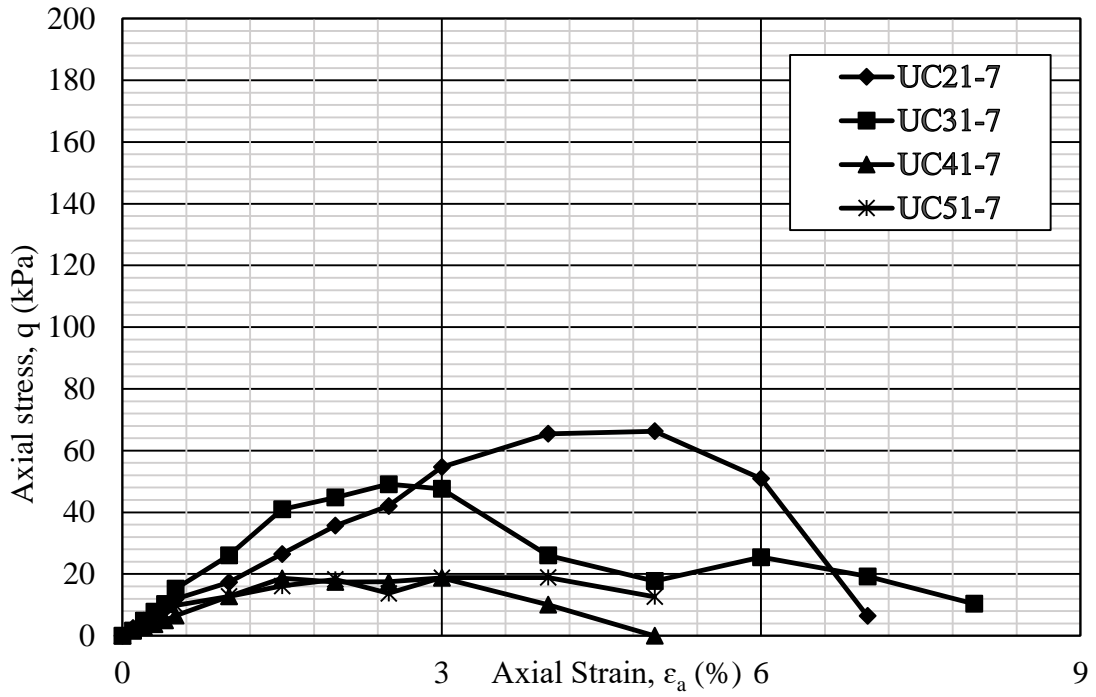
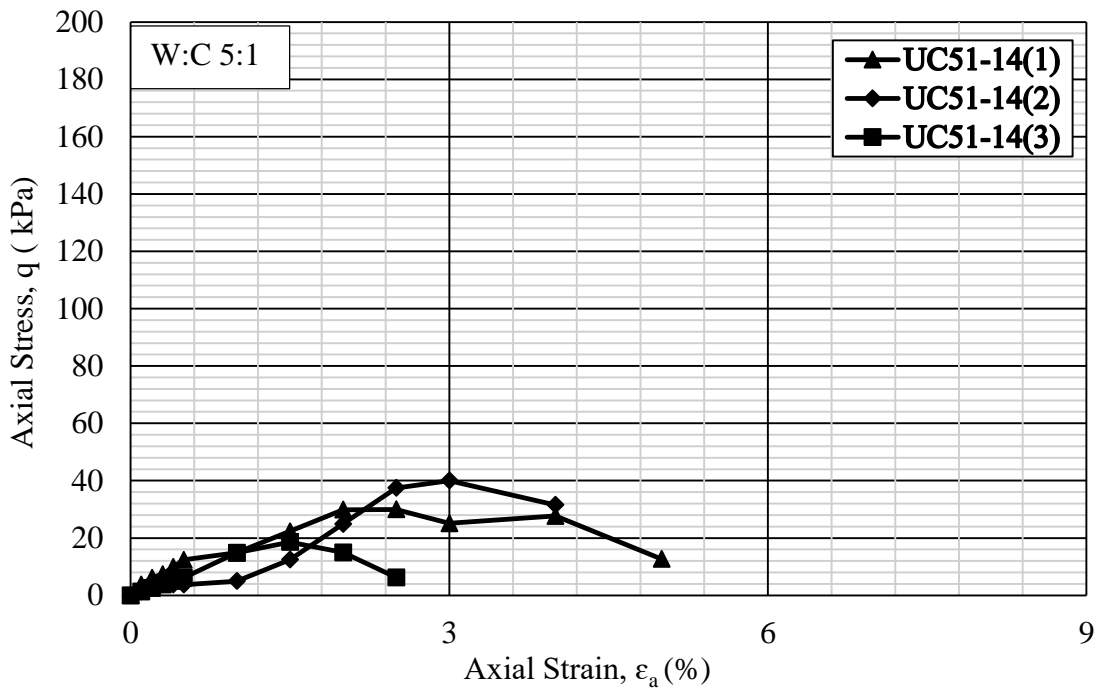
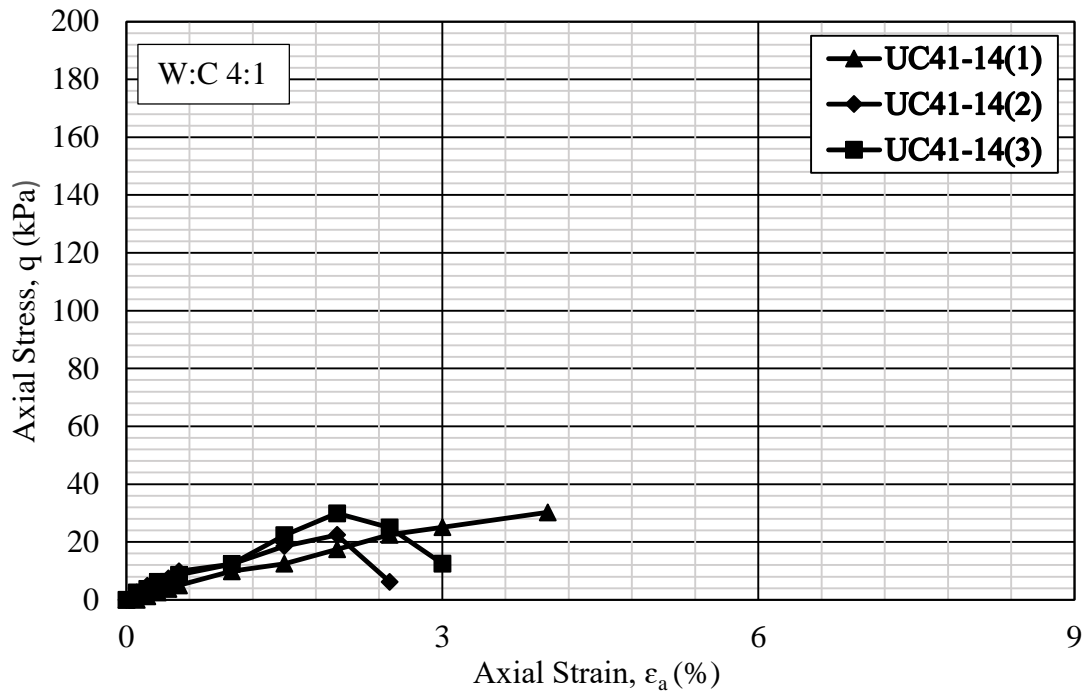


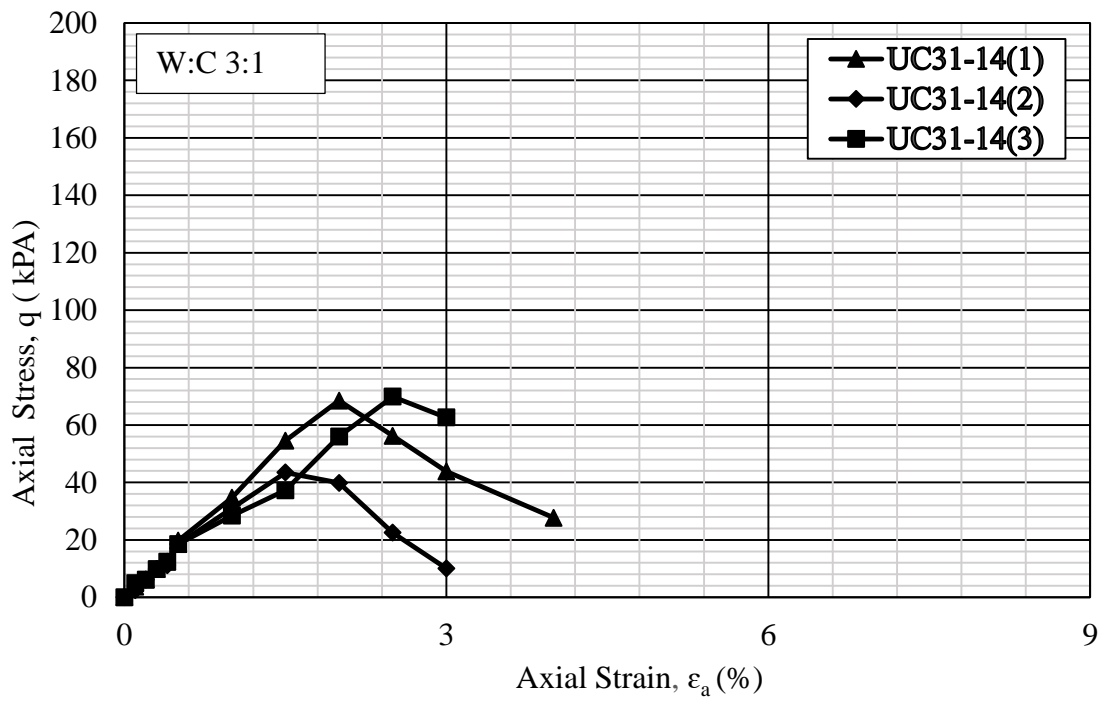
Figure 4.4: Typical axial stress and axial strain curves of different samples cured for 7 days



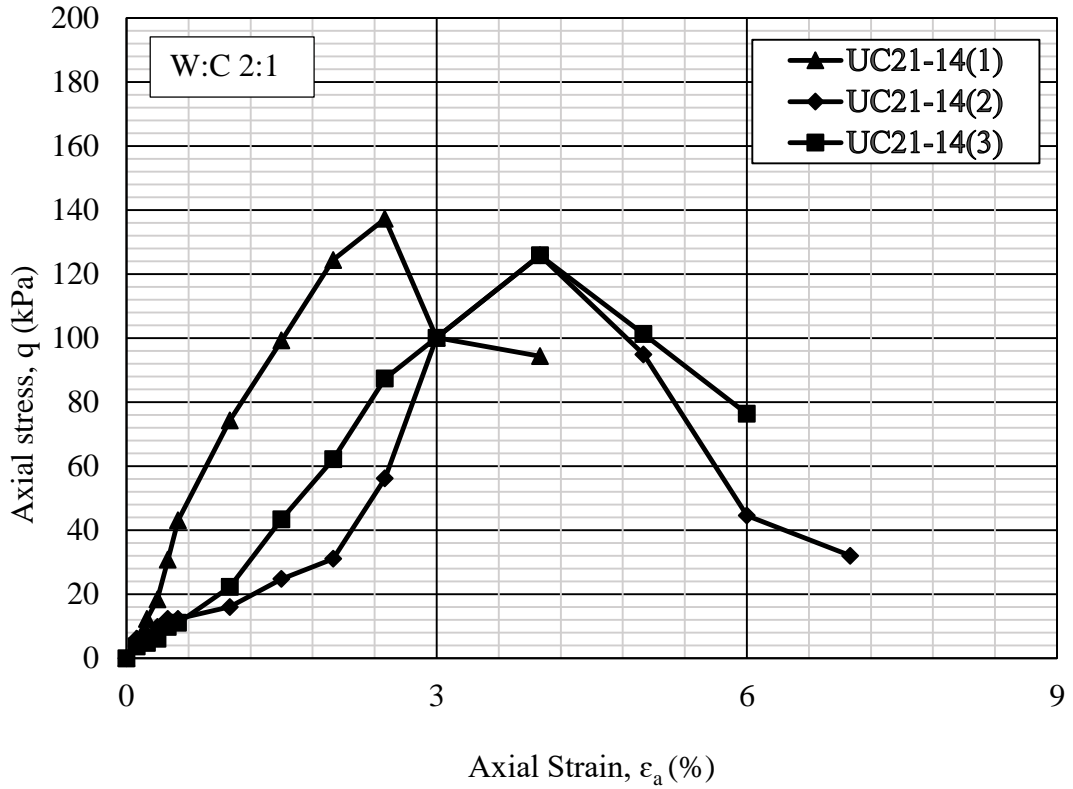
(a)



(b)



(c)



(d)

Figure 4.5: Axial stress vs. axial strain of the samples prepared with different W:C ratio after 14 days of curing: (a) W:C ratio 5:1, (b) W:C ratio 4:1, (c) W:C ratio 3:1, (d) W:C ratio 2:1.

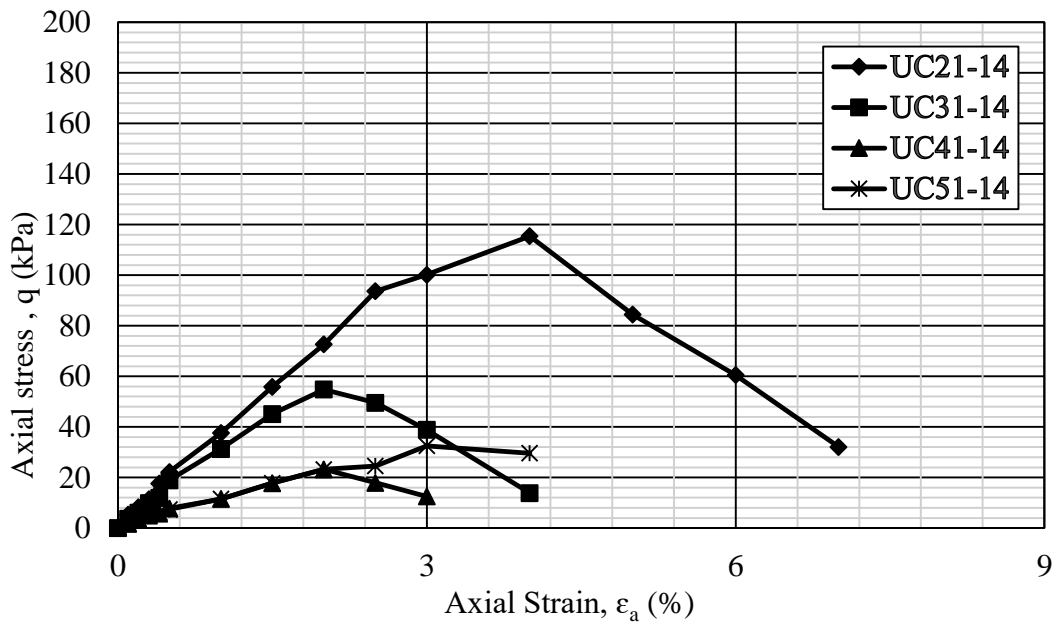
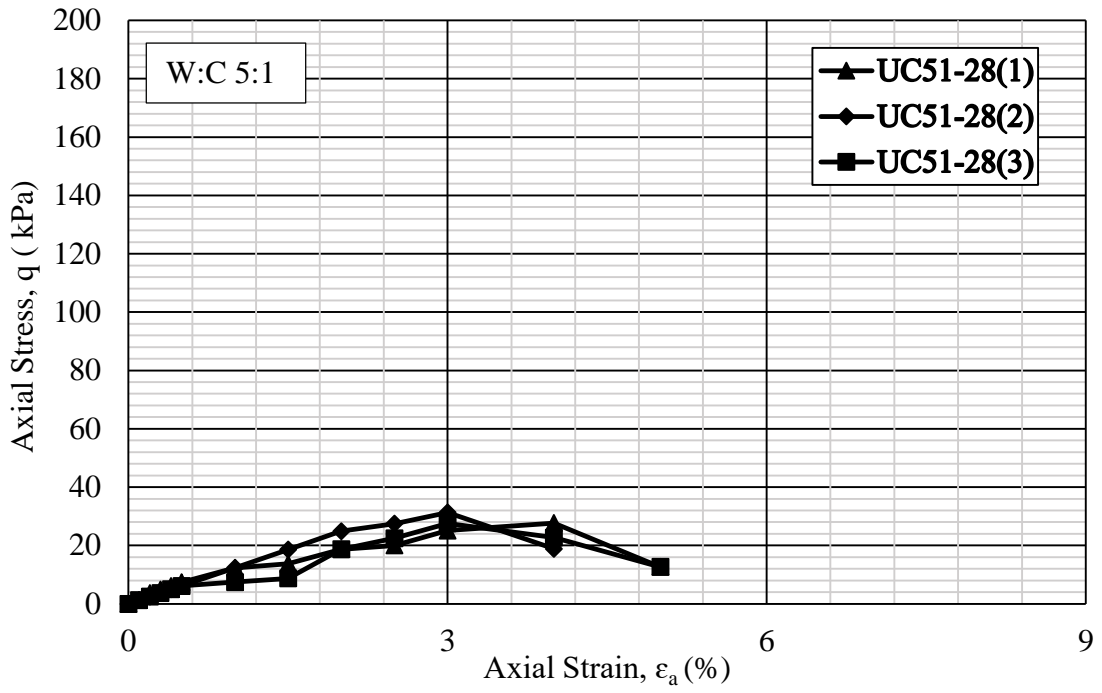
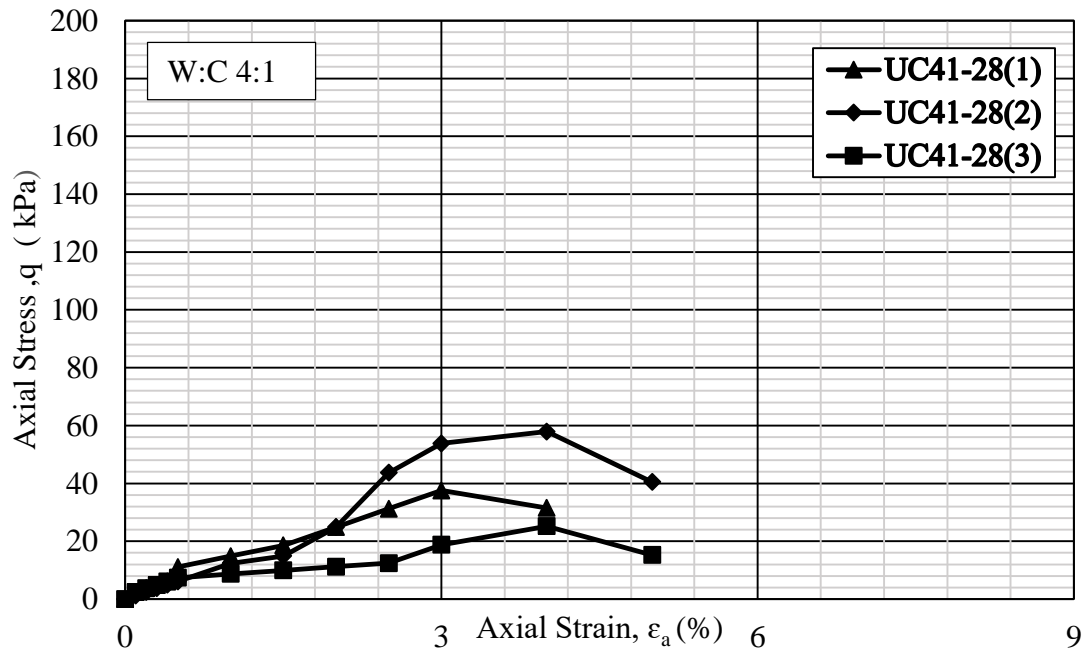


Figure 4.6: Typical axial stress and axial strain curves of different samples cured for 14 days



(a)



(b)

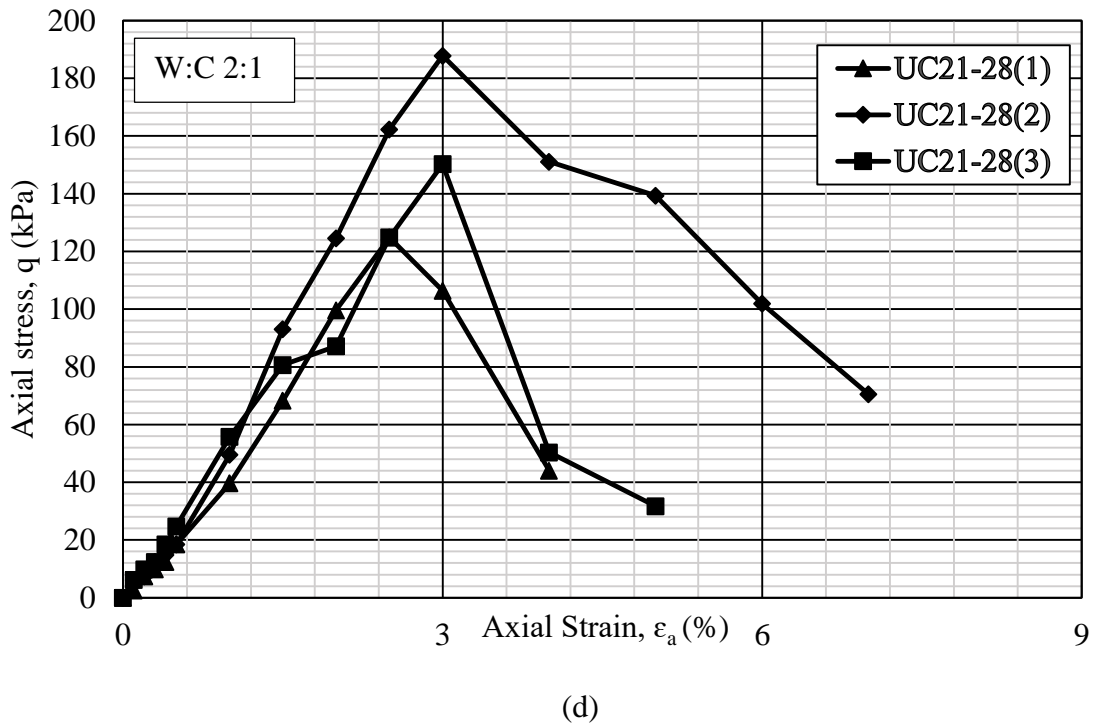
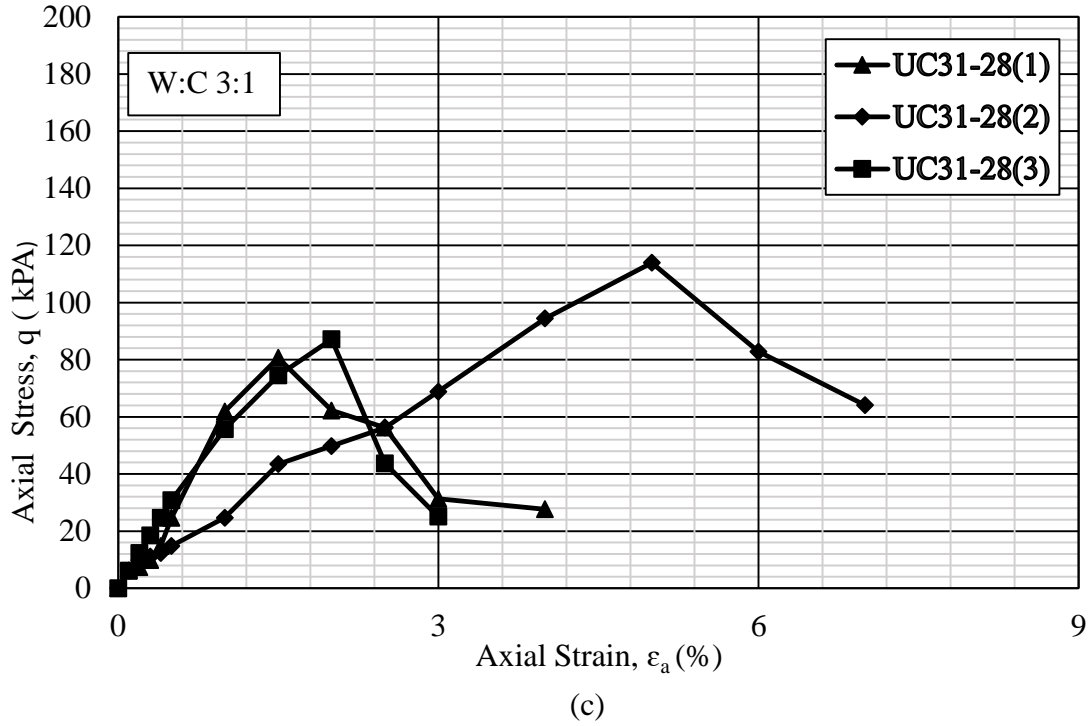


Figure 4.7: Axial stress vs. axial strain of the samples prepared with different W:C ratio after 28 days of curing: (a) W:C ratio 5:1, (b) W:C ratio 4:1, (c) W:C ratio 3:1, (d) W:C ratio 2:1.

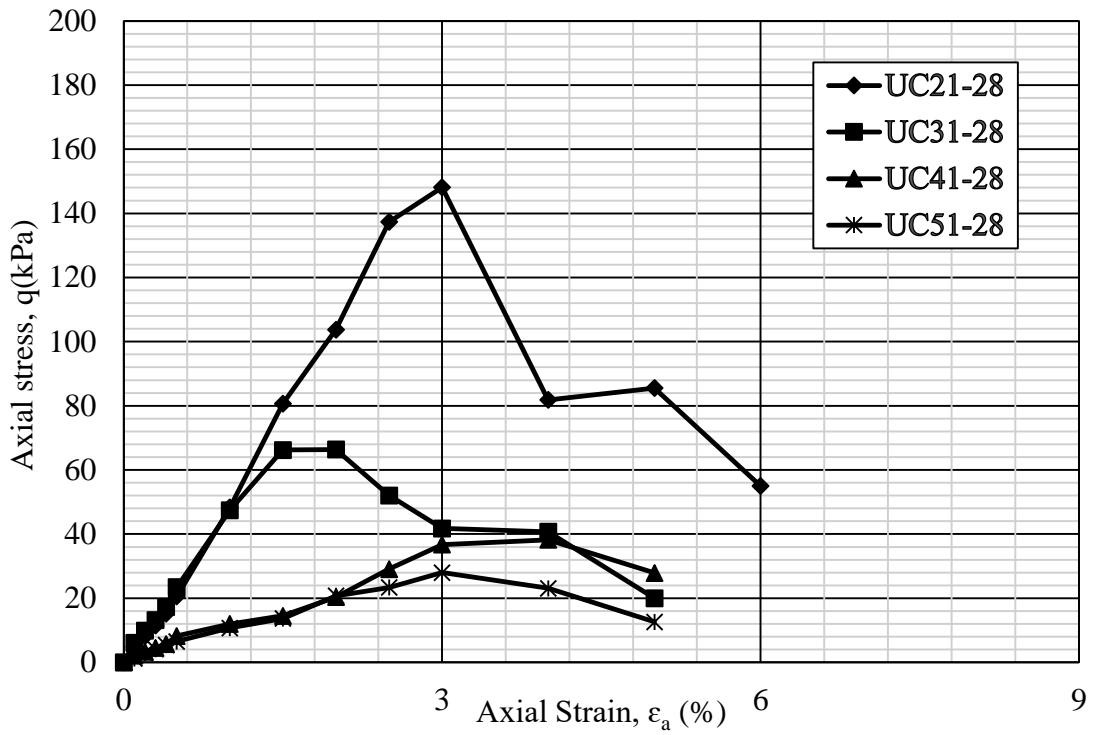
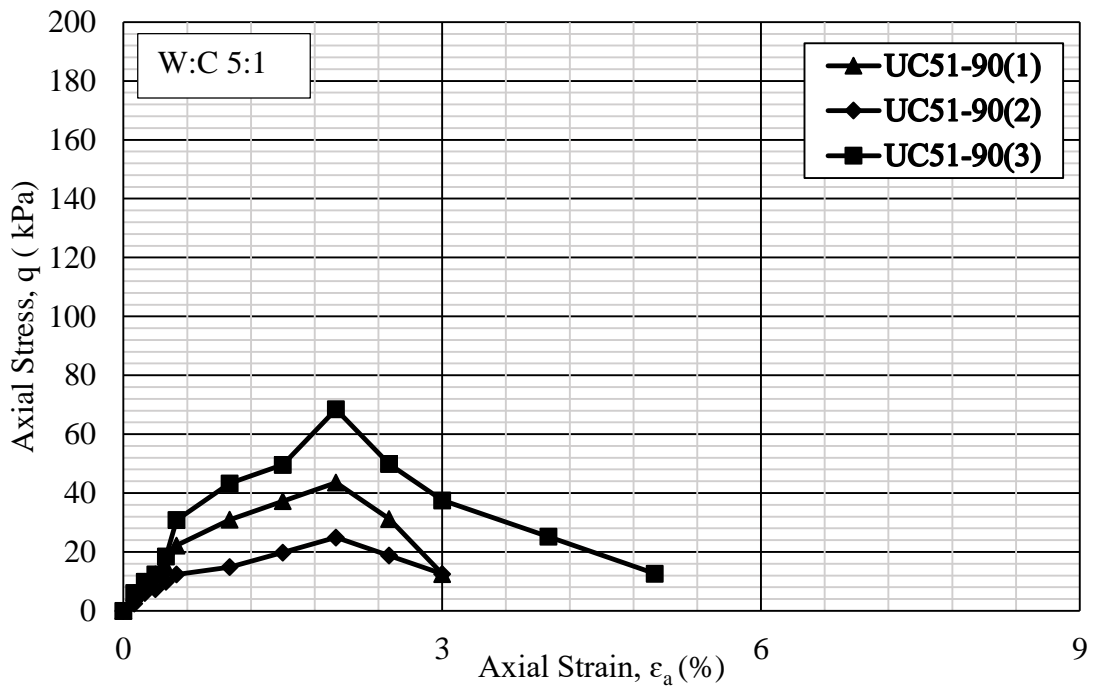
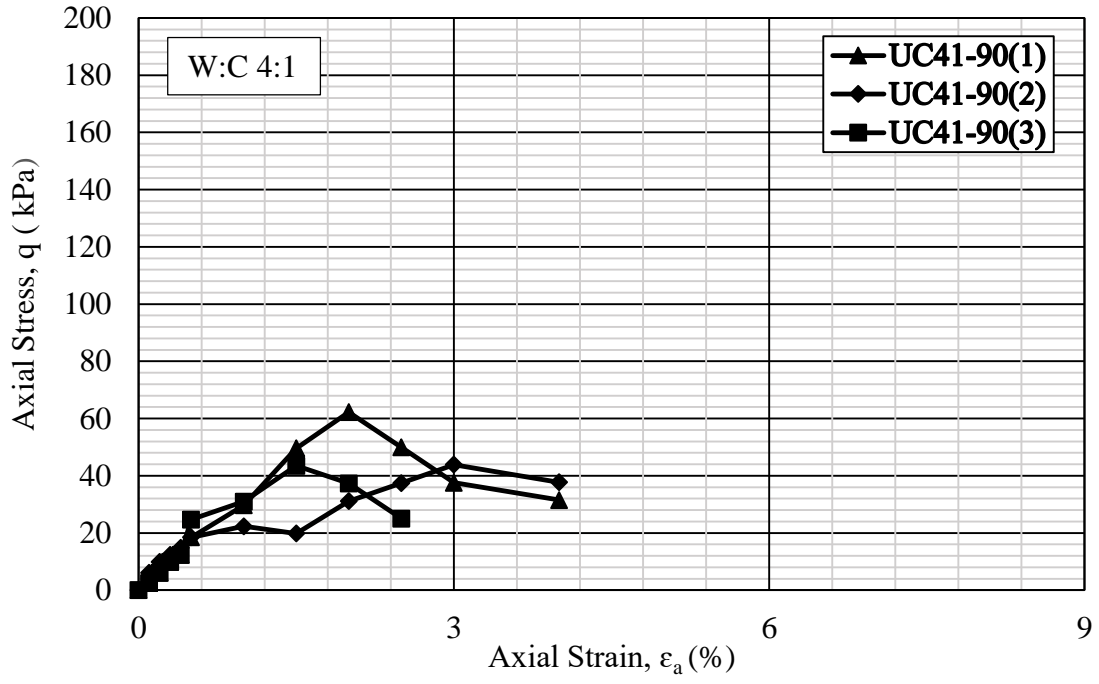


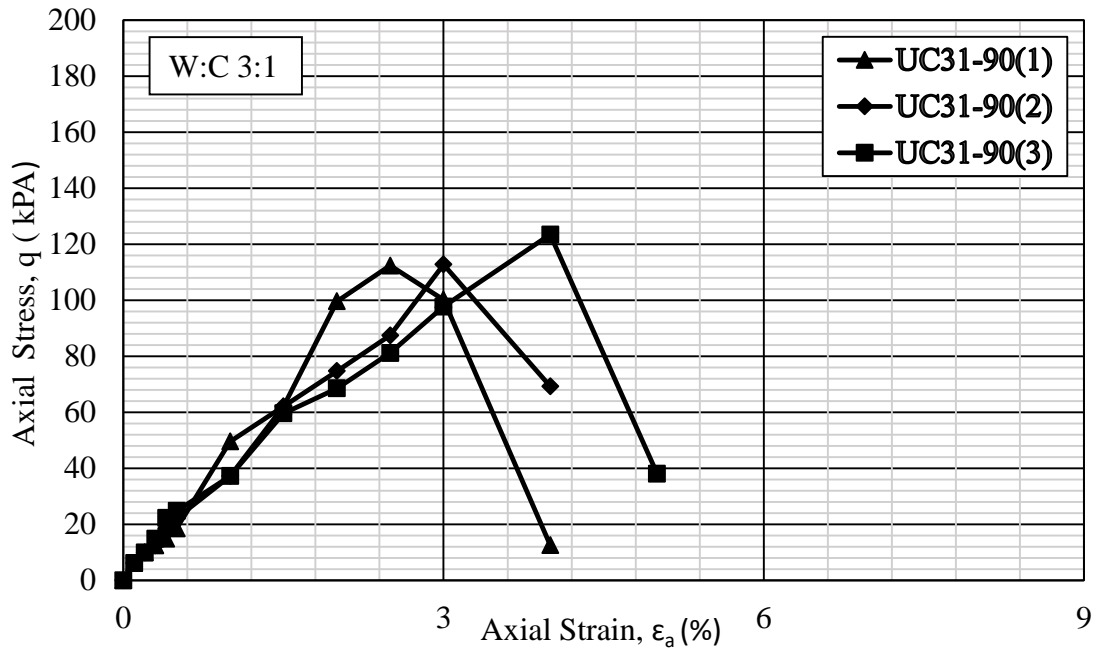
Figure 4.8: Typical axial stress and axial strain curves of different samples cured for 28 days



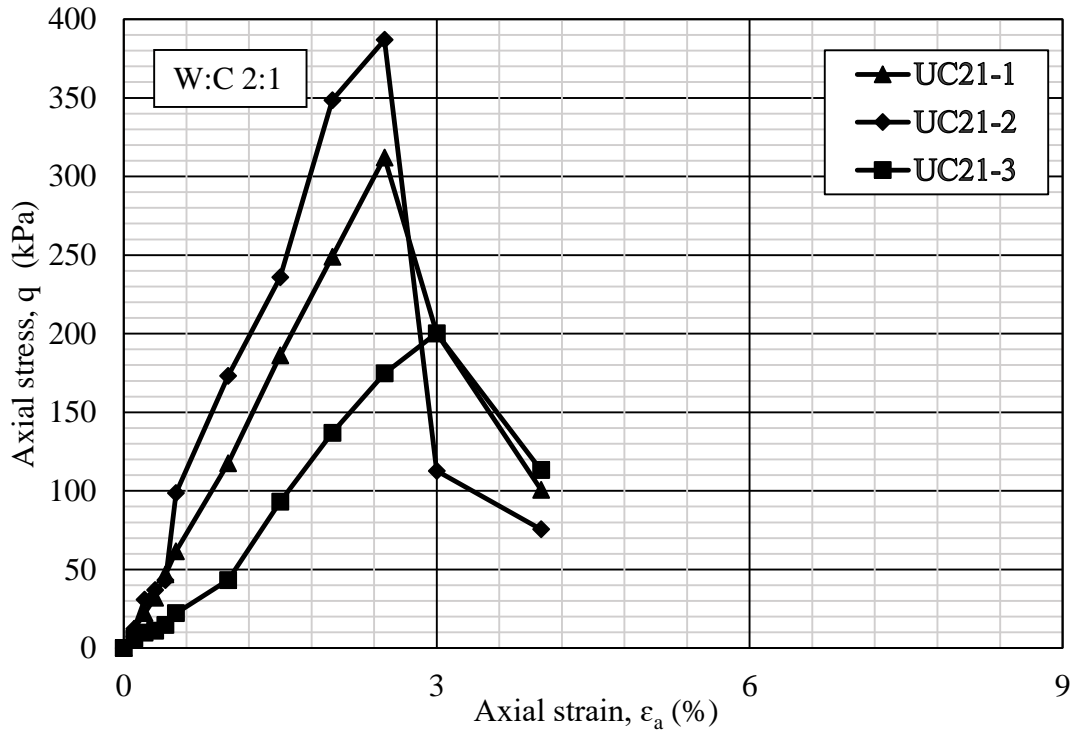
(a)



(b)



(c)



(d)

Figure 4.9: Axial stress vs. axial strain of the samples prepared with different W:C ratio after 90 days of curing: (a) W:C ratio 5:1, (b) W:C ratio 4:1, (c) W:C ratio 3:1, (d) W:C ratio 2:1.

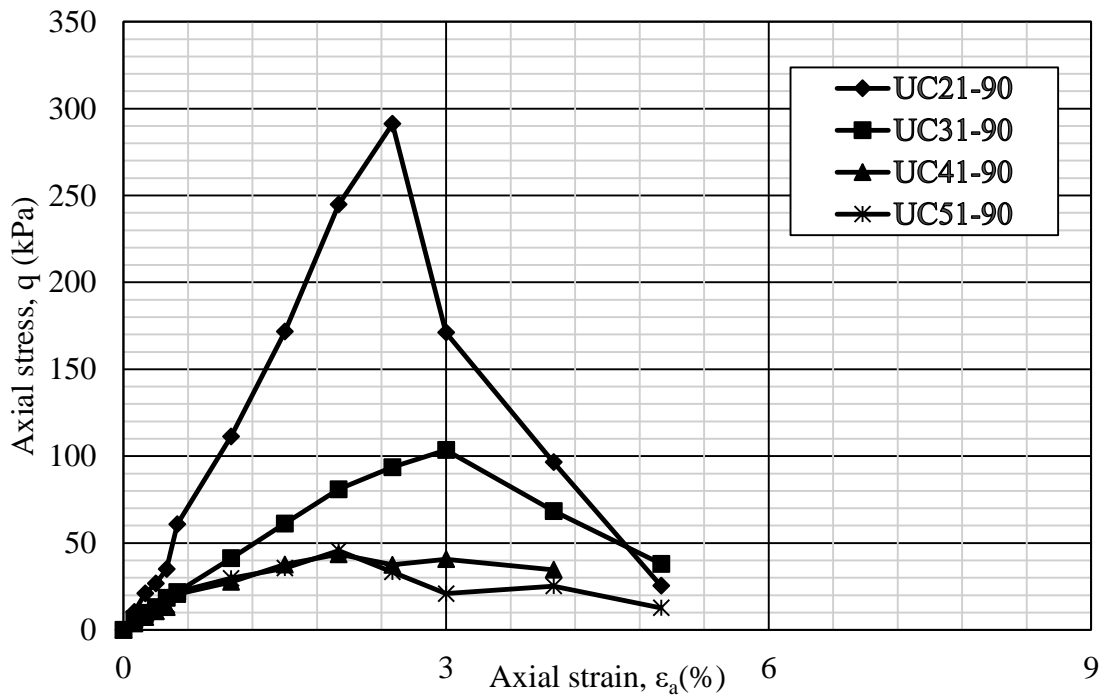


Figure 4.10: Typical axial stress and axial strain curves of different samples cured for 90 days

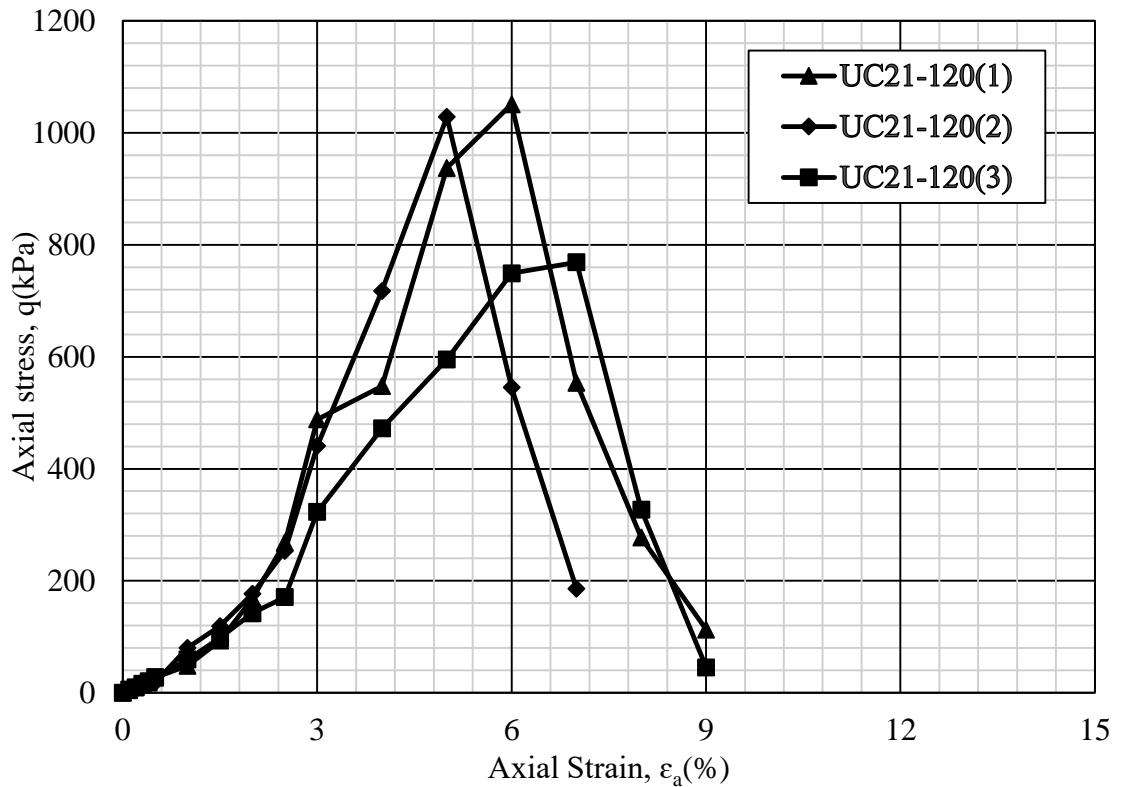


Figure 4.11: Axial stress and axial strain curves of W:C ratio 2:1 samples cured for 120 days

The typical stress and strain curve represents that the axial strain decrease with the increase of cement content and curing time but the confined compressive strength increase with the increase of cement content and curing time. According to Wahab et al. (2021) strength gain due to cement is attributed to decrease soil porosity when the cement content increases. The ductility change with increasing cement and curing time in this research is compatible with the findings of the study by Avci et al. (2021) and Kordnaeij et al. (2019). The ductility significantly decreases for W:C ratio 2:1 and 3:1 with curing time. The brittleness increases with increasing cement content and curing time. According to Dano et al. (2004) engineering properties has a great influence on compressive strength. According to the author the unconfined compression strength increase with higher relative densities. That's why the compressive strength is higher where the particles stay close together. In Haralambos (2009) research presented that the change in compressive strength of soil-cement mixture is dependent upon the grain soil distribution. The strength decrease with the percentage of fines for all cement content. This behavior is independent from the curing time of the cement. The tangent modulus value generally increases with cement content which is compatible with Haralambos (2009).

Although modulus and strength are not always directly related, the improvement in one parameter is often associated with the improvement of the other parameters. Improvement of soil modulus is required for reducing settlements, supporting pavements, or altering seismic response. An increase in strength is required for load-bearing or slope stability improvements. Soil improvement involves modification of site soils to improve their performance in meeting design objectives.

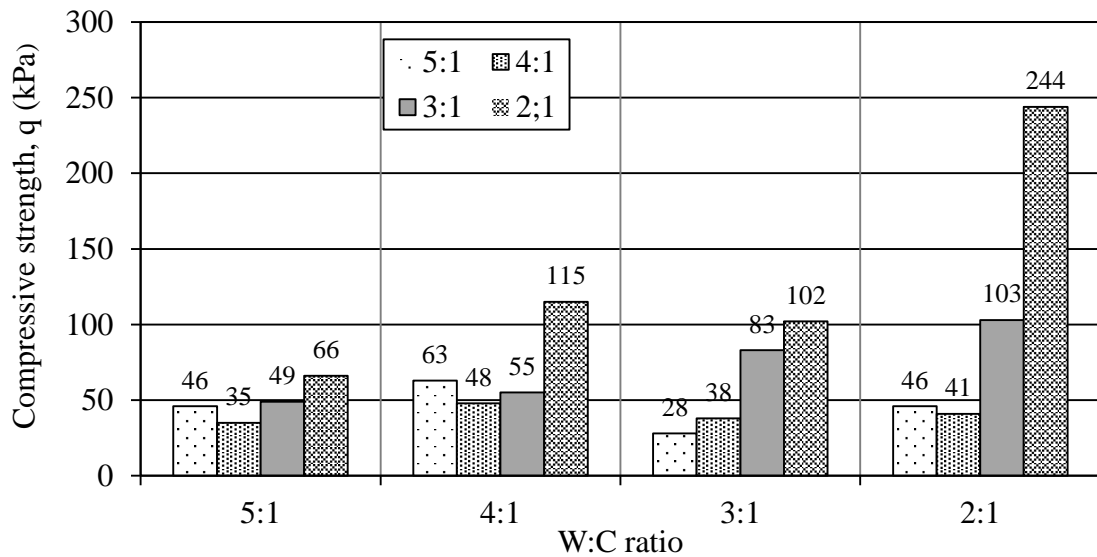


Figure 4.12: Bar chart of compressive strength and W:C ratio

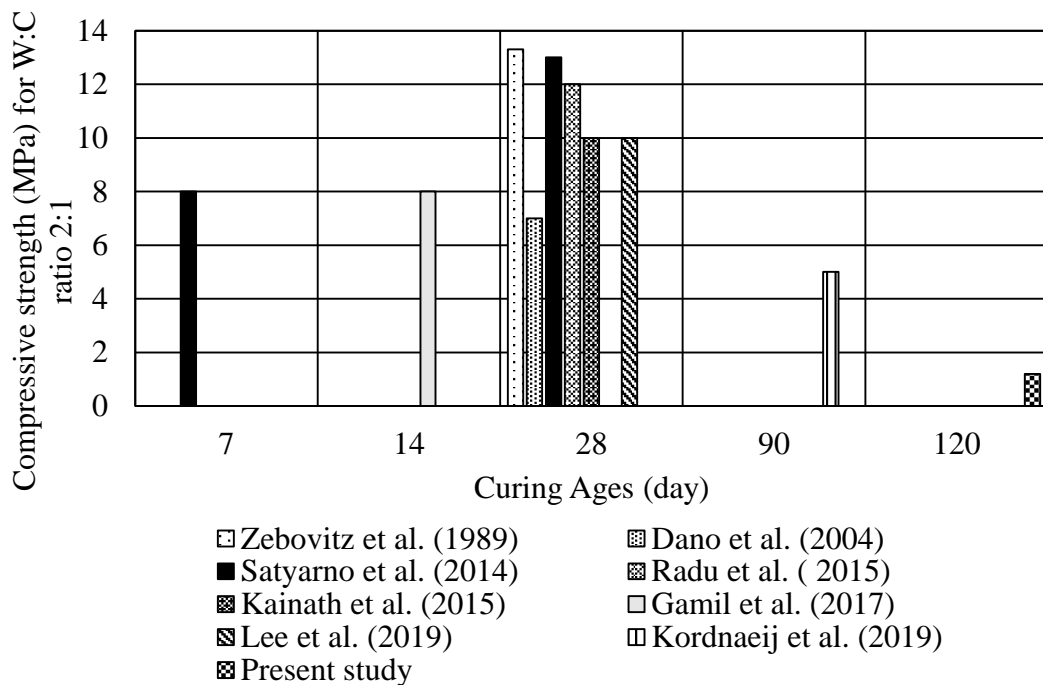


Figure 4.13: Bar chart of comparison of compressive strength (MPa) for W:C ratio 2:1 of present study with other researches for different curing ages

Table 4.6 Comparison of strength properties in grouted samples

Mix Ratio	Curing Time	7 Days	14 Days	28 Days	90 Days	120 Days
5:1	UCS, q (kPa)	27~18	31~27	40~18	68.5~25	
	Cohesion, c,(kPa)	9~13.4	9~20	13.5~15.5	12.5~34.25	-
	Young Modulus, ϵ , (N/m ²)	7~11	3~6	7~18.5	12~31	-
	Failure pattern	Column mode	Column mode	Column mode	Column mode	-
4:1	UCS, q (kPa)	12~28	22~30	37~57	43~62	-
	Cohesion, c,(kPa)	6~14	11~15	18.5~28.5	21.5~31	-
	Young Modulus, ϵ , (N/m ²)	11~14	6~12	7.4~8.7	12.3~28.3	-
	Failure pattern	Collapse	Collapse	Collapse	Collapse	-
3:1	UCS, q (kPa)	50~68	43~69	81~114	112~123	-
	Cohesion, c,(kPa)	25~34	21.5~34.5	40.5~57	56~61.5	-
	Young Modulus, ϵ , (N/m ²)	22~39	18~28	24~55	22~49	-
	Failure pattern	Axial split	Axial split	Axial split	Axial split	-
2:1	UCS, q (kPa)	52~101	100~125	82~187	200~386	1050~769
	Cohesion, c,(kPa)	26~51	50~62.5	41~93.5	100~193	385~525
	Young Modulus, ϵ , (N/m ²)	13~35	11~43	81~150	93~117	489~213
	Failure pattern	Shear failure	Shear failure	Shear failure	Shear failure	Slicken sides

Table 4.7 Comparison of compressive strength (MPa) for W:C ratio 2:1 of present study with other researches for different curing age

Author	Soil type	Device developed	Types of cement	Admixture used	W:C	Curing Ages (Days)	Compressive strength (MPa)
Zebovit et al. (1989)	D ₁₅ =0.15mm	√	Blast furnace slag based cement composed of ultrafine particles	×	2:1	28	13.3
Dano et al. (2004)	FS(D ₅₀ =200μm), SRS (D ₅₀ =530μm), A DM(D ₅₀ =410μm), ADC(D ₅₀ =1300μm), DS (D ₅₀ =240μm)	√	Superfine cement, particles size less than 12 μm	×	2:1	28	7
Satyarno et al. (2014)	D ₁₅ =0.15mm	√	Superfine cement	Bentonite	2:1	7	8
						28	13
Radu et al. (2015)	SP	√	Superfine cement	Slag lead content 30%	2:1	28	12
Kainath et al. (2015)	Sand, C _c = 0.9. C _u = 1.72.	√	Superfine cement	Bentonite	2:1	28	10
Gamil et al. (2017)	D ₆₀ = 1.5 mm and D ₁₀ =0.17 mm	√	Superfine cement	×	2:1	14	8
Kordnae ijeta al. (2019)	SP	√	Superfine cement	Zeolite	2:1	90	5
Lee et al. (2019)	D ₅₀ =1.6	√	Microfine cement	Bentonite	2:1	28	10

4.5.2 Triaxial Test Results

In the present study, triaxial compression tests were conducted for some treated samples in consolidated undrained conditions. From Table 4.4, 2:1 W:C ratio which are cured for 7 days are taken under confining pressures of 50kPa, 100kPa and 200kPa.

The physical properties of this group are dry density is 10.46 gm/cm³, moisture content is 29% and void ratio is 0.4 which are found from Table 4.5.

A summary of triaxial test results at failure is shown in Table 4.7. deviatoric stress (q), mean effective stress (p') are defined using the following equation:

$$q = \sigma'_1 - \sigma'_3 \quad (4.1)$$

$$p' = \sigma'_1 + 2\sigma'_3/3 \quad (4.2)$$

σ'_1 is the major effective principal stress, σ'_3 is the minor effective principal stress (Hamidi, 2014).

Table 4.8 Summary of triaxial test results

Cement content	Confining pressure (kPa)	Deviatoric stress (kPa)	Mean effective stress (kPa)	Axial strain (%)	Void ratio (e)	Pore pressure (kPa)
11	50	980	380	11.86	0.18	-192
11	100	933	413	10.84	0.2	-168
11	200	1354	657	10	0.25	-127

Figure 4.14 shows the typical failure modes of the cemented samples. Although dilation occurred at different confining pressure. Cemented samples with 11% cement content experience a mode of brittle failure and significant expansion of water with peak points in the stress-strain curve. In undrained conditions, cemented soil showed inclination of the shear band with horizontal axis in confining pressure from 50 to 200 kPa.

For cohesionless samples experiments indicates the brittle or dense curve. The dense soil like this grouted samples expands under shear to produce a new void ratio which further modifies to the critical void ratio at some strain. The increase in the void ratio for dense soil forms the dilation or increase in soil volume during shear as the interlocked soil grains with a statistical accumulation of increase in volume.

From the table 4.8, it is found that the deviatoric stress, and mean effective stress are increasing with the increase of confining pressure. In undrained conditions, in the dense samples, an increase of void ratio occurs the dilation and negative pore pressure though in the undrained condition the pore pressure should be increased.

Deviatoric stress – axial strain curves are depicted in Figure 4.14 for the undrained condition. Sample 1 showed some ductility at the first stage of the experiments. The peak axial strain increase with the confining pressure. The samples showed brittleness with the increase of confining pressure.

Using equation 4.1 and 4.2, deviatoric stress and mean effective stress are calculated, then void ratio are calculated from the changing weight of sample and pore pressure are calculated from the difference between first and last pore pressure during triaxial test. all are given in the Table 4.8.

The presence of cement has a significant influence on the triaxial behavior of sand; for sand sheared at a given confining pressure, cementation generally causes an increase in stiffness, peak strength, and the amount and rate of dilation with these effects with cement content. Cementation also influences the failure modes of the sand; brittle failure with the shear plane is often witnessed in cemented specimens. Particle crushing, while a separate phenomenon, also largely affects the stress and strain behavior of granular soils. In triaxial tests, particles breakage decreases the rate of dilation, which in turn influences any peak stress associated with the density.

Hamidi (2014) study that well-graded gravely sands indicated more dilation or negative pore pressure in poorly graded samples when it was tested at confining pressures of 50 kPa, 100 kPa, and 150 kPa. Here concluded that the strain associated with the peak deviatoric stress decreases as the cementation increase. Also, it indicated that the maximum rate of dilation and negative pore water pressure occurs after the maximum shear strength was obtained. Dilation occurred at different

confining pressure under undrained tests and showed barreling mode without shear plane formation. Cemented samples with more cement content experienced a mode of brittle failure and underwent significant dilation with an apparent peak point in the stress-strain curve. It also showed that the inclination of the shear band with the horizontal axis decreased with an increase in confining pressure from 50 kPa to 150 kPa.

Hitcher et al. (2008) investigated the mechanical properties of sand as its stiffness, cohesion, and, to a less extent, friction angle can be increased through the process of grouting. The influence of the cement content in the sand pores can be seen by the increase of the material strength with the increase of W:C at every confining stress. The macroscopic cohesion c due to cemented intergranular bonds and the friction angle ϕ due to interparticle frictional contacts are determined by plotting the maximum strength envelope in Mohr–Coulomb’s diagram. For uncemented granular soils, one obtains a straight-line failure envelope with zero cohesion. For grouted sands, a straight-line failure envelope that is almost parallel to that of the uncemented granular soil is obtained. In other words, the value of the friction angle is approximately the same, probably since permeation grouting with low injection pressures does not cause any disturbance of the particle assembly.

Jaforpour et al. (2014) investigated Zeolite- Cement grouted sand under consolidated undrained test. The peak deviatoric stress increased significantly due to cement grouting. The effect of cementitious bonds is considerable up to the yield stress and beyond that, the bond’s effect dissipates gradually. While uncemented sand specimens show ductile behavior, cement grouting leads to more brittle behavior. All of the specimens grouted with zeolite-cement suspensions show a contractive-like response with positive pore water pressure, followed by negative pore water pressure at the failure state. After q_{max} , the behavior of the specimens is ductile or brittle, depending on the Z and W/CM values.

Figure 4.15 proved that the pore pressure decreased though it was a consolidated undrained test, dilation increased the volume with the confining pressure.

The stress path which is seen at Figure 4.16, it moved linearly in the CU test. It reached a peak point, after that softening caused reversal of the stress path with the

same slope until failure stress reached. In undrained conditions, the peak point was high due to the generation of significant negative pore pressure.

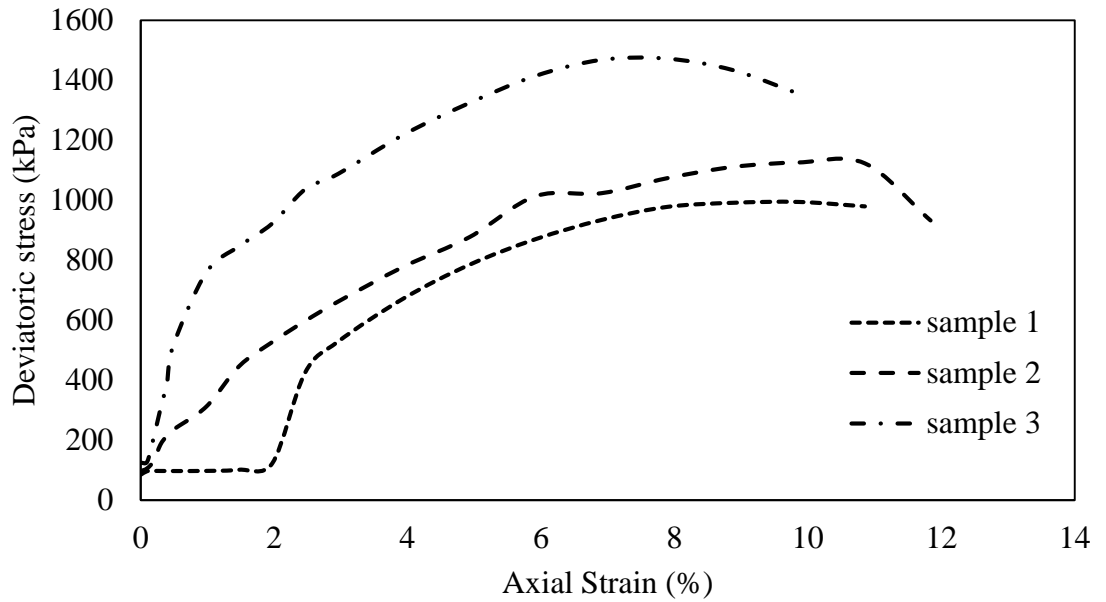


Figure 4.14: Triaxial test results (deviatoric stress vs axial strain curves)

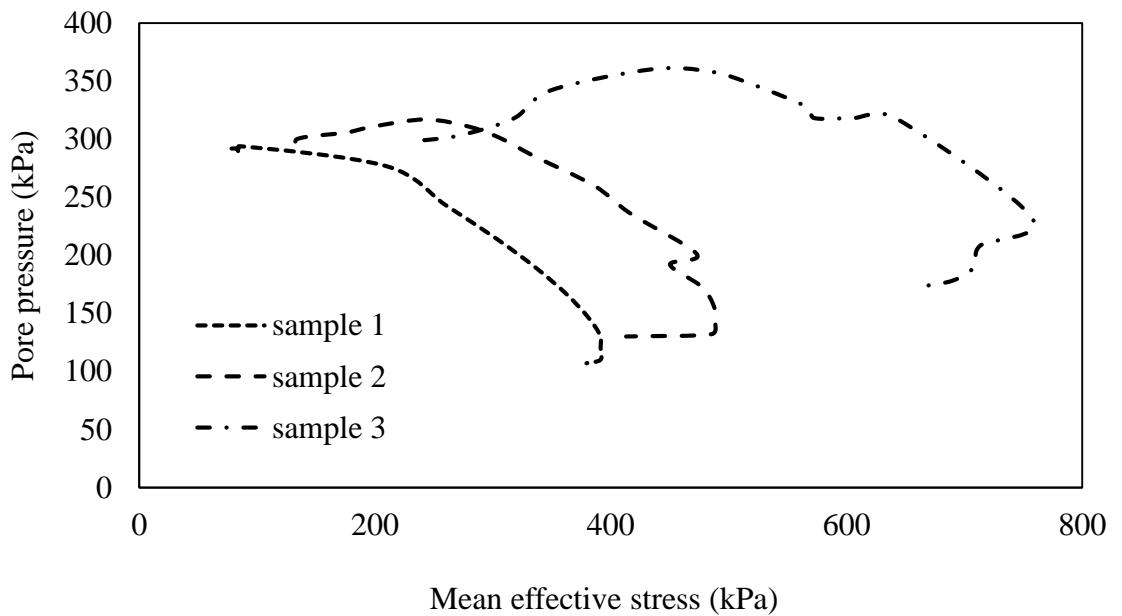


Figure 4.15: Pore pressure vs mean effective stress graph

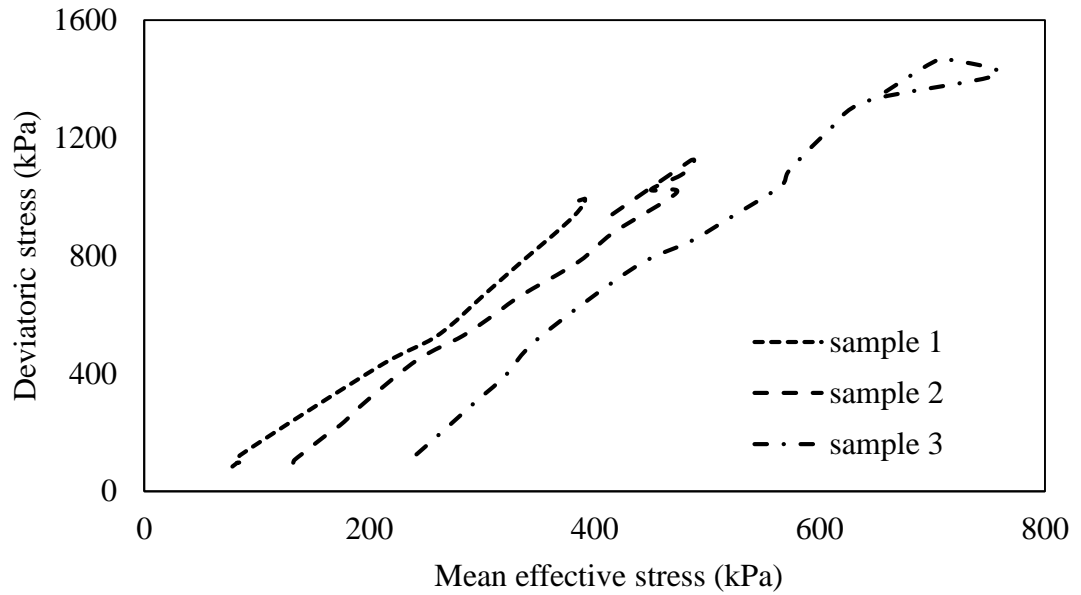


Figure 4.16: Stress path of triaxial test (mean effective stress vs deviatoric stress)

Results of triaxial tests on the cemented well-graded sand indicate the peak stress is associated with the axial strain of 6%. It confirms the more brittle behavior of cemented sand in the CU condition.

From Figure 4.17, upon the effective stress failure envelope, it was observed that the cohesion and angle of internal friction for consolidated undrained samples were $c = 200 \text{ kN/m}^2$ and $\phi = 37.4^\circ$

Finally, a Comparison of the results of a direct shear test on ungrouted samples and the triaxial test on grouted samples is that the cohesion developed after grouting and little change occurred in the angle of internal friction.

4.6 Failure Pattern of Grouted Samples

After injecting cement into sand in 2:1 ratio and give curing time to solidify the sand with cement then cohesion develop into the sand. Under the Unconfined compression test it behaves like a clay and gives multiple shear type failure pattern. However in the case of 5:1 ratio, the cement content is very much low than 2:1. Although the sand gets harden but there are lots of void in the sample. As a result under the test when it gets compression from the upper end then the molecule fills the void and after some time it gives column mode type failure pattern. The schematic diagram of different types of failure pattern are given in Figure 4.18.

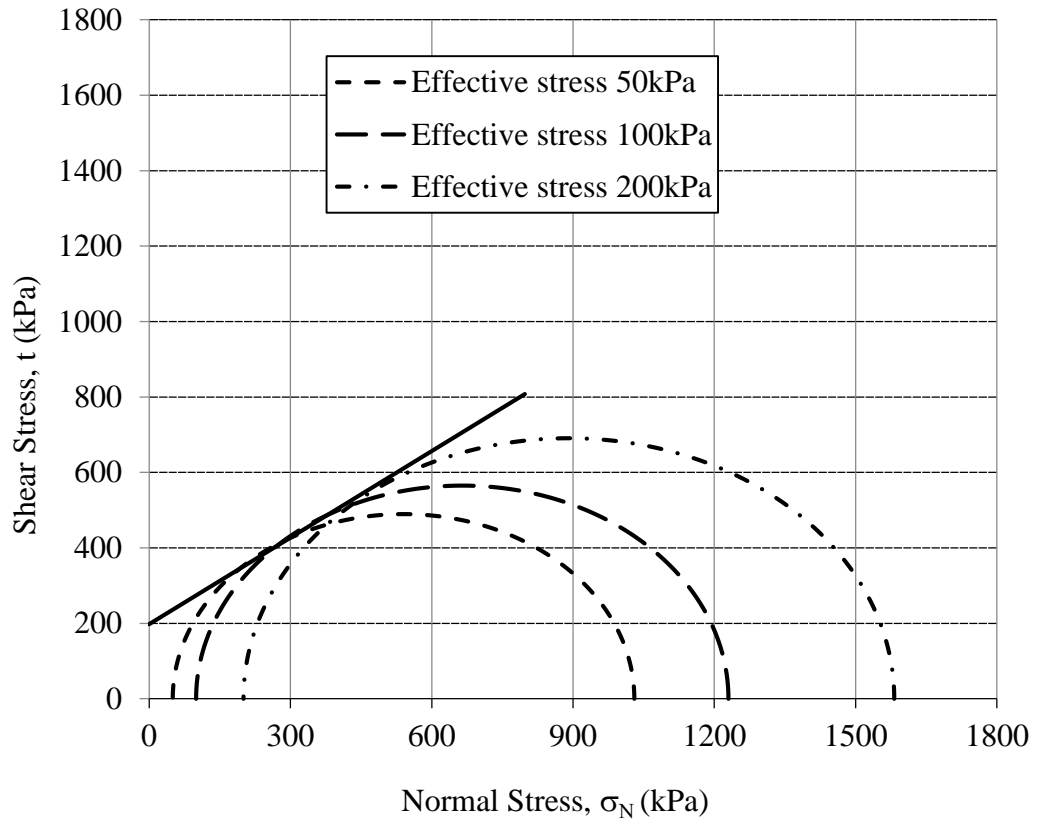


Figure 4.17: Shear stress vs normal stress of grouted samples

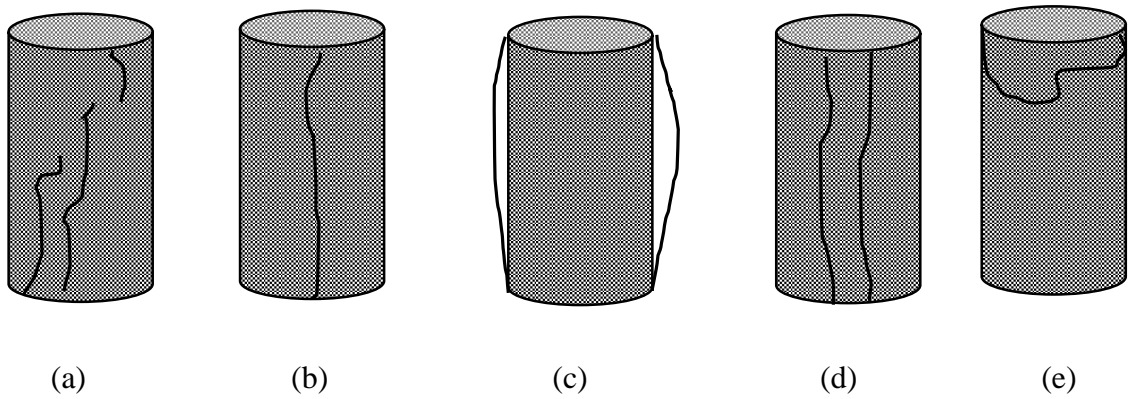


Figure 4.18: Failure patterns of grouted samples: (a) shear failure, (b) axial split, (c) bulging (d) collapse, (e) column mode failure

According to elasticity modulus, combining with table 4.5, the sample with different proportionate with 7 and 14 days curing showing bulging effect because of the low elasticity modulus and with the increasing of elasticity modulus the yielding failure have shown.

The modulus of elasticity refers to the stiffness of material. High modulus materials do not deform under load as much as those of low modulus. The sample were tending to yield or bulge under load. Here the load was perpendicular, the deformation of the low modulus of elasticity was a bulging effect whereas the load for the high modulus of elasticity caused an overstress condition and in extreme cases, failure (Figure 4.19).

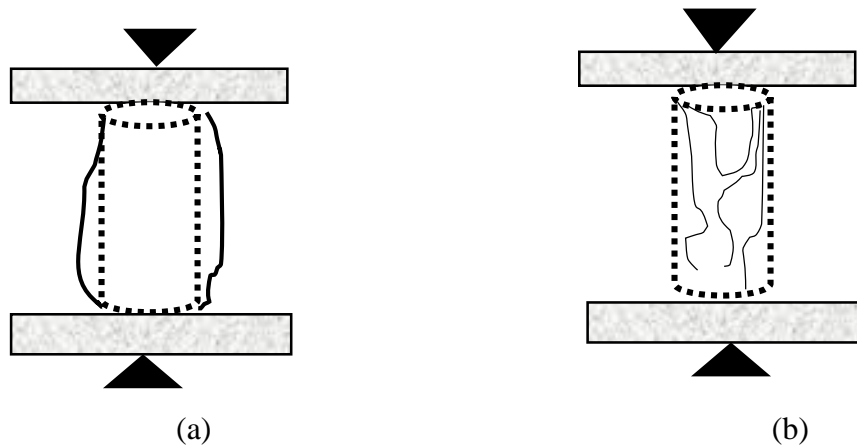


Figure 4.19: Deformed shaped under perpendicular load (a) bulging effect of low modulus of elasticity sample and (b) stress condition of high modulus of elasticity sample (Warner, 2004)

The cohesion developed into the sand by mixing cementitious grout suspension. Cohesion is an important grout property as it has a strong influence on the distance a grout can penetrate. In most cases, it is desirable to have high grout penetrability, which calls for low cohesion. Alternatively, there are instances in which it is desired to limit the travel of the grout in the formation. In such circumstances, travel can be limited through an increase in its cohesion.

After injection, when at rest, the individual particles of a fluid suspension grout tend to settle down of the solution, leaving excess mix water on the top of the settled solids is called bleed. It is of particular significance where injection rate is very slow and

the materials become essentially immobile. The bleed happened on the top of most sample.

The failure patterns obtained in this research are compatible with Wahab et al. (2021). That research paper the ductility changes were shown in the failure patterns, bulging was exhibited in untreated sample and inclined shape were appeared in 6%,9% and 12% cement content sample. In this current paper, 11% and 8% cement content sample shows bulging effect with different curing time. Multiple shear failure, Axial split, Collapse and column mode failure are experienced at different cement content such as 11%, 8%, 6.5% and 5.5% with 7,14,28 and 90 days of curing.

After 120 days there were experienced with new type failure pattern which was not discussed earlier. The name of the failure pattern is slickensides. Under the unconfined compression test the 120 days samples failed at the smoothly polished surface caused by frictional movement. Figure 4.20 showed the failure pattern, slickensides.

Figure 4.21, is tried to give a picture of what is happening after injecting grouting materials into sand. Grouting particles are too smaller than sand particles. The void of sand is filled up with grouting particles and give solid texture and create cohesion.



Figure 4.20: Failure pattern of 2:1 proportionate grouted sand after 120 days

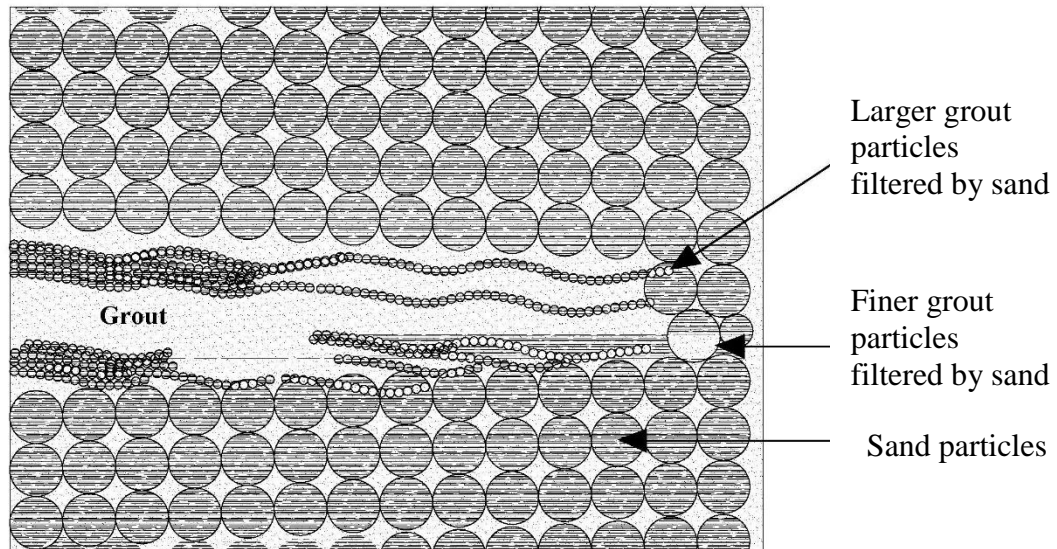
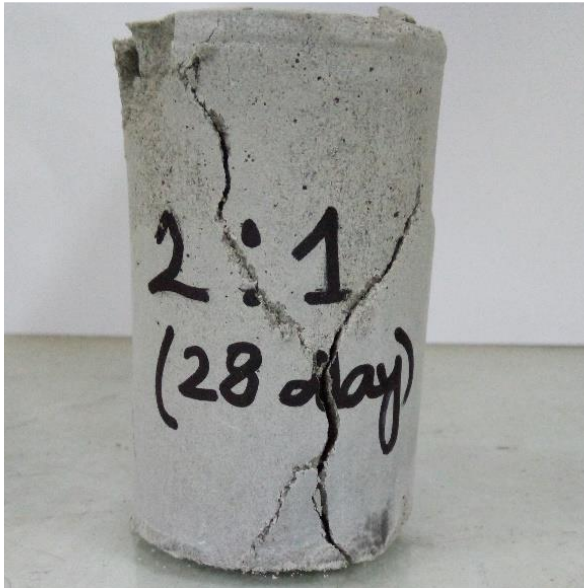


Figure 4.21: Sand compacted with grouting materials (Marchi et al., 2012)

The void of sand samples is filled with grouting materials about 120 days of curing. In this curing period complete bonding occurred between sand and grouting materials. Under the unconfined compression test, the failure occurred parallel with the maximum shear stress due to friction. This type of failure generally occurs on rock samples. That is why it is called slickensides failure as shown in Figure 4.20.

Li et al. (2020) described that permeation grouting has reinforcement effect in a sand layer and When water-cement ratio of slurry increases, compressive strength, deformation modulus, and impermeability of the grouted body reduce significantly. In the figure 4.22 and 4.23 have shown the differernt types of failure pattern which were found at laboratory under unconfined compression test. Here, it was seen that 2:1 W:C sampled always showed multiple shear failure for both the curing time of 28 and 90 days because of high cement content. Modulus of elasticity has influenced on W:C ratio 3:1 for both the cases and showed axial split. For the low cement content collapse and column mode failure were shown respectively of 4:1 and 5:1 W:C sampled. In these two cases there are lots of voids and under compression it has changed its volumn. The volumn decrease with the increase of compression pressure. That time some moisture as well as trapped air evaporated from the samples and after long time they give the following types of failure patterns.



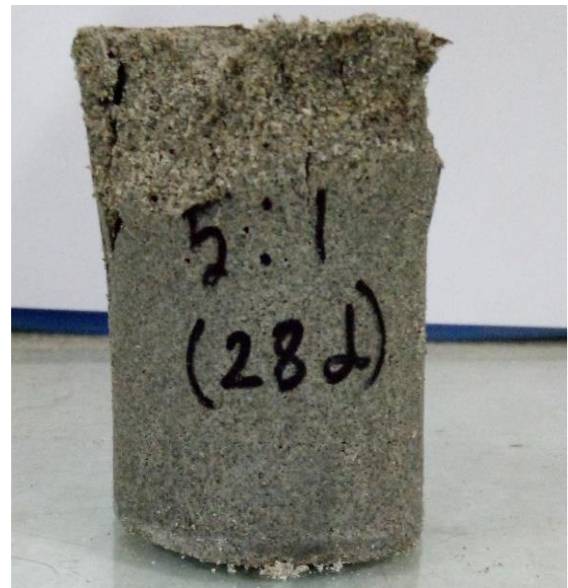
(a)



(b)



(c)



(d)

Figure 4.22: Failure pattern of different proportionate grouted sand after 28 days of curing: (a) Multiple shear failure for W:C 2:1, (b) Axial split for W:C 3:1, (c) collapse failure for W:C 4:1, (d) column mode failure for W:C 5:1



(a)



(b)



(c)



(d)

Figure 4.23: Failure pattern of different proportionate grouted sand after 90 days of curing: (a) Multiple shear failure for W:C 2:1, (b) Axial split for W:C 3:1, (c) collapse failure for W:C 4:1, (d) column mode failure for W:C 5:1

From the tri-axial test, the bulging that occurs at the top or bottom face of the samples proved that the volumetric increase with dilation effect and absorb water made inclined shear failure which was clear from the first two samples in Figure 4.24.

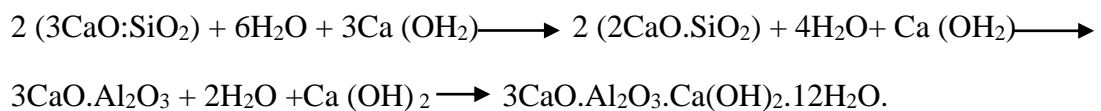


Figure 4.24: Failure pattern of 2:1 proportionate grouted sand under triaxial test

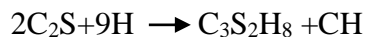
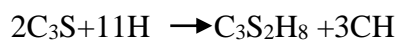
From the failure pattern (Figure 4.24) it was indicated that the maximum rate of dilation and negative pore pressure occurs after the maximum shear strength is obtained. The failure plane of the samples also showed that the failure patterns were combination of bulging and shear plane, although shear plane was not obvious and bulging effect was the predominate mode. Shear failure occurred when the vertical displacement gradually receded and some shear failure was observed when the bulging effect became apparent. These failure patterns also indicated that the cohesion was increased with slow rate of loading as well as confining pressure. The angle of internal friction was increasing with the increase of cohesion. The pore pressure response during the undrained condition is directly inflicted by the compressibility of air water mixture within the voids. Positive pore pressure observed at the initial stage of axial strain and the negative pore pressure are seen to develop with the increasing of axial strain. It was concluded with higher cohesion and also a higher angle of friction.

4.7 Microstructure Analysis

The improvement of the strength characteristics of sand through the addition of small percentage of Portland Composite Cement has been a popular ground improvement technique. Portland composite cement moderates heat generated by hydration and is specifically used for massive concrete structure such as dams. The combined effort has identified three fundamental effects caused by the reaction of cement with sand, namely moisture conditioning, cation exchange and pozzolanic reaction. A particular amount of water is required to achieve an optimum moisture content that coincides with the maximum dry density. The cementing action in granular soils is to produce of compounds and gels that increase the soil strength through complex pozzolanic activity. Cement tends to join at the points of contact between particles, which is dominated by the availability of moisture and the presence of finer particles.

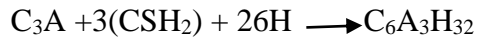


The formation of pozzolanic compounds at the end of the chemical reactions leads to improve strength and workability of the soil. The hydroxyl groups also elevate the pore water pH to a maximum value of approx. 12.45. Calcium hydroxide dissociation is a prerequisite to subsequent changes that determine the engineering properties of cement–sand mixes. The field treatments often provide properties that are less than the laboratory designed properties, hence, the laboratory mix design should always aim at higher properties than those that are stipulated by the specifications.



The principal hydration product is $\text{C}_3\text{S}_2\text{H}_8$, calcium silicate hydrate or C-S-H. C-S-H occupies about 50% of the structural component in a cement paste and forms directly on the surface of cement particles. It is usually called glue gel binder. Another product is CH, calcium hydroxide, produce a good crystalline with a plate shape in most cases.

The primary initial reaction of C_3A with water in the presence of a plentiful supply of gypsum.



The 6-calcium aluminate trisulfate-32-hydrate, is usually known as ettringite. Ettringite is a needle-shaped crystal with a large volume expansion. It will contribute to the early strength development since the needle – shaped crystals can work as reinforcement for the surrounding C-S-H and the expansion is not so significant.

For the purpose of scanning the surface and determine the organic content, the scanning electron microscope has been tested. The SEM picture of grouted sand with amplification factor $\times 2000$.

To confirm the presence of reacted materials found in the grouted sample, the microstructure is also analyzed by using SEM coupled EDS.

In Figure 4.25 and Figure 4.26 it is clearly showed that the void increase with the decrease of cement content. The lower cement content samples, there is the appearance of small particles, which consist mainly of calcium and Sulphur. These might correspond to ettringite which could have developed due to the aqueous relation between gypsum and tri calcium aluminate (C_3A ($3CaO \cdot Al_2O_3$)). The increase in the cement content led to the occurrence of sulphur-calcium rich zones comprised of ettringite. The CSH could have originated from the hydration of the components of cement (C_3S and C_2S ($2CaO \cdot SiO_2$)), but it's partial from the pozzolanic reaction.

In Figure 4.28, the image shows that there are microspores size of $10\mu m$ are visible in 2:1 W:C proportionate grouted sample. The honeycomb forms for the hydration reaction of PCC cement. The ettringite $Ca_3 Al (OH)_6 \cdot 12 H_2O \times (SO_4)_3 \times 2H_2O$ is locally formed in the pore voids. It is crystallized from the solution in the needle like forms, which can be up to $10 \mu m$ long. In Figure 4.27, the image of 3:1 grouted sample, the cement content is less than the 2:1. That causes lots of voids shows in the SEM picture. Also shows more C-S-H gel (calcium silicate hydrate) product reflecting the early hydration stage of the cement paste. The specimens are very heterogeneous, showing huge CH (calcium hydroxide) crystals that are characteristics for the early hydration of cement in initially high water content.

Figure 4.32, pore size distribution, and the amount of $\text{Ca}(\text{OH})_2$ of the stabilized samples compacted at 2:1 water cement contents after 90 days of curing. As the cement content increases, hydration products and the cementitious products significantly increase, which is clearly shown in Figure 4.29 to 4.32. The cementitious products not only enhance the inter-cluster bonding strength but also fill the pore space, as shown in Figure 4.29 to 4.32. As a result, the strength significantly increases with cement. After 90 days of curing the presence of hydration products and cementitious products is almost the same. This results in an insignificant change in the pore size distribution and, thus, the strength. Both the volumes of the highest pore size interval and the total pore tend to increase with cement. This is because the increase in cement content significantly reduces the water content, which decreases the degree of hydration and, thus, cementitious products.

The non-homogeneous shaped sample which we get from the trial 1 to trial 3 method, the 3:1 grouted sample had investigated and found that big formation of layers of C-A-H and C-A-S-H at $10\mu\text{m}$ size. After 14 days curing, very few voids found in the samples (Figure 4.32).

After 120 days, 2:1 samples showed more compressive strength than others. The formation of ettringite crystals, fibrous bundle C-S-H and Tetra calcium aluminate hydrate helped to get stiffening of sand-cement materials. These are the major constituents of Portland cements, are responsible for the main properties of cohesion and the sustainability of the sand-cement materials. From Figure 4.34 to Figure 4.36 showed and increase in ettringite, $\text{Ca}(\text{OH})_2$, CaCO_3 and CSH with an increasing cement content and curing time. This proved that the hydration, pozzolanic and alkali silica reactions increase as the cement content and curing time increase. The increase in the cement content led to the occurrence of Sulphur-calcium rich zones comprised of ettringite. Referring to the findings of some authors (Yu et al., 1999; Mitchell et al., 1998; Millogo et al., 2008; Mengue et al., 2016), the latter CSH could have originated from hydration of the components of cement (C_3S and C_2S), but its partial formation from the pozzolanic reaction involving sand minerals and cement content.

In the research paper Wahab et al. (2021) represent that the increasing cement content and curing time resulted in more hydration and pozzolanic reaction which is shown in Figure 4.29. The agglomerated part, indicating CAH (Calcium Aluminate

Hydrate), CSH (Calcium silicate Hydrate) and CASH (Calcium Aluminate Silicate hydrate) increased with cement content because of pozzolanic reaction with calcium ion of cement which is compatible with Wahab et al (2021) research paper. According to Kordnaeijetal et al., (2019) the consumption of $\text{Ca}(\text{OH})_2$ in the pozzolanic reaction makes secondary gels (C-S-H and C-A-H). In other words, the initial reaction (hydration) is necessary for the secondary reaction (pozzolanic).

Major cementitious bonds are induced by the hydration of cement, and the secondary cementitious products come from the subsequent pozzolanic reactions which is completely similar to this present study. Like calcium aluminate sulphate hydrate (C-A-S-H) minerals which have a very large expansive potential, ettringite absorbs very large quantities of water within its structure. During its formation, very high swelling pressure can develop with disruptive increases in volume. The ettringite occupies a greater volume than the original constituent reactants and grows as rod or needle-shaped crystals which shows in Figure 4.25, 4.26, 4.28, 4.30, 4.33, 4.34 like the research paper Oti et al. (2009).

Figure 4.34 to 4.36 clearly depicts that the voids were decreasing with the increase in curing times. From the three figures, the formation of the ettringite needle was increasing which gives the samples get solidify like a rock. The high cement content in these three samples also influenced to the creation of C-S-H fibrous bundles that give these three samples compact like a rock. Pozzolanic gel-like tetra calcium aluminate hydrate contributed to the samples being as hard as a rock. Therefore, After the unconfined compression test, the failure patterns of these three samples are different from others and identified the new pattern, slickensides. According to Cole et al. (2015) SEM is the modern thin section analysis to find out pores, identify the smallest minerals and distribution of minerals within the pores. In this experiment the sample were made with sand mixed with cement slurry. Therefore, this type of samples are the combination of resultant products of different types of hydration and pozzolonic reaction. The resultant products were distributed within the pores.

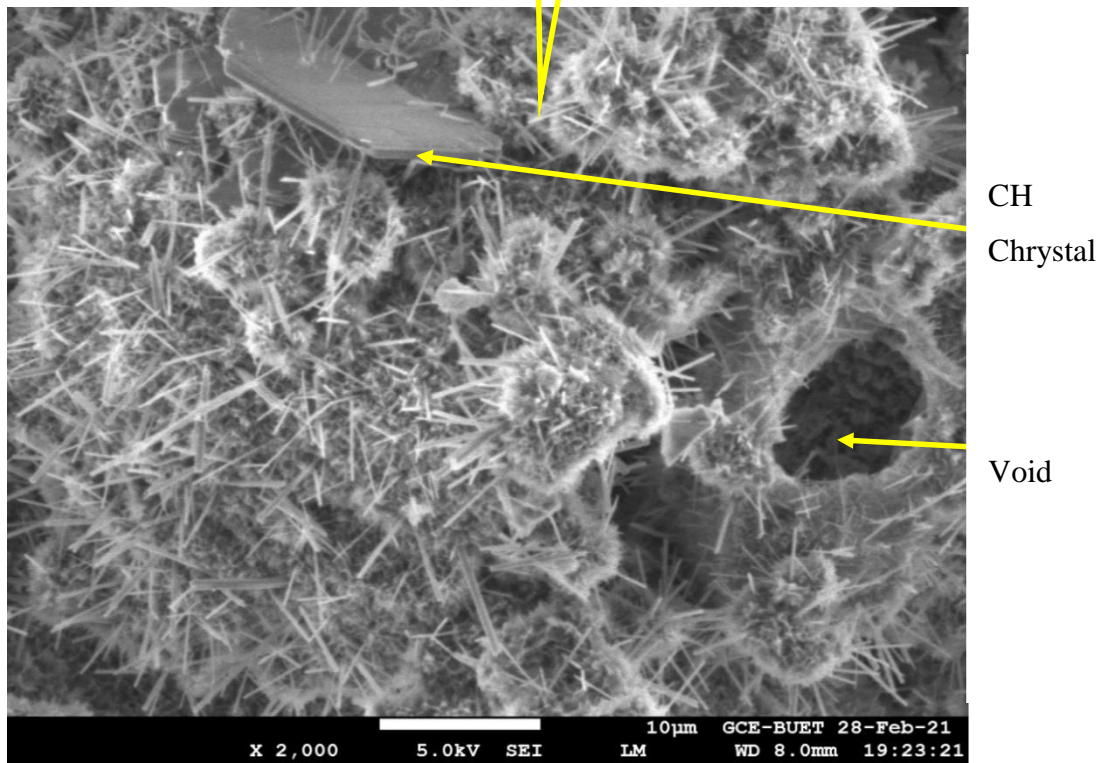
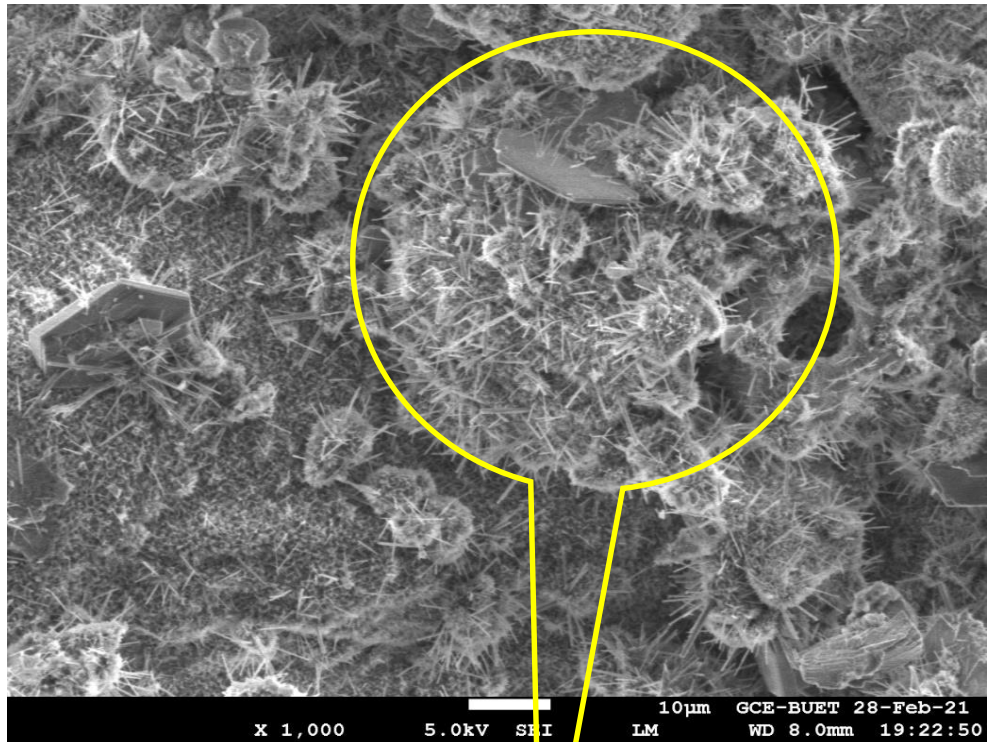
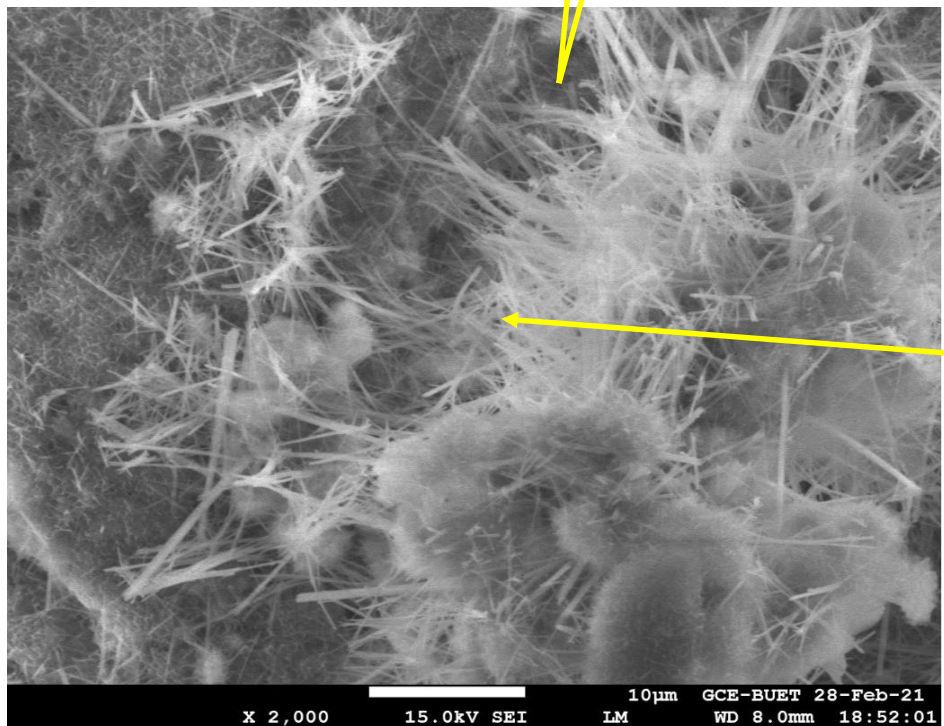
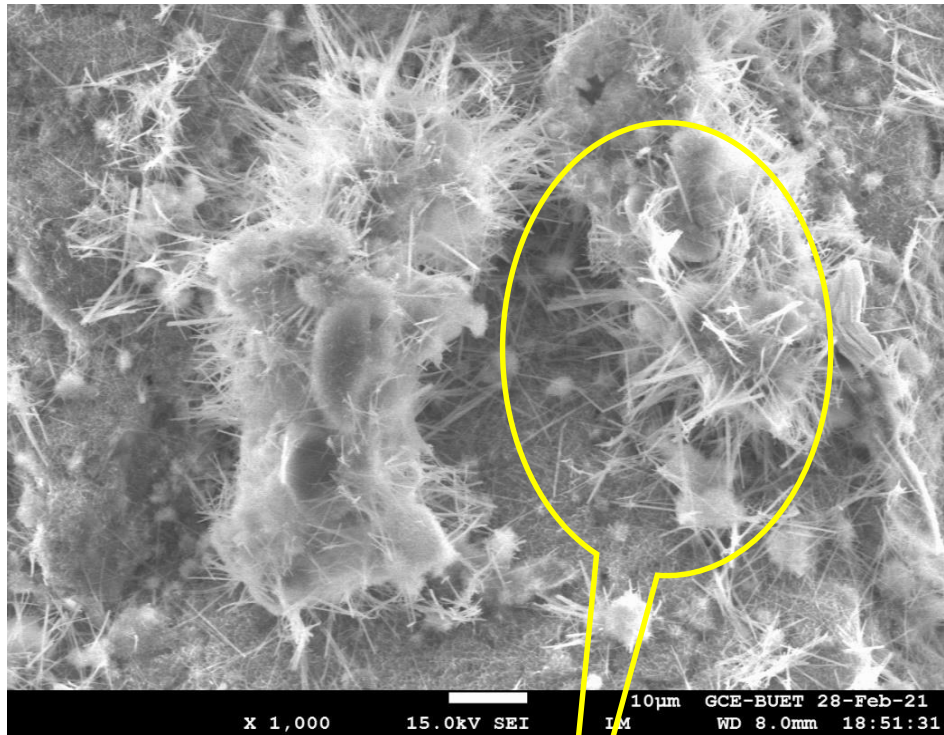


Figure 4.25: SEM image of grouted sand (5:1) after 28days of curing



The ettringite
needle

Figure 4.26: SEM image of grouted sand (4:1) after 28days of curing

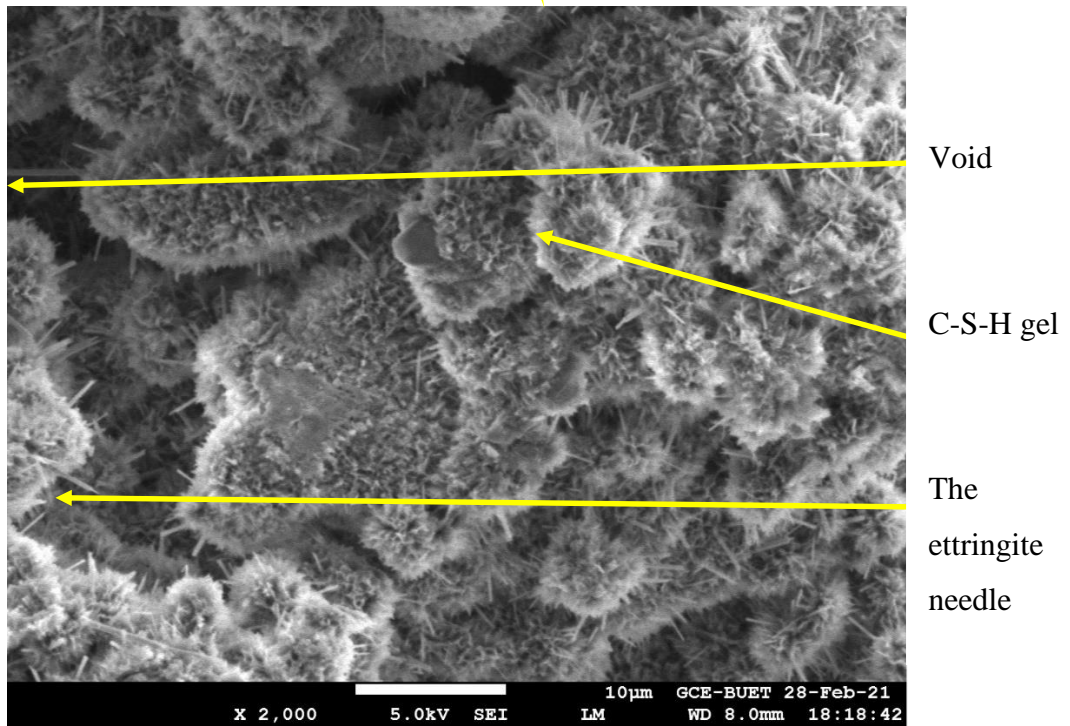
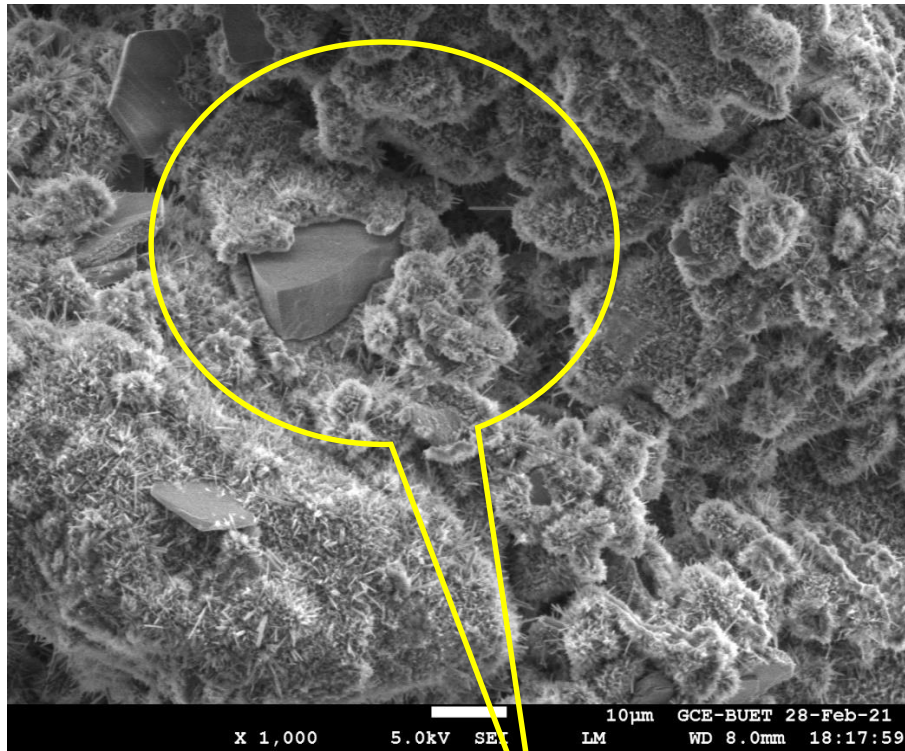


Figure 4.27: SEM image of grouted sand (3:1) after 28days of curing

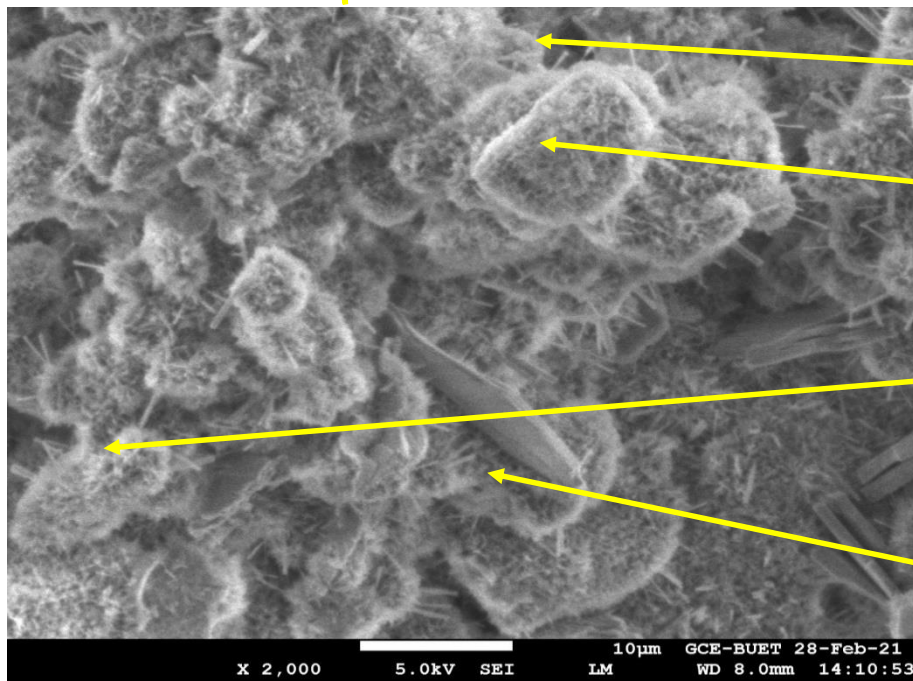
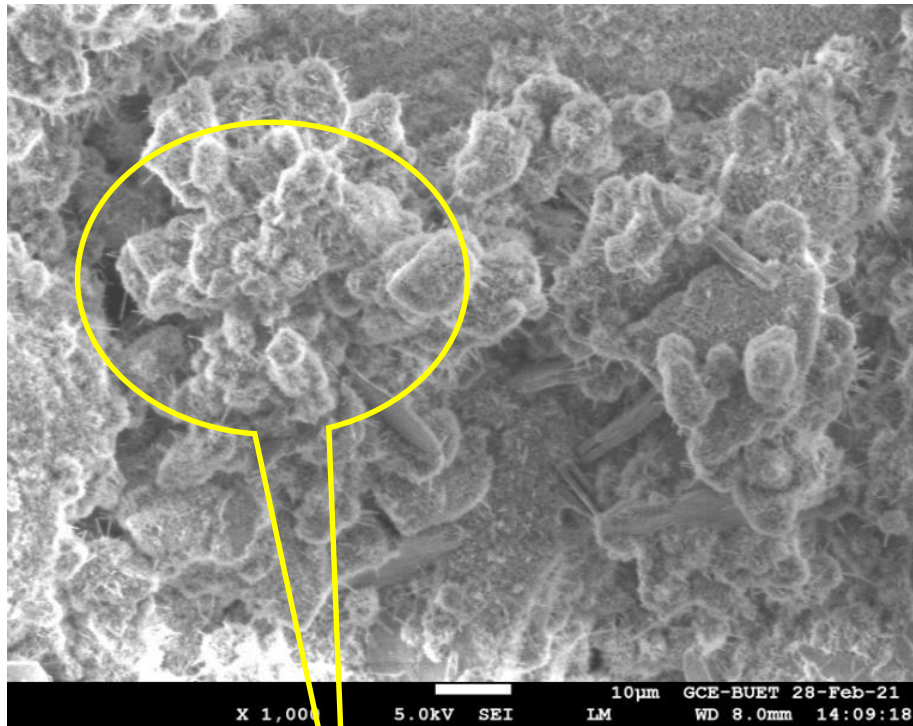
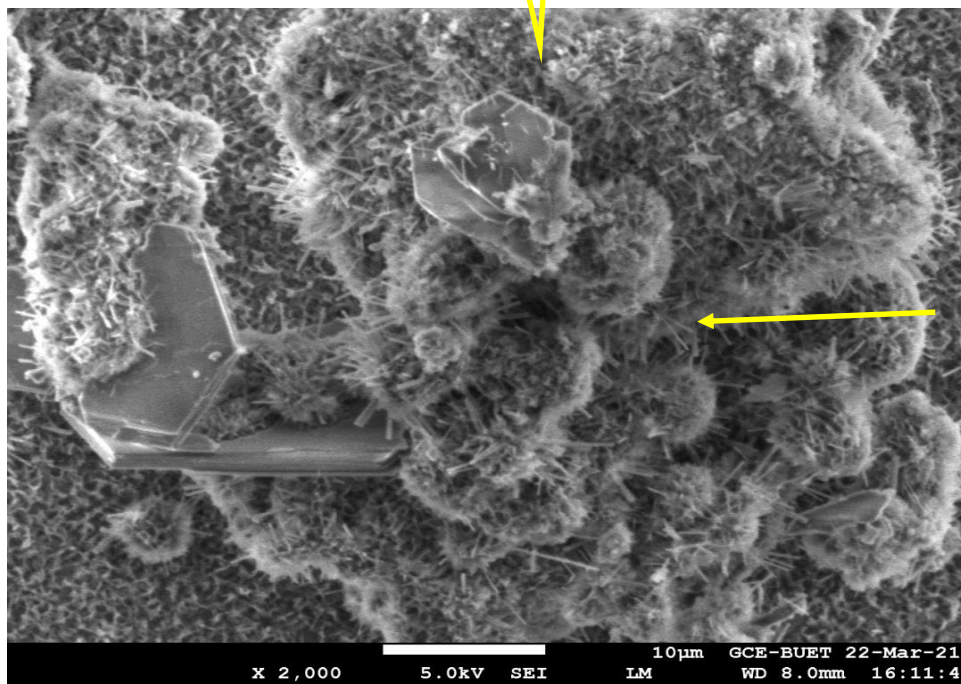
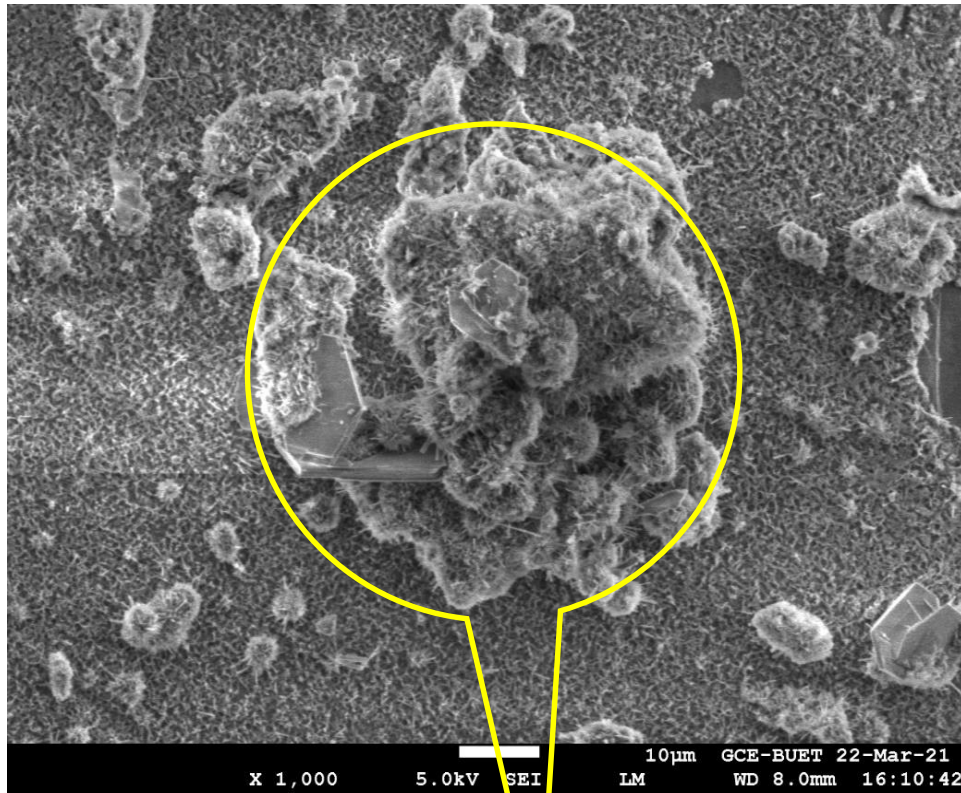
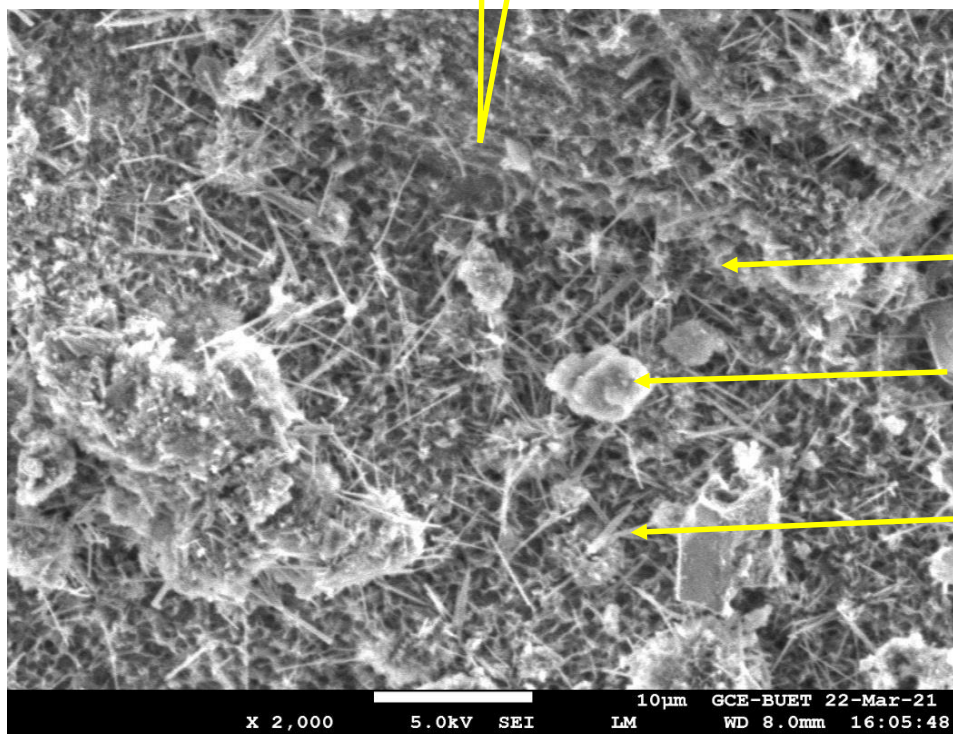
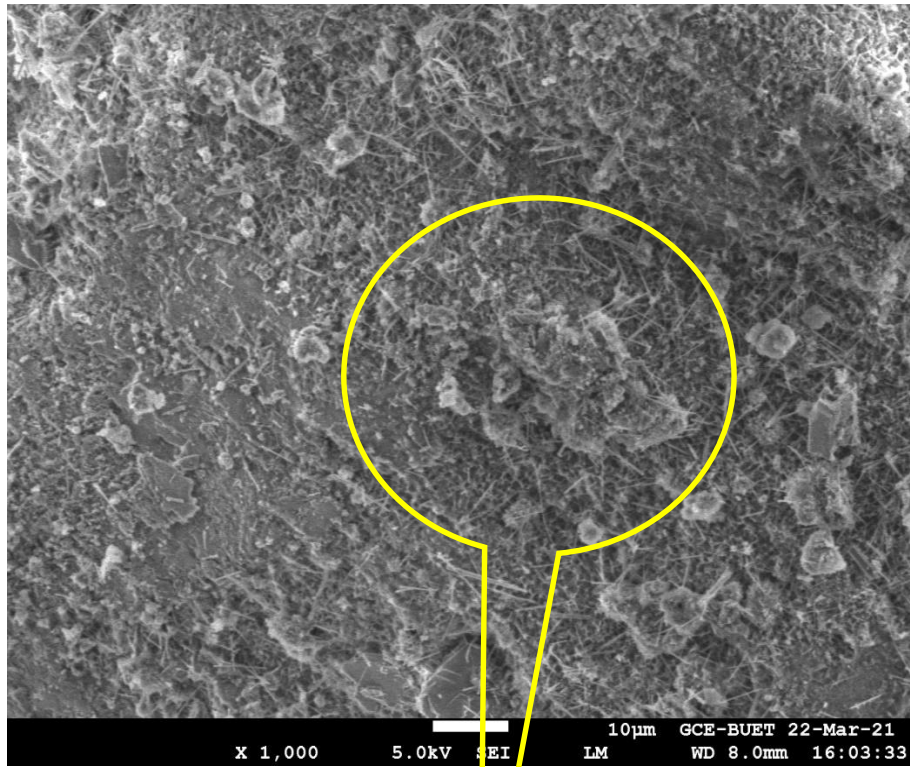


Figure 4.28: SEM image of grouted sand (2:1) after 28days of curing



Big C-S-H
gel

Fig 4.29: SEM Image of grouted sand (5:1) after 90 days of curing



4.30: SEM Image of grouted sand (4:1) after 90 days of curing

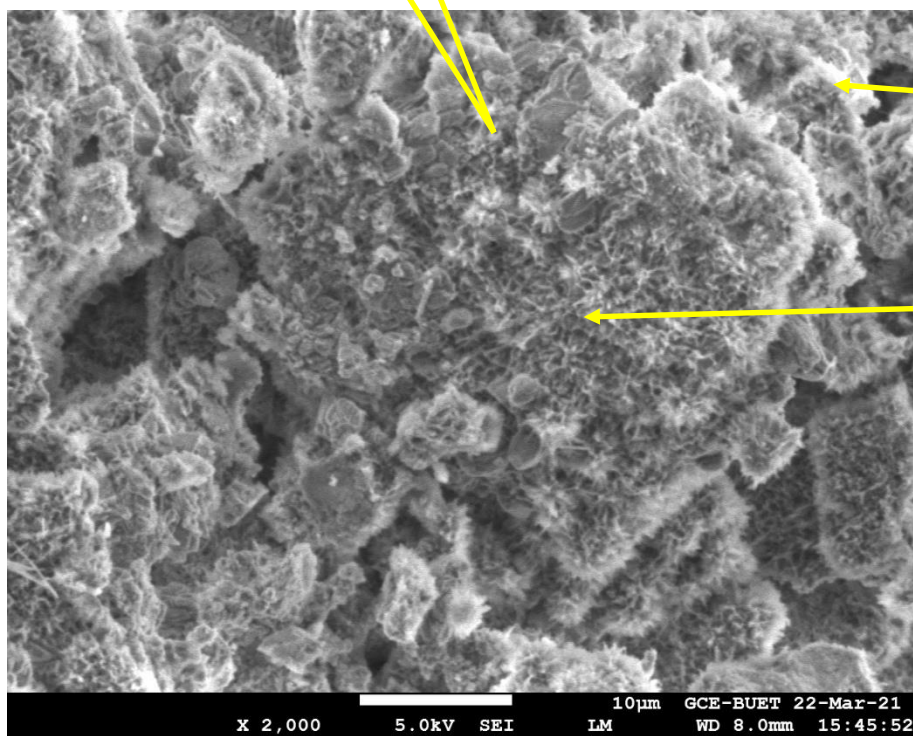
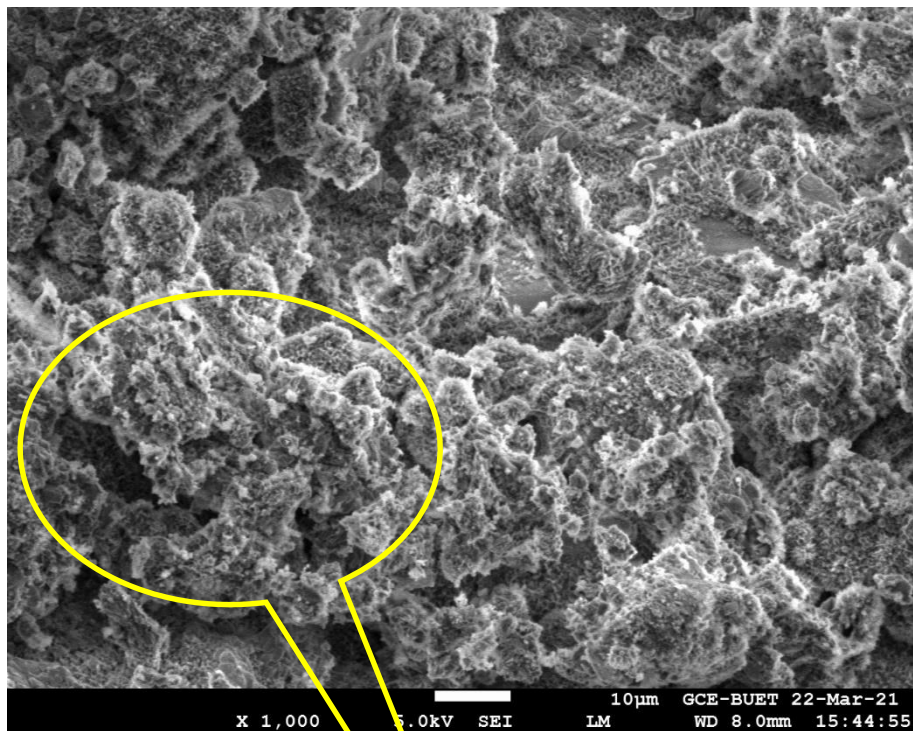


Figure 4.31: SEM Image of grouted sand (3:1) after 90 days of curing

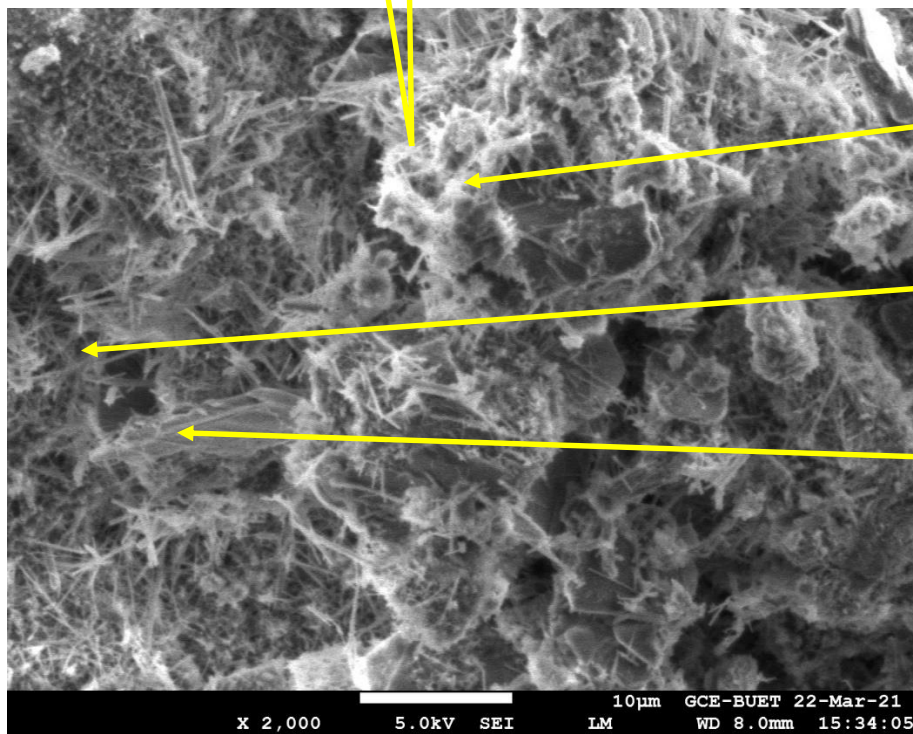
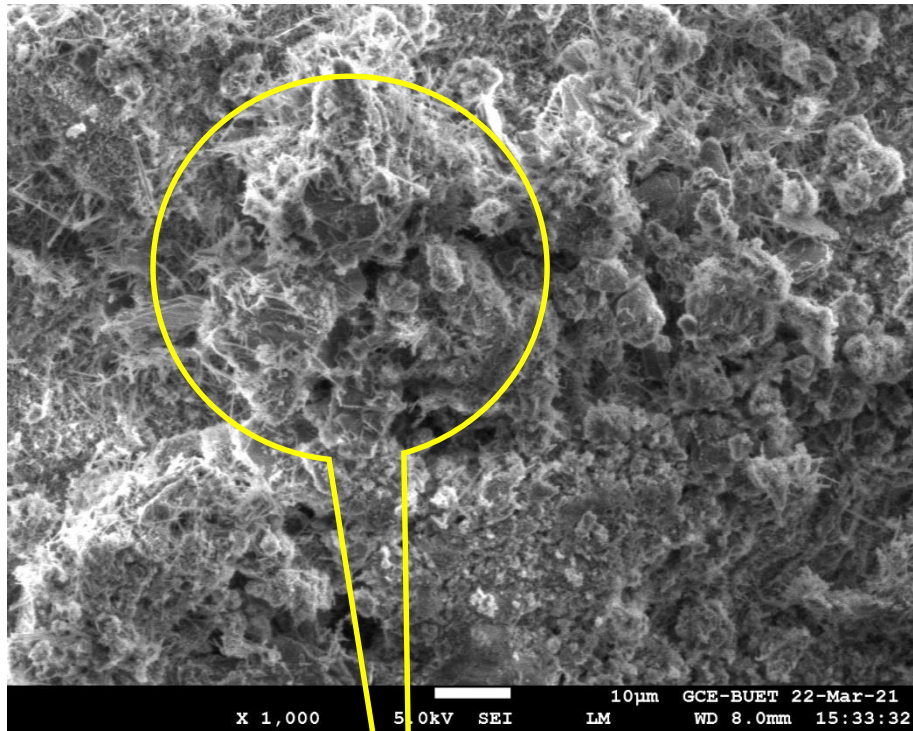
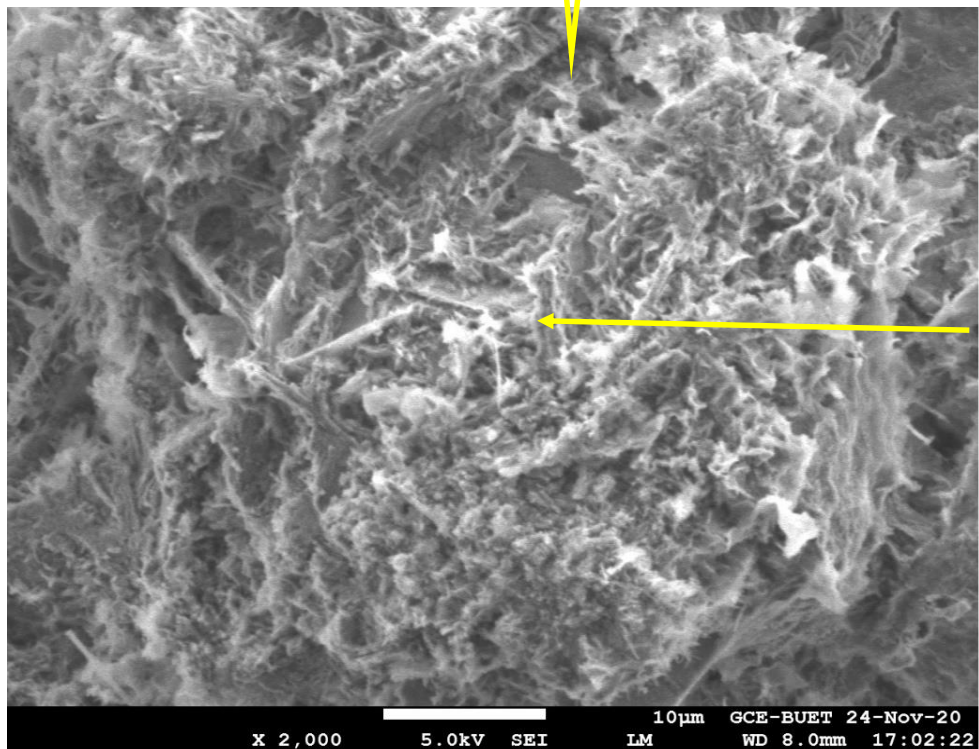
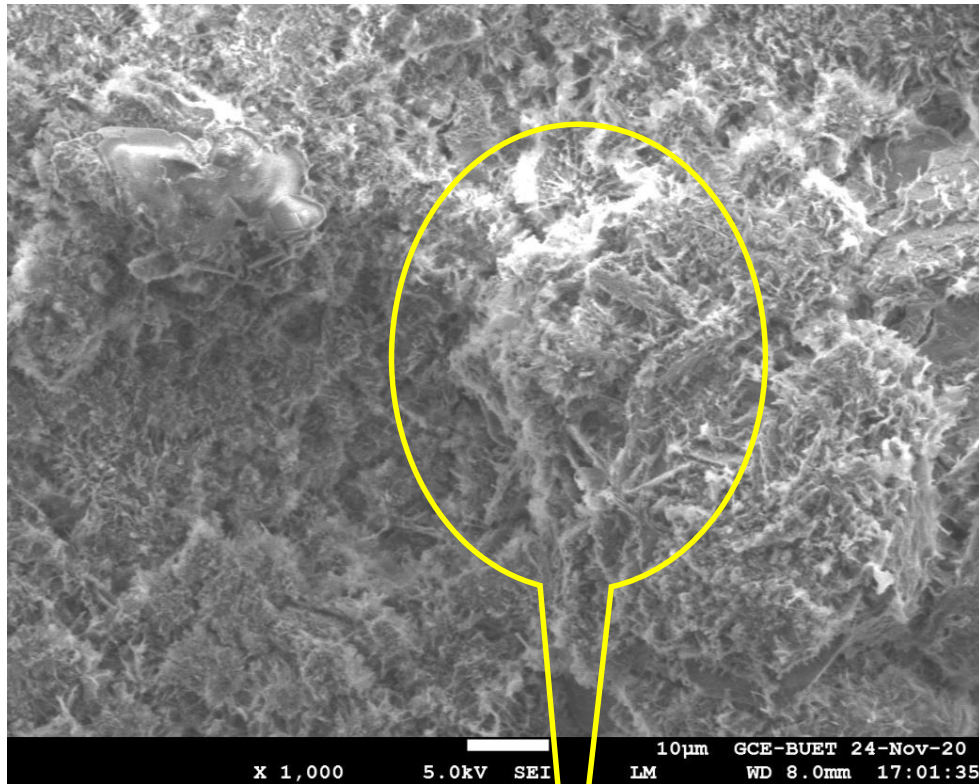
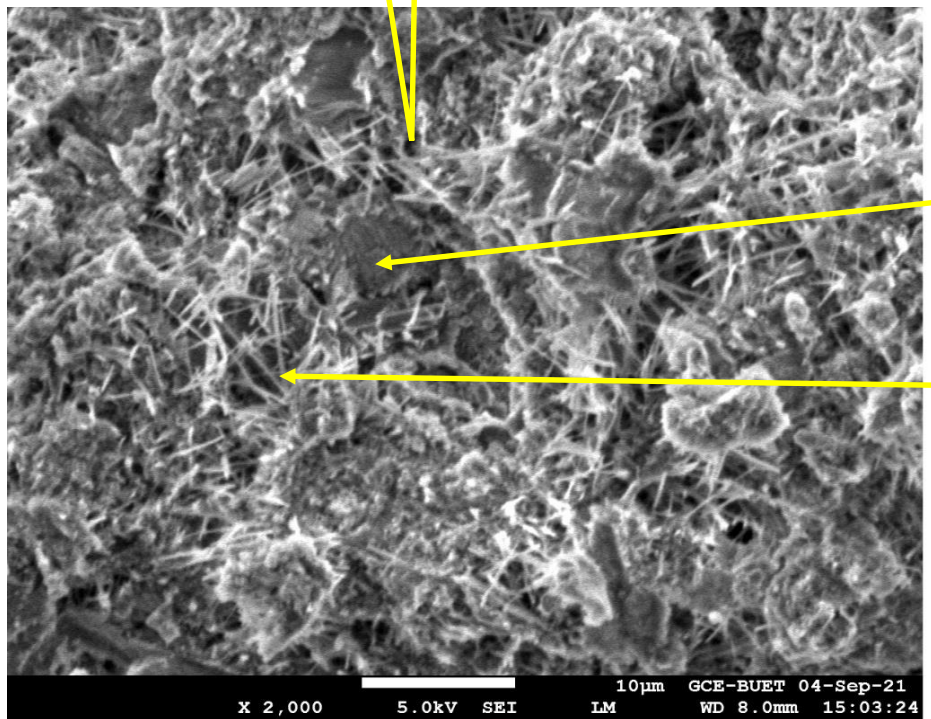
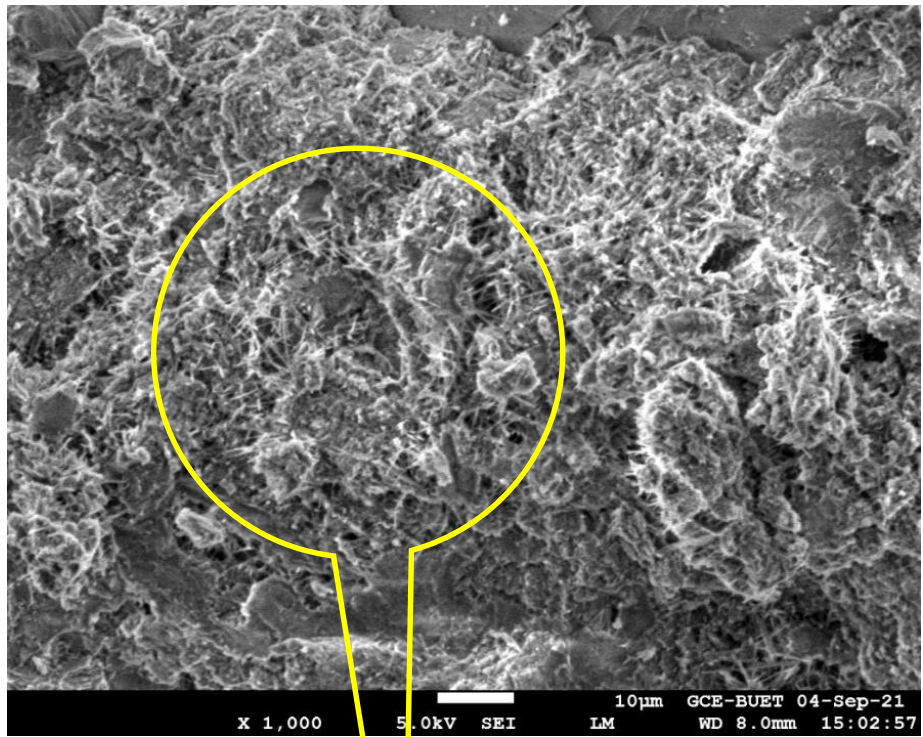


Figure 4.32: SEM image of grouted sand (2:1) after 90 days of curing



Layer of
formation
of C-A-H
and C-A-
S-H

Figure 4.33: SEM Image of grouted sand (3:1) after 14 days of curing (nonhomogeneous shaped sample)



C-S-H
fibrous
bundles

The
ettringite
needle

Figure 4.34: SEM Image of grouted sand (2:1) after 120 days of curing (sample 1)

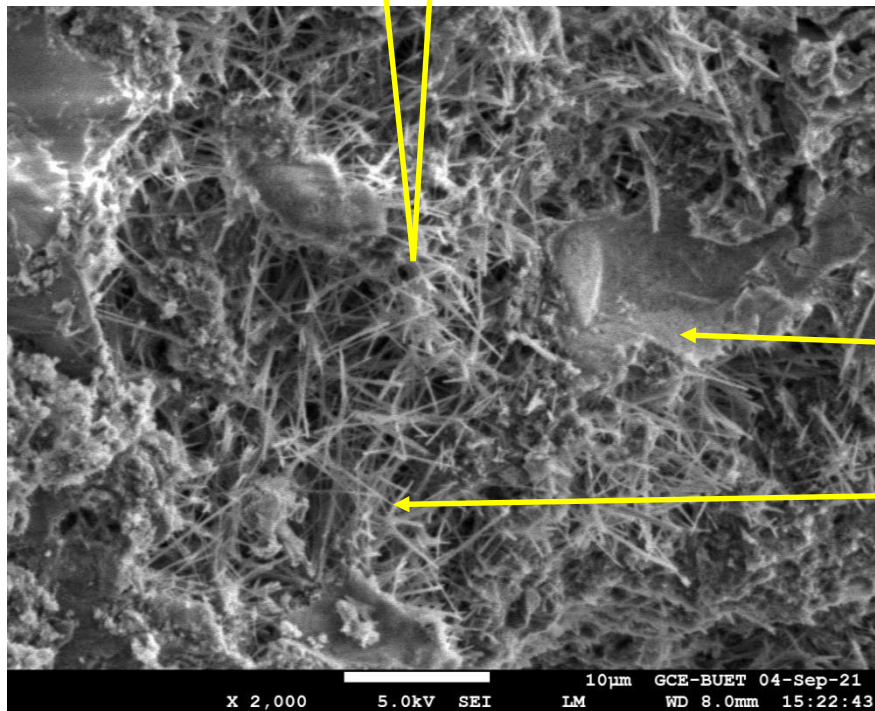
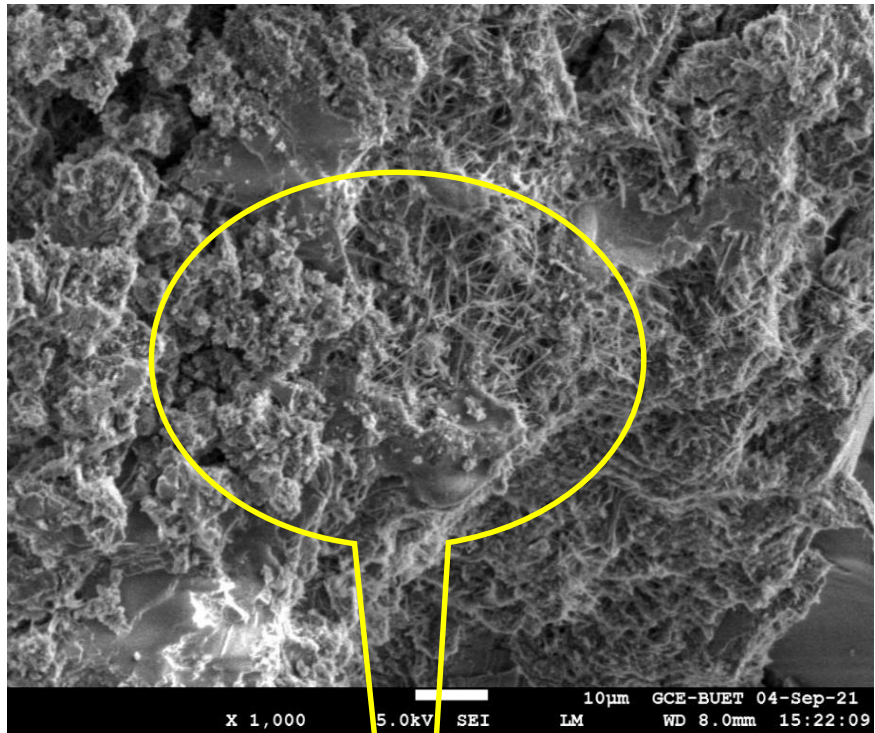
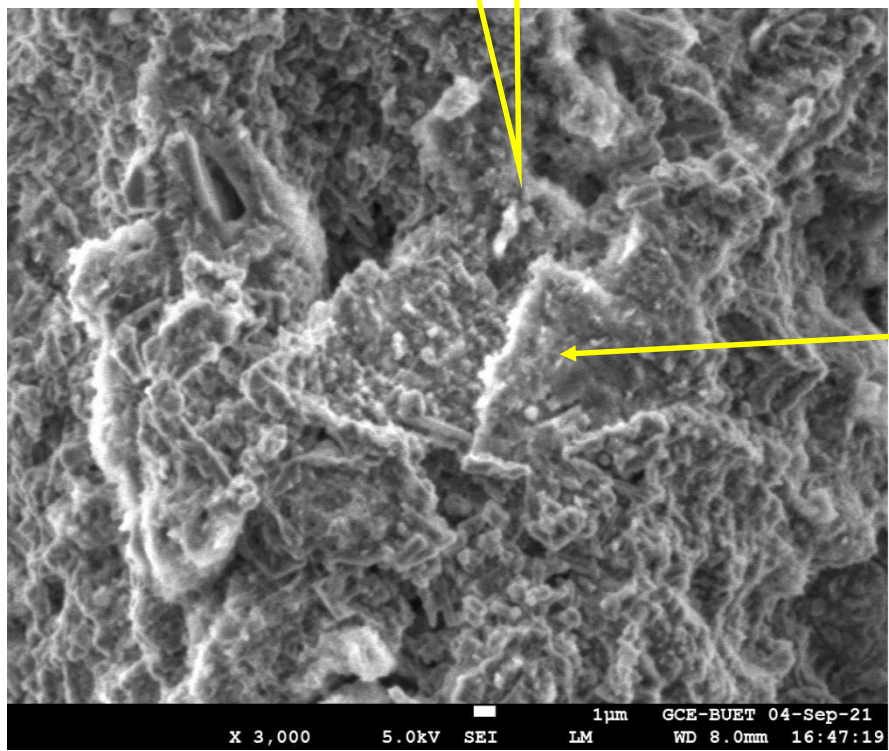
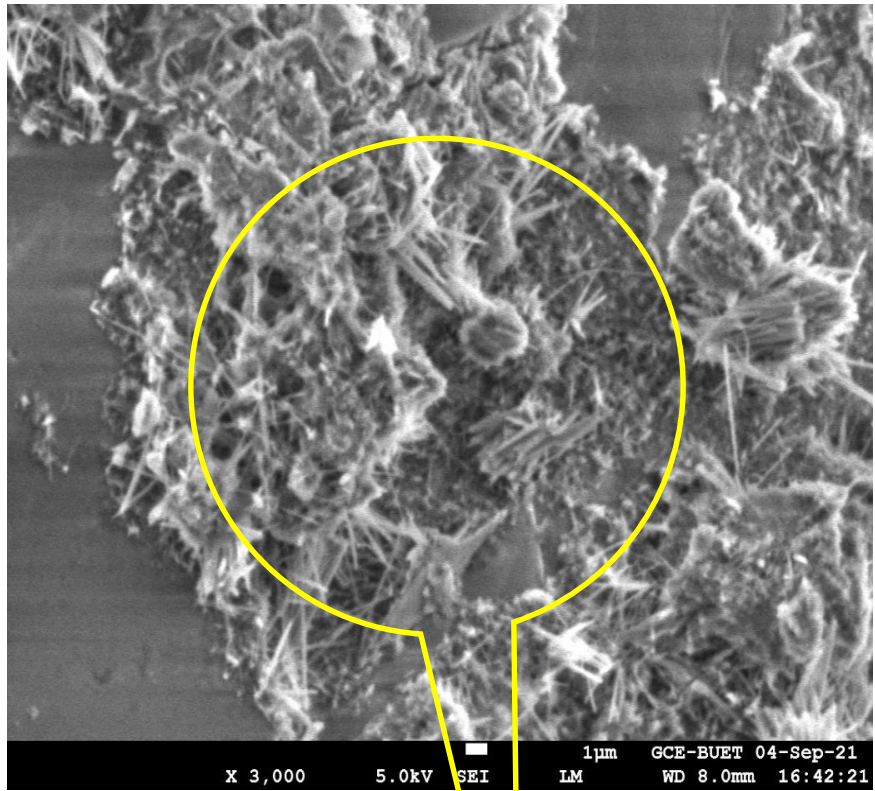


Figure 4.35: SEM Image of grouted sand (2:1) after 120 days of curing (sample 2)



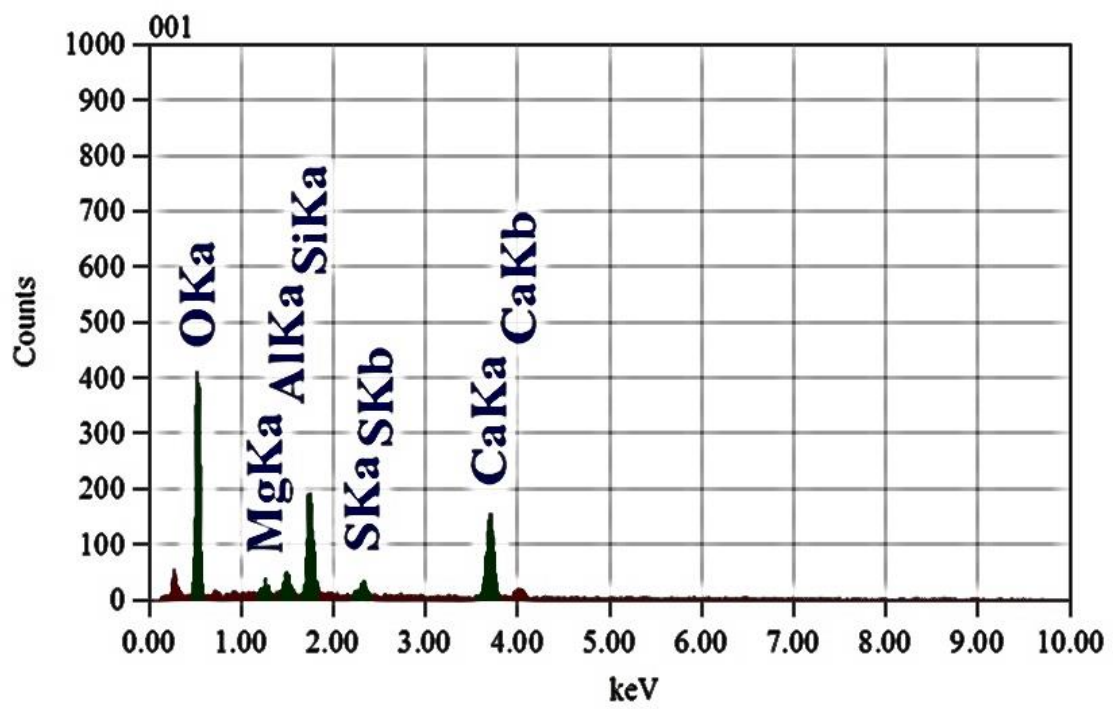
C₄AH₁₉

Figure 4.36: SEM Image of grouted sand (2:1) after 120 days of curing (sample 3)

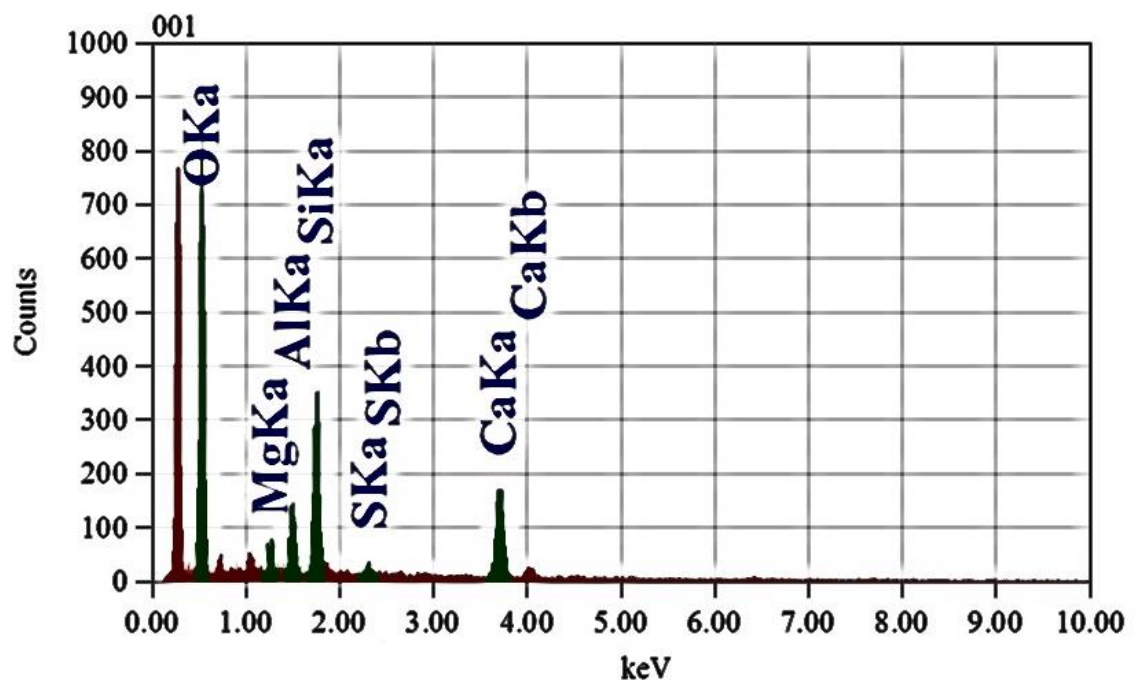
4.8 Energy Dispersive Spectroscopy (EDS)

Energy Dispersive Spectroscopy (EDS) can be used to determine which chemical elements are present in a sample, and can be used to estimate their relative abundance. Scanning Electron Microscopy (SEM) coupled with Energy Dispersive Spectroscopy (EDS) has many applications in cementitious materials. For example, it can be used to obtain the C-A-S-H composition, to analyse the composition of complex SCMs, to calculate the degree of reaction. Elemental analysis of surfaces in SEM is performed using energy dispersive spectroscopy (EDS), which measures the energy and intensity distribution of X-ray signals generated by the electron beam striking the surface of the specimen. As can be seen on the EDS of grouted sand, high intensities of Oxygen(O₂) was observed from the all the proportioned samples of 5.5%, 6.5%,8% and 11% cement content. Second high intensities of (Al) was found from the following EDS. The strove peak (keV) is high at 0 in Figure 4.37, because in an X-ray spectrum, a noise peak sometimes appears near the zero voltage level. This small amount of electrical noise is always present from any type of detector. Peaks at low energies below 1 keV might indicate various elements (such as the K α line for carbon, L α line for calcium, or M α line for lanthanum).

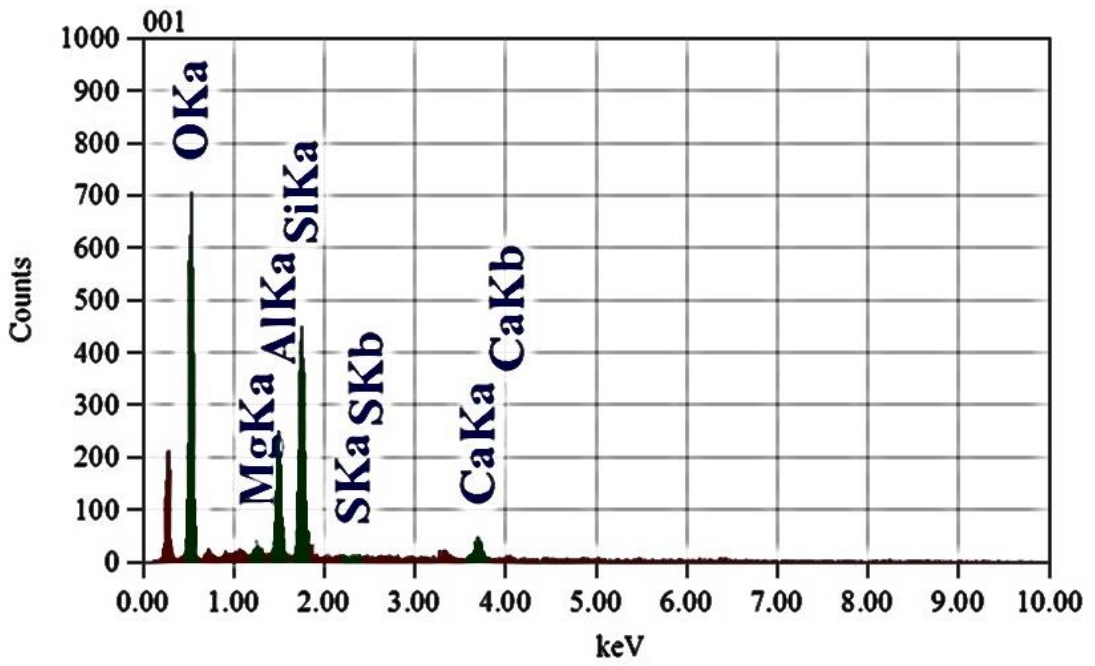
In Figure 4.38, the same condition was observed but the electrical noise is not very high in 2:1 proportionate grouted samples. The third image the count of chemical reaction is very negligible. From two cases, most of the atom of oxygen travel from M to L and from L to K and lowest number of atom of calcium travel from M to K. The most common component of sand is silicon dioxide in the form of quartz. The intensities of Oxygen as well as Silicon were observed specially in Figure 4.38 (a) and (b). These two componants dominated the cementitious reaction for 2:1 grouted samples after 120 days of curing. From EDS, the traveling of Oxygen and silicon atom prove the presence of filling sand.



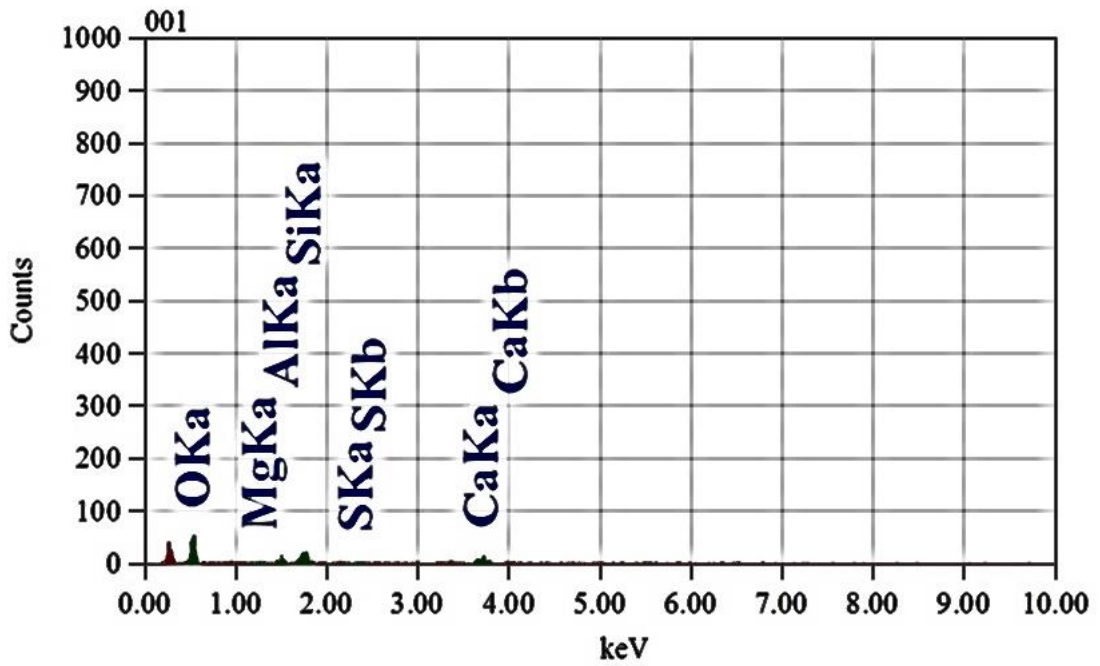
(a)



(b)

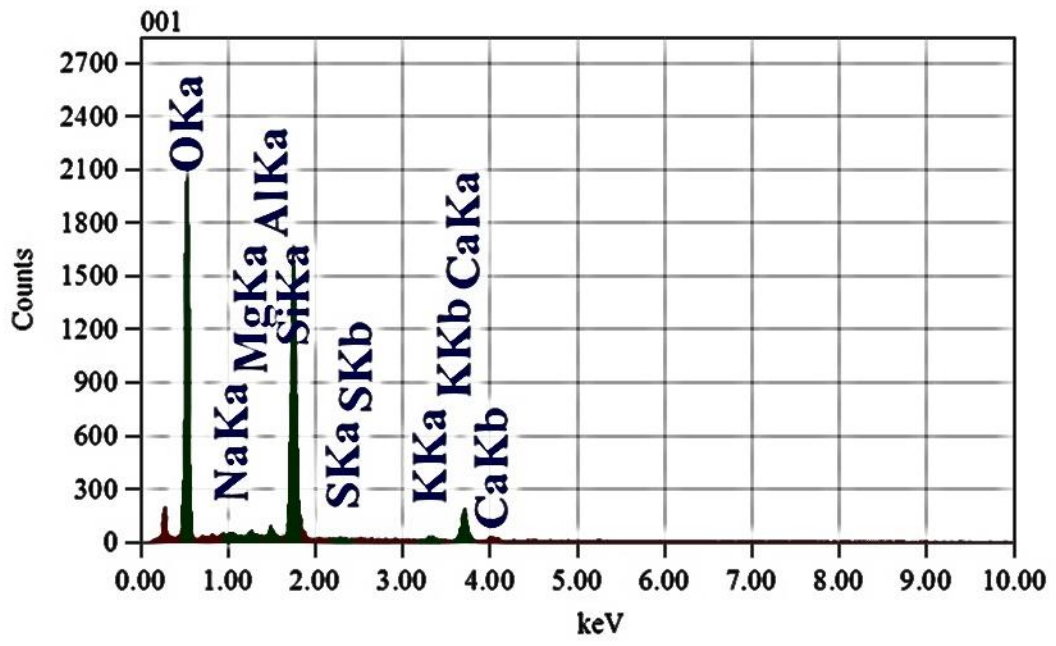


(c)

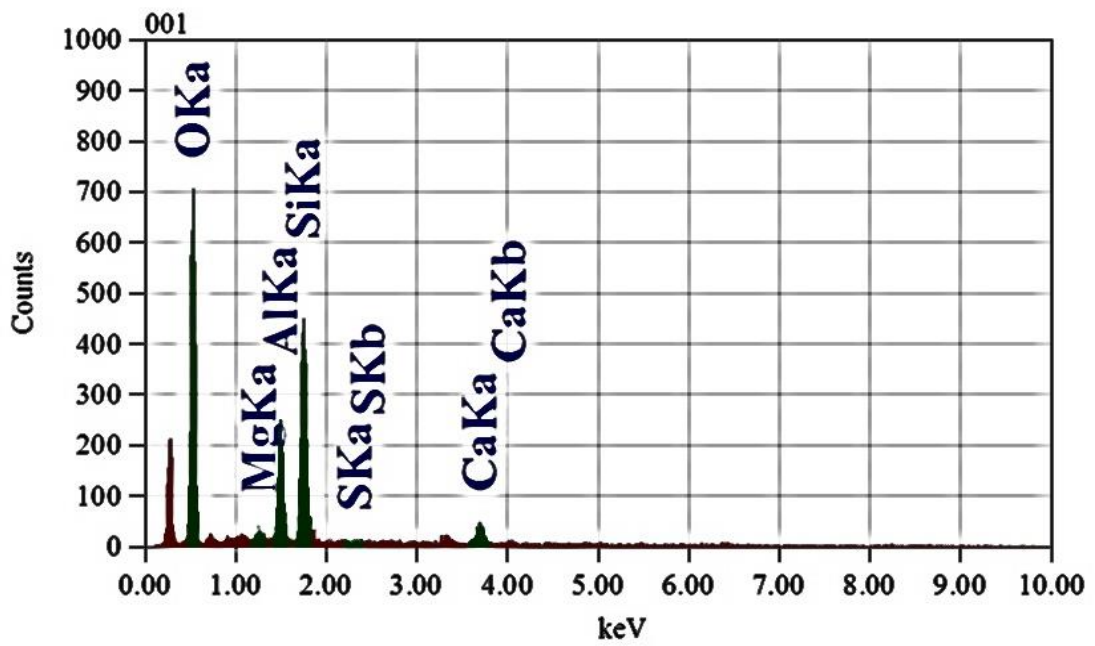


(d)

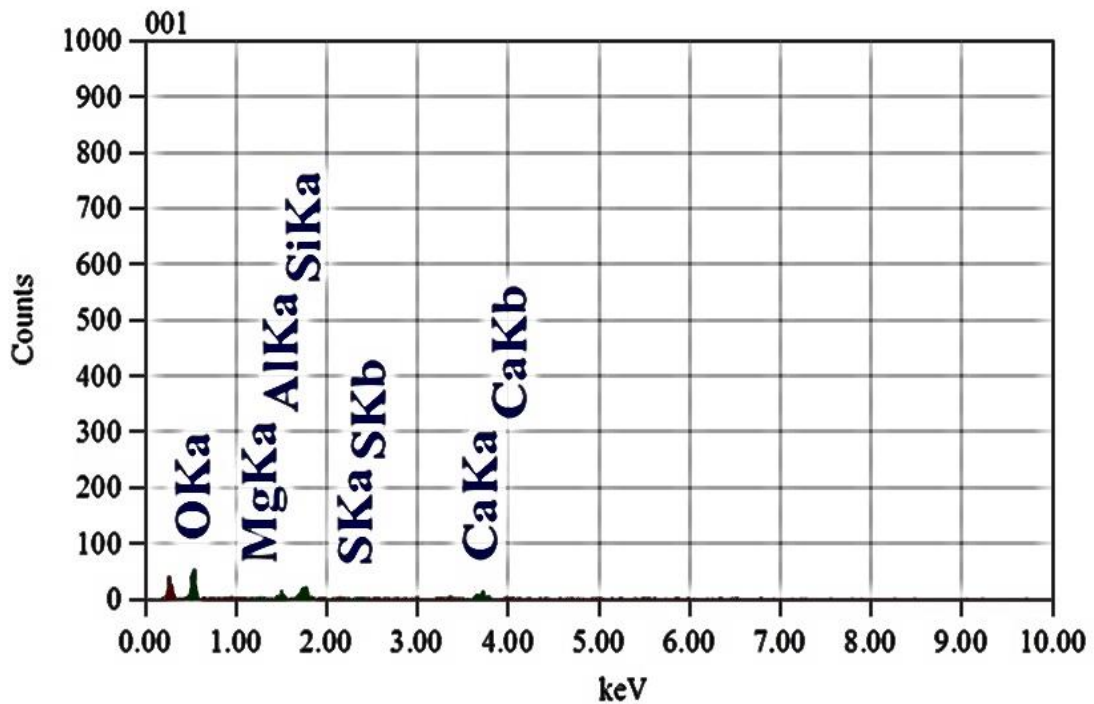
Figure 4.37: EDS analysis of grouted sand samples cured for 90 days: (a) W:C 2:1, (b) W:C 3:1, (c) W:C 4:1 and (d) W:C 5:1



(a)



(b)



(c)

Figure 4.38: EDS analysis of Grouted sample (2:1) after 120 days of curing: (a) sample 1, (b) sample 2 and (c) sample 3

4.9 Summary

In this chapter, the suitability of sandy soil for grouting was investigated. The water to cement (W:C) ratio was fixed through trials. Strength properties were determined by unconfined compression test and triaxial tests. SEM and EDS analyses were done to conduct microstructural study with the aim to understand the mechanism of stabilization. This chapter discusses the strength characteristics of grouted soil by compiling a variety of graphs, bar charts, and tables. From the graphs, it is observed that curing time and water-cement ratio influence the strength as well as physical properties of the grouted samples. To explore the mechanical properties of grouted sand, CU triaxial tests were done for three samples. From this test, it was clear that some cohesion developed in grouted samples. In this test, dilation effects and negative pore pressures were also observed. In both UCS and Triaxial test, failure patterns seemed to differ with different W:C ratio and curing ages. It was observed that the engineering parameters like modulus of elasticity, cohesion, brittleness, and ductility influence the failure patterns of grouted samples. Eventually, with the microstructure analysis, it was clear that the chemical reaction made the soil samples

solid by reducing the porosity and void ratio. Different chemical components were produced through hydration reaction of cement with water. These chemical reactions also depended on curing time and cement content. Finally, the Energy Dispersive Spectroscopy (EDS) helped in visualizing the traveling of atoms from one orbital to another. By analyzing the energy dispersion particular atom in the grouted sand was identified. The summary of the results is:

- (i) The value of specific gravity, permeability, density index and F.M. of the sand are 2.89, 8.84×10^{-6} cm/sec, 4.92% and 1.12 respectively. From the direct shear test, it is found that the angle of internal friction ϕ is 35° .
- (ii) While dry density of grouted sand is increased, moisture content as well as void ratio is decreased with the cement content and curing ages.
- (iii) From unconfined compression test the axial strength of 5:1 (W:C) at 7, 14, 28 days range from 35 kPa to 40 kPa where in 90 days it reached the highest value of about 70 kPa. Different curing ages have almost no effect on the axial strain. In the case of 4:1 W:C ratio the axial stress is about 30 kPa from 7 to 14 days of curing. After 28 days it reached about 60 kPa and similar results are found after 90 days of curing. The axial strain for each group is about 4%. On the other hand, the axial stress of 3:1 and 2:1 showed highest value for each group. The axial stress of 3:1 (W:C) after 7, 14, 28 and 90 days are 70 kPa, 72 kPa, 114 kPa and 125 kPa respectively. The strength of the samples of the group of W:C 2:1 is 101 kPa, 137 kPa, 190 kPa and 400 kPa respectively after 7, 14, 28 and 90 days curing with small amount of axial strain. It was found that when the axial stress reached the peak value then the materials became brittle. It was also observed that axial stress increased with increasing cement content and curing ages whereas the axial strain decreased with increasing axial stress. Young's modulus of grouted sand increased with increasing W:C ratios and curing ages.
- (iv) One group of samples with W:C of 2:1 was cured for 7 days and were examined in triaxial test. From triaxial test, the peak axial stress increased with the increase of confining pressure and showed brittleness. During the test, dilation increased the volume and decreased pore water pressure. From the

stress path graphs, it was observed that once it reached a peak point, softening caused reversal of the stress path with the same slope until failure stress was reached. In undrained condition, the peak point was high due to the generation of significant negative pore pressure. For this composition, the cohesion was about 200 kN/m².

- (v) Grouted samples showed different failure pattern for different proportioned W:C ratios and curing time. 2:1 grouted sample showed multiple shear failure whereas 3:1 showed axial split at every case. Collapse and column failure were found for 4:1 and 5:1. After 120 days, a new type of failure pattern, slickenside, occurred in 2:1 grouted sample. All these above-mentioned failure patterns were found via unconfined compression test. After triaxial test on selected samples, bulging failure was also observed.
- (vi) From microstructure analysis, it was found that the formation of pozzolanic compounds at the end of the chemical reactions lead to improved strength of the soil. From SEM images, it was clearly showed that with the increase of cement content, the void ratio decreased.
- (vii) Finally, from Energy Dispersive Spectroscopy (EDS) it was clear that the most common component of sand, silicon dioxide was in the form of quartz. From EDS, the traveling of oxygen and silicon atom proved the presence of filling sand.

Chapter 5

CONCLUSIONS AND FUTURE RECOMMENDATIONS

5.1 Introduction

The main objectives of this research are to characterize the shear strength, determine permeability and investigate the microstructure of grouted sandy soil. After four different trials, fifty-one homogeneous grouted samples were prepared with varying water: cement ratio and then the prepared samples were cured for different ages. Unconfined compression test, direct shear test, triaxial test and microstructure analysis, i.e., SEM and EDS were conducted. Conclusions obtained from these studies and some future recommendations are presented in this chapter.

5.2 Conclusions

The main findings are as follows:

- (i) From the unconfined compression test, it was found that axial stress of the samples prepared with W:C ratio 5:1 ranged between 35 kPa and 40 kPa cured for 7, 14, and 28 days. However, the strength of the samples cured for 90 days, was 70 kPa. There was no effect of curing age on the axial strain. The failure strain was close to 4% for all the curing ages. In the case of the samples prepared with 4:1 W:C ratio, the axial strain was found to be 3%. The axial strength of the samples cured 7 to 14 days is about 30 kPa. The axial strength of the samples cured for 28 days, and 90 days was same (60 kPa). The axial strain of the samples of this group was also about 4% for both curing ages. On the other hand, the axial strength of the samples prepared with W:C ratio 3:1 and 2:1 was found to be maximum. The axial strengths of the samples prepared with 3:1 are 70 kPa, 72 kPa, 114 kPa and 125 kPa which were cured for 7, 14, 28 and 90 days respectively. The axial strengths of the samples prepared with W:C ratio 2:1 are 101 kPa, 137 kPa, 190 kPa and 400 kPa which were cured for 7, 14, 28 and 90 days respectively. Axial strain of that samples was found

to be 4%. Samples with high strength showed brittle behavior. It was also observed that axial strength increased with the increase of cement content and curing ages, whereas the axial strain decreased with the increase of axial strength. Young's modulus of the grouted sand increased with the increase of water-cement ratio and curing age.

Grouted samples showed different types of failure patterns for different samples with different W:C ratios and curing ages. Samples of 2:1, 3:1, 4:1 and 5:1 W:C ratios showed shear failure, axial split, collapse, and column failure respectively. Under the unconfined compression test, the samples behave like clayey samples and produce multiple types of failure pattern. The modulus of elasticity refers to the stiffness of materials. Samples with high modulus of elasticity do not deform under load as much as those of low modulus. High modulus of elasticity of 2:1 W:C ratio showed overstress condition and caused shear failure in extreme cases. The cohesion of 2:1 W:C ratio sample varied from 26 to 193 kPa and the modulus of elasticity varied from 13 to 117 kN/m². 3:1 W:C ratio sample showed axial split when cohesion was 25 to 61.5 kPa and the modulus of elasticity was 22 to 61.5 kN/m². The cohesion and modulus of elasticity of 4:1 and 5:1 W:C samples were lower than 2:1 and 3:1 W:C samples. The range of cohesion was 6 to 31 kPa and the range of modulus of elasticity was between 11 and 28 kN/m² for 4:1 W:C ratio and these samples showed collapse failure. In the case of 5:1 W:C ratio, the cement content was lower than other proportioned samples, therefore there were lots of void in samples. As a result, under this test when it was subjected to compression from the upper end the molecules filled the void and after some time it produced column mode failure pattern. After 120 days, new type of failure pattern, slickenside, occurred in 2:1 W:C grouted samples, when the samples have shown highest cohesion of 385 kPa and highest modulus of elasticity of 489 kN/m². Here it was determined that cohesion and modulus of elasticity increased with the cement content and curing ages.

- (ii) From the consolidated undrained (CU) triaxial test, it is found that, the deviatoric stress increased with the increase of confining pressure. The well-graded sands indicated more dilation or negative pore pressure with increased

confining pressure. The stress path moved linearly and reached a peak point under CU condition. Then softening caused reversal of the stress path with the same slope until failure stress was reached. In undrained condition, the peak point was high due to the generation of significant negative pore pressure. The higher the cement content, the higher the cohesion value and angle of internal friction. Deviatoric stress and mean effective stress were increased with the increase of confining pressure. The deviatoric stresses are 980, 983 and 1354 kPa for 50, 100 and 200 kPa confining pressure respectively. Mean effective stresses were 380, 413 and 657 kPa for the same confining pressure. However, the axial strain, and pore pressure were decreasing with the increasing confining pressure. In the dense samples, an increase of void ratio caused dilation and produced negative pore pressure under the undrained condition. The axial strains were 11.86%, 10.84% and 10% for the confining pressure 50, 100 and 200 kPa. The void ratio was 0.18, 0.20 and 0.25 respectively with decreasing negative pore pressure of 192, 168 and 127 kPa for the same confining pressure.

The failure pattern observed in the triaxial test was that the sample showed some ductility at the primary stage of low confining pressure. Afterwards the brittle failure occurred with the increase of confining pressure. The bulging that occurred at the top or bottom face of the samples proved that volumetric increase and absorbance of water caused this type of failure. The failure patterns of the samples were a combination of bulging and shear failure. Shear failure occurred when the vertical displacement gradually receded. Shear failures were more clearly observed after the bulging effect became apparent. These failure patterns also indicated that the cohesion was increased with the slow rate of loading as well as confining pressure.

- (iii) The moisture content and the void ratio decreased with the increase of cement content and the curing ages. After 7 days of curing, the moisture contents were 32.6% for 5:1, 30.5% for 4:1, 30.2% for 3:1 and 29% for 2:1 w:c ratio samples. The moisture contents decreased with the increasing curing time and it went to 8.7%, 4.5%, 3.9%, and 3.5% after 90 days of curing for 5:1, 4:1, 3:1 and 2:1 w:c ratio samples respectively. After 90 days of curing, the void ratio of 5:1,

4:1, 3:1 and 2:1 W:C ratio samples were 0.11, 0.14, 0.15 and 0.12 respectively. With more time, the voids started to fill up with grouting materials. After 120 days, it came to 0.1 void ratio for 2:1 W:C sample. Dry density decreased with increasing cement content and curing ages. The dry density of 5:1, 4:1, 3:1 and 2:1 W:C ratio samples after 90 days of curing are 9.89, 9.6, 9.3 and 8.4 gm/cm³ respectively. The compressive strength was about 70, 90, 125 and 200 kPa for 5:1, 4:1, 3:1 and 2:1 W:C samples respectively after 90 days of curing. After 120 days, the sample showed the maximum compressive strength of about 500 kPa, which meant that strength increased with the increase of curing time whereas the permeability and the void ratio decreased. The injected pressure depended on the loose condition of sand and the W:C ratio. In this research, the injected pressure was almost the same for all proportioned grouted samples.

- (iv) From the scanning electron microscope images, it was found that the strength depended on the chemical and hydration reaction. Formation of pozzolanic and hydroxyl compounds gave strength to different grouted samples. The cementing action in granular soil produced compounds and C-S-H gels that increased the soil strength through complex pozzolanic activity. The formation of pozzolanic compounds at the end of the chemical reactions led to improved strength and workability of the soil. The hydroxyl groups also elevated the pore water pH to a maximum value of approx. 12.45. The principal hydration product was C₃S₂H₈, calcium silicate hydrate or C-S-H. C-S-H occupied about 50% of the structural component in a cement paste and formed directly on the surface of cement particles. Another product was CH, calcium hydroxide, which produced plate shaped crystalline in most cases. C-S-H formed a glue gel binder that helped to form a solid state of cohesion characteristics in sand. CH crystalline also worked as the strength provider. Ettringite needle helped to absorb water that decreased the moisture content. The appearance of small particles in the lower cement content samples, which consisted mainly of calcium and sulphur were observed. These might correspond to ettringite which could have developed due to the aqueous relation between gypsum and tri calcium aluminate (C₃A (3CaO. Al₂O₃)). The increase in the cement content led to the occurrence of sulphur-calcium rich zones comprised of ettringite. The C-S-H could have originated from the hydration of the components of

cement (C_3S and C_2S ($2CaO.SiO_2$)), but it was partially from the pozzolanic reaction. The honeycomb shaped were formed due to the hydration reaction of PCC cement. The ettringite $Ca_3Al(OH)_6. 12H_2O.(SO_4)_3.2H_2O$ was locally formed in the pore voids. It was a needle shaped crystalline whose length was up to $10\ \mu m$ long. SEM images also showed more C-S-H gel (calcium silicate hydrate) products reflecting the early hydration stage of the cement paste. The specimens were very heterogeneous, showing huge CH (calcium hydroxide) crystals that were the reason for the early hydration of cement in initially high-water content. The same type of chemical reaction happened at different proportioned grouted samples. This chemical reaction helped to decrease microspores and voids in the samples.

The presence of different chemical elements was found from Energy Dispersive Spectroscopy test. The travelling oxygen and silicon ion represented the sand which was collected from river side.

From the study it was observed that, strength properties and Young's modulus improved with the cement content, whereas porosity and void ratio decreased. It means that grouting effectively stabilized the alluvial sand to increase bearing capacity and decrease the settlement potential of existing embankments and dams. It also effectively decreased seepage potential which is necessary for the durability of embankments under flooded conditions.

5.3 Future Recommendations

Following are the recommendations for future study:

- (i) The research work was conducted using Portland Composite Cement. However, micro fine cement can be used in future studies for better results.
- (ii) The same research can be done on the clayey soil.
- (iii) Viscosity can be measured with curing time for both fine and coarse particles.
- (iv) Strength tests should be conducted for larger size samples in future studies.
- (v) In this study, triaxial tests were conducted for a particular case. Further investigation considering all the cases will help understanding the complete scenario.

- (vi) Field level work and studies are highly recommended to understand the effectiveness of permeation grouting to protect the dam from erosion. Further research should be conducted in the field to consider the actual confinement pressure of the site.
- (vii) After the grouting process, to stabilize the slope even further, geotextile or turf can be used in future studies.

This experiment would have come to its optimum level if it was done in field condition which is very expensive, so this work was done under patronage.

REFERENCES

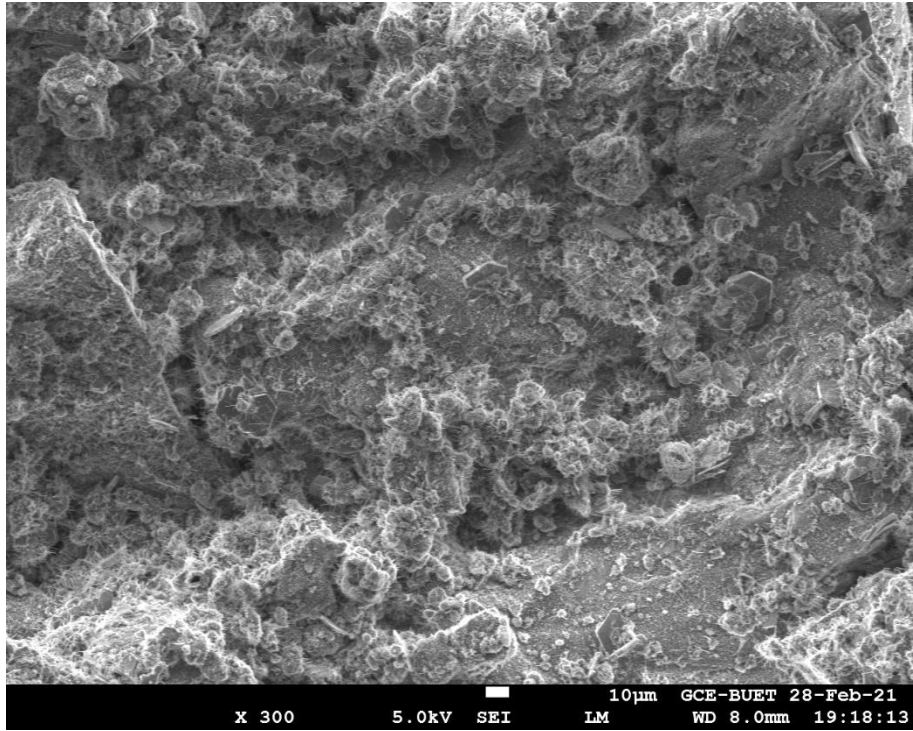
- Abraham, B., Kumar, S., Sridharan, A. and Jose, B. (2014) “Strength Improvement of Loose Sandy Soils through Cement Grouting”, *Journal of Indian Geotech*, Vol. 44(3), pp. 234-240.
- Anovitz, L. and Cole, R. (2015) “Characterization and Analysis of Porosity and Pore Structures”, *Journal of Mineralogy and Geochemistry*, Vol. 80, pp. 61-164.
- ASTM D2434-68, Standard Test Method of Permeability of Granular Soils (Constant Head)”, *ASTM International*, West Conshohocken, PA, 2007.
- ASTM D3080/D3080M-11, “Standard Test Method for Direct Shear Test of Soils Under Consolidated Drained Conditions” ,*ASTM International*, West Conshohocken, PA, 2011.
- ASTM D422-63, “Standard Test Method for Particle-Size Analysis of Soils”, *ASTM International*, West Conshohocken, PA, 2007.
- ASTM D7012-14, “Standard Test Method for Unconfined Compressive Strength of Cohesive Soil”, *ASTM International*, West Conshohocken, PA, 2007.
- ASTM D854-14, “Standard Test Methods for Specific Gravity of Soil Solids by Water Pycnometer”, *ASTM International*, West Conshohocken, PA, 2012.
- ASTM D9767-95, “Standard Test Method for Consolidated Undrained Triaxial Compression Test for Cohesive Soil”, *ASTM International*, West Conshohocken, PA, 2007.
- Beetham, P., Dijkstra, T., Dixon, N., Flaming, P., Hutchison, R. and Bateman, J. (2015) “Lime Stabilization for Earthworks: U.K Perspective”, *ICE, ground Improvement*, Vol. 168, pp. 81-95.
- Bhuiyan, M., Wang, S., Sloan, S., Carter, J. and Raka, T. “Effects of Grout Injection Techniques in Pressure Grouted Soil Nail System”, *E3S Web of Conferences 92*, 17010, 2019.
- Bonno, J., Mcdowell, G. and Wanatoski, D. (2014) “DEM of Triaxial Test on Crushable Cemented Sand”, *Journal on Graanular Matter, Springer*. Vol. 1(16), pp. 563-572.
- Byle, J., and Borden, H. (1995) “Verification of Geotechnical Grouting”, *Journal of Americans Society of Civil Engineers*. Vol.1(2), pp. 10-25.
- Celik, F. (2019) “The Observation of Permeation Grouting Method as Soil Improvement Technique with Different Grout Flow Models”, *Journal of Geomechanics and Engineering*, Vol. 17, pp. 367-374.
- Chinchillas, M., Casarez, C., Rea, S., Soberon, J. and Higuera, R. (2019) “SEM Image Analysis in Permeable Recycled Concretes with Silica Fume. A Quantitative Comparison of Porosity and the ITZ”, *Journal materials*. Vol. 12(01), pp. 1-19.

- Dano, C., Hicher, P. and Tailliaz, S. (2004) “Engineering Properties of Grouted Sand”, *Journal of Geotechnical and Geoenvironmental Engineering*, Vol. 130(1), pp. 25-34.
- Dayakar, P., Venkat, K. and Raju, K. (2012) “Effect of Permeation Grouting Using Cement Bentonite Grout in Sandy Soil”, *International Journal of Engineering Trends and Technology*. Vol. 3(5), pp. 8-10.
- Dias, D.; Camarini, G. and Miguel, M. (2012) “Preliminary Laboratory Tests to Study the Increase of Strength in Samples of Soft Soils with Cement, for Treatments using Dry-Mix System”, *Journal of American Society of Civil Engineering : Grouting and Deep Mixing*. Vol. 1(2), pp. 57-58.
- Eyuvan, A. and Murat, M. (2017) “Permeability Characteristics of Superfine Cement- Grouted Sand”, *ACI Materials Journal*. Vol.1(03), pp. 103-105.
- Eyuvan, A., Deveci, A., and Gokce, A. (2021) “Effect of Sodium Silicate on the Strength and Permeability Properties of Ultrafine Cement Grouted Sands”, *ASCE Journal of Materials in Civil Engineering*, Vol.2(5), pp. 120-123.
- GeoGrout (2019) *Hydro Fracture Grouting*. Available at: <https://www.gggms.com/services/hydro-fracture-grouting/>. [Accessed on: 23 March 2019]
- Guangxuan, Z., Qingsong, Z., Rentai, L., Jiwen, B., Wei, L. and Xiao, F. (2021) “Experimental and Numerical Study on the Permeation Grouting Diffusion Mechanism considering Filtration Effects”, *Journal of Hindawi, Geofluids*. Vol.2(13), pp. 11-13.
- Hamidi, A. (2014) “ Triaxial Shear Behavior of a Cement-Treated Sand-Gravel Mixture”, *Journal of Rock Mechanics and Geotechnical engineering*. Vol.1(5), pp. 455-465
- Haralambos, S. (2009) “Compressive Strength of Soil Improved with Cement”, *Journal of Ground Modification, Problem Soils and Geo-Support*. Vol. 1(2), pp.289-296.
- Hashimoto, K., Nishihara, S., Oji, S., Kanazawa, T., Nishie, S., Seko, I., Hyodo, T. and Tsukamoto, Y. (2016), “ Field Testing of Permeation Grouting using Microfine Cement”, *Institution of Civil Engineers*. Vol. 169(G12), pp 134-142.
- Hicher, P., Chang, C. and Dano, C. (2008) “ Multi Scale Modeling of Grouted Sand Behavior”, *Int. Journal of Solids and Structures*. Vol 45, pp. 4362-4374.
- Horpibulsuk, S. (2006) “Strength and Microstructure of Cement Stabilized Clay” , *Journal of Intechopen*. Vol.1, pp. 20-23.
- Islam, T., Islam, M., Islam, M., and Abedin, M., “Effect of fine content on shear strength behavior of sandy soil”, *presented at 14th Global Engineering and Technology Conf.2017*.
- Jadid, R. and Abedin, M. (2015) “Permeation of Bentonite Suspensions through Loose Sandy Soil”, *Malaysian Journal of Civil Engineering*, Vol. 27, pp. 413-424.
- Jafarpour, P., Moayed, R., and Kordnaeij, A. (2019) “Behavior of Zeolite- Cement Grouted Sand under Triaxial Compression Test”, *Journal of Rock Mechanics and Geotechnical Engineering*. Vol 12, pp 149-159.

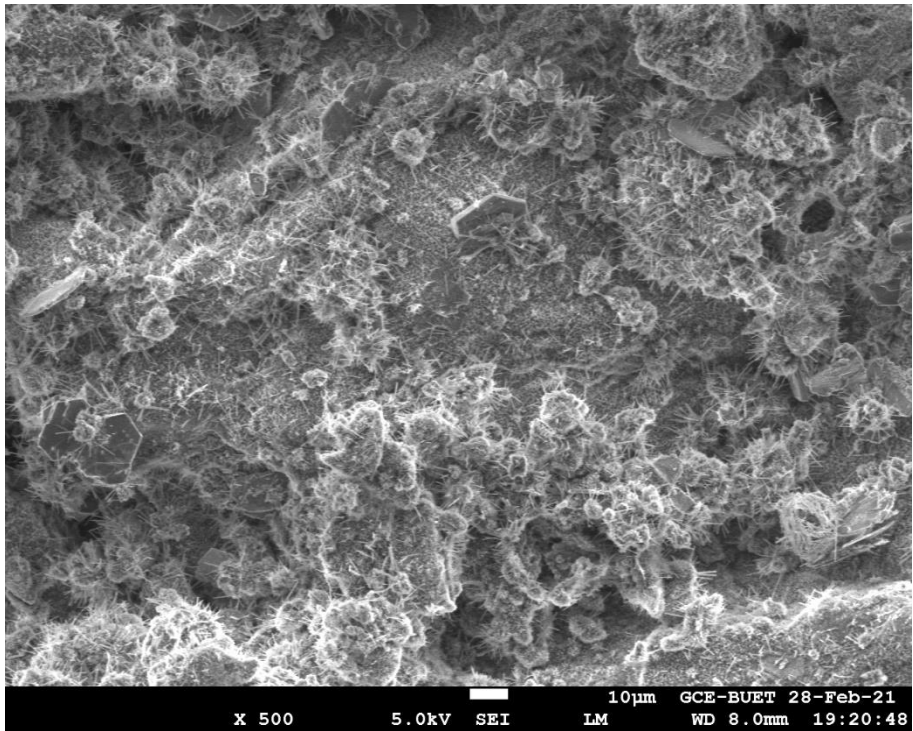
- Jin, Y., Han, L., Meng, Q., Ma, D., Han, G., Geo, F. and Wang, S. (2018) “Experimental Investigation of the Mechanical Behaviors of Grouted Sand with UF-OA Grouts”, *Living Archive for Process Systems Engineering*. Vol. 6, pp. 1-13.
- Kainrath, A. and Adam, D. (2015) “Influences on the Mechanical Behavior of Grouted soil”, *Journal of Geotechnical Engineering for Infrastructure and Development*. ICE Publishing. Vol1, pp. 20-26.
- Kamata, T., Tsukamoto, Y. and Ishihara, K. (2009) “Undrained Shear Strength of Partially Saturated Sand in Triaxial Tests”, *Bulletin of the New Zealand society for Earthquake Engineering*, Vol.42, pp. 35-40.
- Kazemian, S. and Huat, B. (2009) “Assessment and Comparison of Grouting and Injection Methods in Geotechnical Engineering”, *European Journal of Scientific Research*. Vol. 27(2), pp.234-247.
- Keong, S. *Properties of Cement Based Permeation Grout used in Ground Engineering*, M.Sc. Engg. Thesis, Department of Civil Engineering, National University of Singapore. 2015.
- Khan, N., Khan, I., Ullah, A., Yasir, M. and Naseer, S., (2018) “Performance Evaluation of Cement Grouting by Universal Testing Machine to Improve the Bearing Capacity of Sandy Soil”, *Journal of Irrigation & Drainage Systems Engineering*. Vol 7, pp 1-4.
- Kordnaeij, A., Moayed, R.Z. and Soleimani, M. (2019) “Unconfined Compressive Strength of Loose Sandy Soils Grouted with Zeolite and Cement”, *Soils and Foundations*. Vol. 59, pp 905-919.
- Lee, C., Nam, H., Lee, W., Coe, H. and Ku, T. (2019) “Estimating UCS of Cement-Grouted Sand Using Characteristics of Sand and UCS of Pure Grout”, *Research gate, article in Geomechanics and Engineering*. Vol.1, pp.20-23.
- Lees, D.(2021), “Permeation Grouting in Sydney”, *Researchgate*. Vol. 1(2), pp. 1-10.
- Mainmark (2019) *Permeation grouting is the longest-established and most widely used pressure grouting technique*. Available at: <https://mainmark.com/products/permeation-grouting/>. [Accessed on: 10 January 2019]
- Nonveiller, E. (1989) “Grouting Theory and Practice”, *Elsevier*. Vol.3, pp-20-24.
- Oti, J.E., Kinuthia, J.M., and Bai, J. (2009) “Compressive strength and microstructural analysis of unfired clay masonry bricks”, *Journal of Engineering Geology, Elsevier*. Vol. 109, pp 230-240.
- Puppala, A., Pedarla, A.vand Bheemasetti, T. (2015) “Soil Modifications by Admixture”, *Elsevier: Chemicals, Electrokinetic, Thermal and Bioengineering method*. Vol.1(10), pp 291-309.
- Rahman, R., *Horizontal infiltration of grouts and its effect on shear strength of sandy soil*, M.Sc. Engg. Thesis, Department of Civil Engineering, Bangladesh University of Engineering and Technology (BUET), Dhaka, Bangladesh, 2016.
- Raman, K.V., Deyakar, P. and Raju, K. (2016) “Improvement of Sandy Soil by Low Pressure Grouting using Cement Grout”, *Journal of Chemicals and Pharmaceutical Sciences*. Vol 9, pp 190-194.

- Raman, K.V., Deyakar, P., and Raju, K.V.B. (2016) “Study on Permeation Grouting Using Cement Grout In Sandy Soil” , *Journal of Mechanical and Civil Engineering*. Vol. 4, pp 05-10.
- Ryan, C. *Mechanical Behavior of Grouted Sands*, M.Sc. Engg. Thesis, College of Engineering, University of Kentucky, USA, 2015.
- Sarker, D. and Abedin, Z. (2015) “ A Review on Ground Improvement Techniques to Improve Soil Stability against Liquefaction”, *International Journal of Science and Engineering Investigations*. Vol. 4(40), pp. 53-55.
- Satyarno, I., Solehudin, P., Meyarto, C., Hadiyatmoko, D., Mohammad, P. and Afnan, R. “Practical method for mix design of cement-based grout,” *presented at 2nd Int. Conf. on Sustainable Civil Engineering Structures and Construction Materials, 2014*.
- Schwarz, G. and Krizek, R. (2006) “Hydrocarbon Residuals and Containment in Microfine Cement Grouted Sand”, *Journal of Materials in Civil Engineering*, Vol. 18(2), pp-290-294.
- TAEHWA (2020) *Jet Grout Pile*. Available at: <https://taehwa.com.sg/jet-grout-pile/> [Accessed on: 17 November 2021]
- U.S. Department of Transportation Federal Highway Administration (2017) *Ground Modification Methods Reference Manual – Volume I, USA*. Available at: <https://www.fhwa.dot.gov/engineering/geotech/pubs/nhi16027.pdf>. [Accessed on: 10 June 2020]
- Warner, J. (2004) , “*Practical Handbook of Grouting*”, Chap. 2, pp. 16, Published by John Wiley and Sons, Inc., Hoboken, New Jersey.
- Yaser, G., Ismail, B. and Kemas, A. (2017) “Simulation and Development of Instrumental Setup to be Used for Cement Grouting of Sand Soil”, *Italian Journal of Science and Engineering*. Vol 1(1), pp. 16-27.
- Zebovitz, S., Krizek, R.J. and Atmatzidis, D. (1989) “Injection of Fine Sands with very Fine Cement Grout”, *Journal of Geotechnical Engineering*. Vol. 115, pp. 1717-1723.
- Zhang, F., Chen, X., Feng, T., Wang, Y. and Liu, X. (2022) “Experimental Study of Grouting Protection against Local Scouring of Monopile Foundations for Offshore Wind Turbines” , *Elsevier, Ocean Engineering*. Vol. 258, pp. 50-55.
- Zongjin, Li (2011), “*Advanced Concrete Technology*”, Chap 4, Published by John Wiley and Sons, Inc., Hoboken, New Jersey.

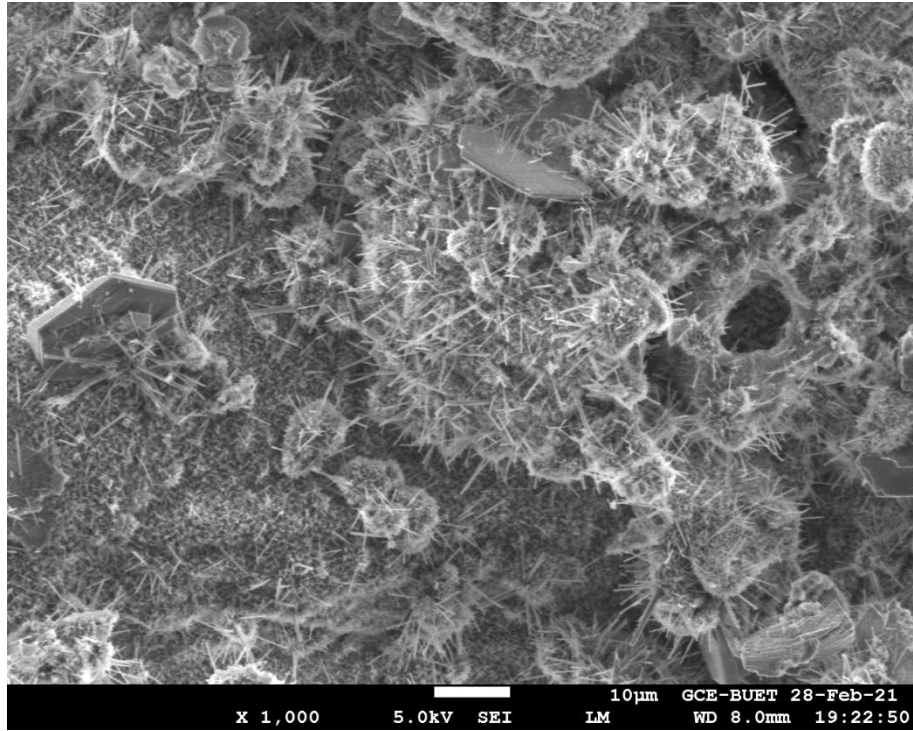
Appendix A
Scanning Electron Microscope Images of Grouted
Samples with W:C ratio 5:1, 4:1, 3:1 and 2:1
Cured for 28 days



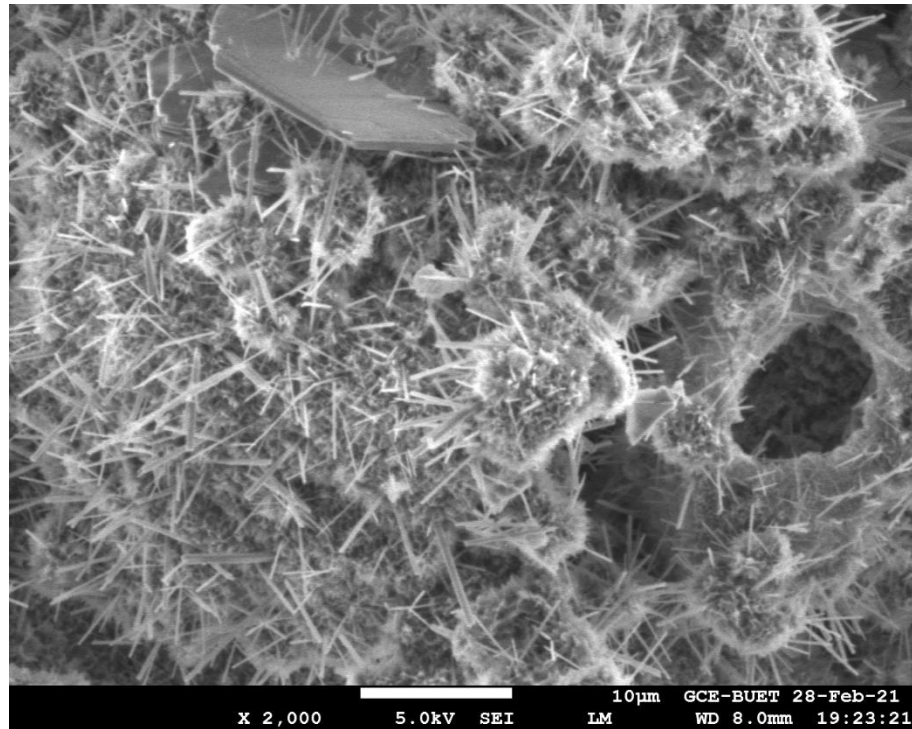
(a)



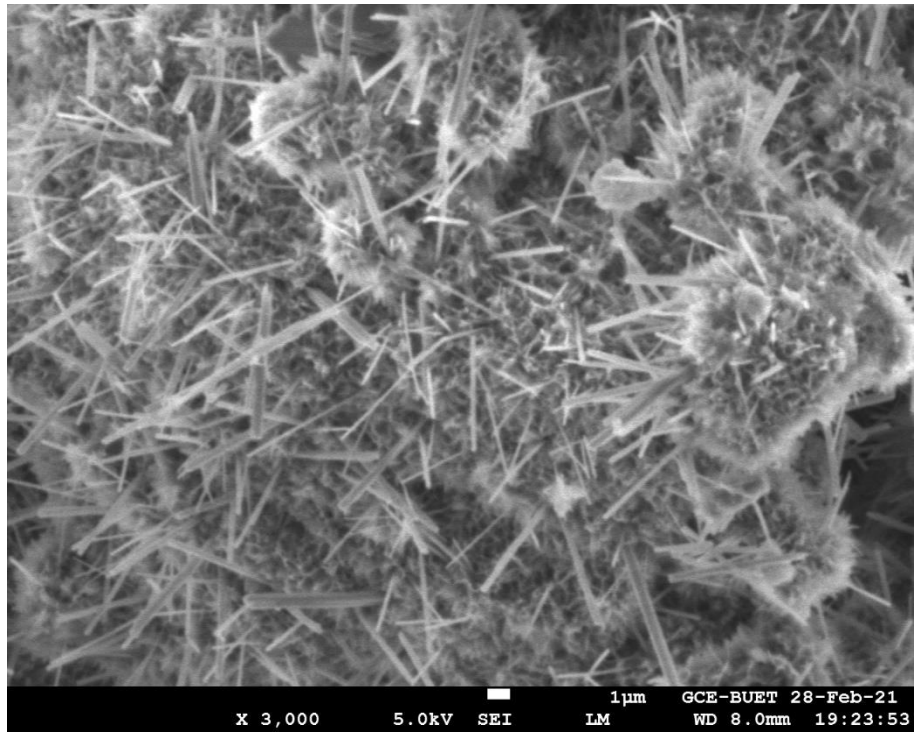
(b)



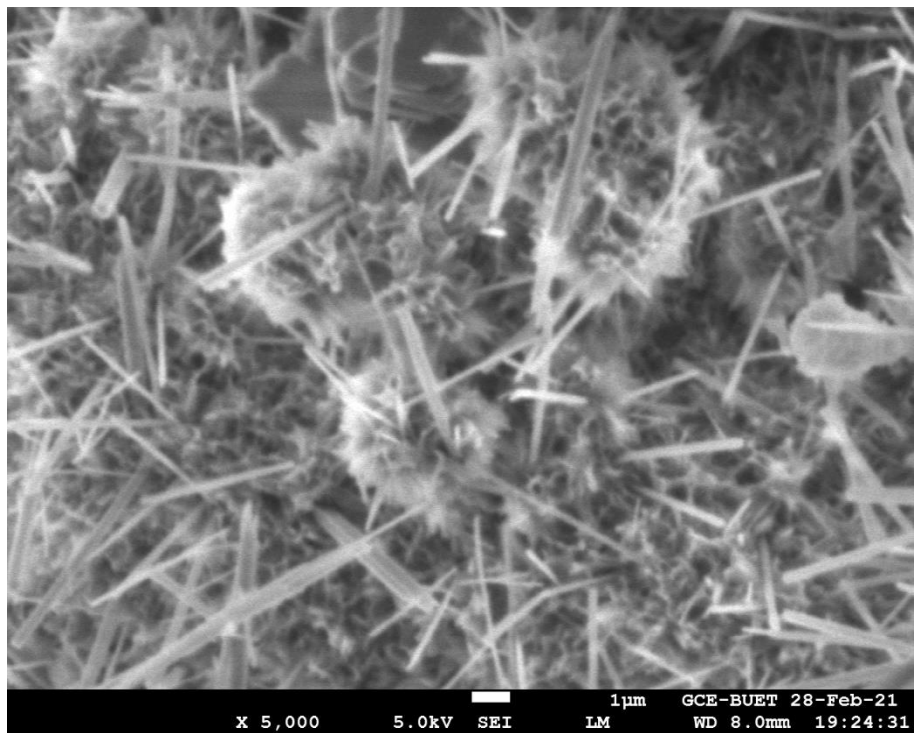
(c)



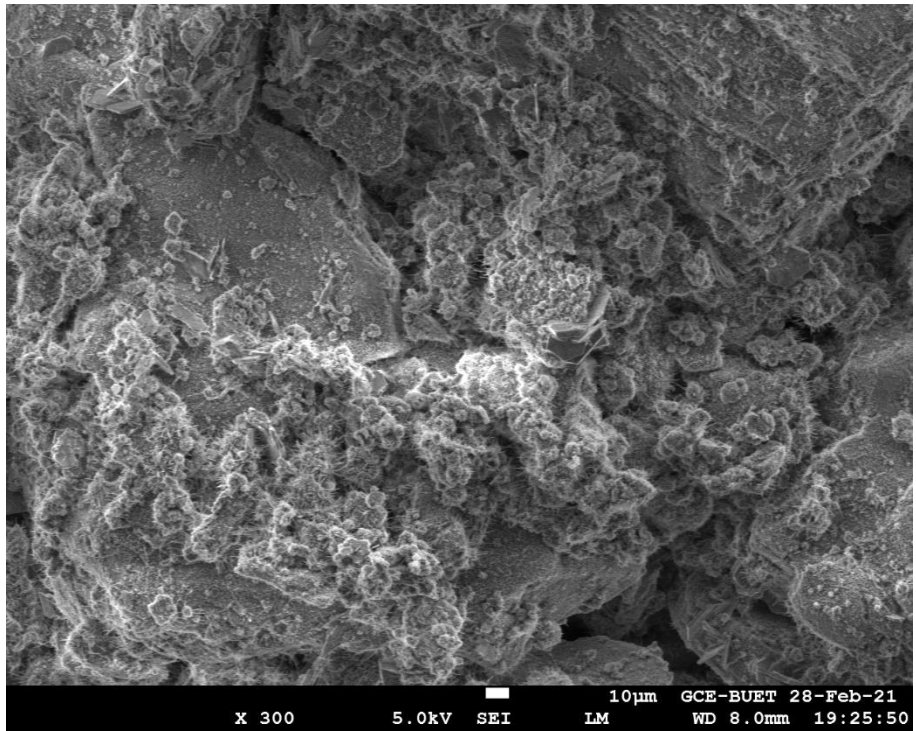
(d)



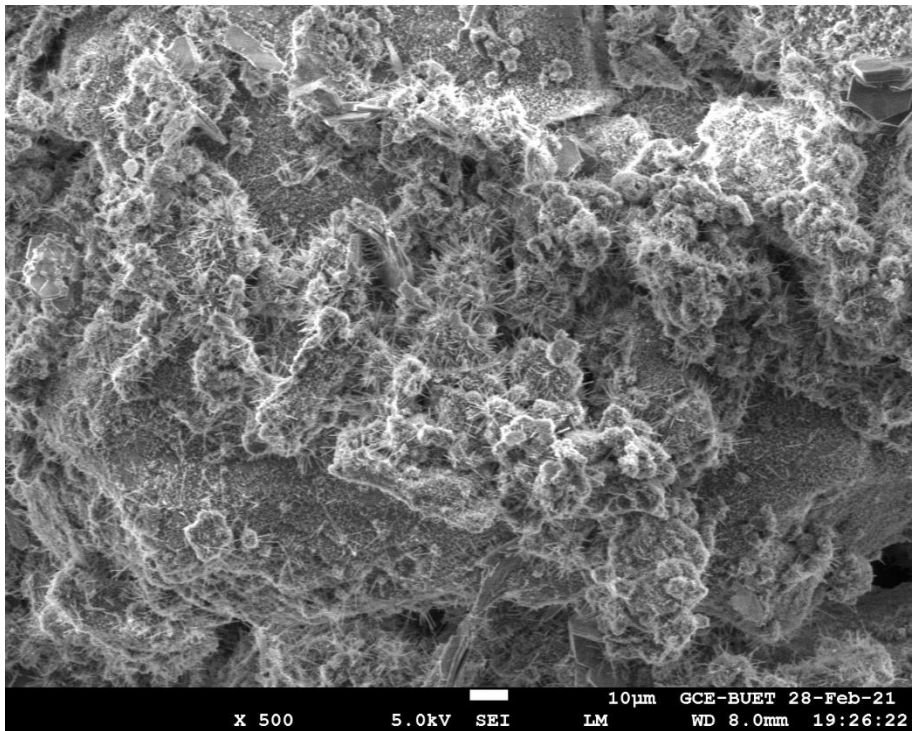
(e)



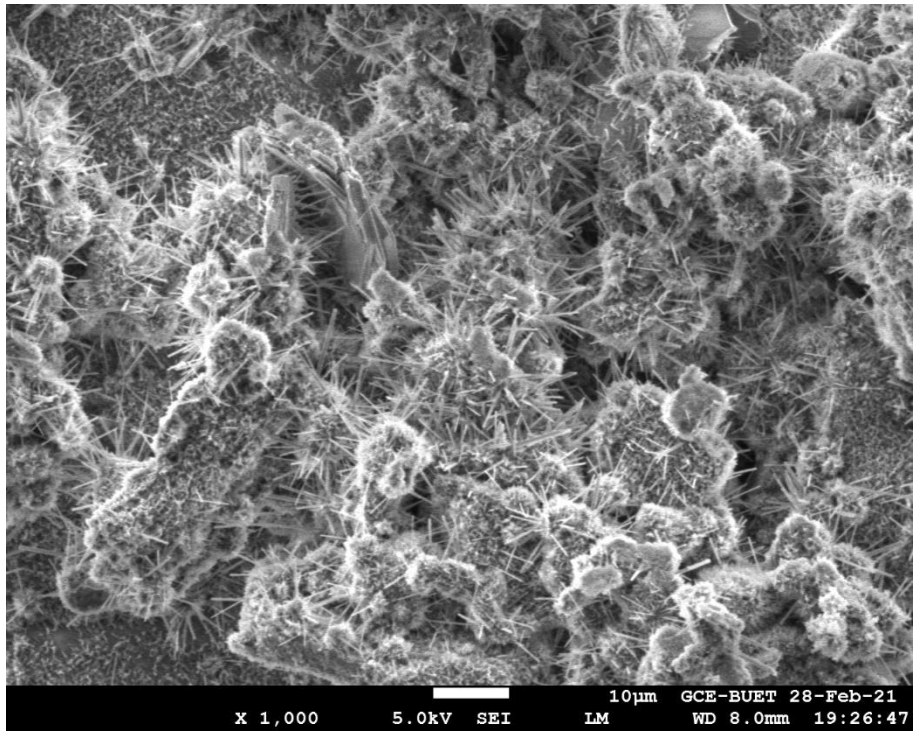
(f)



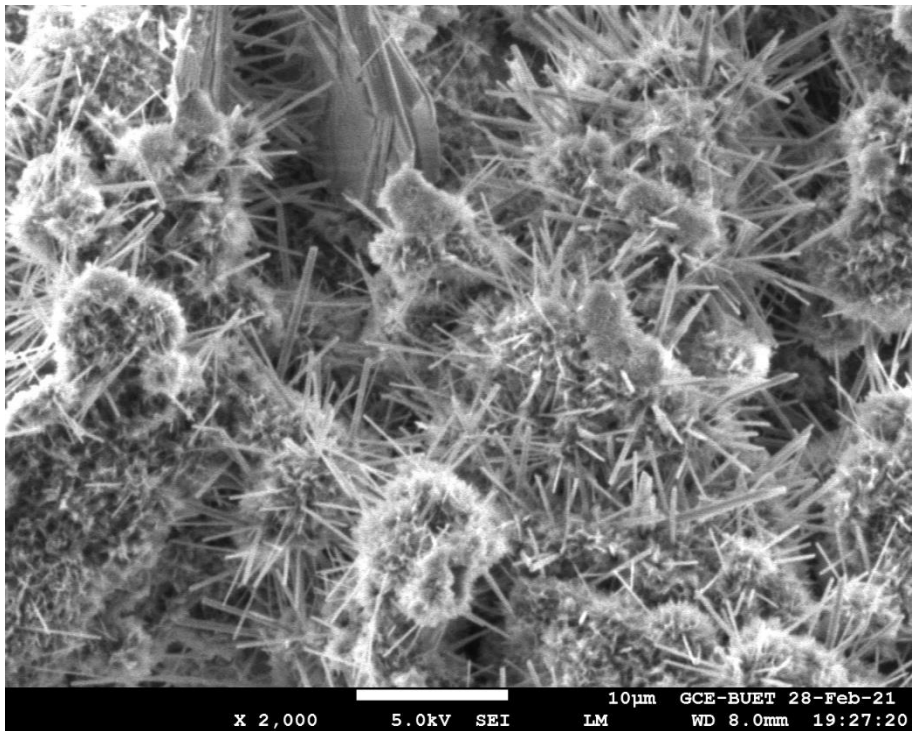
(g)



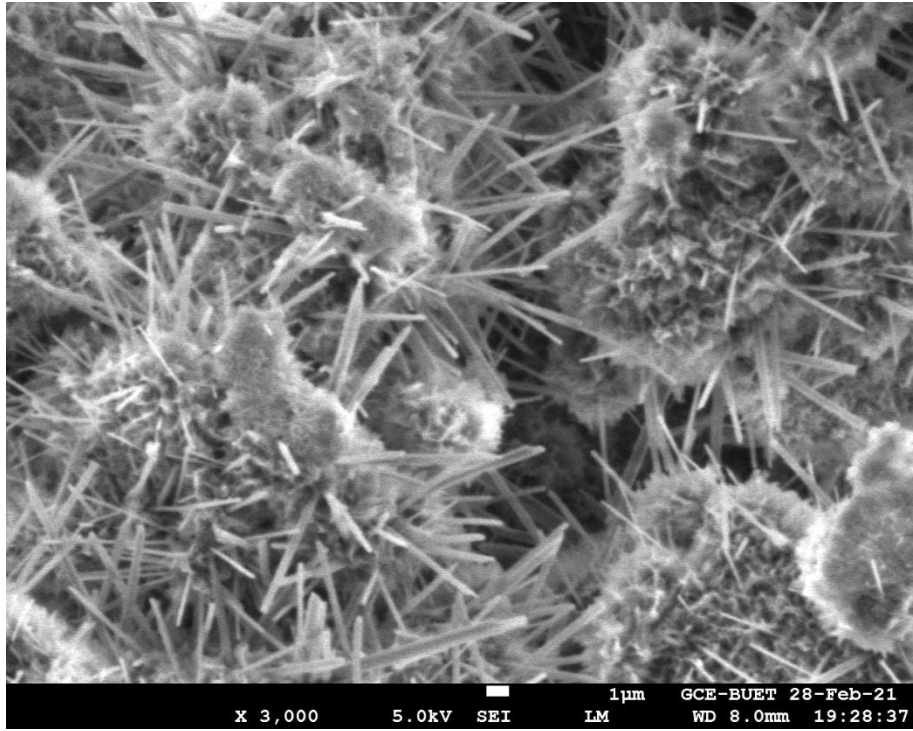
(h)



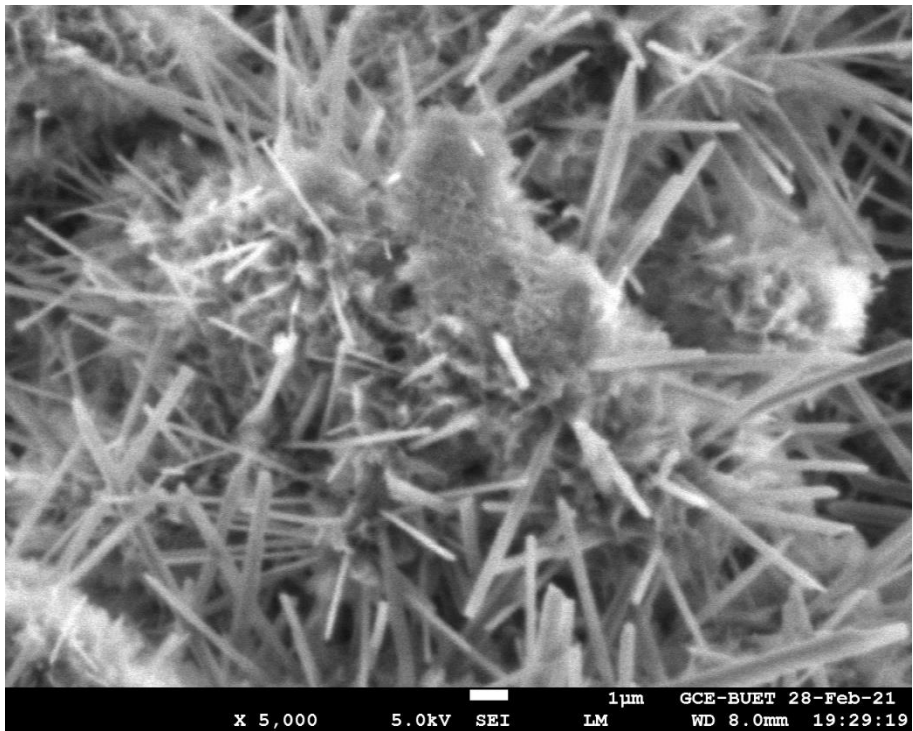
(i)



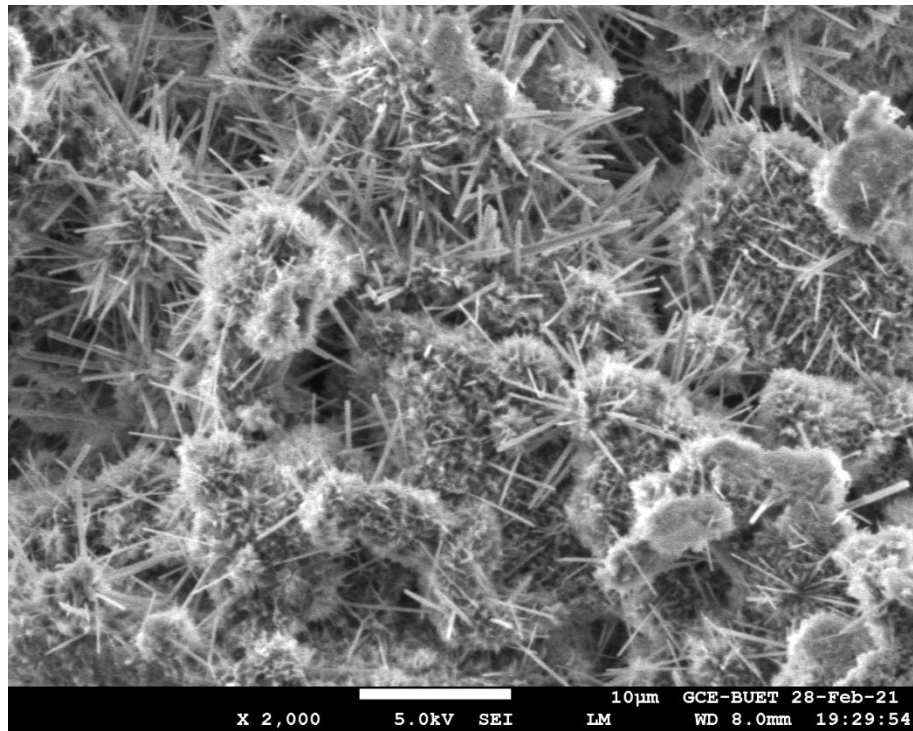
(j)



(k)

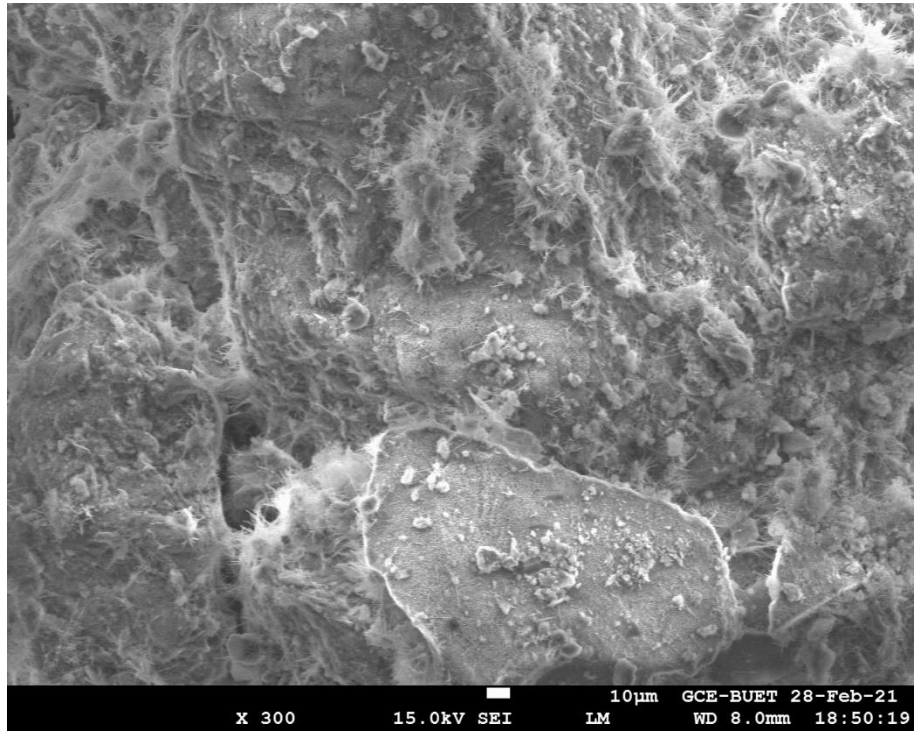


(l)

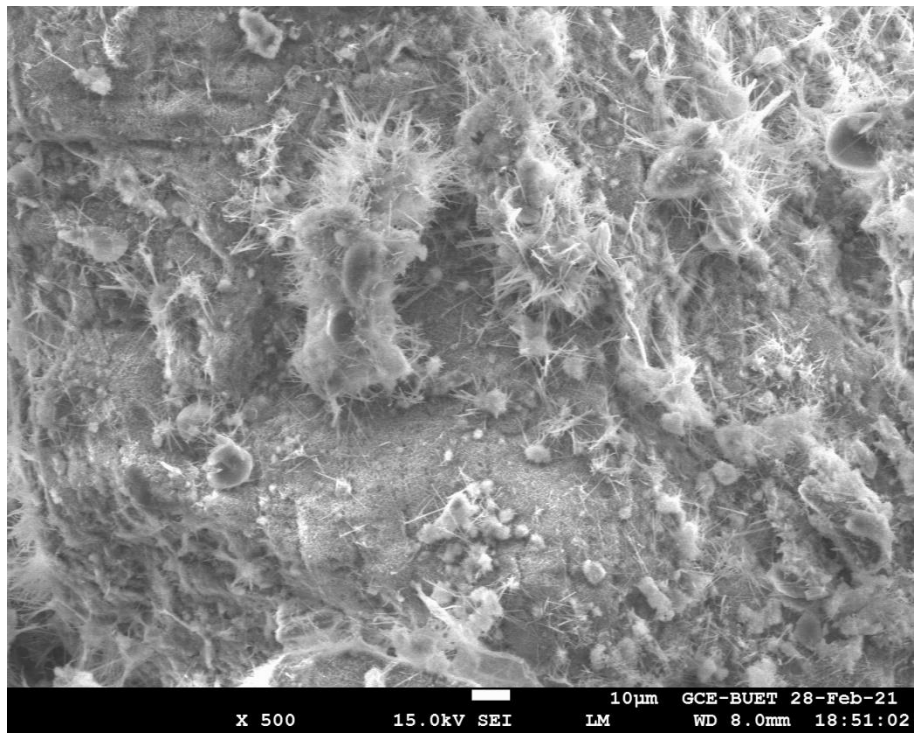


(m)

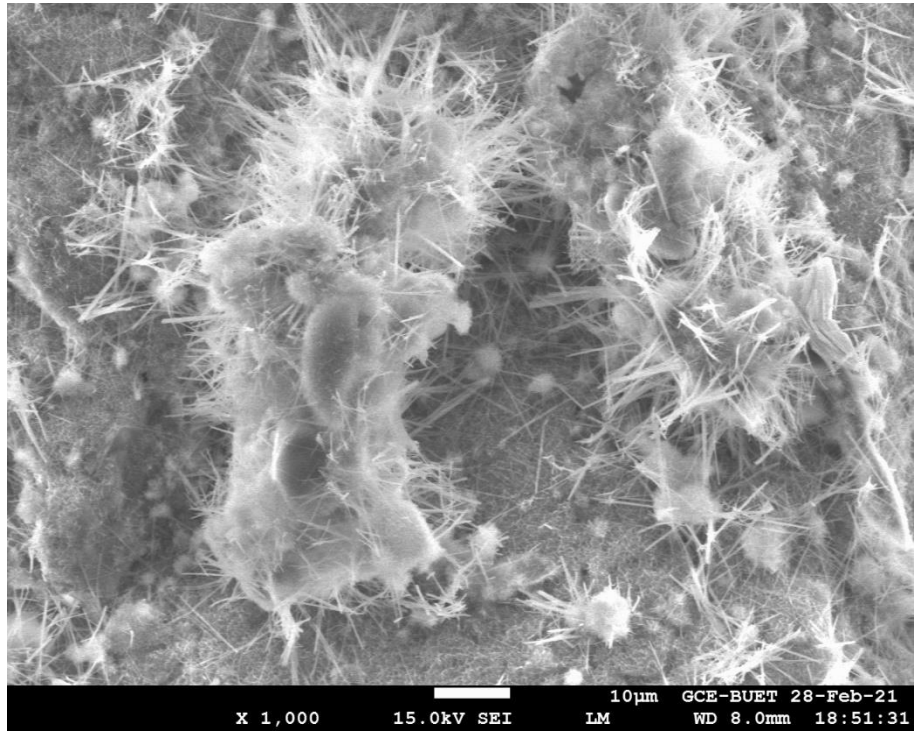
Figure A1: SEM Image of grouted three samples (5:1) after 28 days of curing of different wavelength: (a) 300 Hz (10 μ m) sample 1, (b) 500 Hz(10 μ m) sample 1, (c) 1000 Hz(10 μ m) sample 1 , (d) 2000 Hz (10 μ m) sample 1, (e) 3000 Hz (1 μ m), sample 1 (f) 5000Hz (1 μ m), sample 1 (g) 300 Hz (10 μ m), sample 2, (h) 300 Hz (10 μ m), sample 3 (i) 1000 Hz(10 μ m) sample 2, (j) 2000 Hz (10 μ m) sample 2, (k) 3000 Hz (1 μ m), sample 3, (l) 5000Hz (1 μ m), sample 2, (m) 2000 Hz (10 μ m) sample 3.



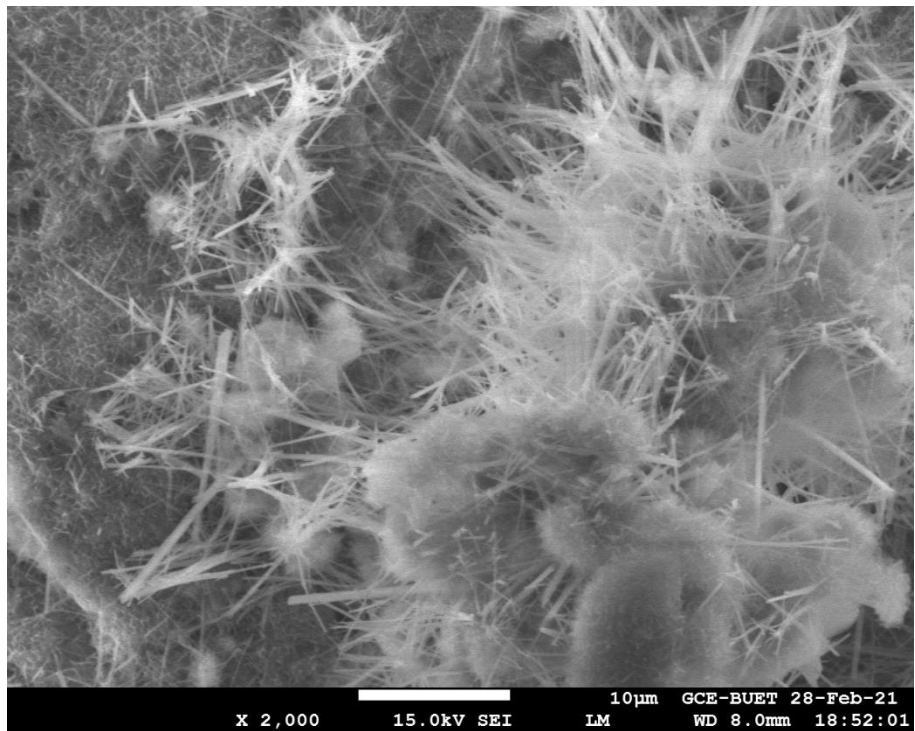
(a)



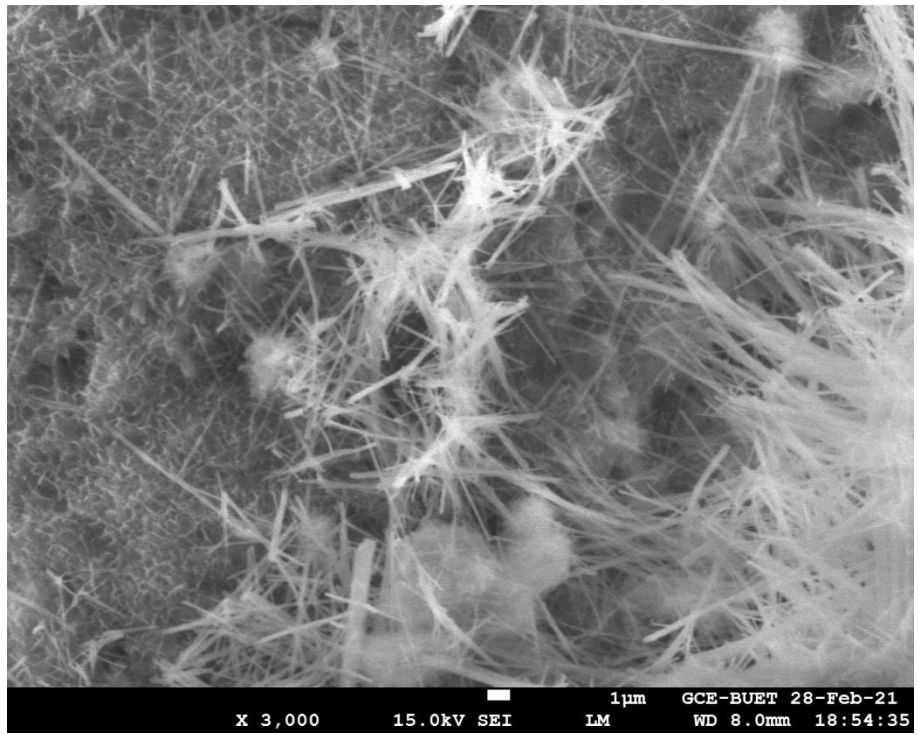
(b)



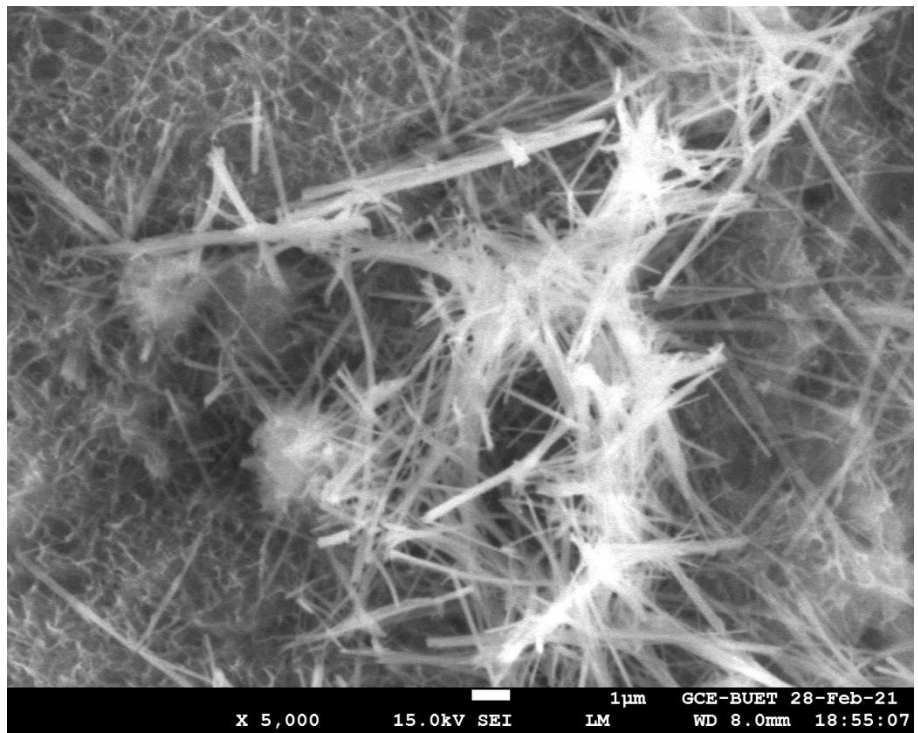
(c)



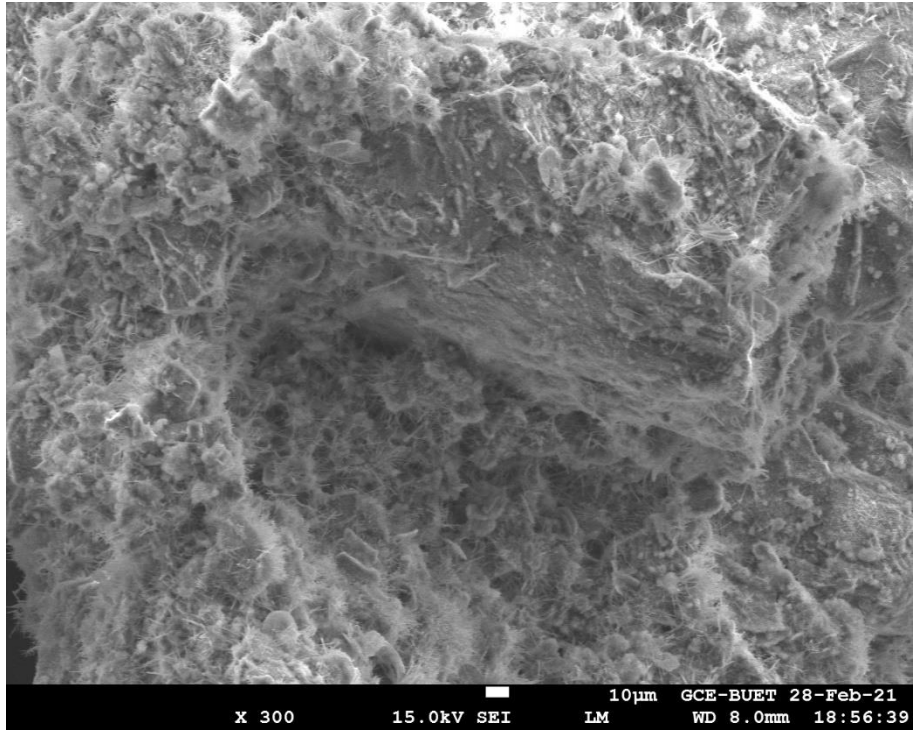
(d)



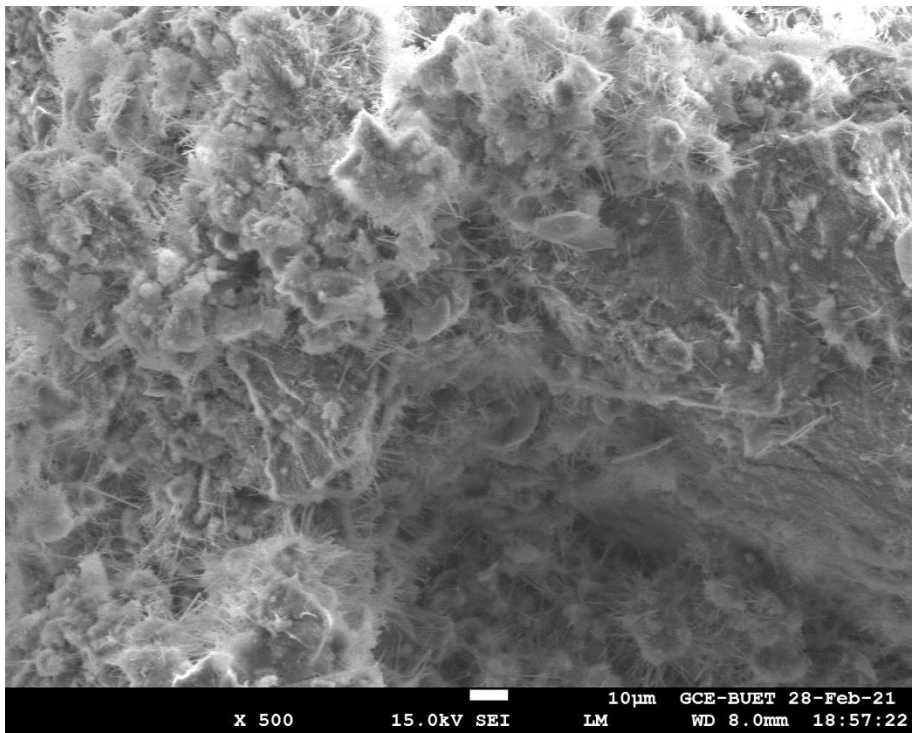
(e)



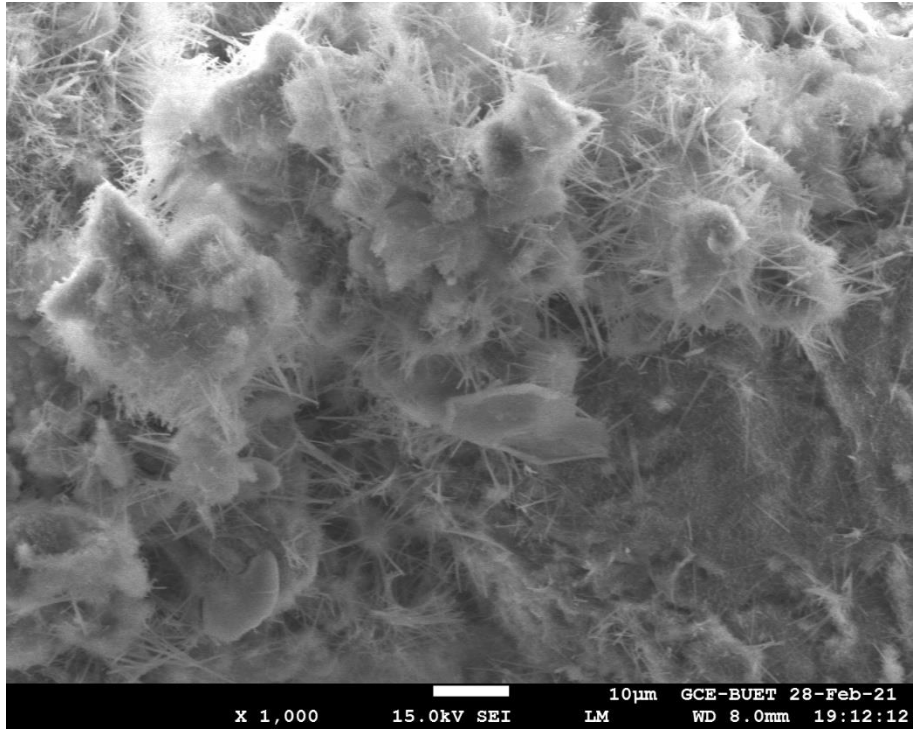
(f)



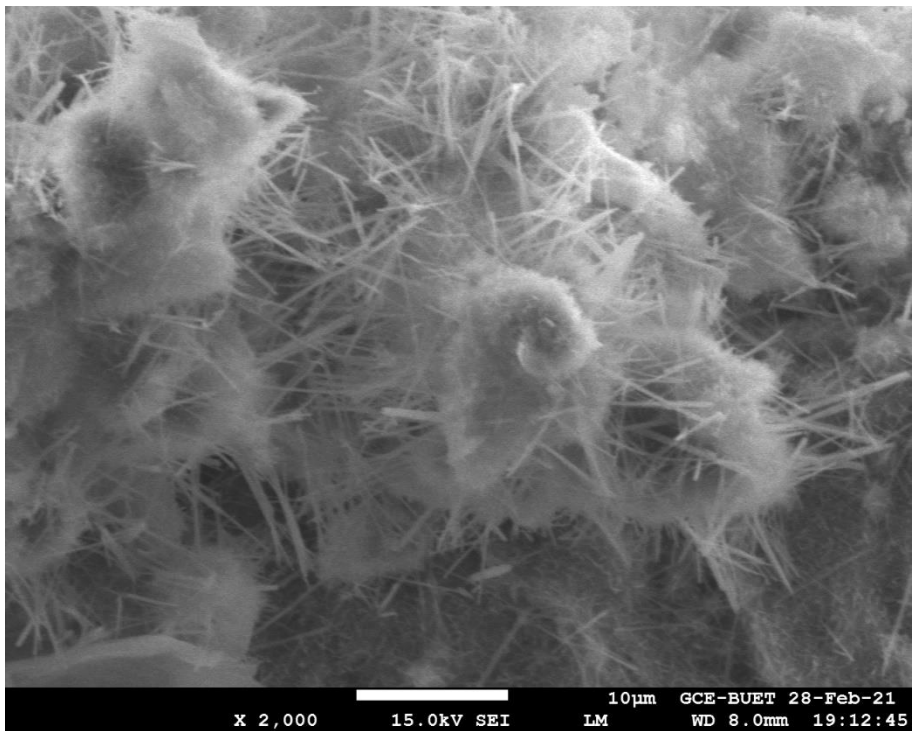
(g)



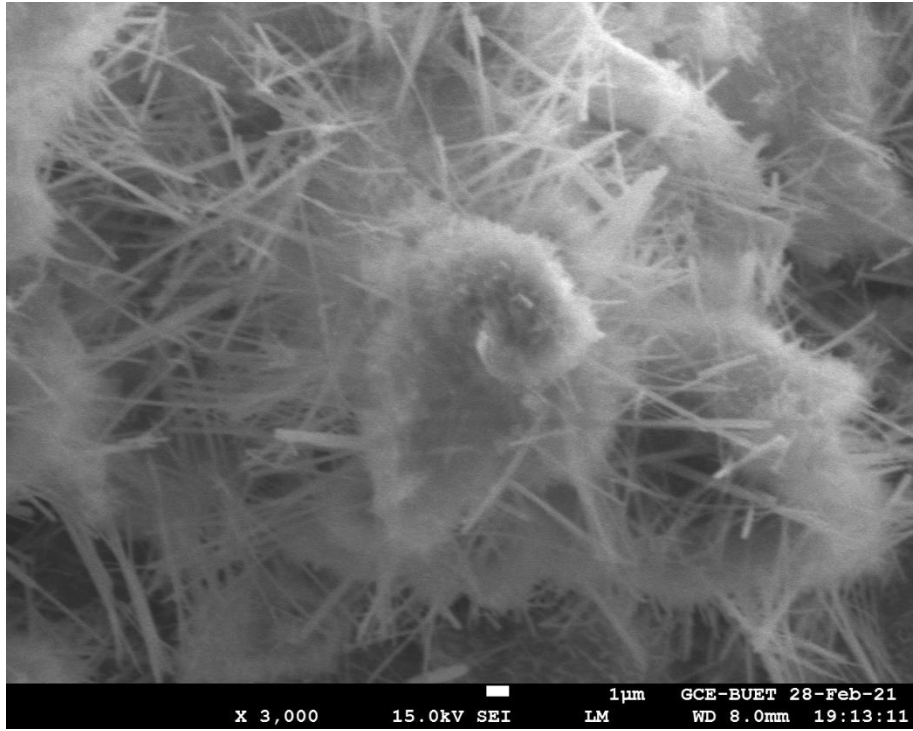
(h)



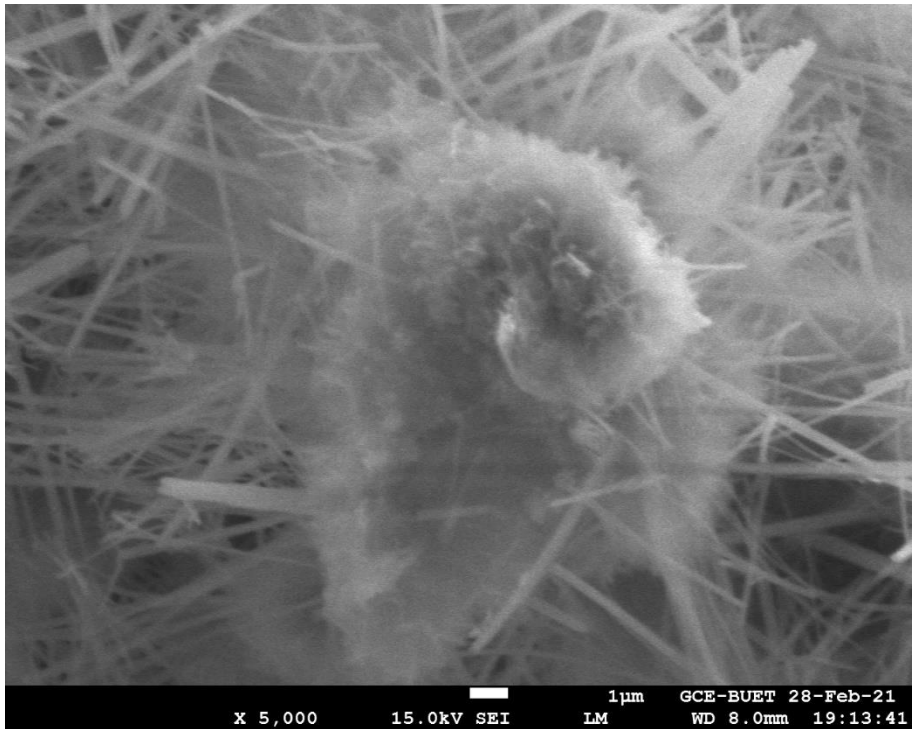
(i)



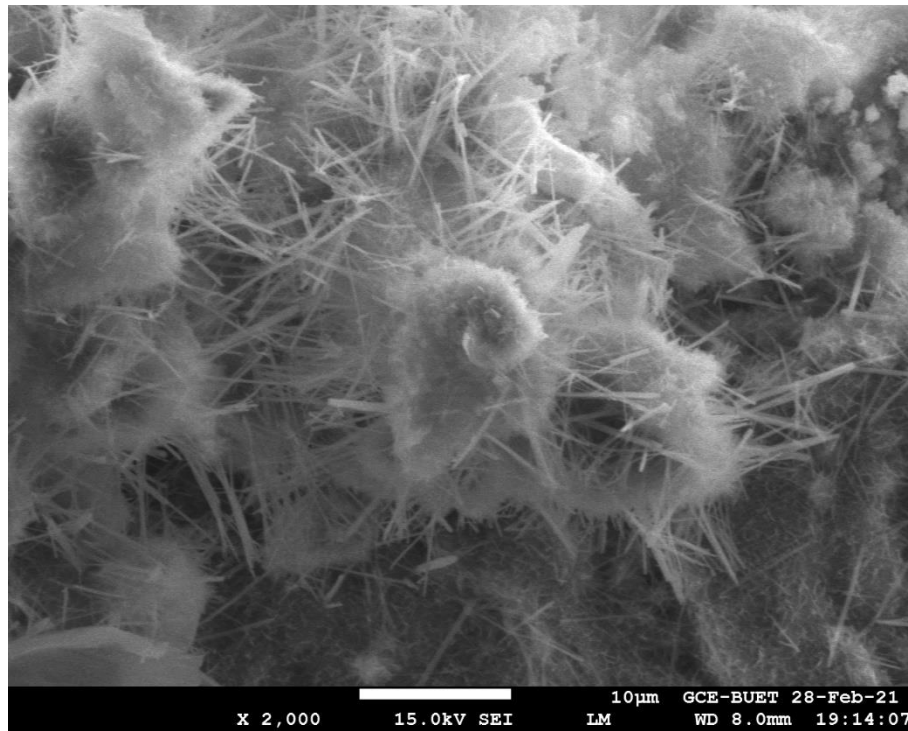
(j)



(k)

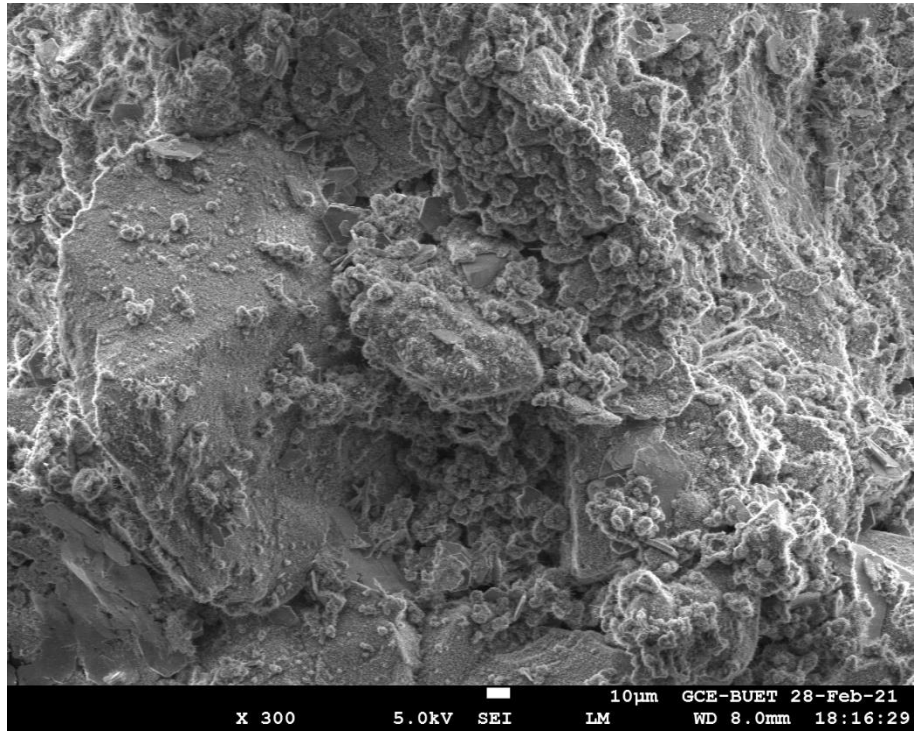


(l)

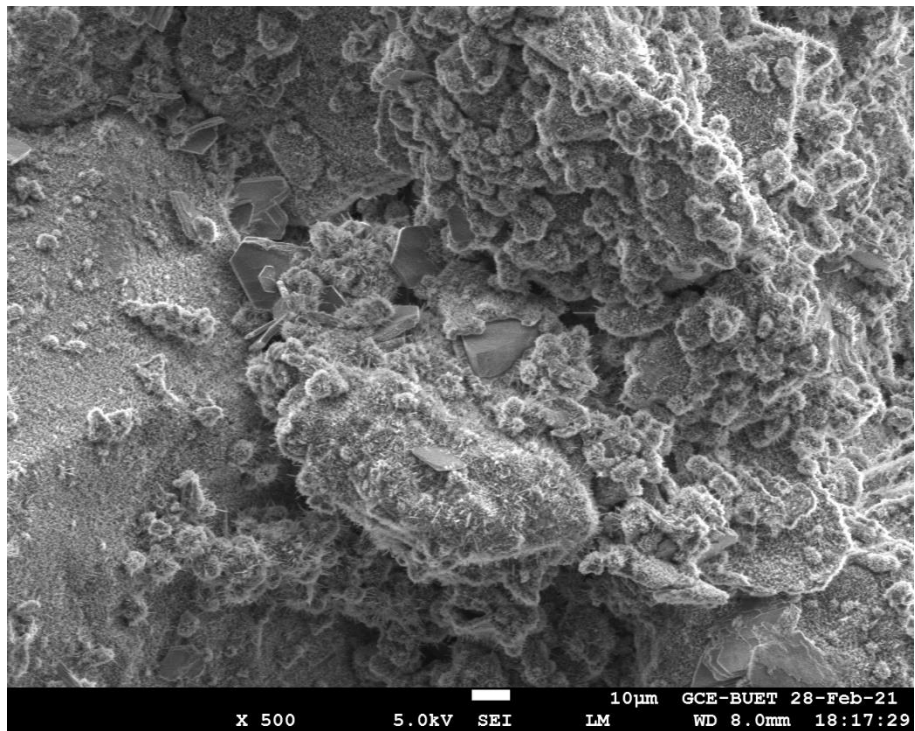


(m)

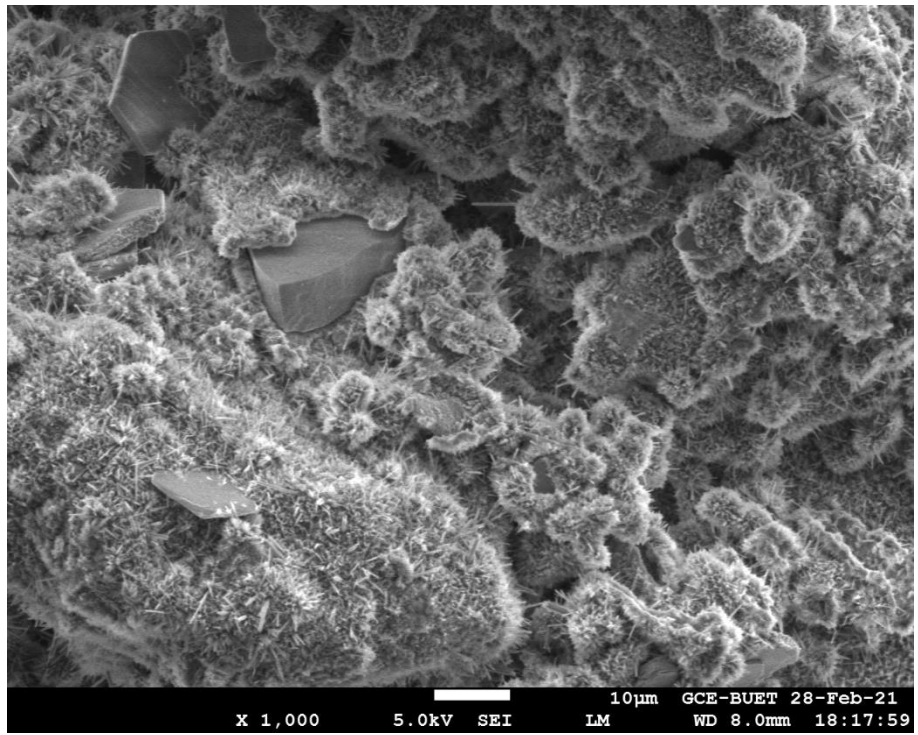
Figure A2: SEM Image of grouted three samples (4:1) after 28 days of curing of different wavelength: (a) 300 Hz (10µm) sample 1, (b) 500 Hz(10µm) sample 1, (c) 1000 Hz(10µm) sample 1 , (d) 2000 Hz (10µm) sample 1, (e) 3000 Hz (1µm), sample 1 (f) 5000Hz (1µm), sample 1 (g) 300 Hz (10µm), sample 2, (h) 300 Hz (10µm), sample 3 (i) 1000 Hz(10µm) sample 2, (j) 2000 Hz (10µm) sample 2, (k) 3000 Hz (1µm), sample 3, (l) 5000Hz (1µm), sample 2, (m) 2000 Hz (10µm) sample 3.



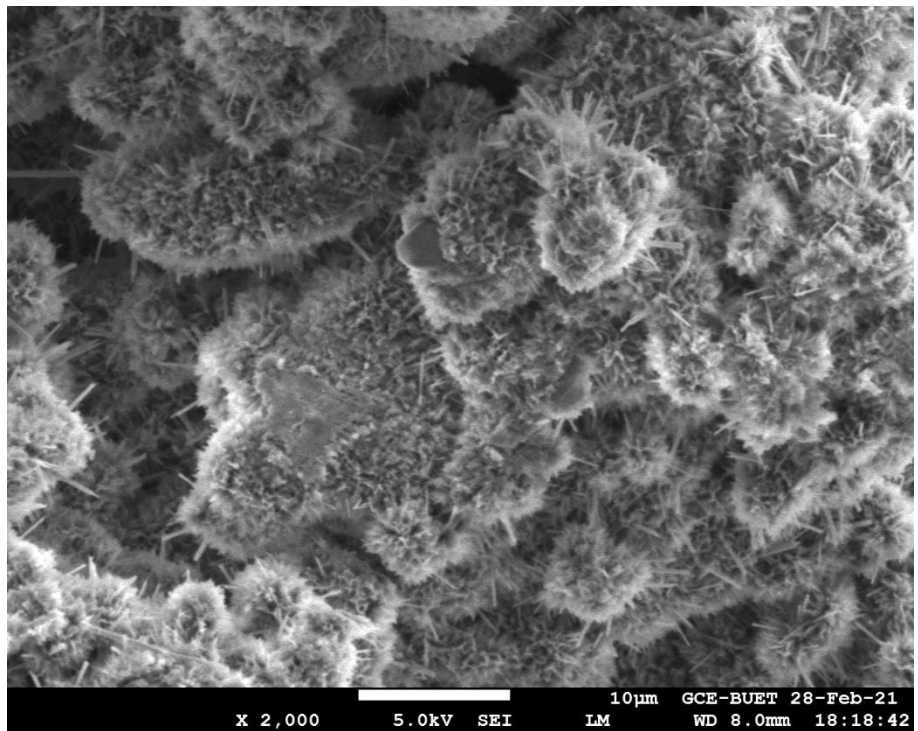
(a)



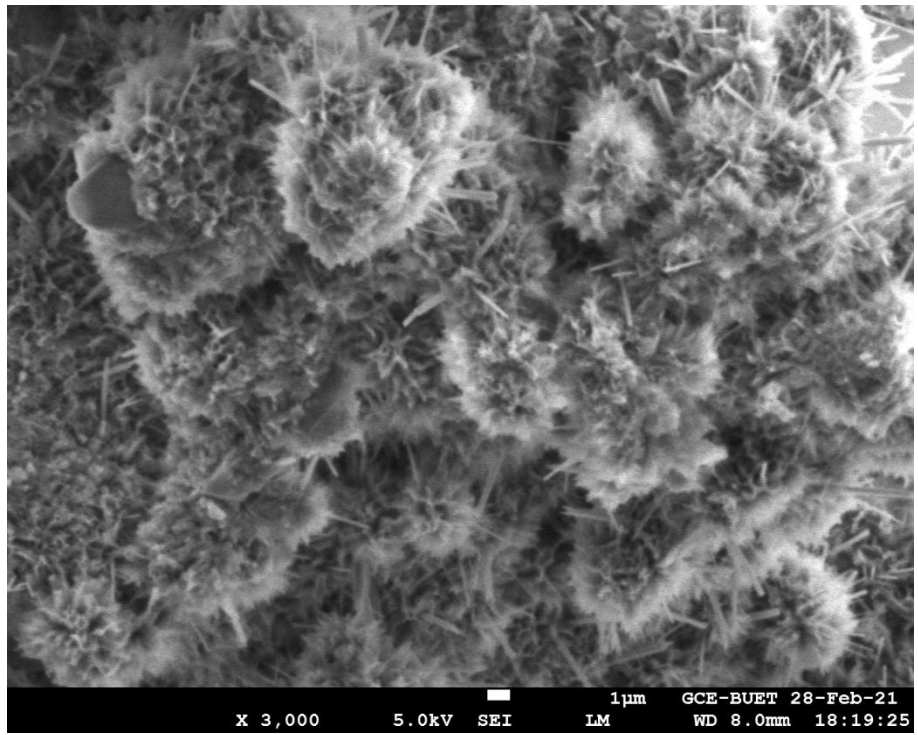
(b)



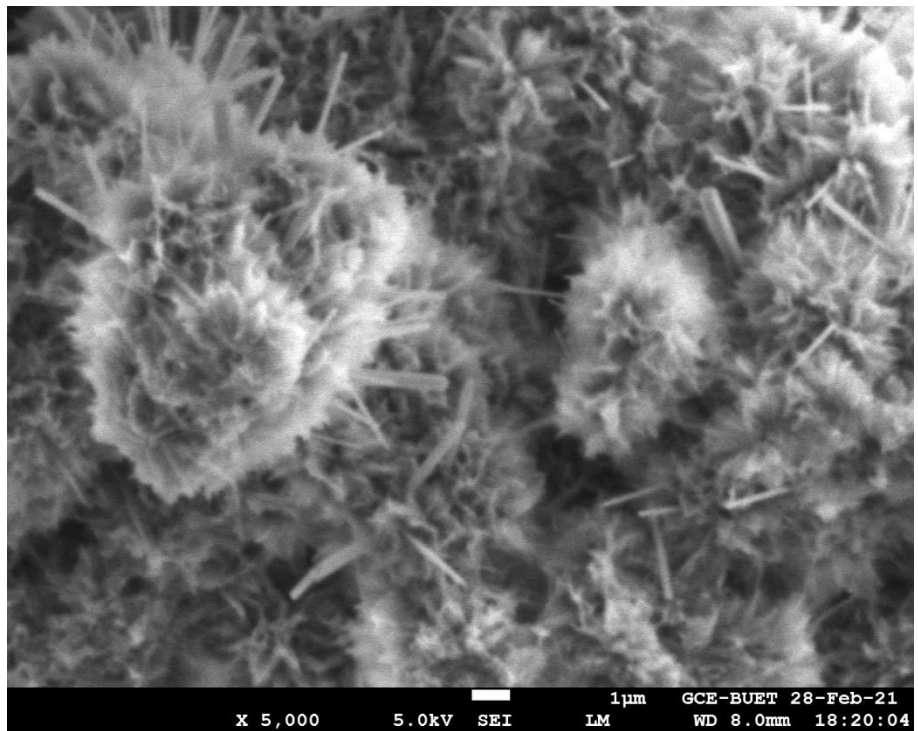
(c)



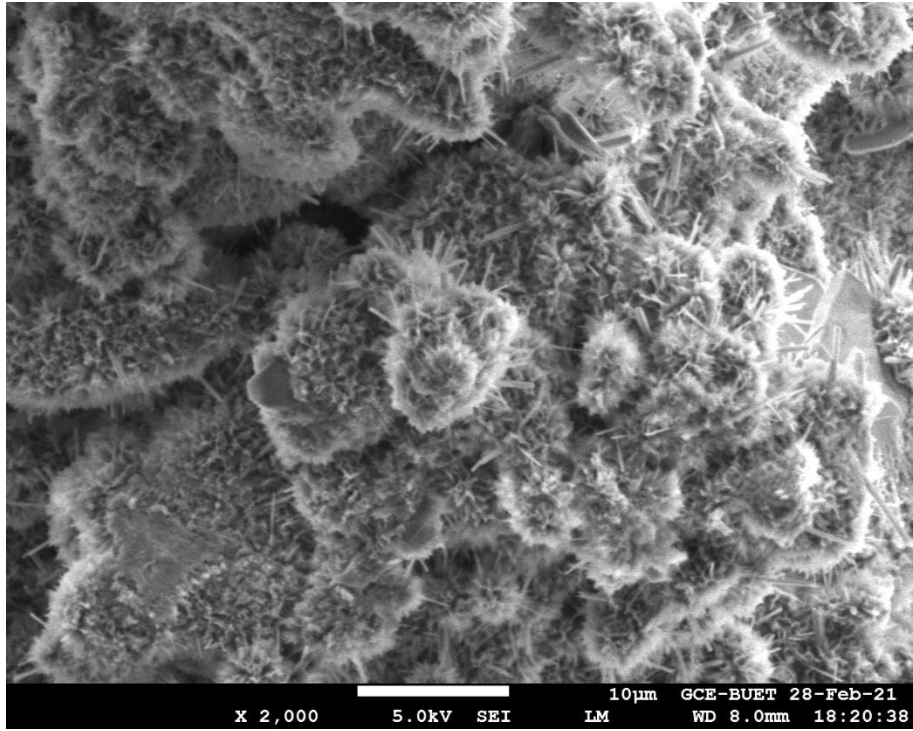
(d)



(e)

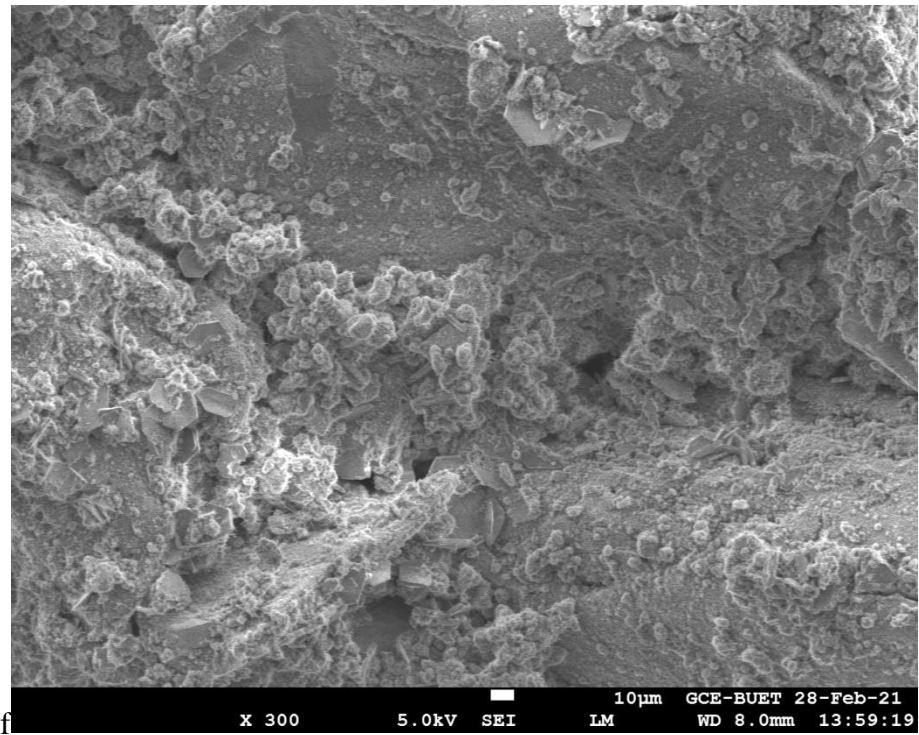


(f)

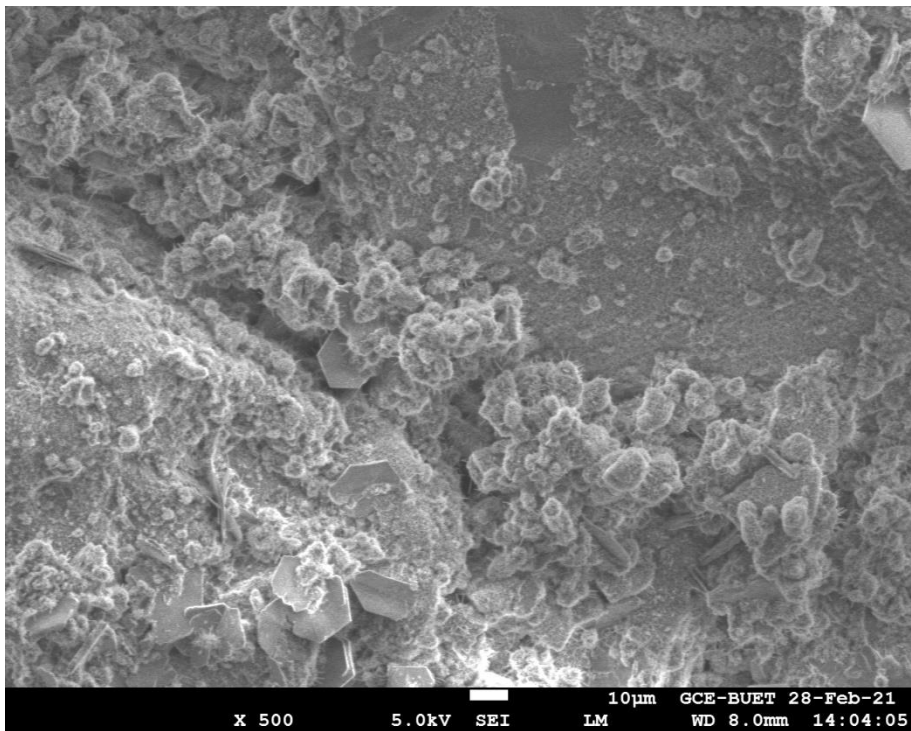


(g)

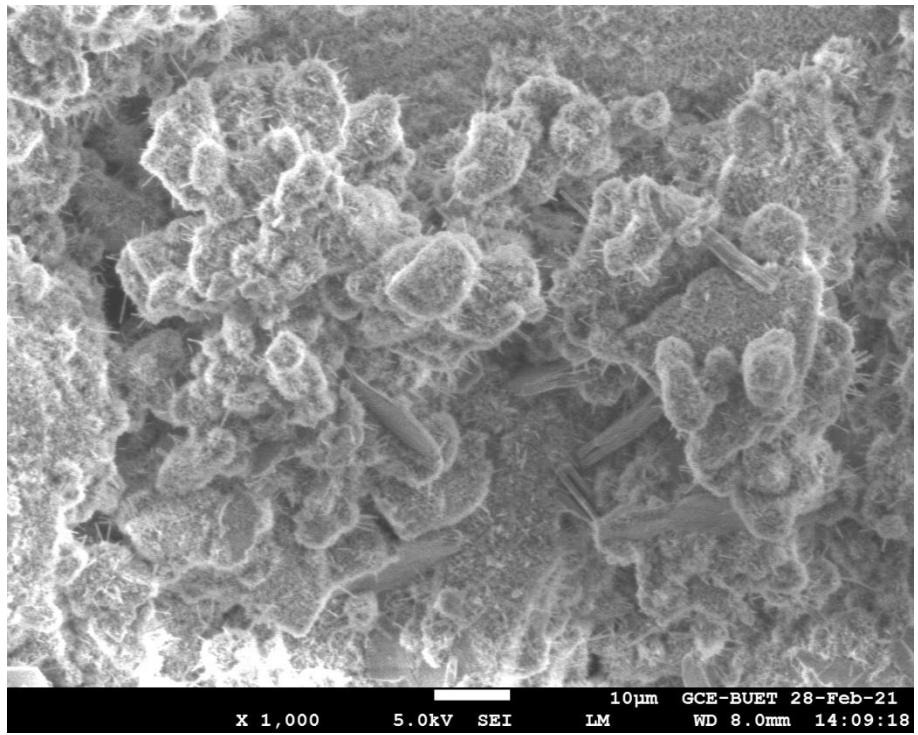
Figure A3: SEM Image of grouted three samples (2:1) after 28 days of curing of different wavelength: (a) 300 Hz (10µm) sample 1, (b) 500 Hz(10µm) sample 1, (c) 1000 Hz(10µm) sample 1 , (d) 2000 Hz (10µm) sample 2, (e) 3000 Hz (1µm), sample 2 (f) 5000Hz (1µm), sample 3 (g) 200 Hz (10µm), sample 3.



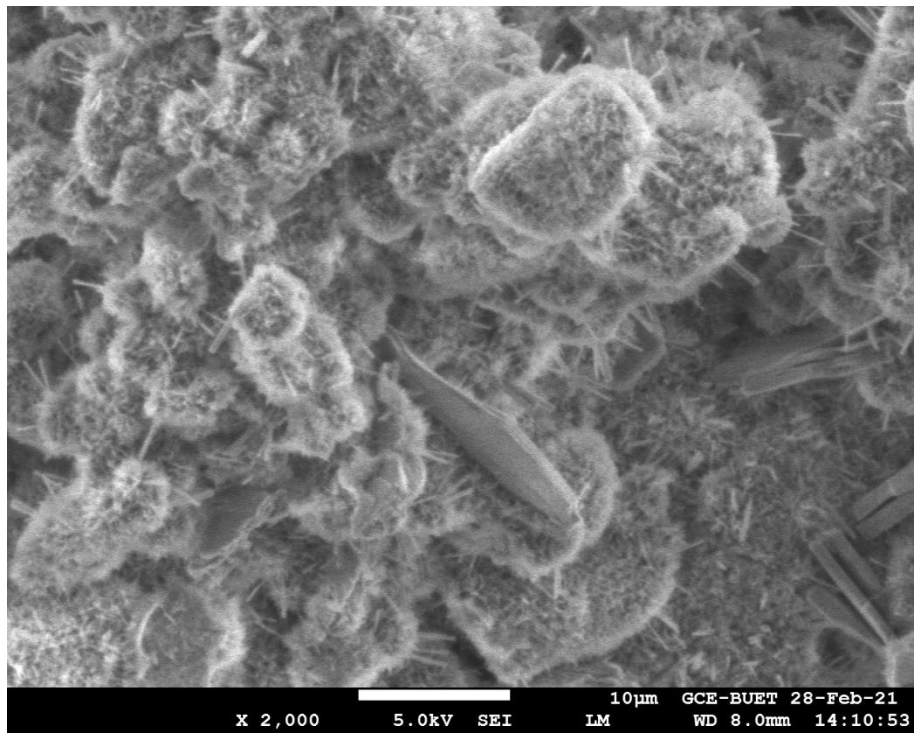
(a)



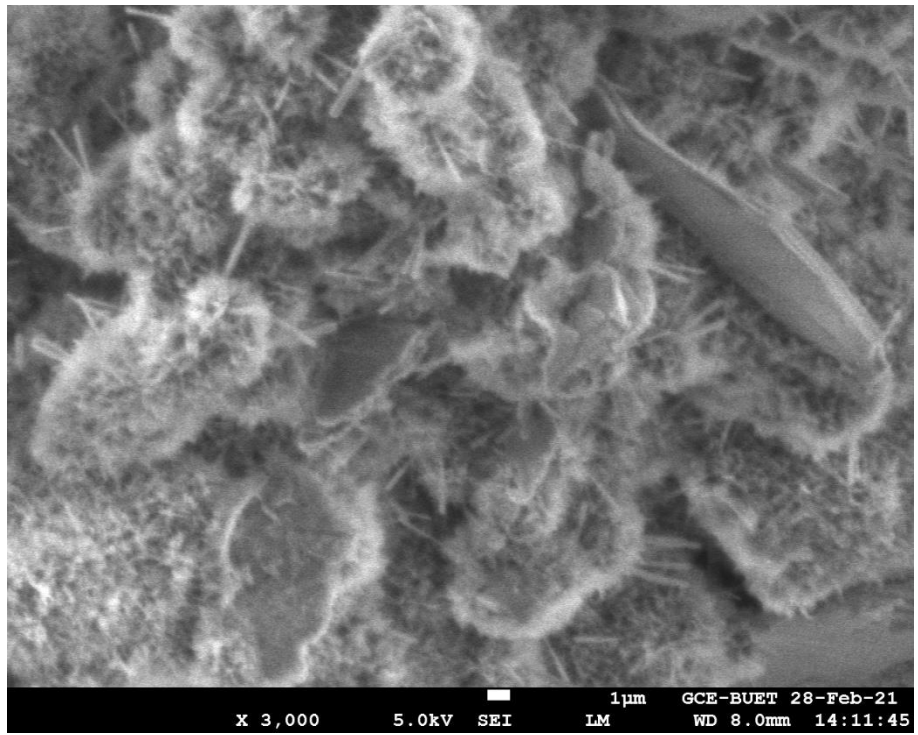
(b)



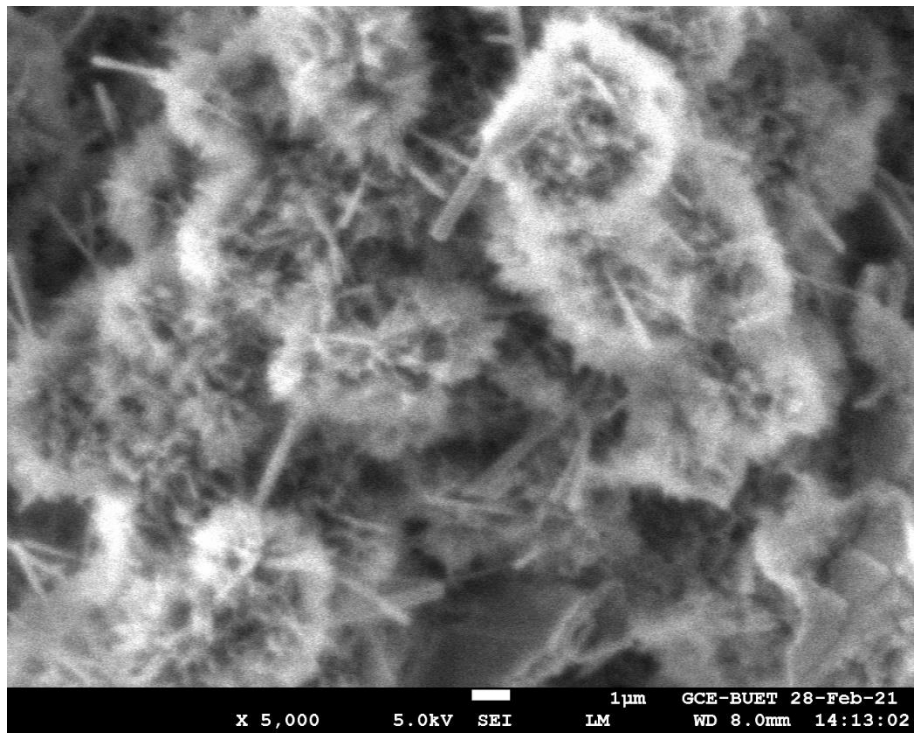
(c)



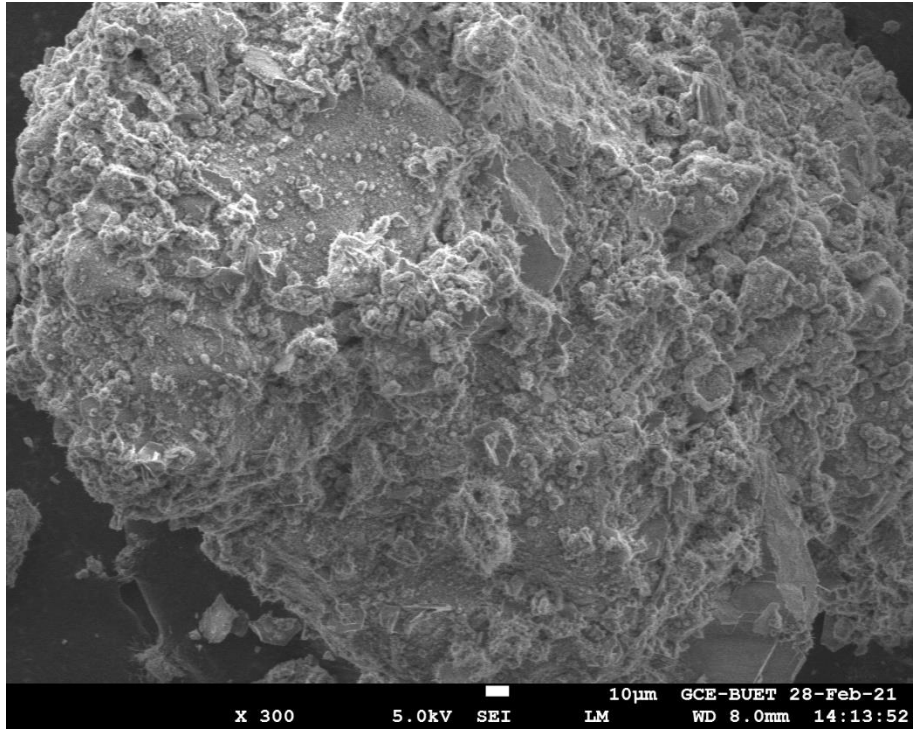
(d)



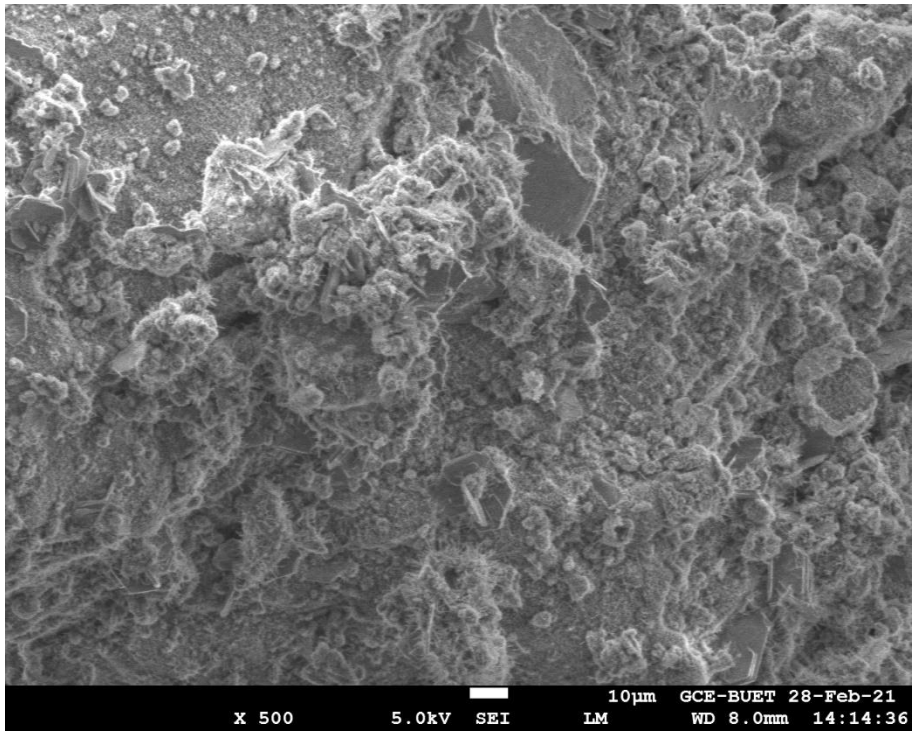
(e)



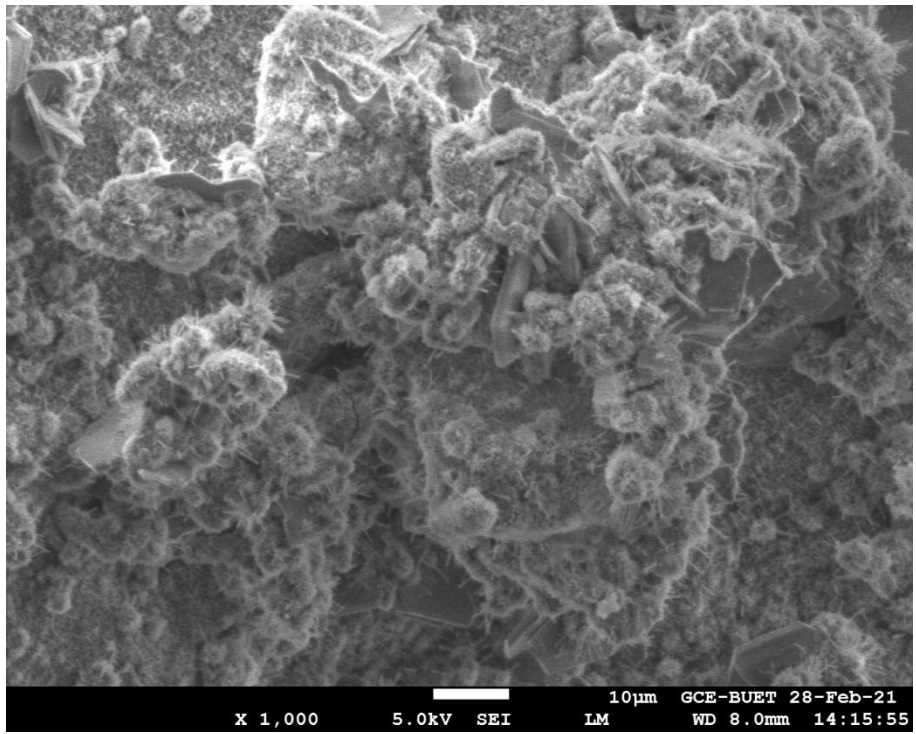
(f)



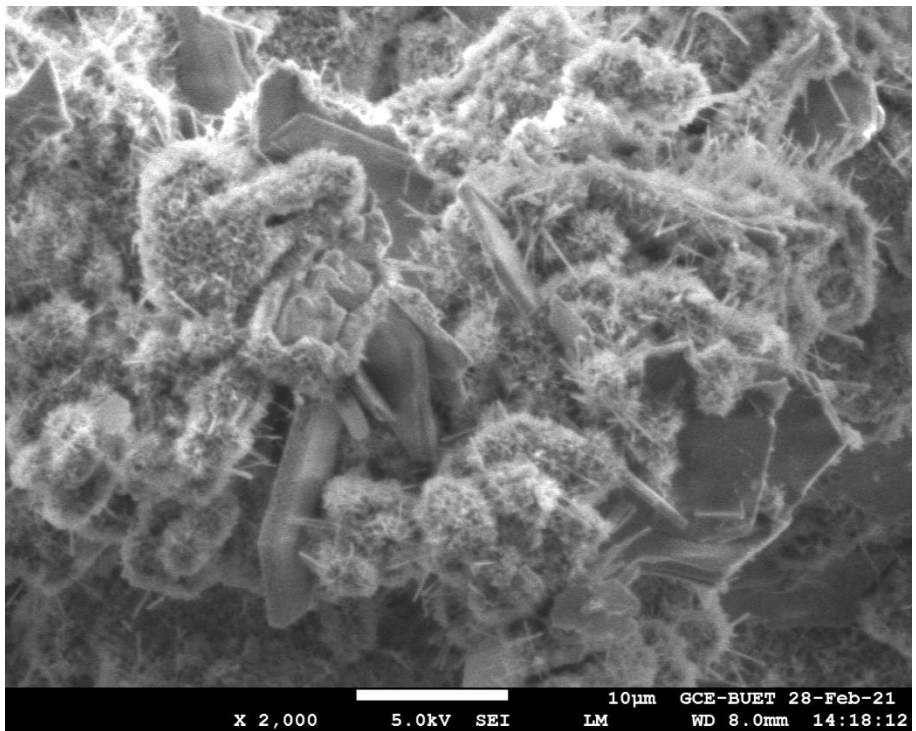
(g)



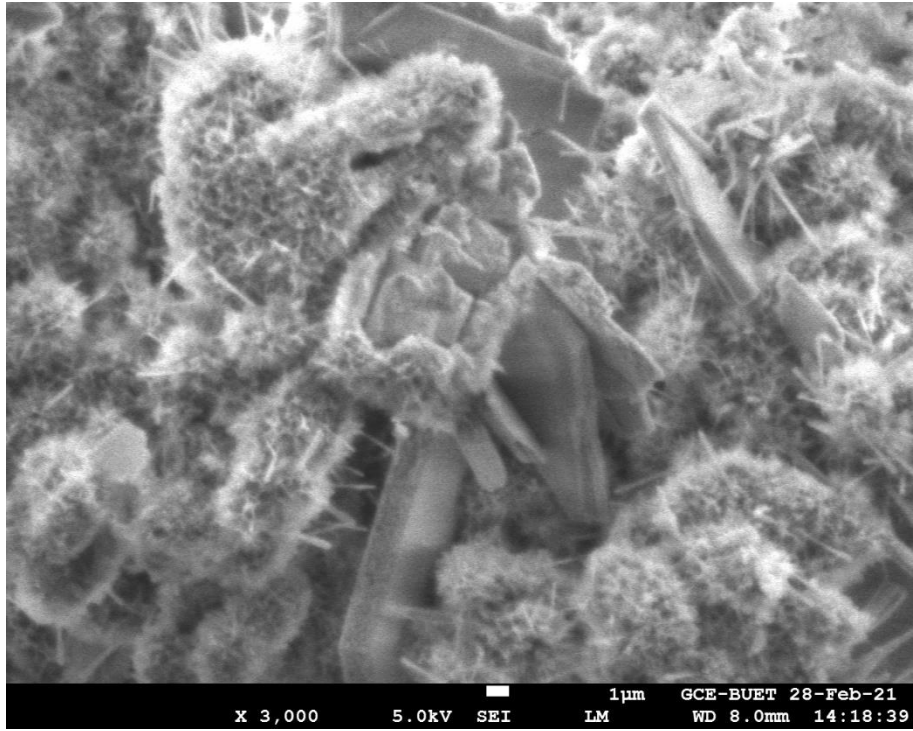
(h)



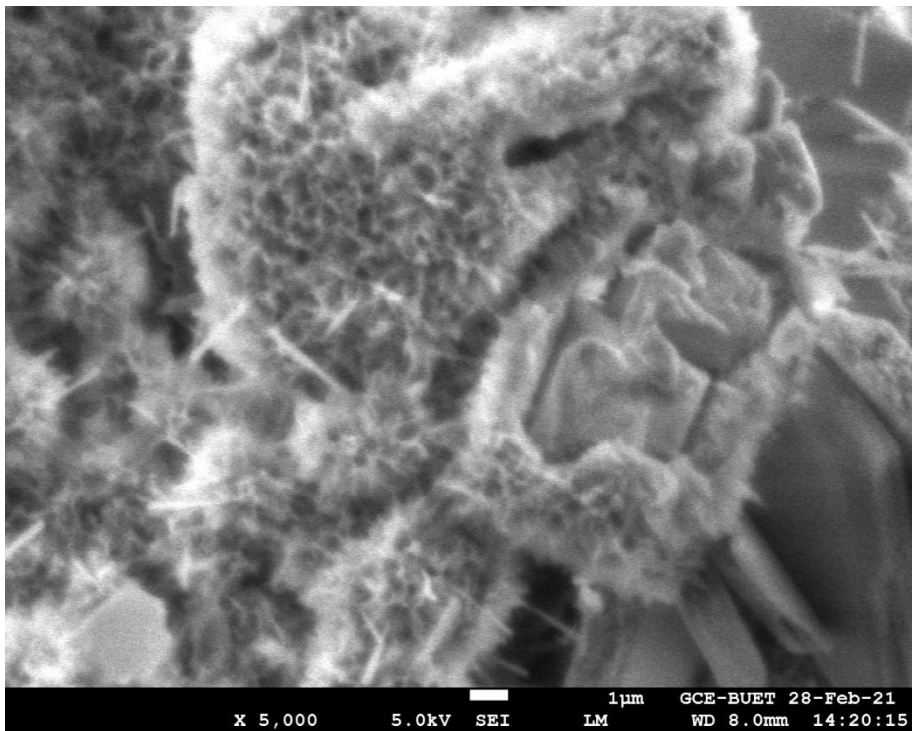
(i)



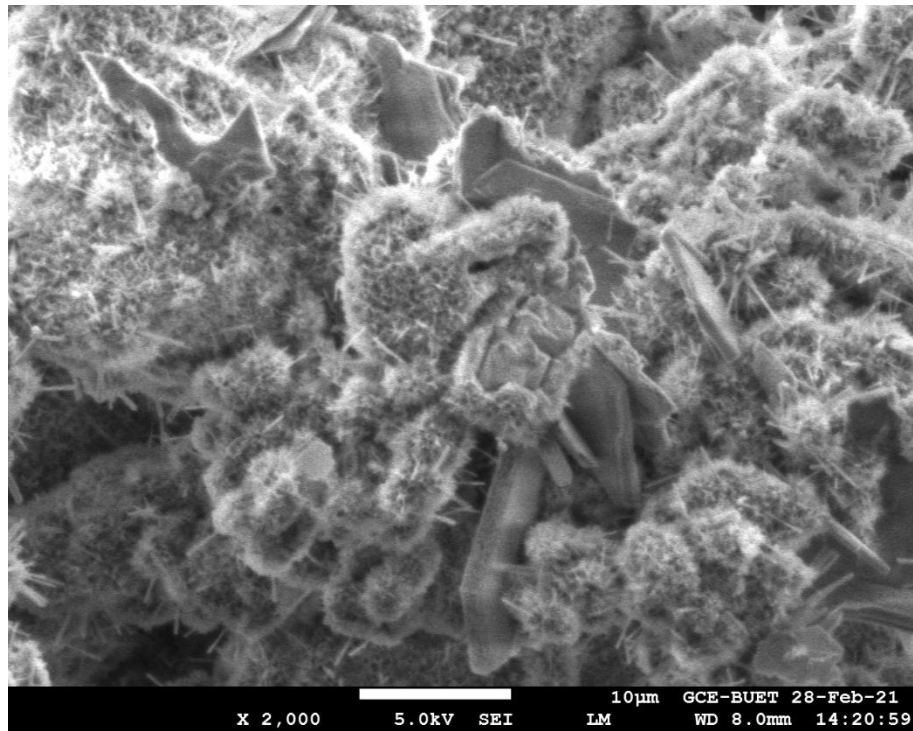
(j)



(k)



(l)

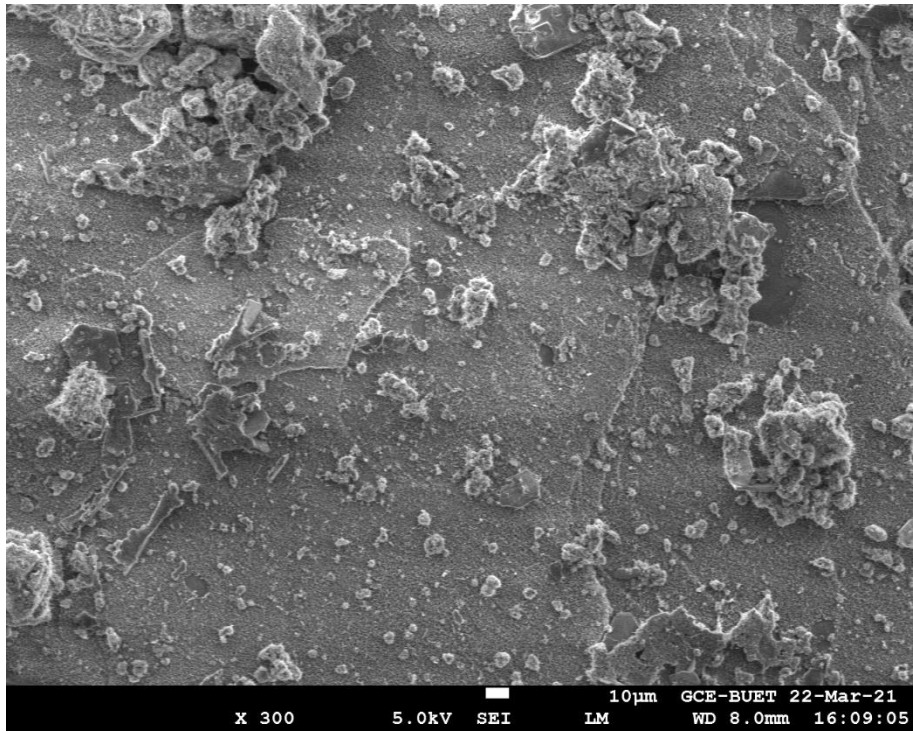


(m)

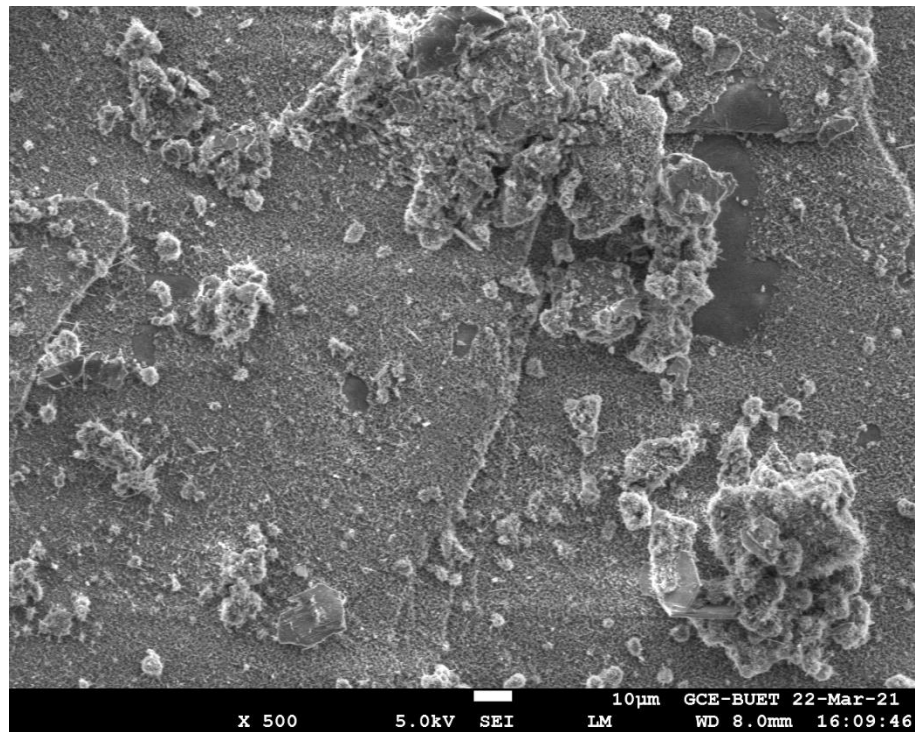
Figure A4: SEM Image of grouted three samples (2:1) after 28 days of curing of different wavelength: (a) 300 Hz (10µm) sample 1, (b) 500 Hz(10µm) sample 1, (c) 1000 Hz(10µm) sample 1 , (d) 2000 Hz (10µm) sample 1, (e) 3000 Hz (1µm), sample 1 (f) 5000Hz (1µm), sample 1 (g) 300 Hz (10µm), sample 2, (h) 300 Hz (10µm), sample 3 (i) 1000 Hz(10µm) sample 2, (j) 2000 Hz (10µm) sample 2, (k) 3000 Hz (1µm), sample 3, (l) 5000Hz (1µm), sample 2, (m) 2000 Hz (10µm) sample 3.

Appendix B

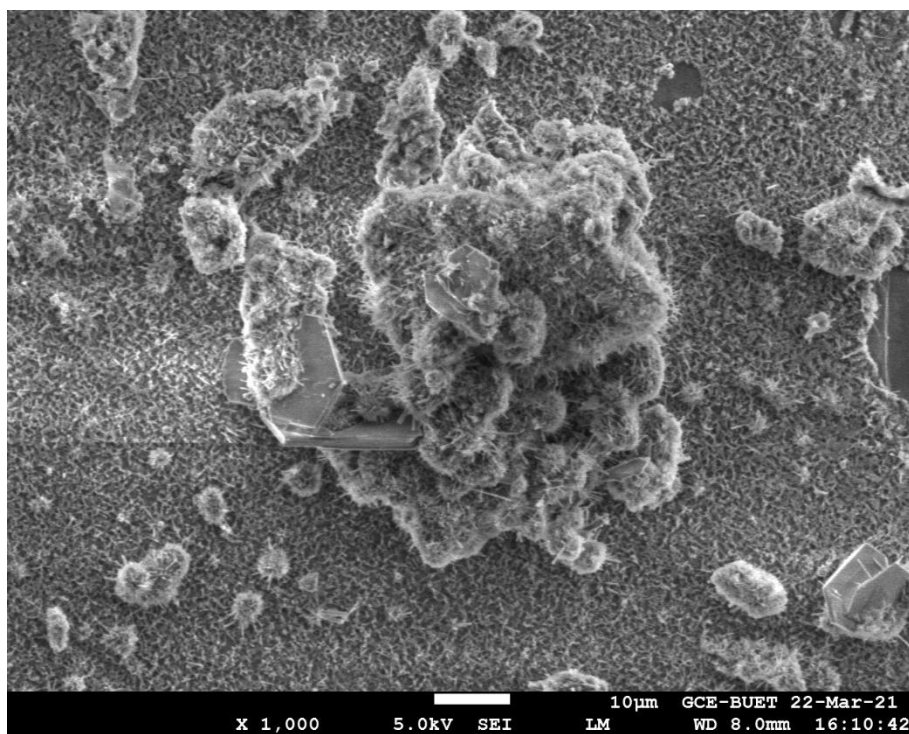
Scanning Electron Microscope Images of Grouted
Samples with W:C ratio 5:1, 4:1, 3:1 and 2:1
Cured for 90 days



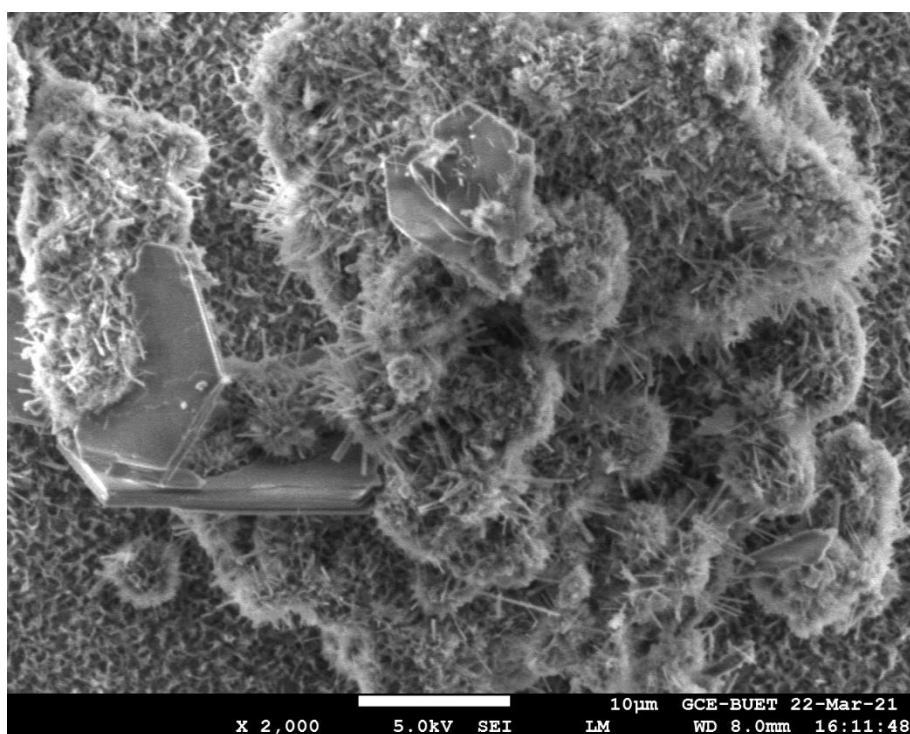
(a)



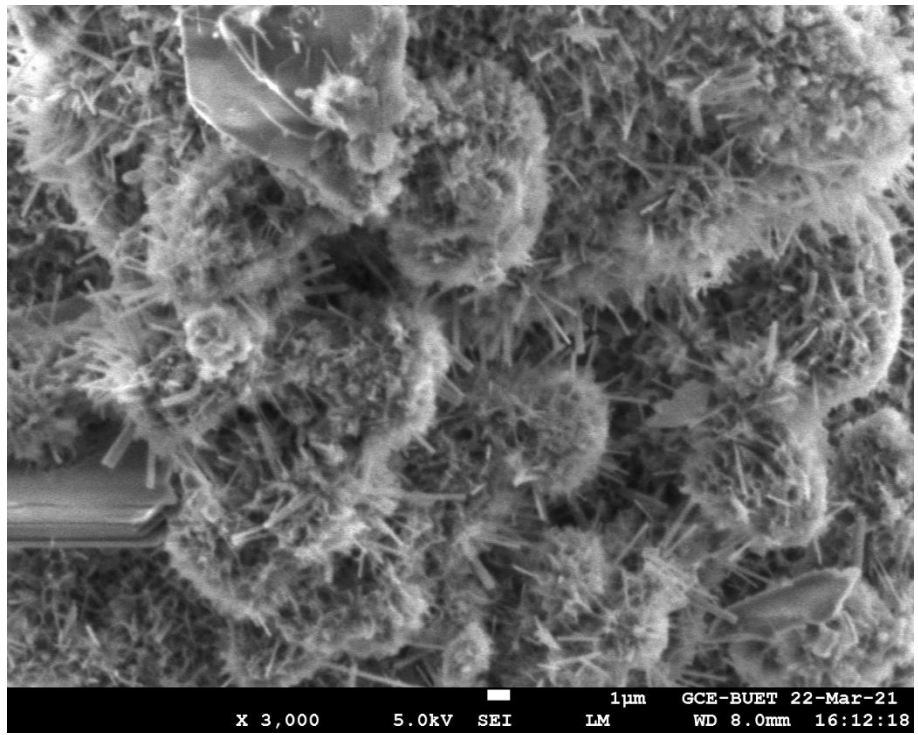
(b)



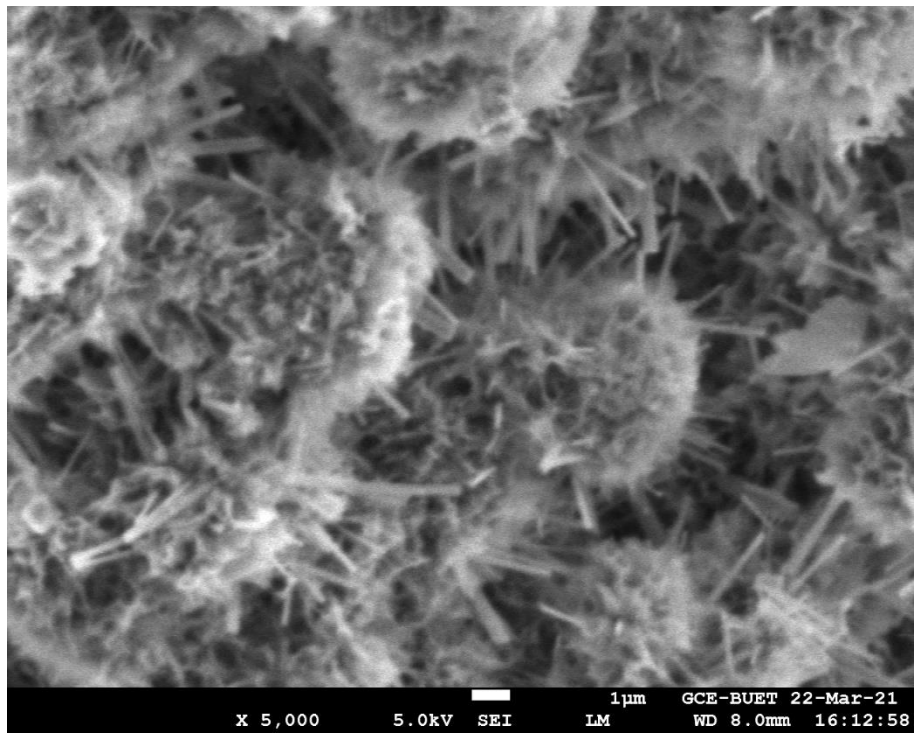
(c)



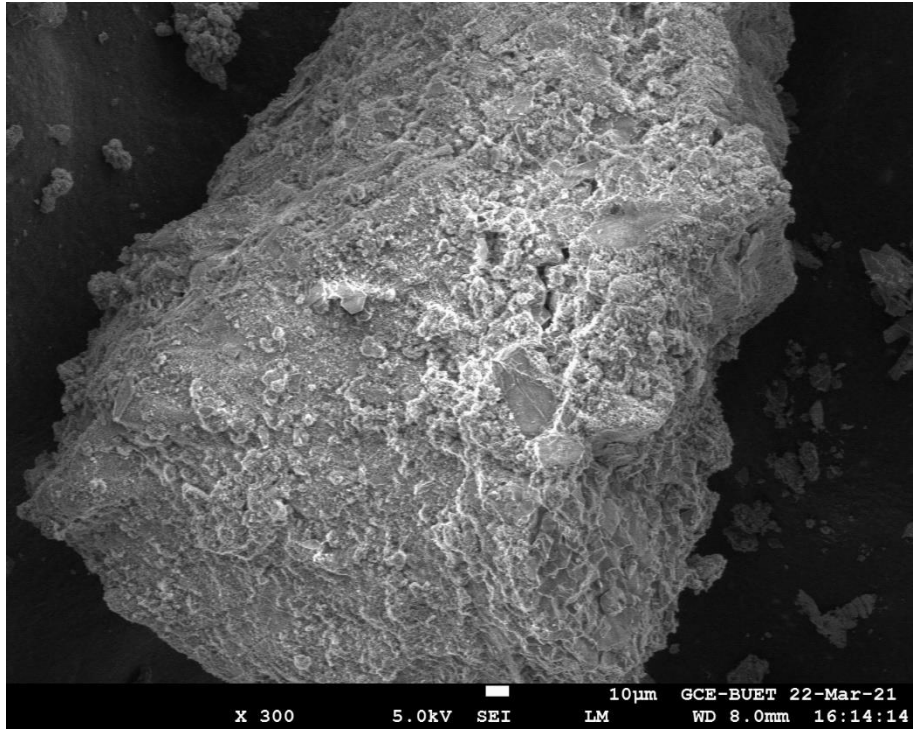
(d)



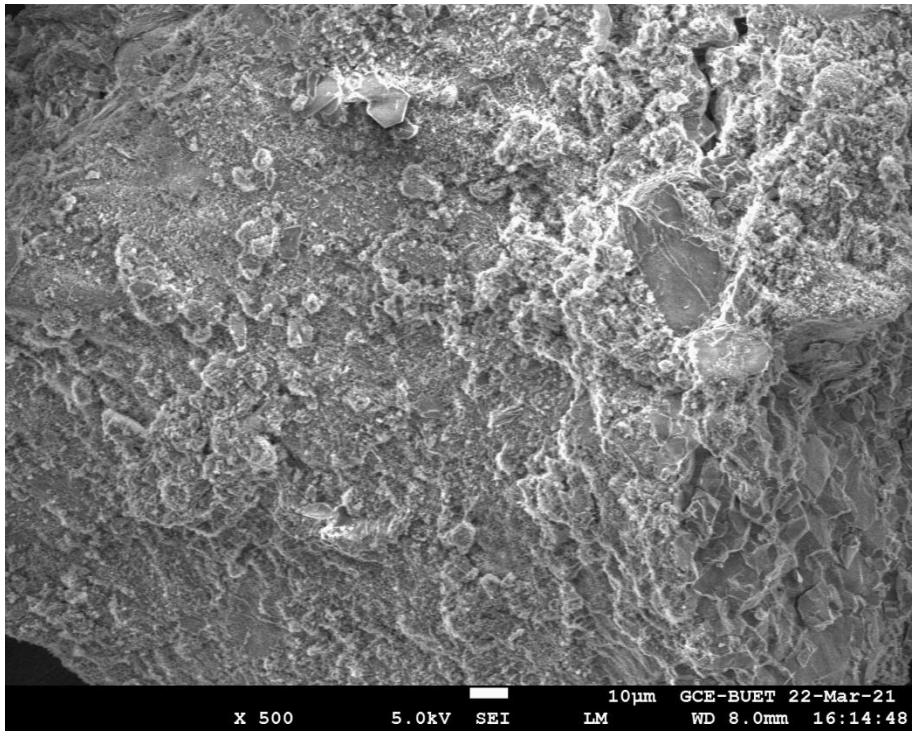
(e)



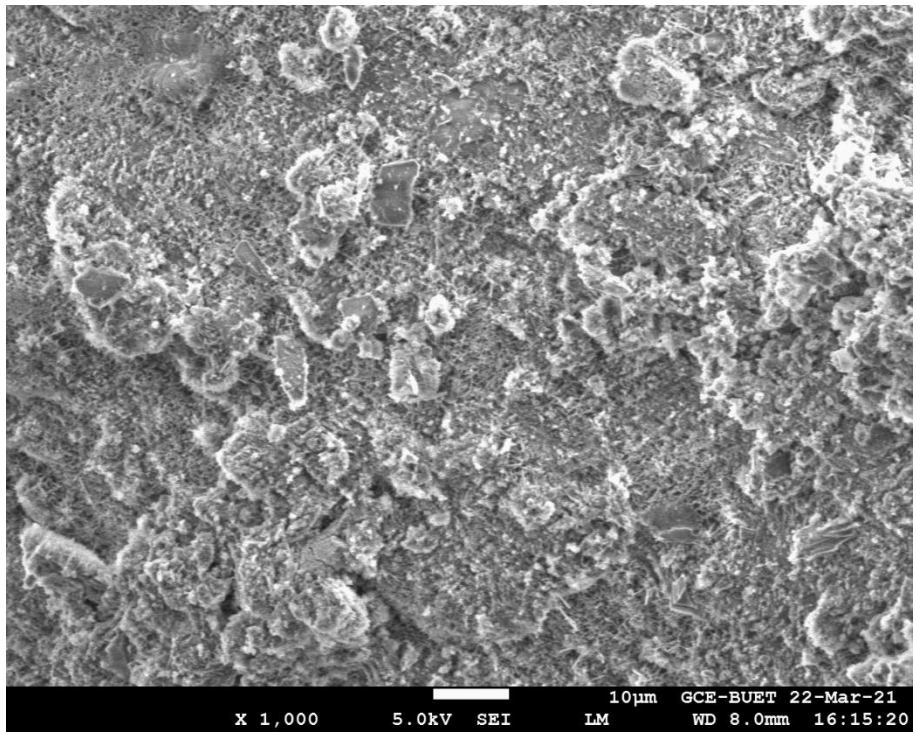
(f)



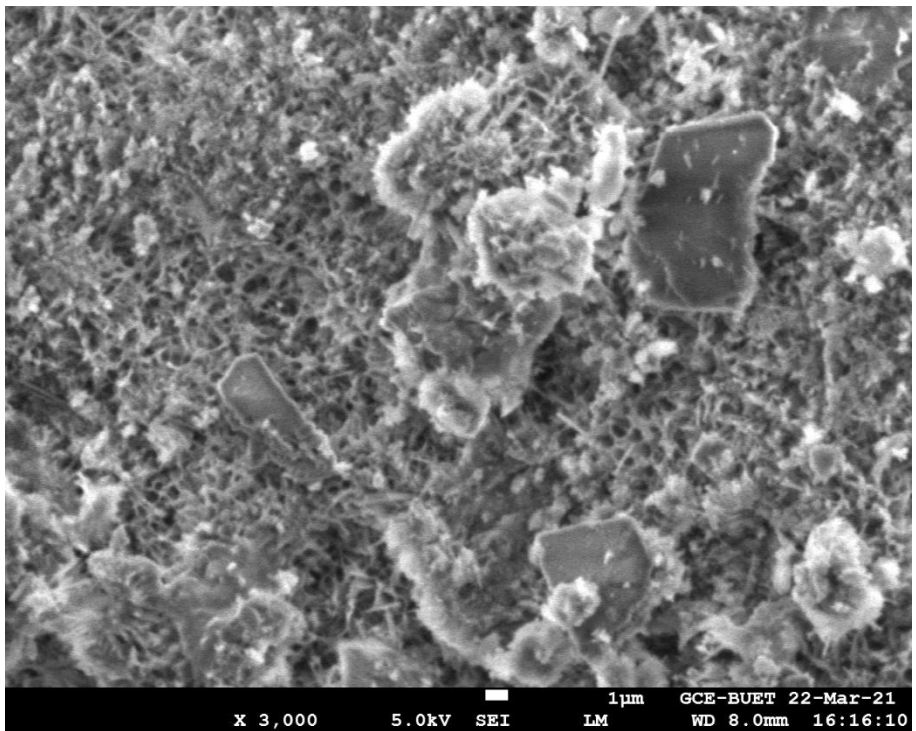
(g)



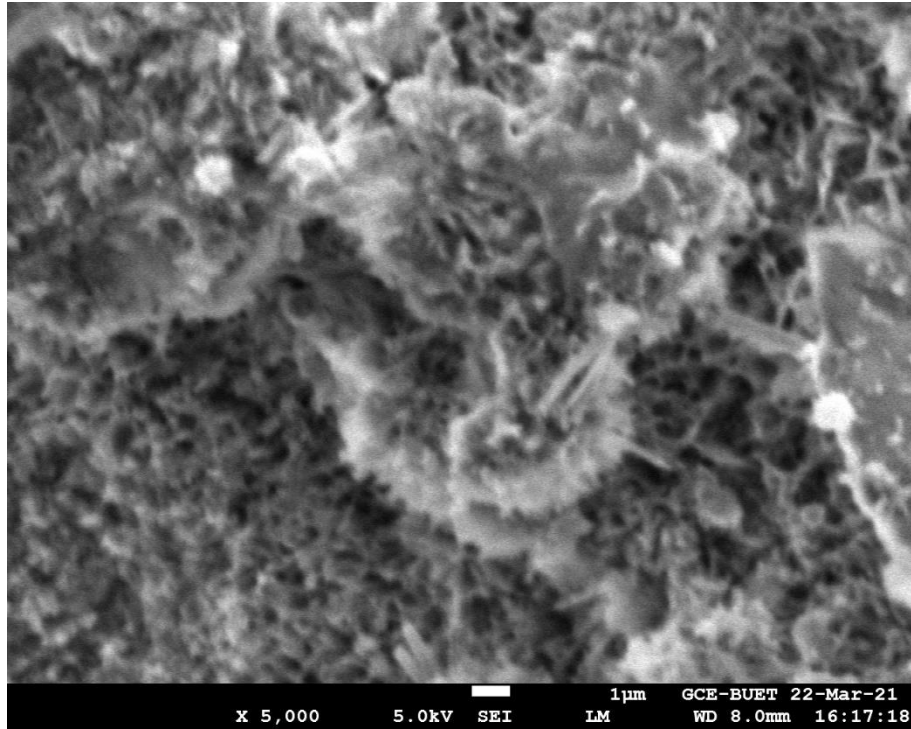
(h)



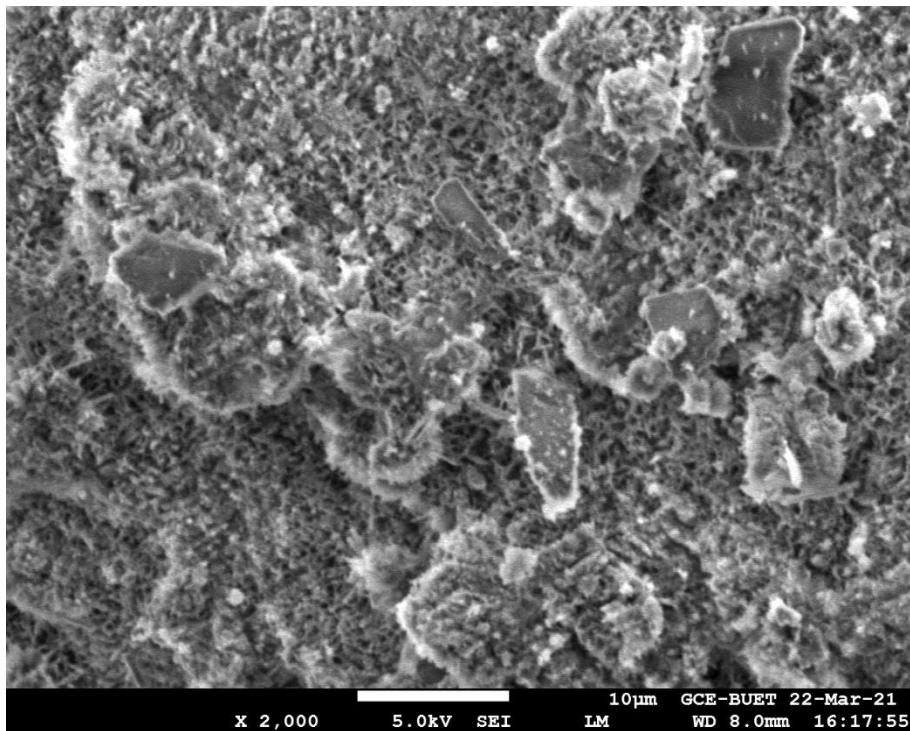
(i)



(j)

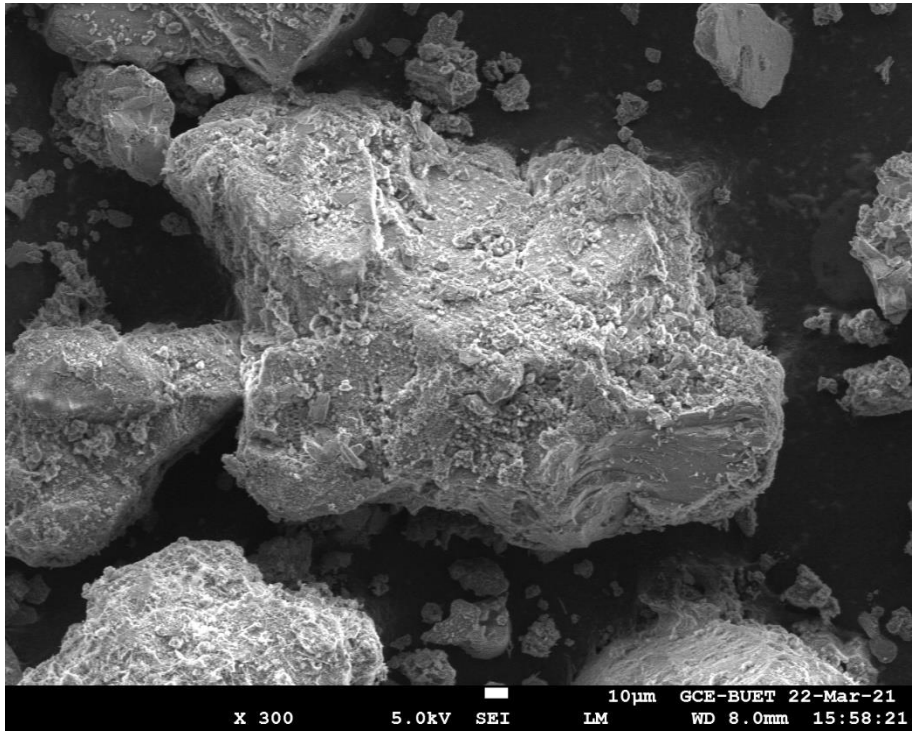


(k)

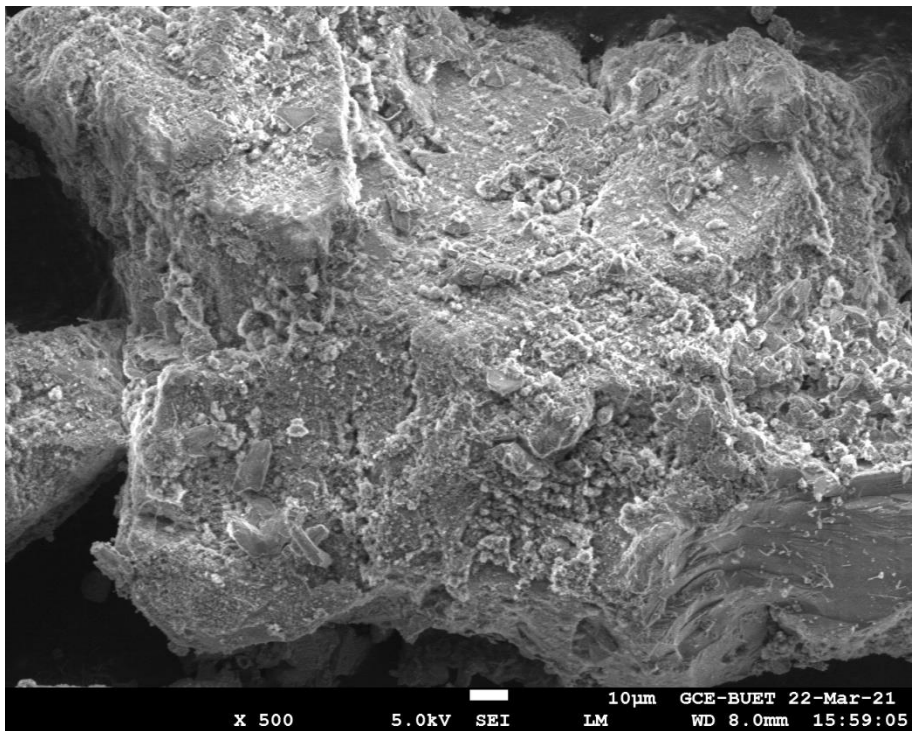


(l)

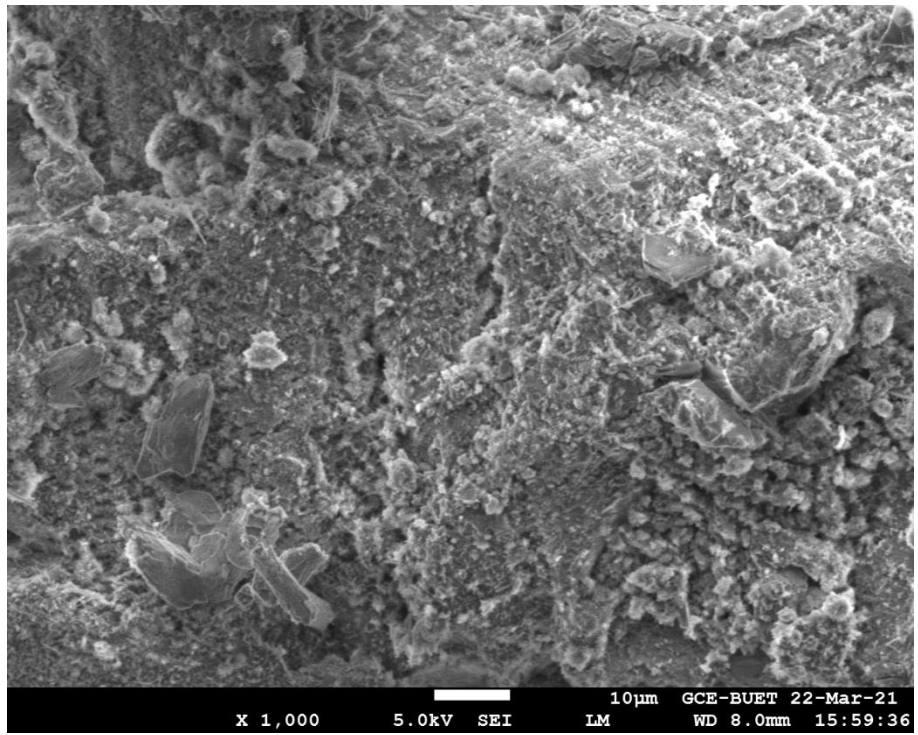
Figure B1: SEM Image of grouted three samples (5:1) after 90 days of curing of different wavelength: (a) 300 Hz (10 μ m) sample 1, (b) 500 Hz(10 μ m) sample 1, (c) 1000 Hz(10 μ m) sample 1, (d) 2000 Hz (10 μ m) sample 1, (e) 3000 Hz (1 μ m), sample 1 (f) 5000Hz (1 μ m), sample 1 (g) 300 Hz (10 μ m), sample 2, (h) 500 Hz (10 μ m), sample 3 (i) 1000 Hz(10 μ m) sample 2, (j) 3000 Hz (10 μ m) sample 2, (k) 5000 Hz (1 μ m), sample 3, (l) 2000Hz (1 μ m), sample 2,



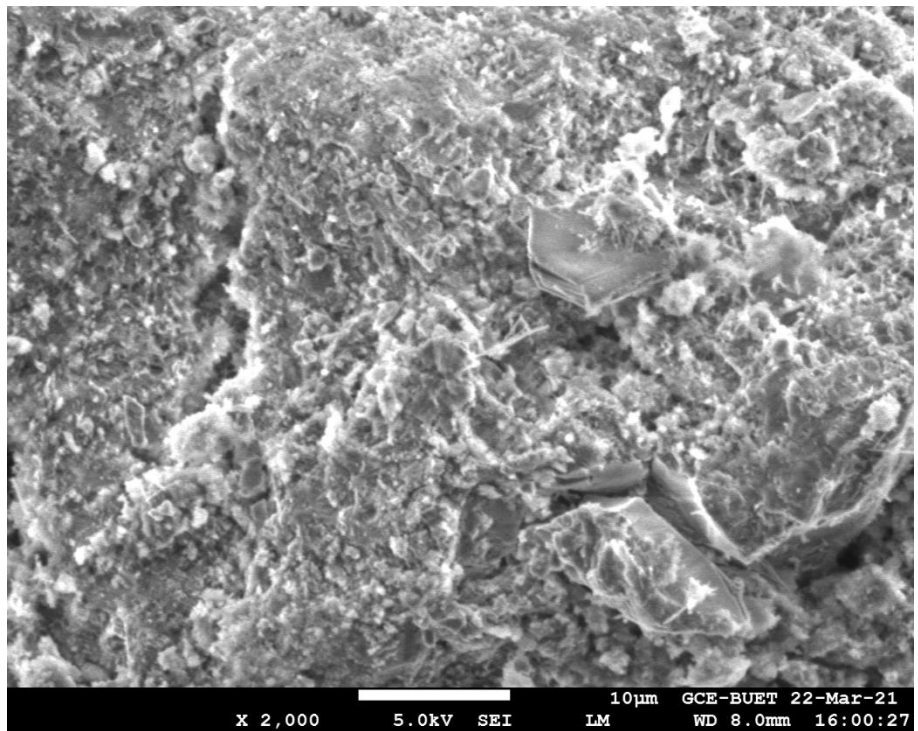
(a)



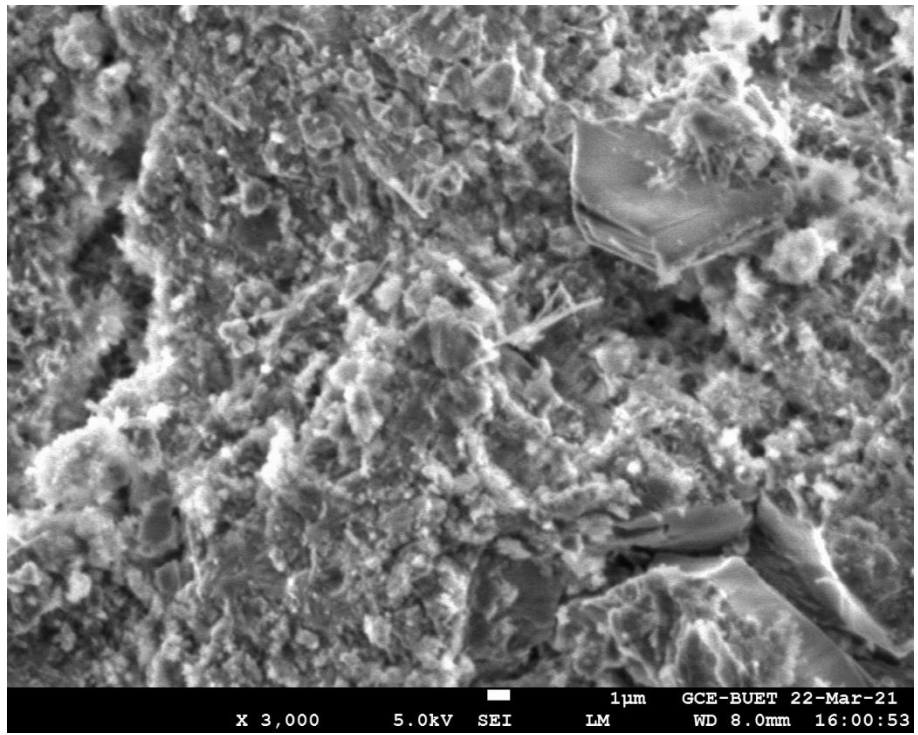
(b)



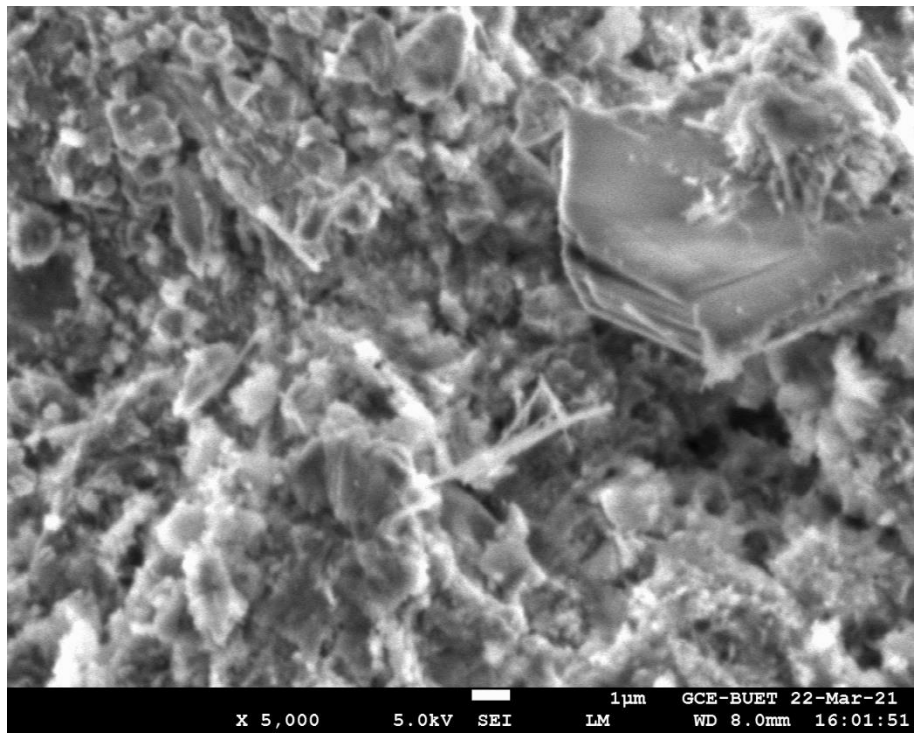
(c)



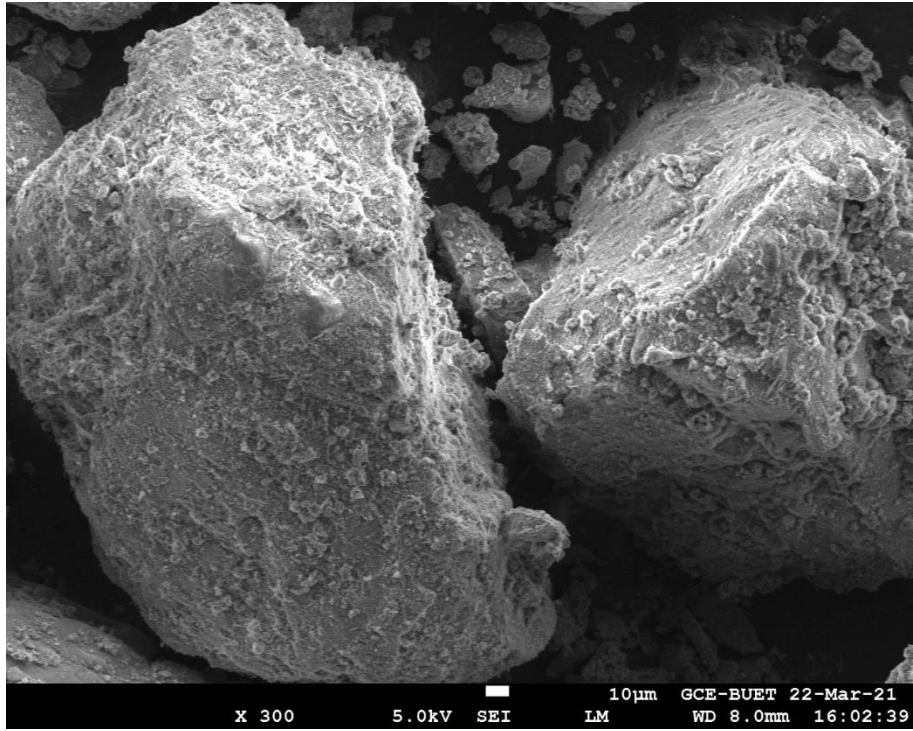
(d)



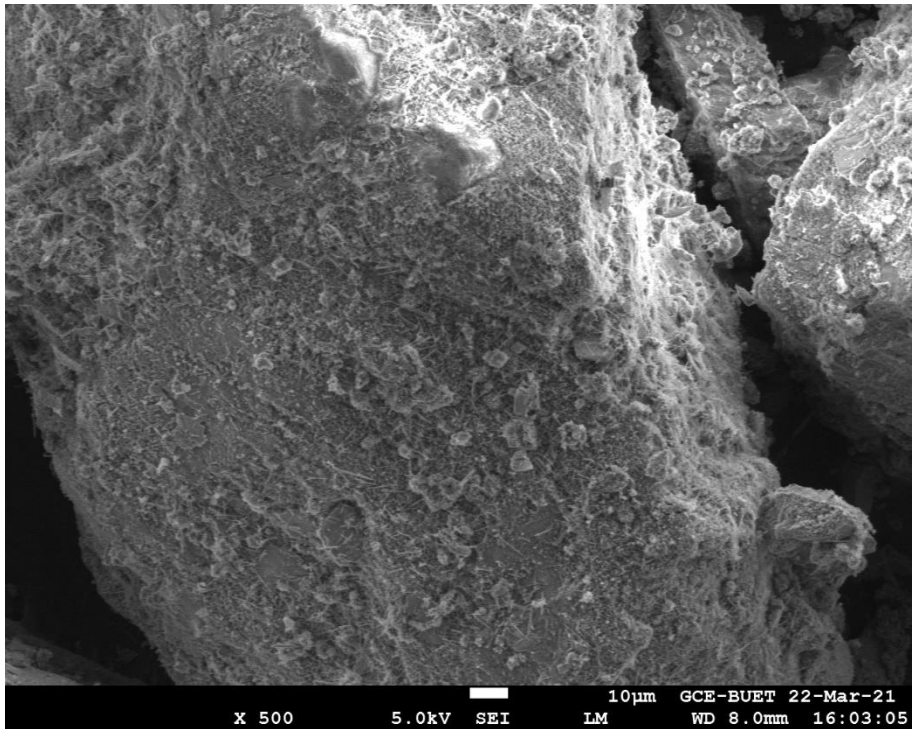
(e)



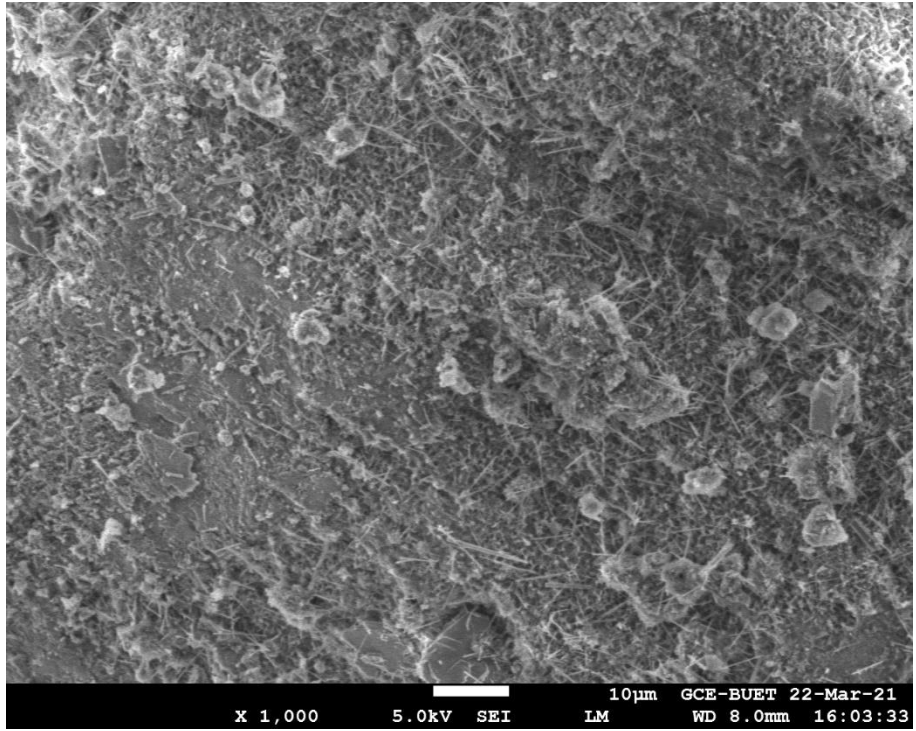
(f)



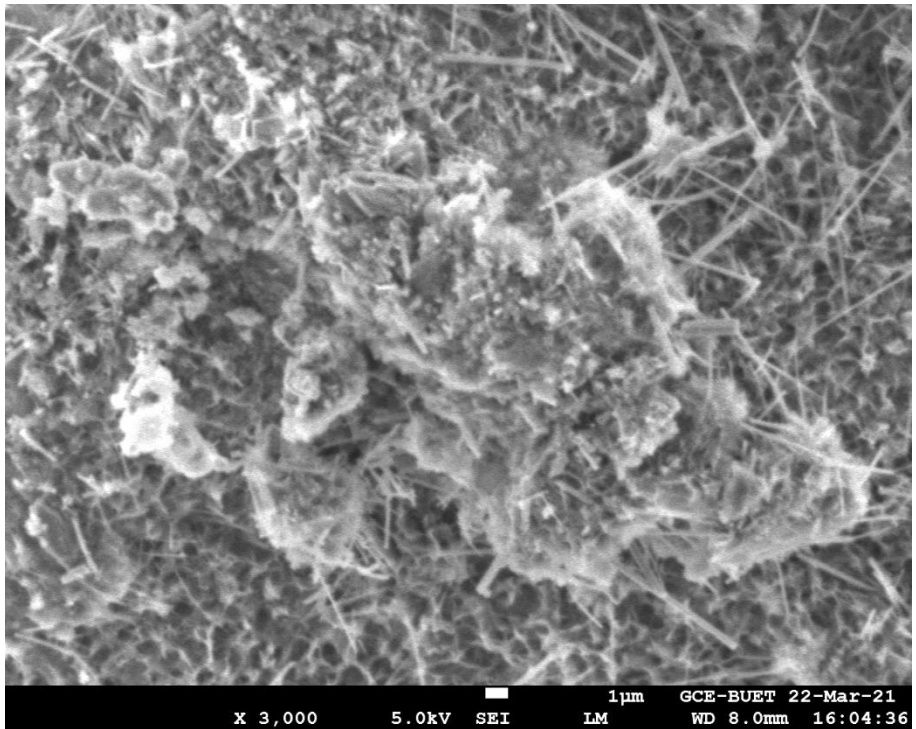
(g)



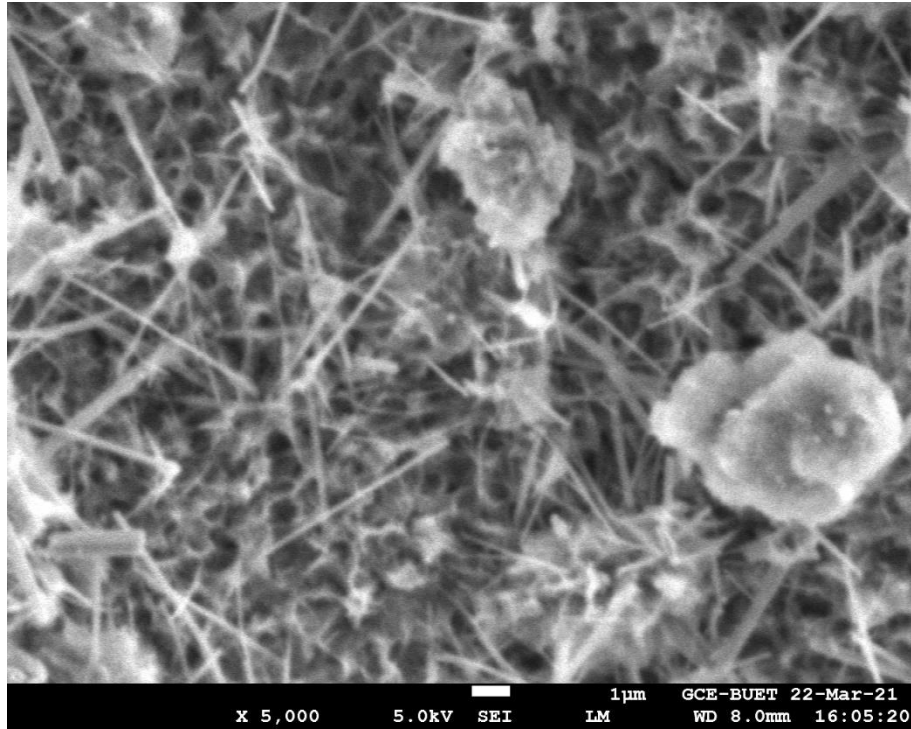
(h)



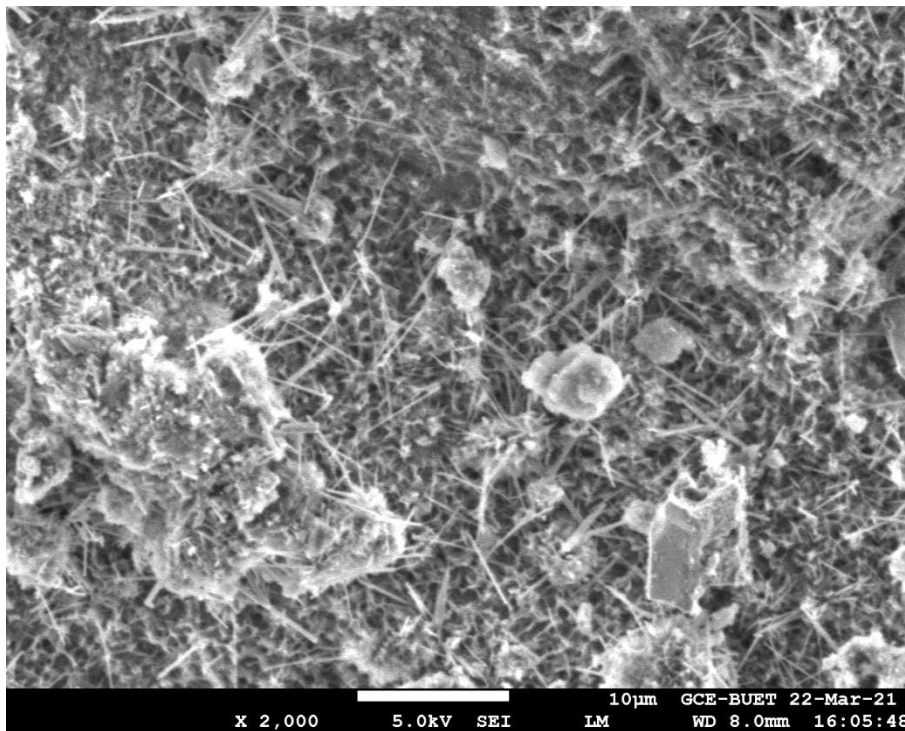
(i)



(j)

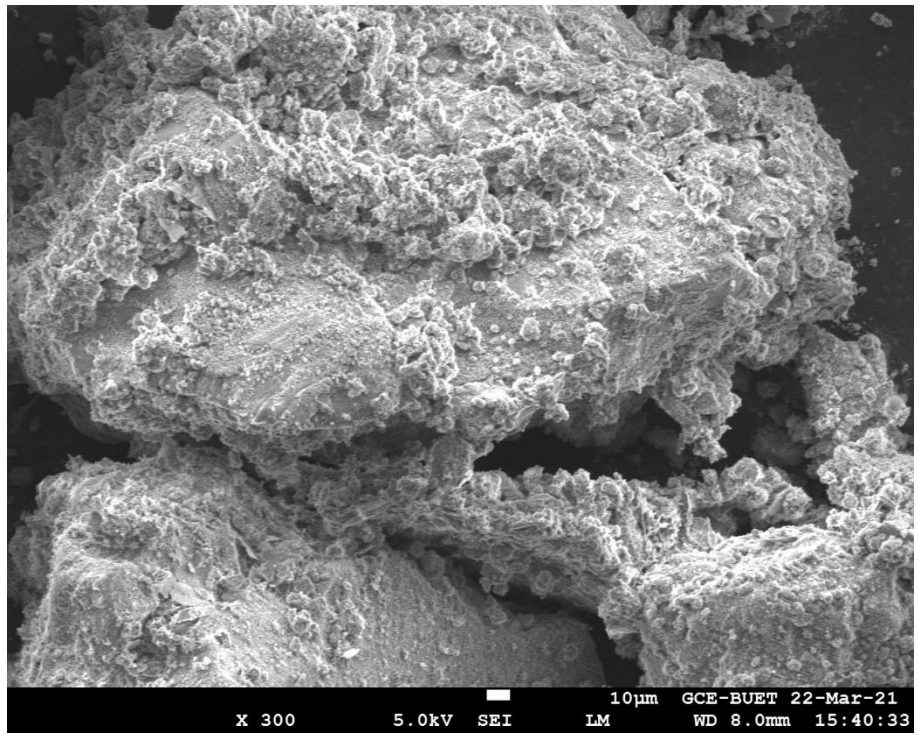


(k)

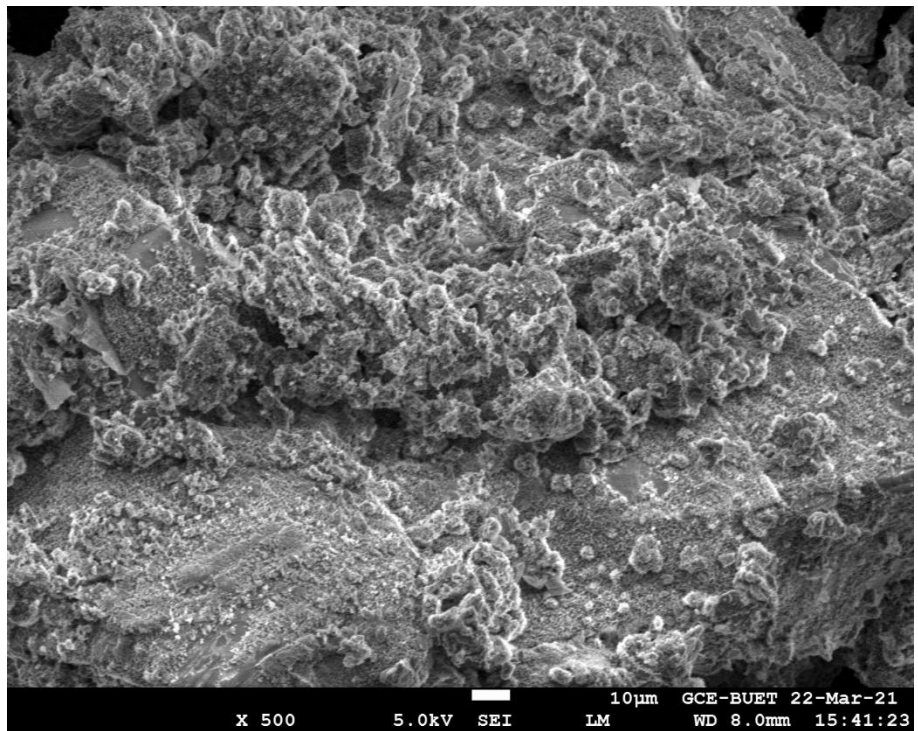


(l)

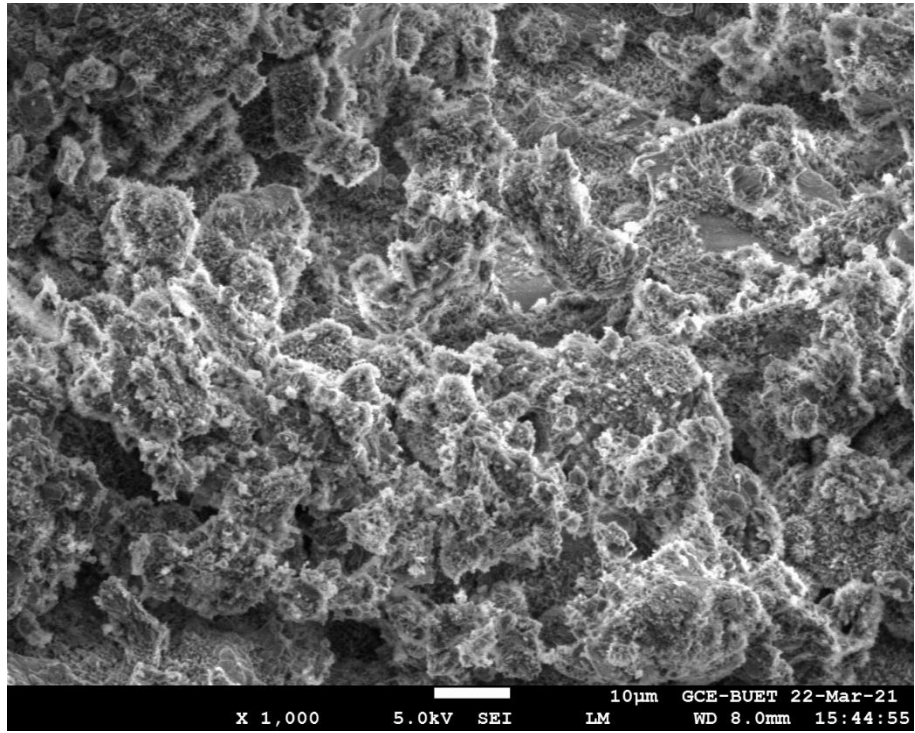
Figure B2: SEM Image of grouted three samples (4:1) after 90 days of curing of different wavelength: (a) 300 Hz (10 μ m) sample 1, (b) 500 Hz(10 μ m) sample 1, (c) 1000 Hz(10 μ m) sample 1, (d) 2000 Hz (10 μ m) sample 1, (e) 3000 Hz (1 μ m), sample 1 (f) 5000Hz (1 μ m), sample 1 (g) 300 Hz (10 μ m), sample 2, (h) 500 Hz (10 μ m), sample 3 (i) 1000 Hz(10 μ m) sample 2, (j) 3000 Hz (10 μ m) sample 2, (k) 5000 Hz (1 μ m), sample 3, (l) 2000Hz (1 μ m), sample 2,



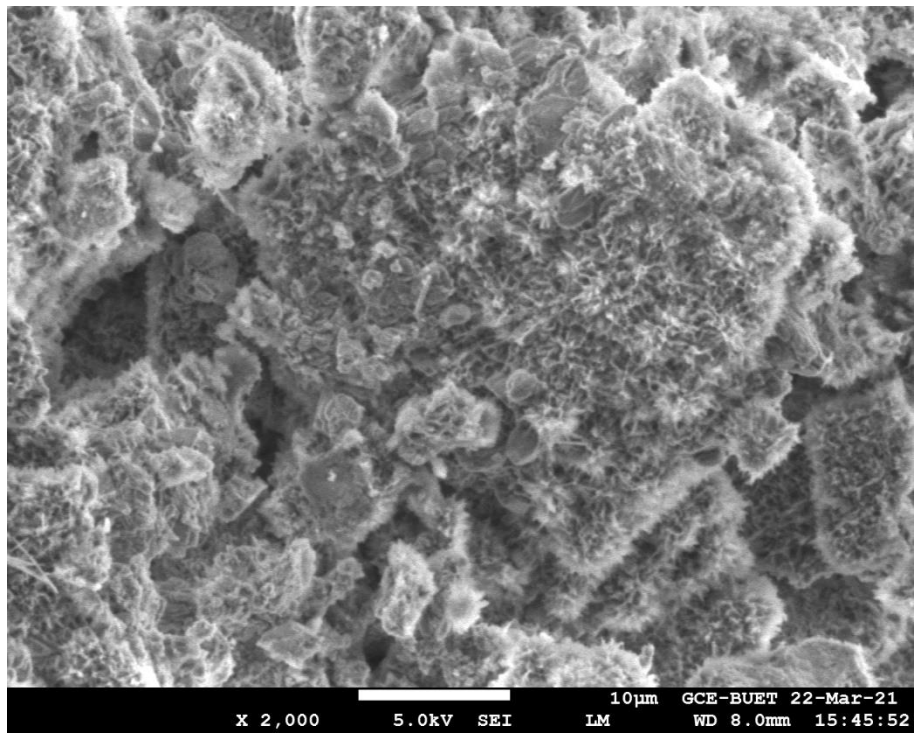
(a)



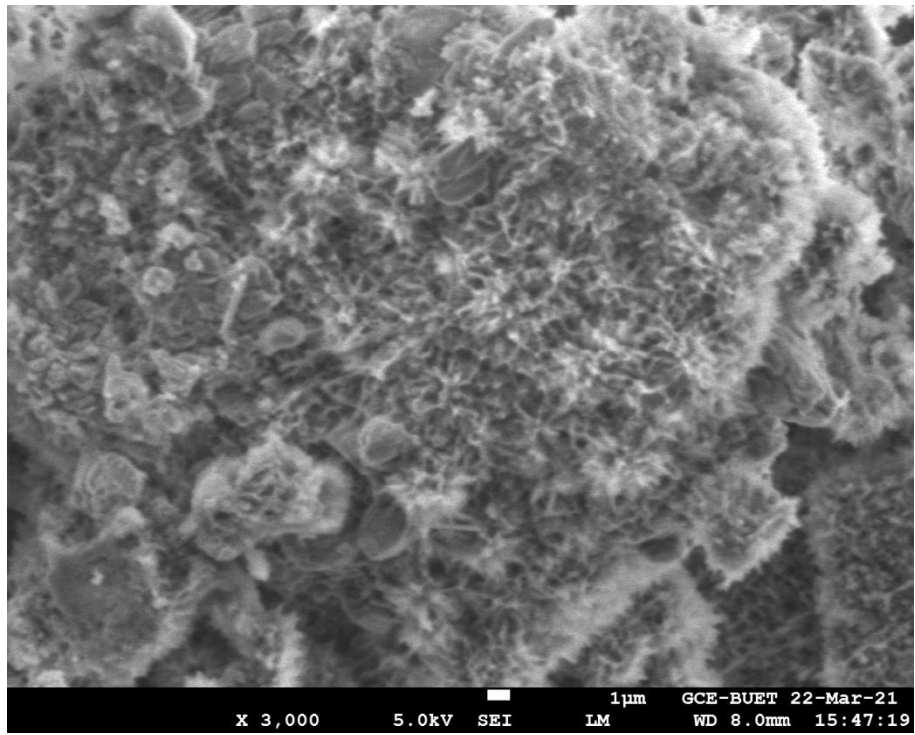
(b)



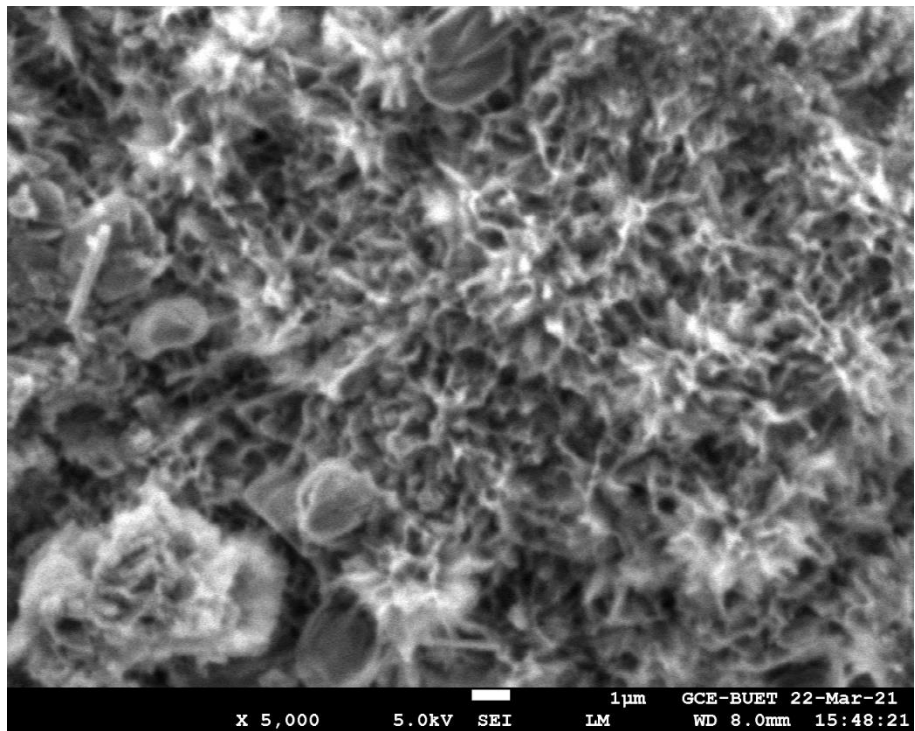
(c)



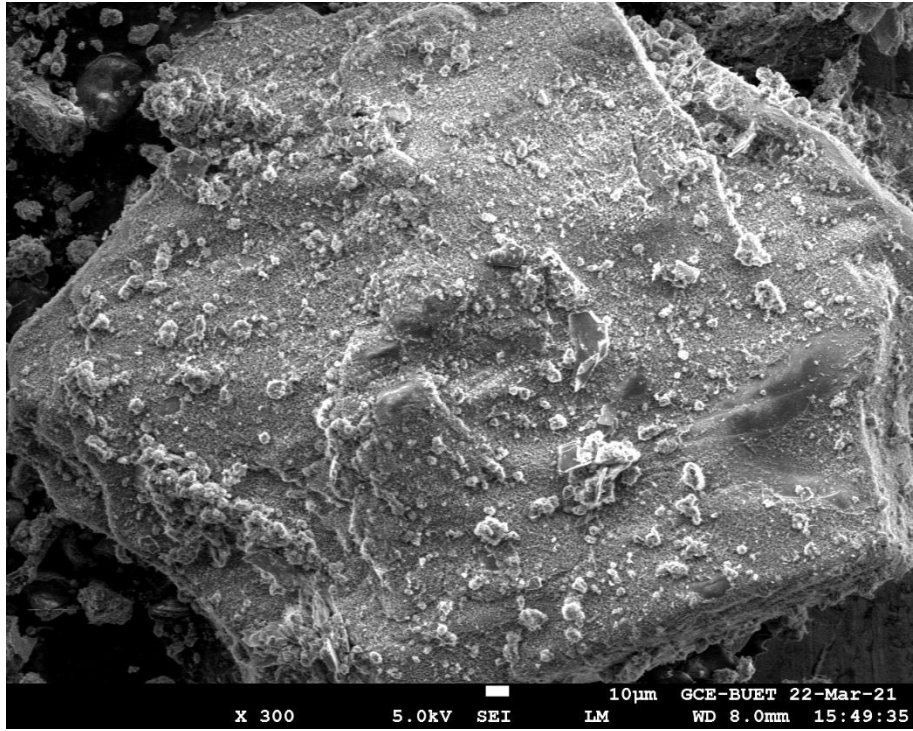
(d)



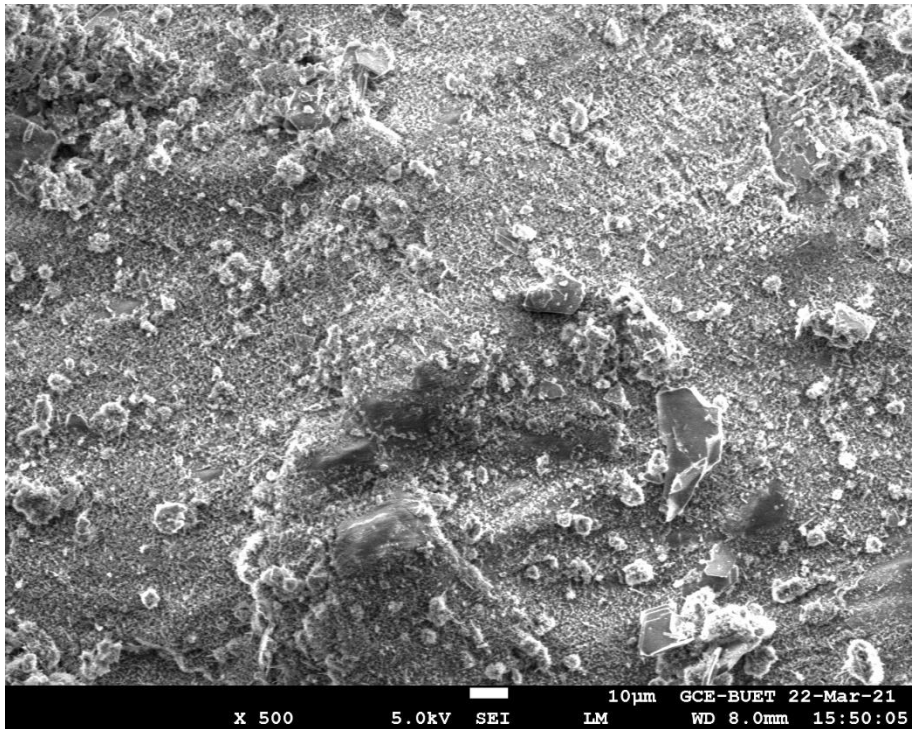
(e)



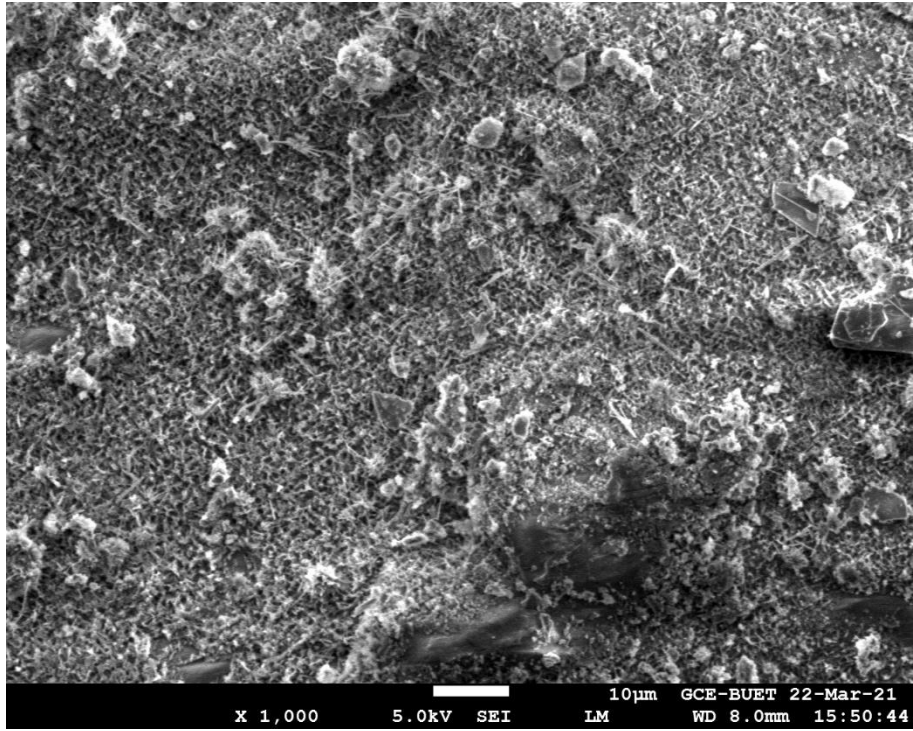
(f)



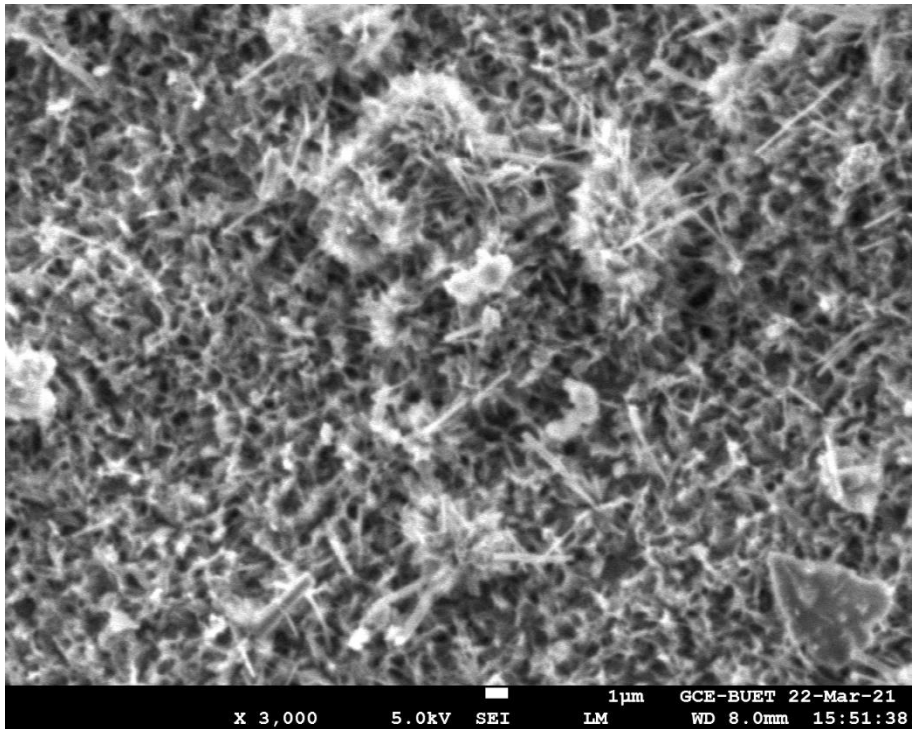
(g)



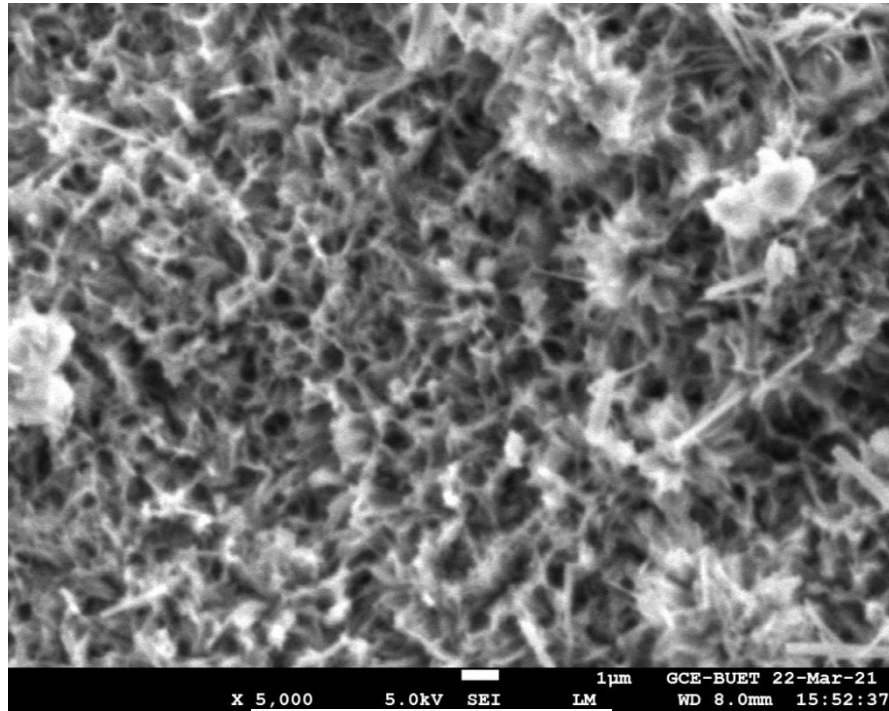
(h)



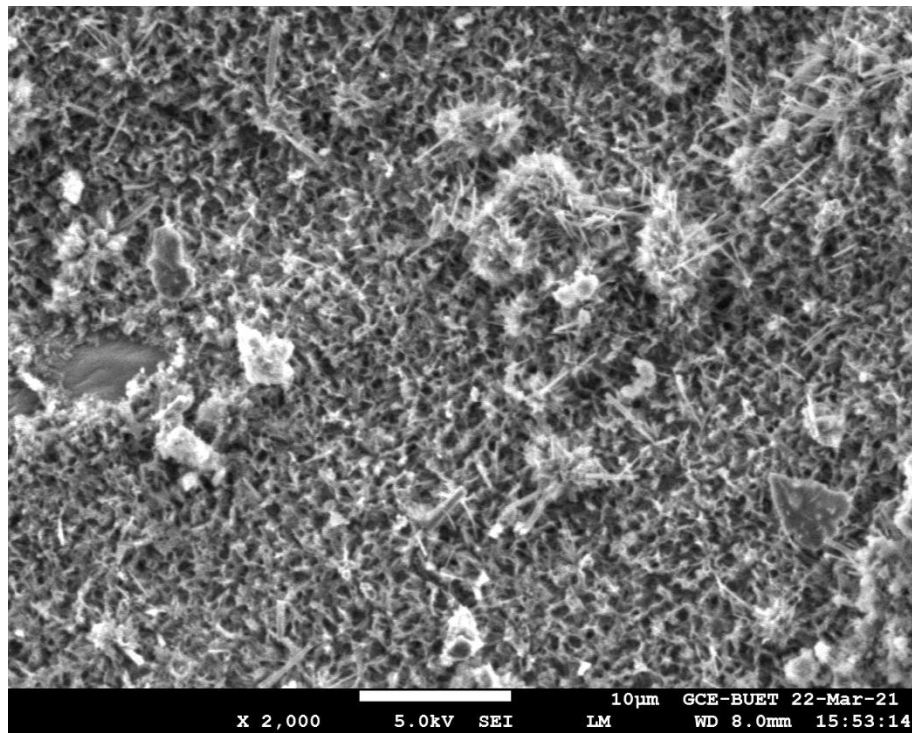
(i)



(j)

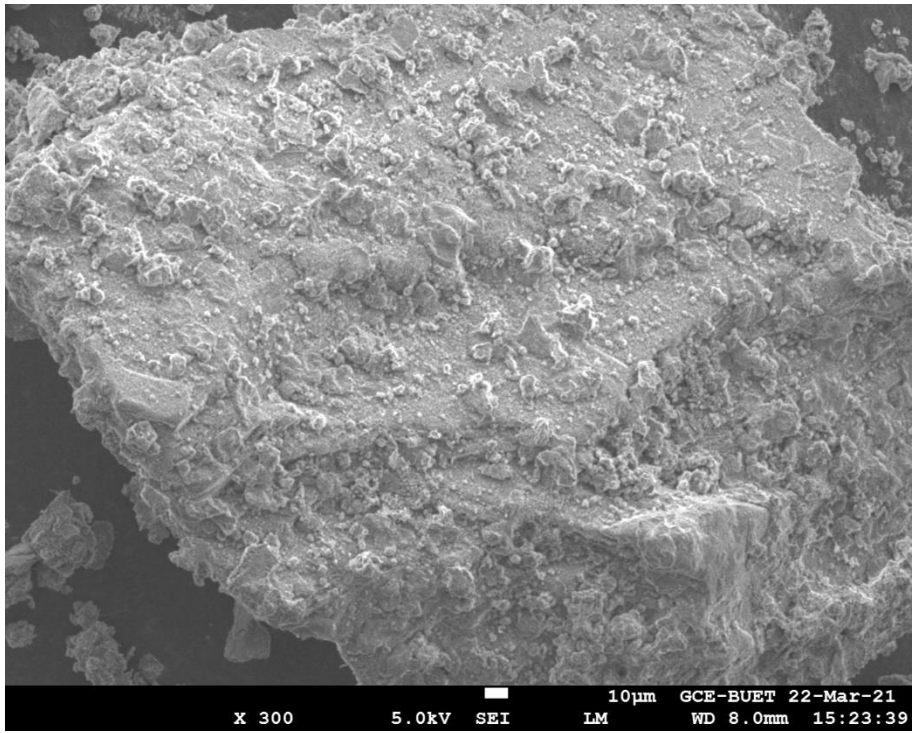


(k)

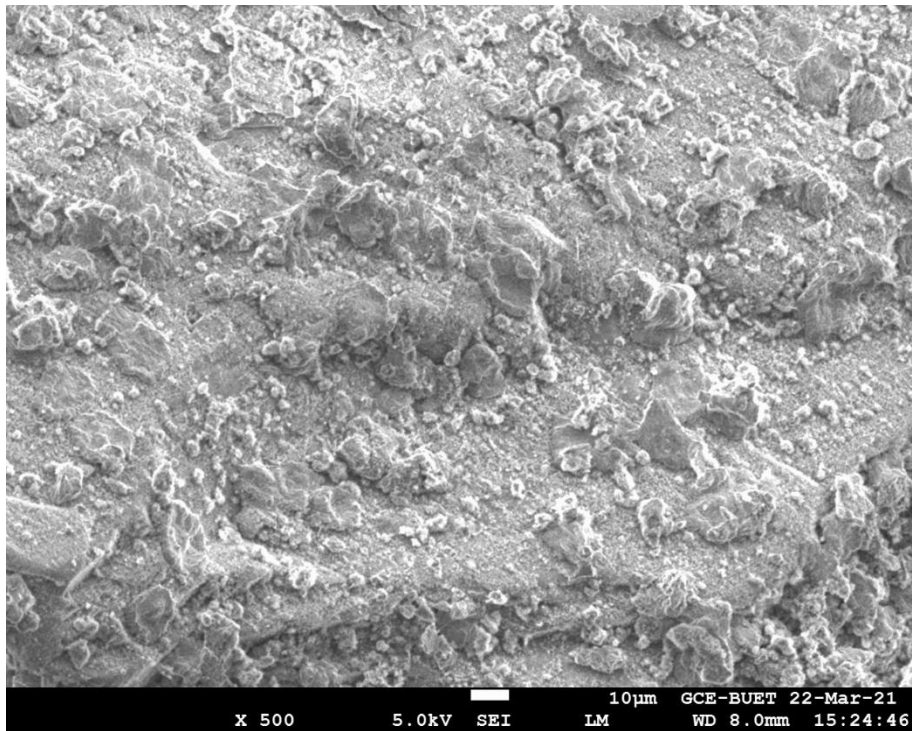


(l)

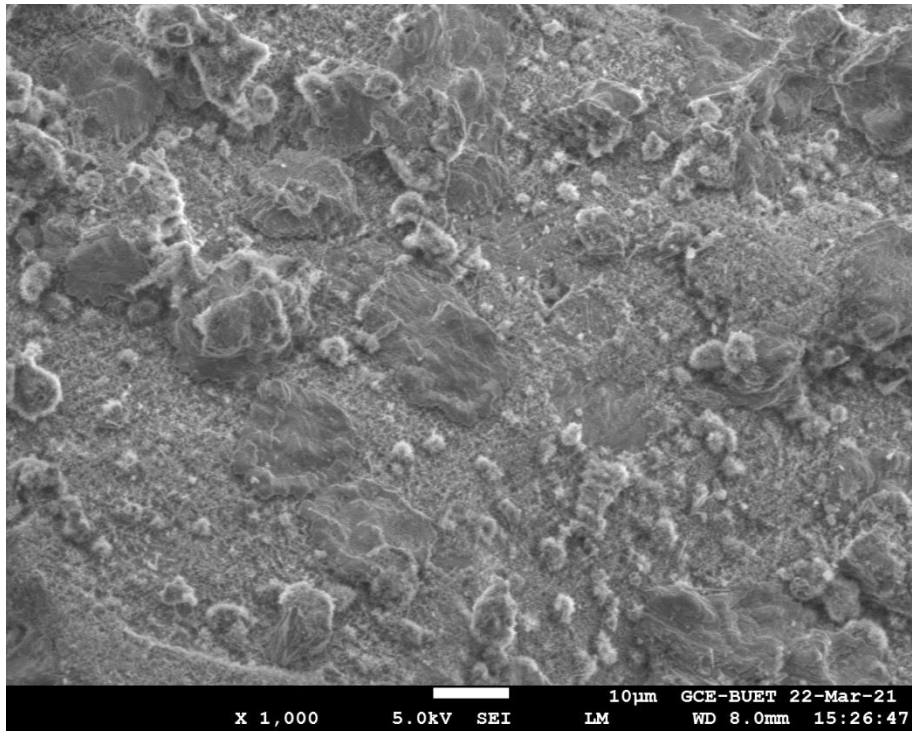
Figure B3: SEM Image of grouted three samples (3:1) after 90 days of curing of different wavelength: (a) 300 Hz (10µm) sample 1, (b) 500 Hz(10µm) sample 1, (c) 1000 Hz(10µm) sample 1, (d) 2000 Hz (10µm) sample 1, (e) 3000 Hz (1µm), sample 1 (f) 5000Hz (1µm), sample 1 (g) 300 Hz (10µm), sample 2, (h) 500 Hz (10µm), sample 3 (i) 1000 Hz(10µm) sample 2, (j) 3000 Hz (10µm) sample 2, (k) 5000 Hz (1µm), sample 3, (l) 2000Hz (1µm), sample 2,



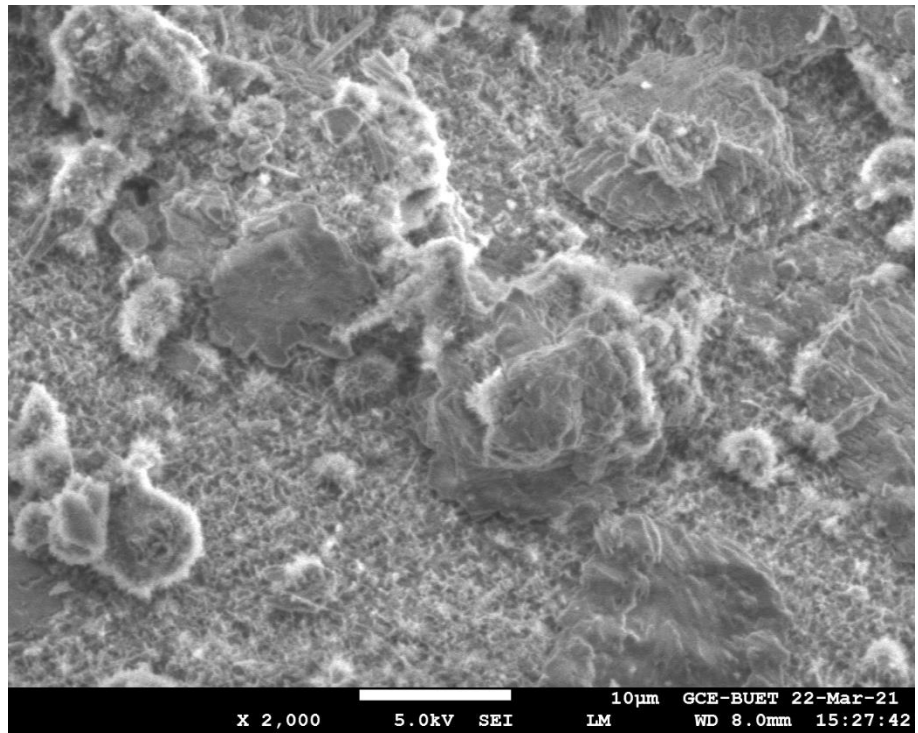
(a)



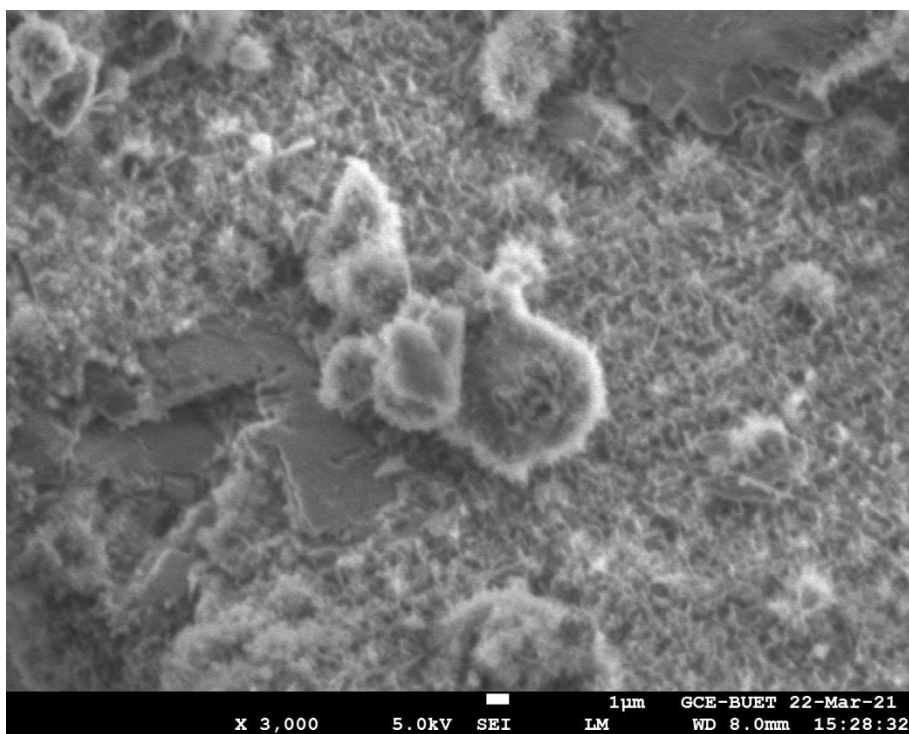
(b)



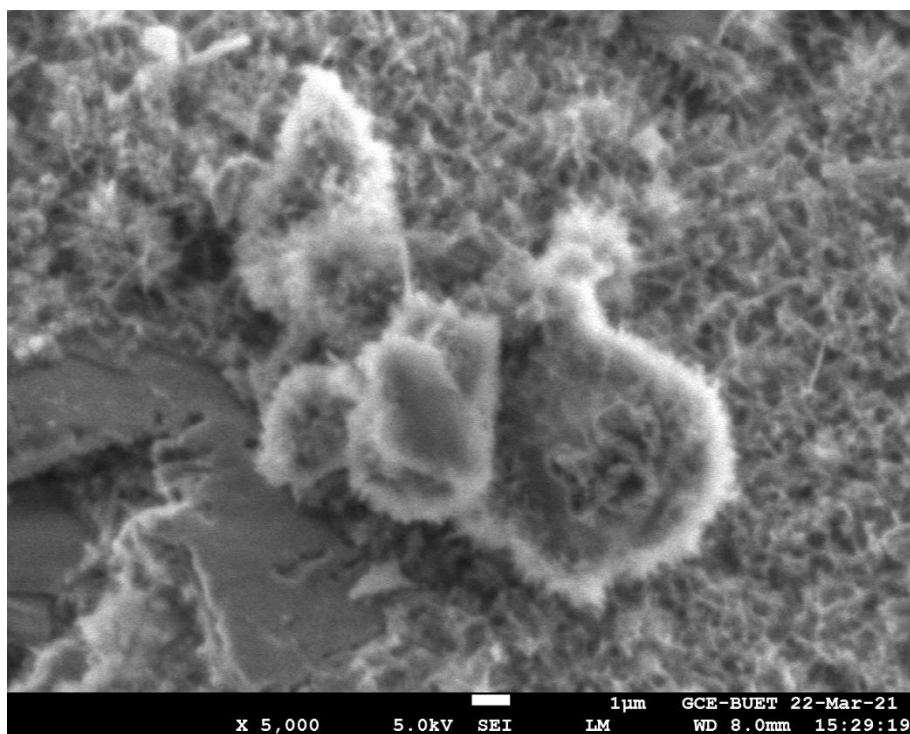
(c)



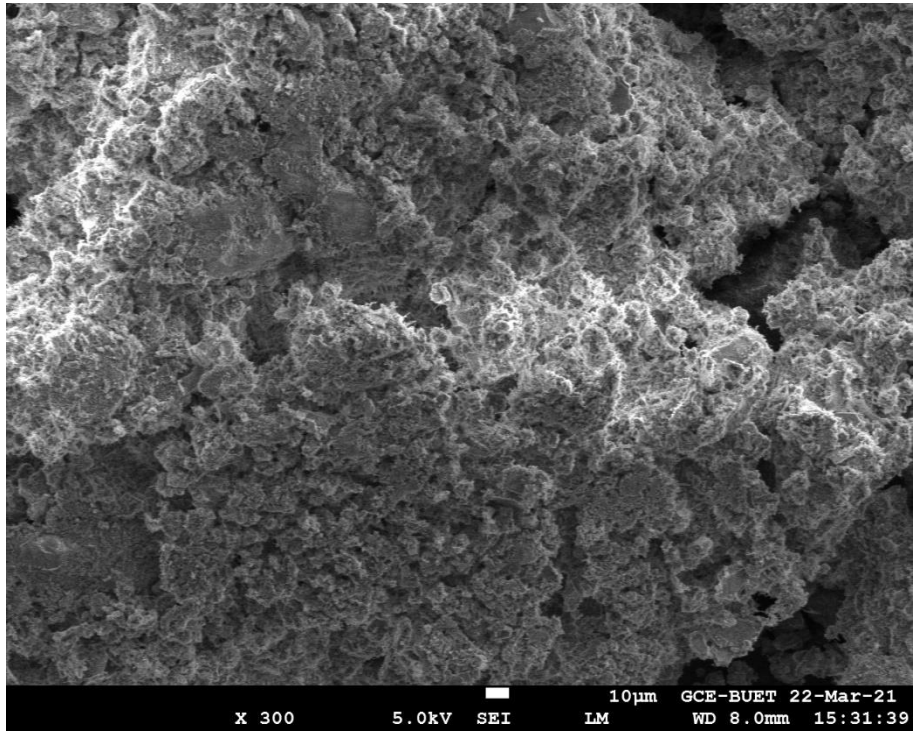
(d)



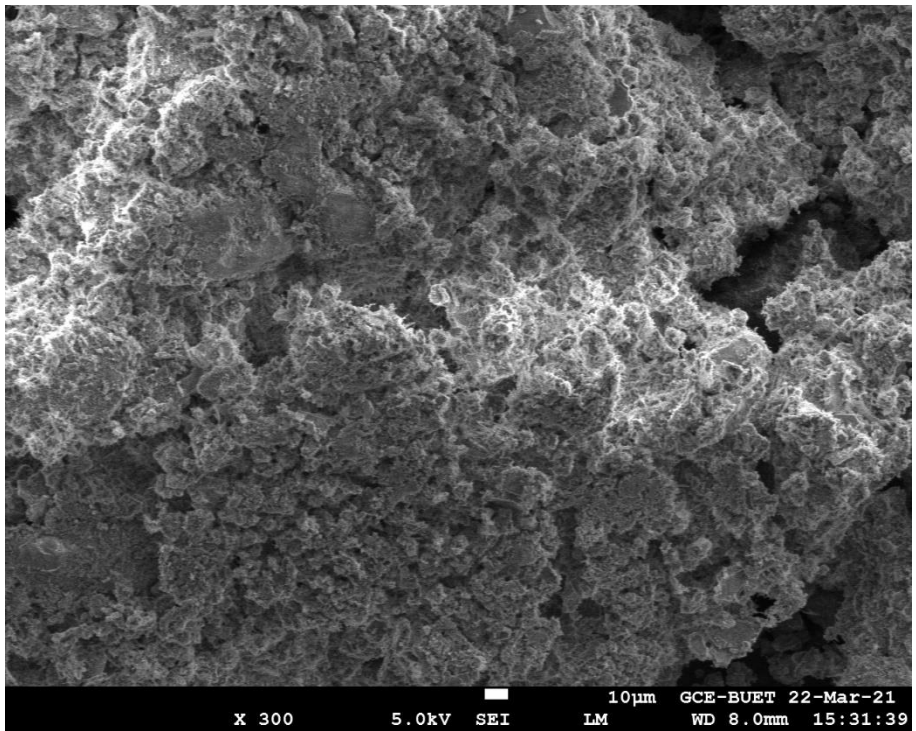
(e)



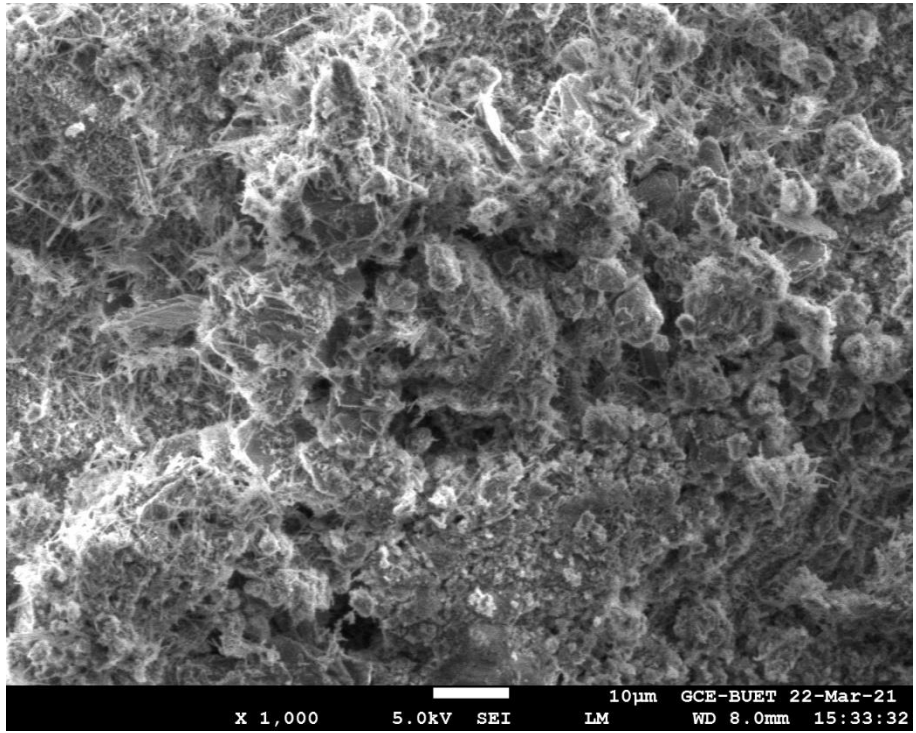
(f)



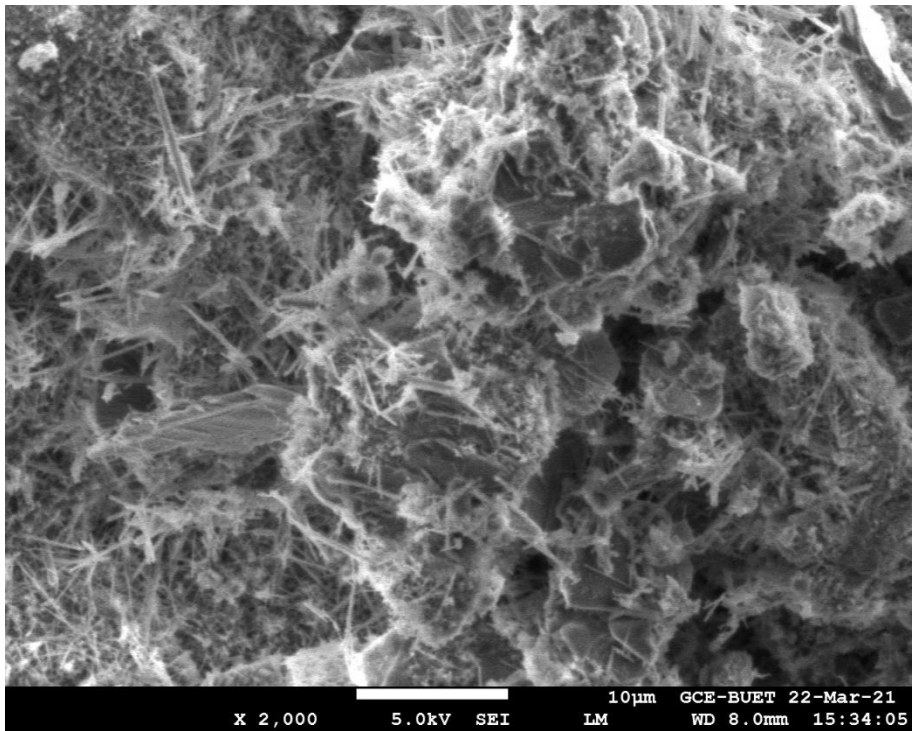
(g)



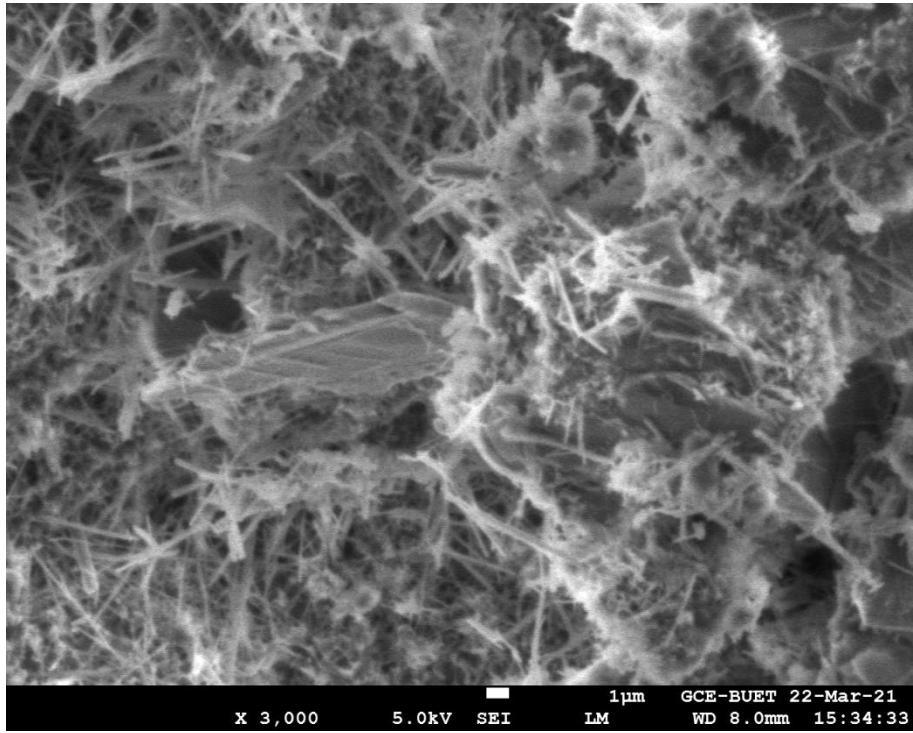
(h)



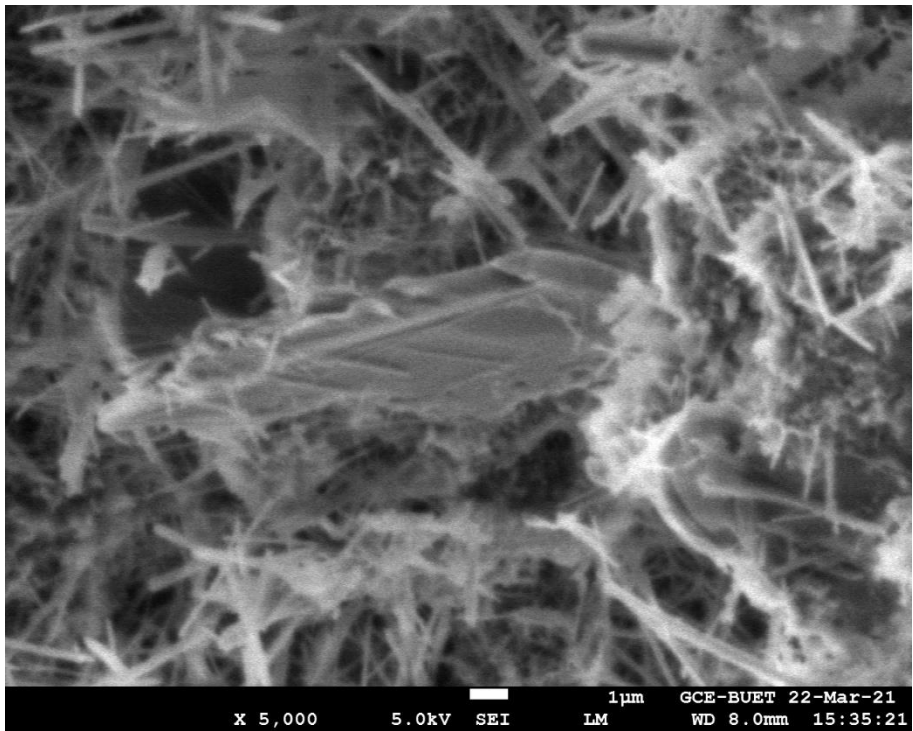
(i)



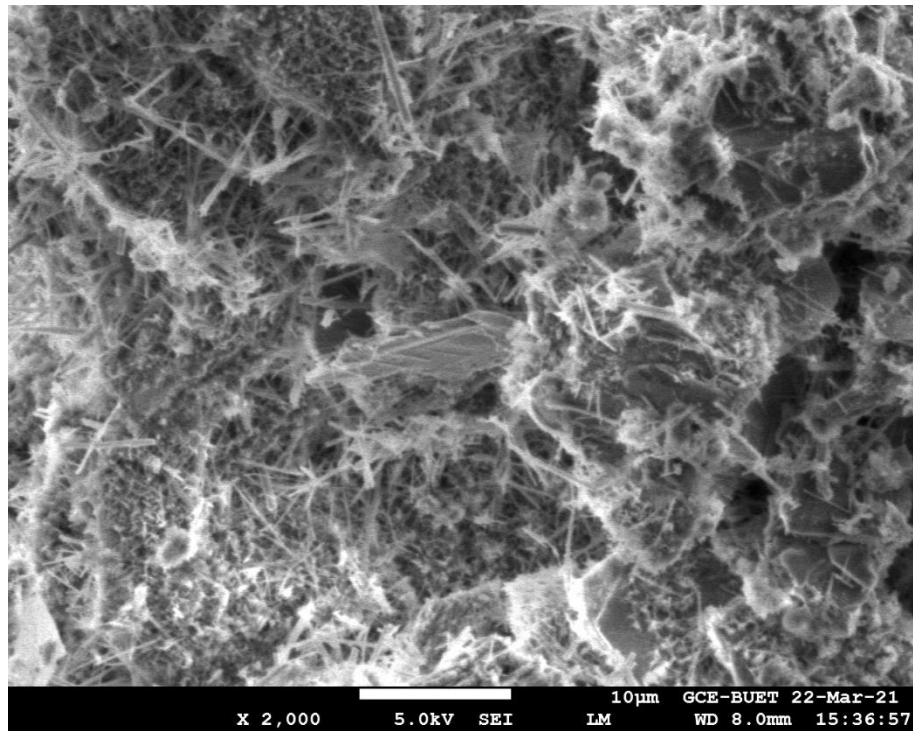
(j)



(k)



(l)



(m)

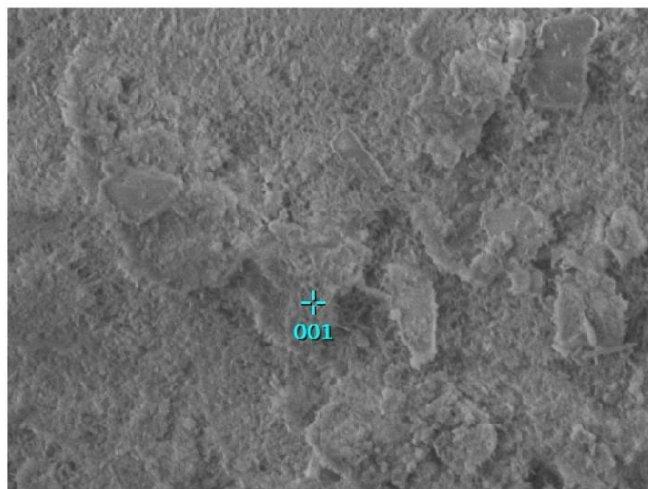
Figure B4: SEM Image of grouted three samples (2:1) after 90 days of curing of different wavelength: (a) 300 Hz (10 μ m) sample 1, (b) 500 Hz(10 μ m) sample 1, (c) 1000 Hz(10 μ m) sample 1 , (d) 2000 Hz (10 μ m) sample 1, (e) 3000 Hz (1 μ m), sample 1 (f) 5000Hz (1 μ m), sample 1 (g) 300 Hz (10 μ m), sample 2, (h) 300 Hz (10 μ m), sample 3 (i) 1000 Hz(10 μ m) sample 2, (j) 2000 Hz (10 μ m) sample 2, (k) 3000 Hz (1 μ m), sample 3, (l) 5000Hz (1 μ m), sample 2, (m) 2000 Hz (10 μ m) sample 3.

Appendix C

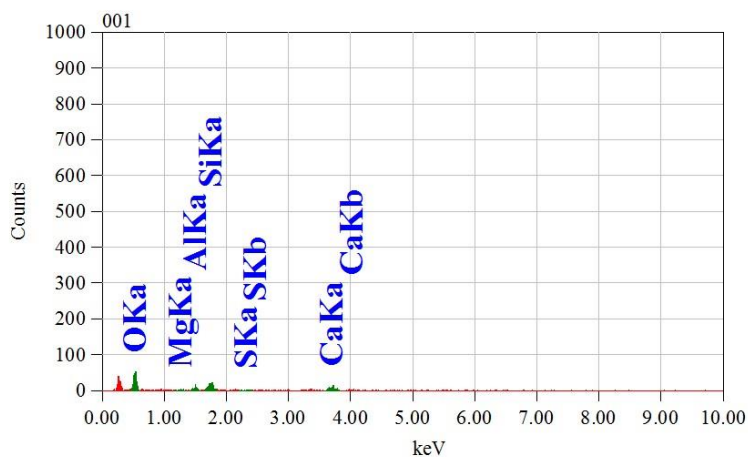
Energy Dispersive Spectroscopy Images of
Grouted Samples with W:C ratio 5:1, 4:1, 3:1 and
2:1 Cured for 28 days

View000

JEOLUSER 1/1



Title : IMG1
 Instrument : 7600F
 Volt : 5.00 kV
 Mag. : x 2,000
 Date : 2021/03/22
 Pixel : 512 x 384



Acquisition Parameter
 Instrument : 7600F
 Acc. Voltage : 10.0 kV
 Probe Current: 1.00000 nA
 PHA mode : T3
 Real Time : 30.03 sec
 Live Time : 30.00 sec
 Dead Time : 0 %
 Counting Rate: 50 cps
 Energy Range : 0 - 20 keV

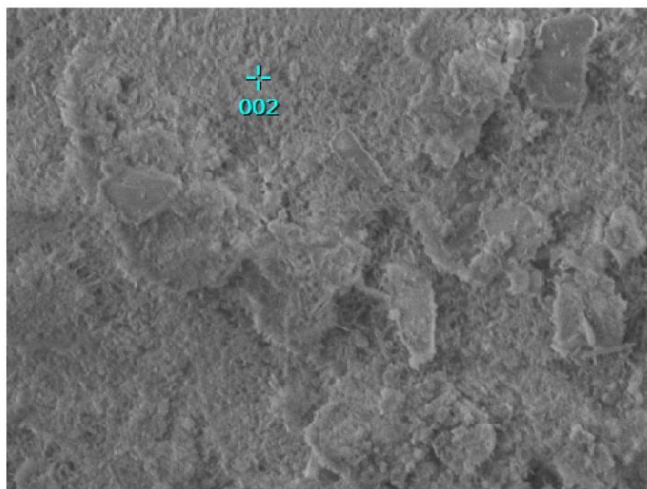
ZAF Method Standardless Quantitative Analysis
 Fitting Coefficient : 0.5420

Element	(keV)	Mass%	Sigma	Atom%	Compound	Mass%	Cation	K
O	0.525	62.33	3.21	77.38				57.4536
Mg	1.253	0.65	0.35	0.54				0.6128
Al	1.486	5.14	0.79	3.79				5.2749
Si	1.739	11.82	1.34	8.36				13.0952
S								
Ca	3.690	20.06	2.57	9.94				23.5635
Total		100.00		100.00				

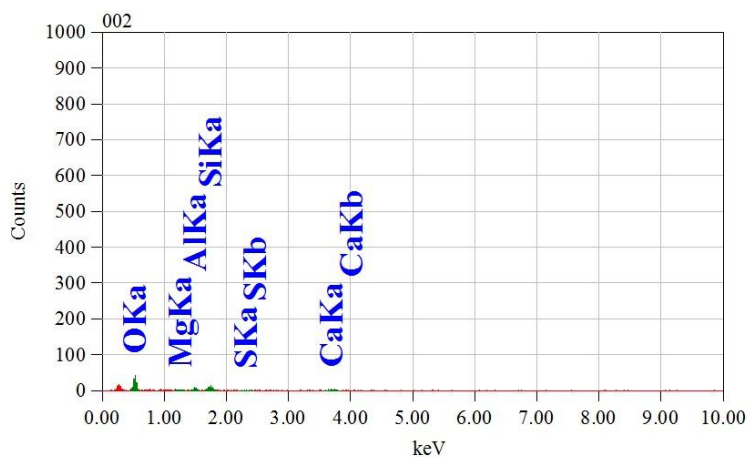
(a)

View000

JEOLUSER 1/1



Title : IMG1
 Instrument : 7600F
 Volt : 5.00 kV
 Mag. : x 2,000
 Date : 2021/03/22
 Pixel : 512 x 384



Acquisition Parameter
 Instrument : 7600F
 Acc. Voltage : 10.0 kV
 Probe Current: 1.00000 nA
 PHA mode : T3
 Real Time : 30.02 sec
 Live Time : 30.00 sec
 Dead Time : 0 %
 Counting Rate: 31 cps
 Energy Range : 0 - 20 keV

ZAF Method Standardless Quantitative Analysis

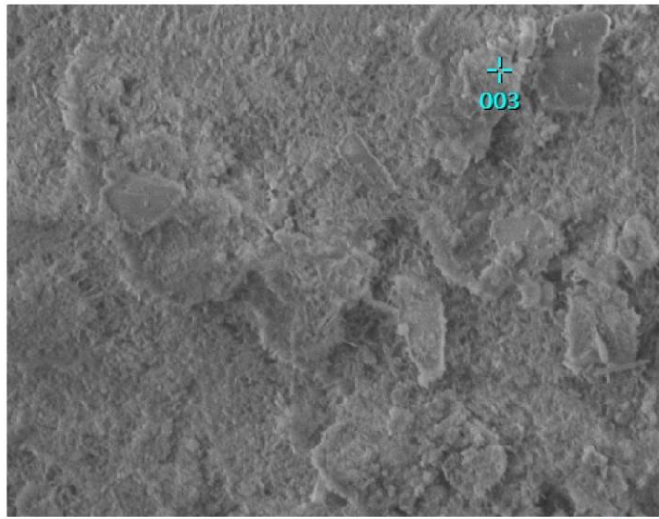
Fitting Coefficient : 0.5602

Element	(keV)	Mass%	Sigma	Atom%	Compound	Mass%	Cation	K
O	0.525	73.08	4.68	83.76				75.4134
Mg	1.253	0.16	0.60	0.12				0.1255
Al	1.486	4.19	1.25	2.85				3.5359
Si	1.739	14.96	2.32	9.77				13.6579
S	2.307	0.12	0.45	0.07				0.1148
Ca	3.690	7.49	2.73	3.43				7.1526
Total		100.00		100.00				

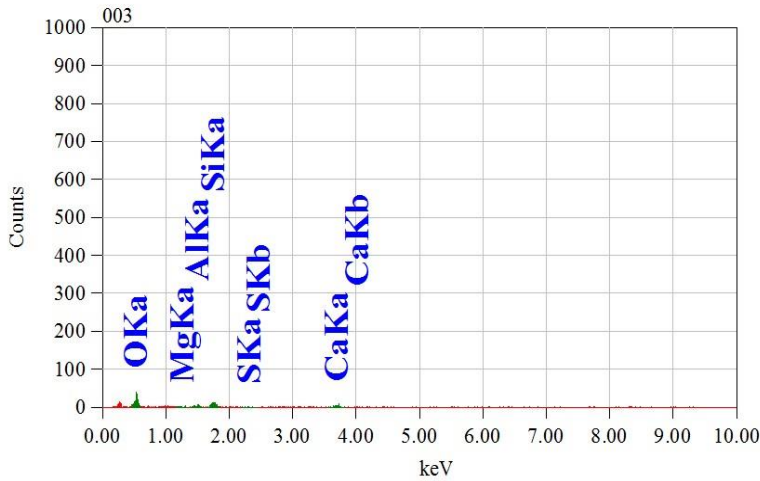
(b)

View000

JEOLUSER 1/1



Title : IMG1
 Instrument : 7600F
 Volt : 5.00 kV
 Mag. : x 2,000
 Date : 2021/03/22
 Pixel : 512 x 384



Acquisition Parameter
 Instrument : 7600F
 Acc. Voltage : 10.0 kV
 Probe Current: 1.00000 nA
 PHA mode : T3
 Real Time : 30.02 sec
 Live Time : 30.00 sec
 Dead Time : 0 %
 Counting Rate: 33 cps
 Energy Range : 0 - 20 keV

ZAF Method Standardless Quantitative Analysis
 Fitting Coefficient : 0.6411

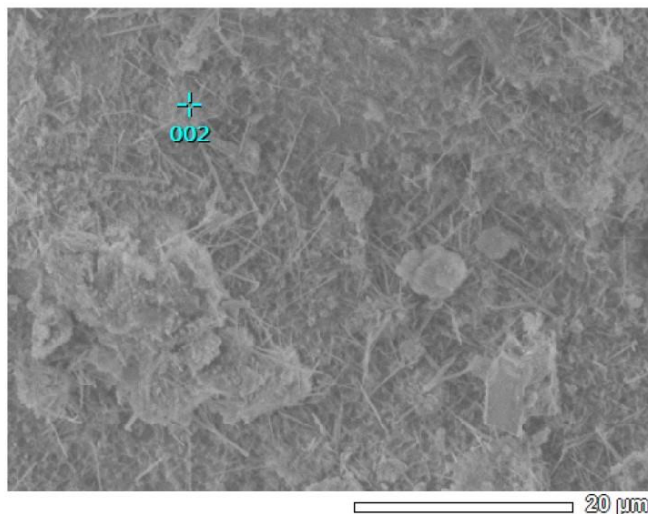
Element	(keV)	Mass%	Sigma	Atom%	Compound	Mass%	Cation	K
O K	0.525	66.22	4.72	80.51				62.0718
Mg K								
Al K	1.486	2.90	0.95	2.09				2.9096
Si K	1.739	11.42	1.83	7.91				12.5619
S K	2.307	0.34	0.37	0.21				0.3863
Ca K	3.690	19.12	3.48	9.28				22.0704
Total		100.00		100.00				

(c)

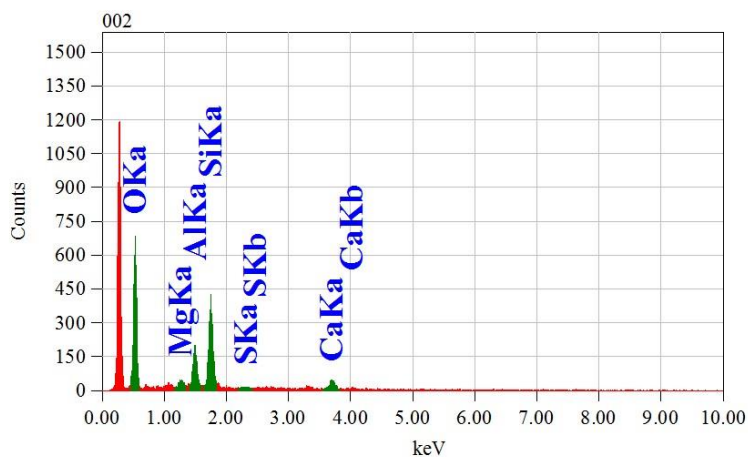
Figure C1: EDS Image of grouted three samples (5:1) after 90 days of curing
 (a) sample 1, (b) sample 2, (c) sample 3

View000

JEOLUSER 1/1



Title : IMG1
 Instrument : 7600F
 Volt : 5.00 kV
 Mag. : x 2,000
 Date : 2021/03/22
 Pixel : 512 x 384



Acquisition Parameter
 Instrument : 7600F
 Acc. Voltage : 10.0 kV
 Probe Current: 1.00000 nA
 PHA mode : T3
 Real Time : 30.22 sec
 Live Time : 30.00 sec
 Dead Time : 0 %
 Counting Rate: 707 cps
 Energy Range : 0 - 20 keV

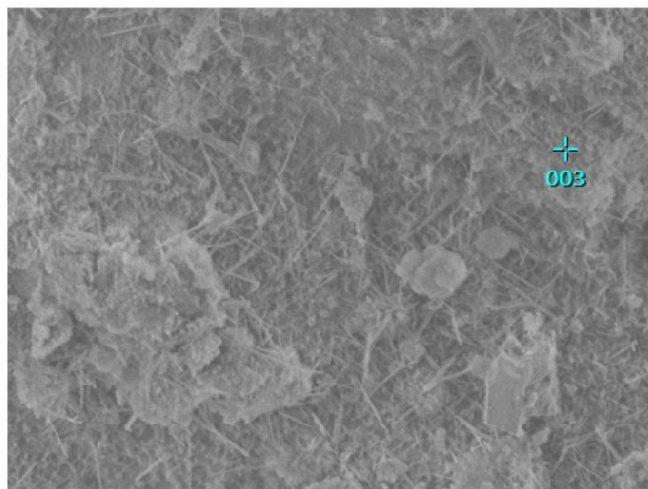
ZAF Method Standardless Quantitative Analysis
 Fitting Coefficient : 0.5865

Element	(keV)	Mass%	Sigma	Atom%	Compound	Mass%	Cation
O	0.525	60.73	0.86	73.93			K
Mg	1.253	1.49	0.15	1.19			61.8452
Al	1.486	8.87	0.32	6.40			1.2903
Si	1.739	21.24	0.53	14.73			8.2691
S	2.307	0.21	0.10	0.13			20.7253
Ca	3.690	7.46	0.51	3.63			0.2026
Total		100.00		100.00			7.6676

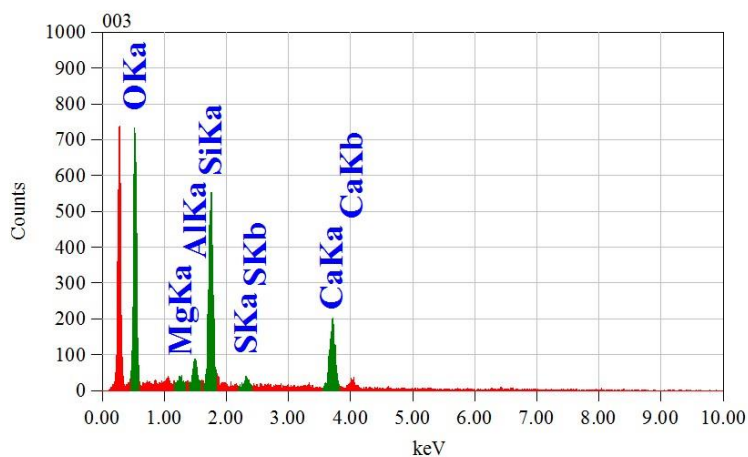
(a)

View000

JEOLUSER 1/1



Title : IMG1
 Instrument : 7600F
 Volt : 5.00 kV
 Mag. : x 2,000
 Date : 2021/03/22
 Pixel : 512 x 384



Acquisition Parameter
 Instrument : 7600F
 Acc. Voltage : 10.0 kV
 Probe Current: 1.00000 nA
 PHA mode : T3
 Real Time : 30.21 sec
 Live Time : 30.00 sec
 Dead Time : 0 %
 Counting Rate: 761 cps
 Energy Range : 0 - 20 keV

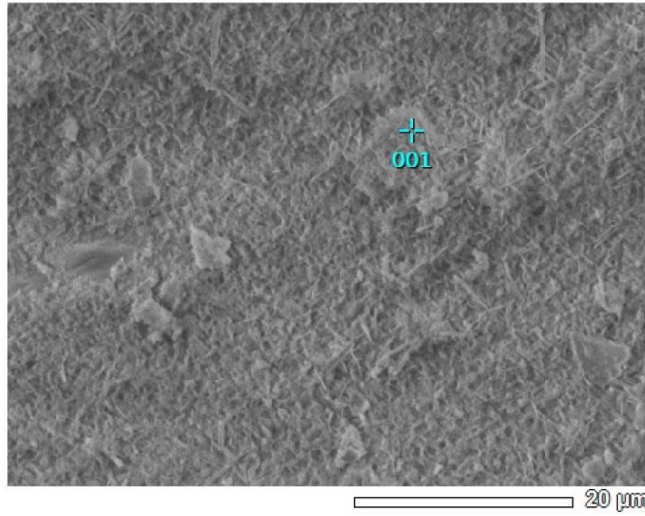
ZAF Method Standardless Quantitative Analysis
 Fitting Coefficient : 0.4085

Element	(keV)	Mass%	Sigma	Atom%	Compound	Mass%	Cation	K
O	0.525	56.20	0.74	72.59				48.6758
Mg	1.253	0.51	0.08	0.43				0.4936
Al	1.486	2.11	0.13	1.62				2.2395
Si	1.739	18.01	0.37	13.25				20.8946
S	2.307	1.22	0.11	0.78				1.4121
Ca	3.690	21.96	0.63	11.32				26.2844
Total		100.00		100.00				

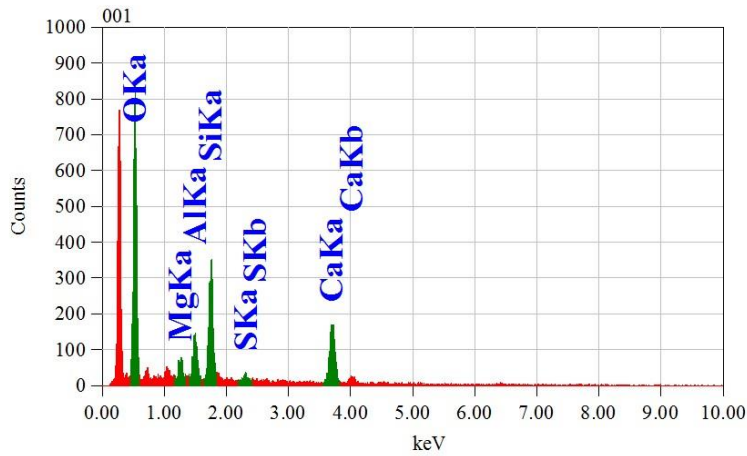
(b)

View000

JEOLUSER 1/1



Title : IMG1
 Instrument : 7600F
 Volt : 5.00 kV
 Mag. : x 2,000
 Date : 2021/03/22
 Pixel : 512 x 384



Acquisition Parameter
 Instrument : 7600F
 Acc. Voltage : 10.0 kV
 Probe Current: 1.00000 nA
 PHA mode : T3
 Real Time : 30.20 sec
 Live Time : 30.00 sec
 Dead Time : 0 %
 Counting Rate: 727 cps
 Energy Range : 0 - 20 keV

ZAF Method Standardless Quantitative Analysis

Fitting Coefficient : 0.4426

Element	(keV)	Mass%	Sigma	Atom%	Compound	Mass%	Cation	K
O	0.525	60.56	0.29	76.04				54.9184
Mg	1.253	1.84	0.09	1.52				1.7462
Al	1.486	3.93	0.12	2.92				4.0529
Si	1.739	11.80	0.19	8.44				13.2782
S	2.307	0.93	0.07	0.58				1.0786
Ca	3.690	20.95	0.35	10.50				24.9256
Total		100.00		100.00				

JED-2300 AnalysisStation

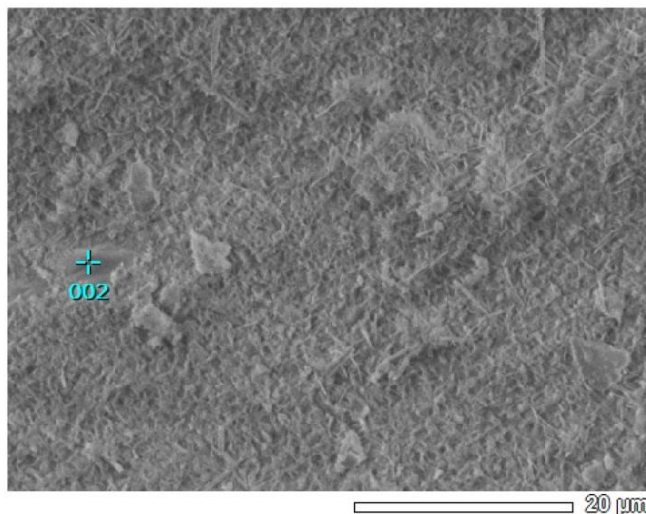
JEOL

(c)

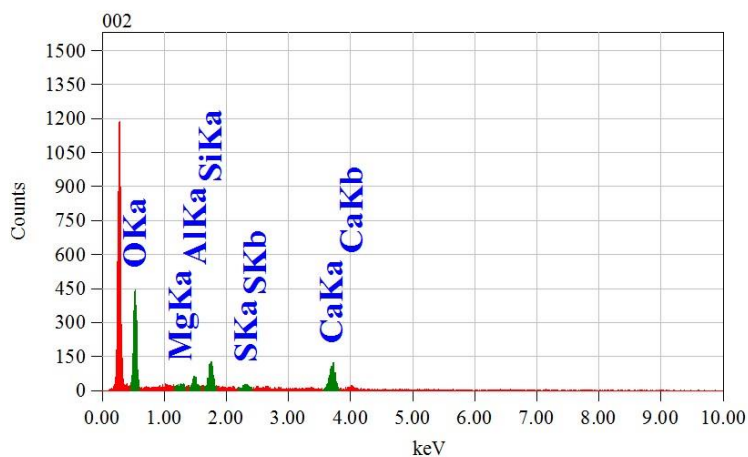
Figure C2: EDS Image of grouted three samples (4:1) after 90 days of curing (a) sample 1, (b) sample 2, (c) sample 3

View000

JEOLUSER 1/1



Title : IMG1
 Instrument : 7600F
 Volt : 5.00 kV
 Mag. : x 2,000
 Date : 2021/03/22
 Pixel : 512 x 384



Acquisition Parameter
 Instrument : 7600F
 Acc. Voltage : 10.0 kV
 Probe Current: 1.00000 nA
 PHA mode : T3
 Real Time : 30.16 sec
 Live Time : 30.00 sec
 Dead Time : 0 %
 Counting Rate: 581 cps
 Energy Range : 0 - 20 keV

ZAF Method Standardless Quantitative Analysis
 Fitting Coefficient : 0.6747

Element	(keV)	Mass%	Sigma	Atom%	Compound	Mass%	Cation	K
O	0.525	63.19	0.39	79.03				55.9953
Mg	1.253	0.25	0.11	0.21				0.2400
Al	1.486	2.89	0.14	2.15				3.0506
Si	1.739	7.22	0.22	5.14				8.3630
S	2.307	2.19	0.11	1.37				2.6596
Ca	3.690	24.26	0.52	12.11				29.6916
Total		100.00		100.00				

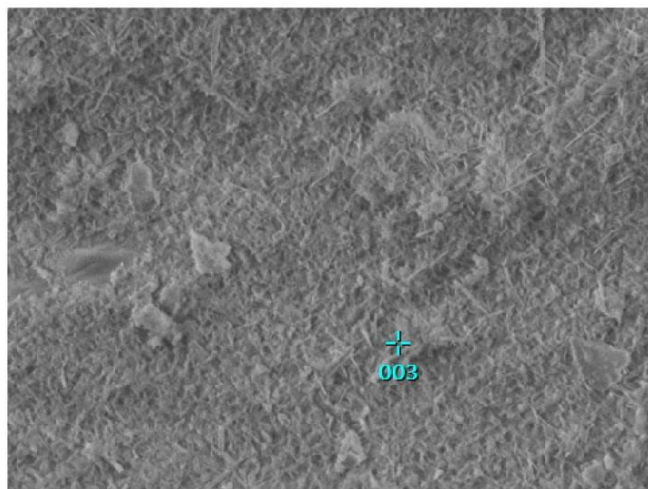
JED-2300 AnalysisStation

JEOL

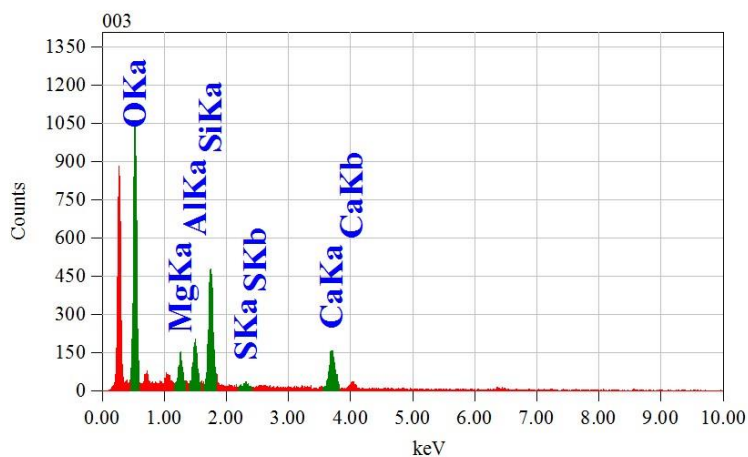
(a)

View000

JEOLUSER 1/1



Title : IMG1
 Instrument : 7600F
 Volt : 5.00 kV
 Mag. : x 2,000
 Date : 2021/03/22
 Pixel : 512 x 384



Acquisition Parameter
 Instrument : 7600F
 Acc. Voltage : 10.0 kV
 Probe Current: 1.00000 nA
 PHA mode : T3
 Real Time : 30.25 sec
 Live Time : 30.00 sec
 Dead Time : 0 %
 Counting Rate: 944 cps
 Energy Range : 0 - 20 keV

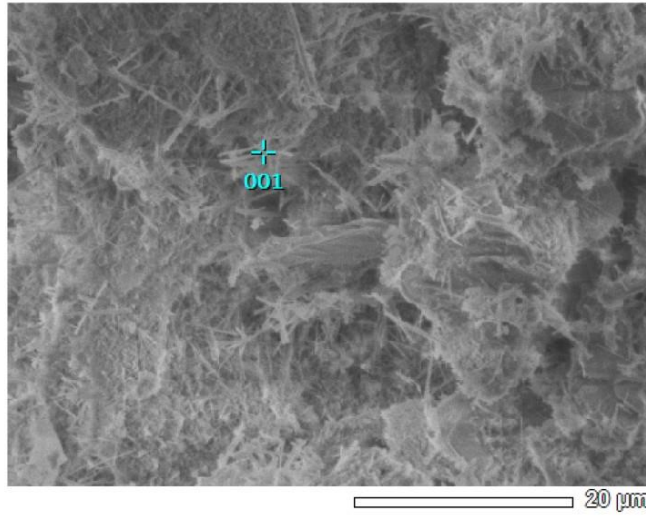
ZAF Method Standardless Quantitative Analysis
 Fitting Coefficient : 0.3907

Element	(keV)	Mass%	Sigma	Atom%	Compound	Mass%	Cation	K
O	0.525	61.35	0.68	75.80				58.3854
Mg	1.253	3.05	0.14	2.48				2.8137
Al	1.486	4.72	0.18	3.46				4.6663
Si	1.739	13.93	0.31	9.80				14.9275
S	2.307	0.81	0.09	0.50				0.8959
Ca	3.690	16.14	0.51	7.96				18.3113
Total		100.00		100.00				

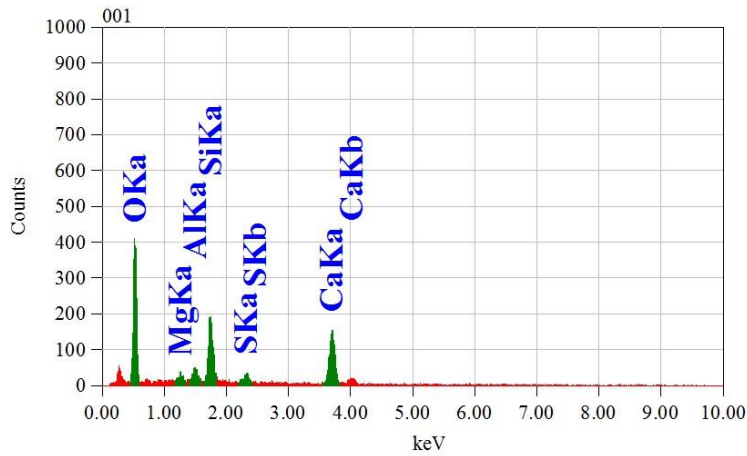
(b)

View000

JEOLUSER 1/1



Title : IMG1
 Instrument : 7600F
 Volt : 5.00 kV
 Mag. : x 2,000
 Date : 2021/03/22
 Pixel : 512 x 384



Acquisition Parameter
 Instrument : 7600F
 Acc. Voltage : 10.0 kV
 Probe Current: 1.00000 nA
 PHA mode : T3
 Real Time : 30.10 sec
 Live Time : 30.00 sec
 Dead Time : 0 %
 Counting Rate: 342 cps
 Energy Range : 0 - 20 keV

ZAF Method Standardless Quantitative Analysis
 Fitting Coefficient : 0.1246

Element	(keV)	Mass%	Sigma	Atom%	Compound	Mass%	Cation	K
O K*	0.525	57.30	0.36	74.66				47.2823
Mg K*	1.253	0.60	0.09	0.51				0.5914
Al K*	1.486	1.69	0.12	1.31				1.8419
Si K*	1.739	10.19	0.23	7.57				12.2581
S K*	2.307	1.76	0.11	1.15				2.1909
Ca K*	3.690	28.45	0.50	14.80				35.8354
Total		100.00		100.00				

JED-2300 AnalysisStation

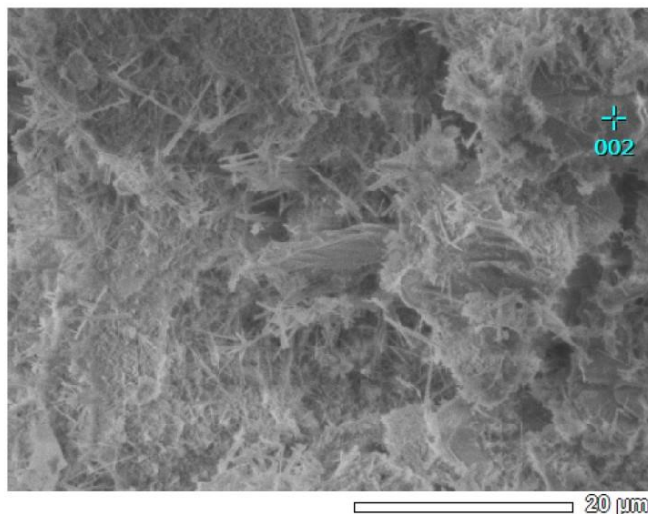
JEOL

(c)

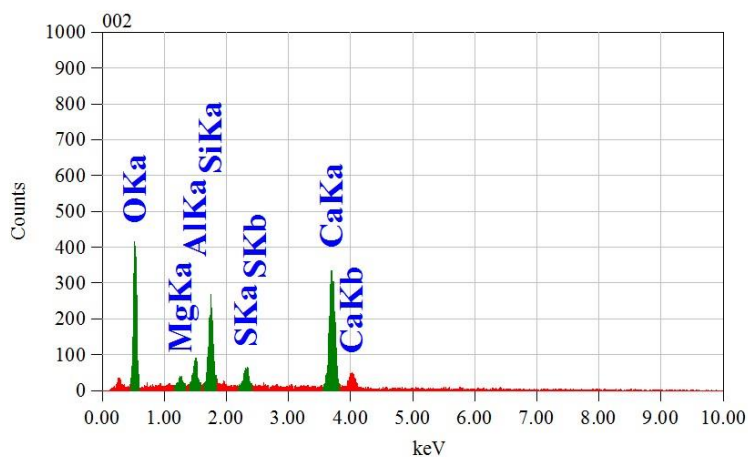
Figure C3: EDS Image of grouted three samples (3:1) after 90 days of curing (a) sample 1, (b) sample 2, (c) sample 3

View000

JEOLUSER 1/1



Title : IMG1
 Instrument : 7600F
 Volt : 5.00 kV
 Mag. : x 2,000
 Date : 2021/03/22
 Pixel : 512 x 384



Acquisition Parameter
 Instrument : 7600F
 Acc. Voltage : 10.0 kV
 Probe Current: 1.00000 nA
 PHA mode : T3
 Real Time : 30.15 sec
 Live Time : 30.00 sec
 Dead Time : 0 %
 Counting Rate: 532 cps
 Energy Range : 0 - 20 keV

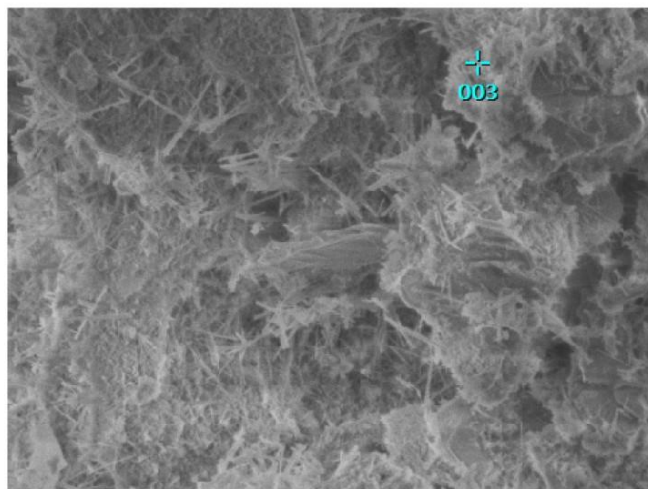
ZAF Method Standardless Quantitative Analysis
 Fitting Coefficient : 0.1022

Element	(keV)	Mass%	Sigma	Atom%	Compound	Mass%	Cation	K
O K*	0.525	46.16	0.81	66.09				31.3129
Mg K*	1.253	0.88	0.09	0.83				0.8881
Al K*	1.486	2.01	0.14	1.71				2.2370
Si K*	1.739	7.84	0.26	6.40				9.6511
S K*	2.307	2.44	0.15	1.75				3.1478
Ca K*	3.690	40.66	0.86	23.24				52.7630
Total		100.00		100.00				

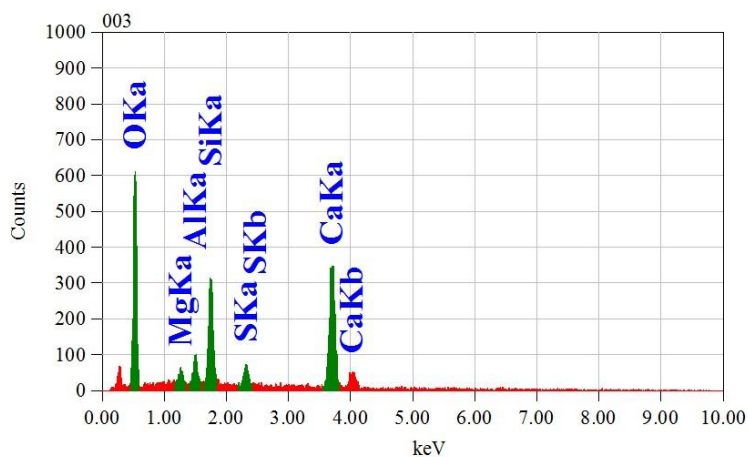
(a)

View000

JEOLUSER 1/1



Title : IMG1
 Instrument : 7600F
 Volt : 5.00 kV
 Mag. : x 2,000
 Date : 2021/03/22
 Pixel : 512 x 384



Acquisition Parameter
 Instrument : 7600F
 Acc. Voltage : 10.0 kV
 Probe Current: 1.00000 nA
 PHA mode : T3
 Real Time : 30.17 sec
 Live Time : 30.00 sec
 Dead Time : 0 %
 Counting Rate: 666 cps
 Energy Range : 0 - 20 keV

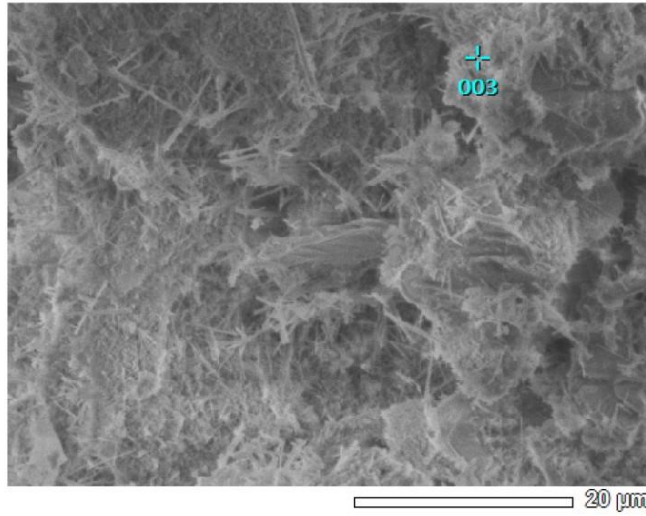
ZAF Method Standardless Quantitative Analysis
 Fitting Coefficient : 0.1049

Element	(keV)	Mass%	Sigma	Atom%	Compound	Mass%	Cation	K
O K*	0.525	50.40	0.72	69.48				37.1182
Mg K*	1.253	1.06	0.09	0.96				1.0707
Al K*	1.486	1.85	0.12	1.51				2.0575
Si K*	1.739	8.49	0.24	6.67				10.4287
S K*	2.307	2.64	0.14	1.82				3.3858
Ca K*	3.690	35.55	0.72	19.56				45.9391
Total		100.00		100.00				

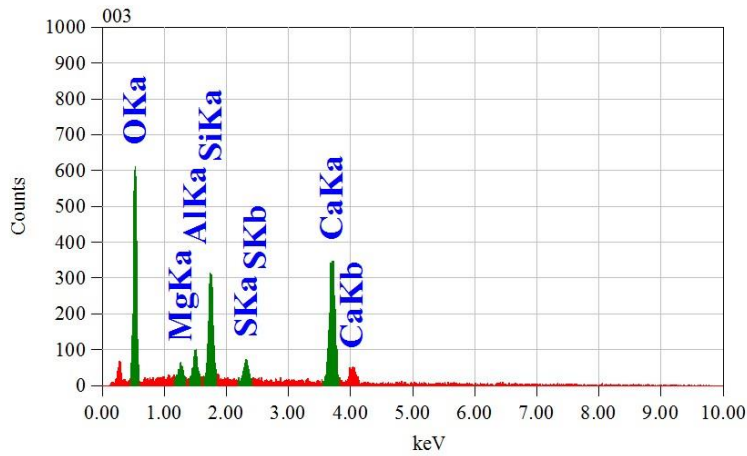
(b)

View000

JEOLUSER 1/1



Title : IMG1
 Instrument : 7600F
 Volt : 5.00 kV
 Mag. : x 2,000
 Date : 2021/03/22
 Pixel : 512 x 384



Acquisition Parameter
 Instrument : 7600F
 Acc. Voltage : 10.0 kV
 Probe Current: 1.00000 nA
 PHA mode : T3
 Real Time : 30.17 sec
 Live Time : 30.00 sec
 Dead Time : 0 %
 Counting Rate: 666 cps
 Energy Range : 0 - 20 keV

ZAF Method Standardless Quantitative Analysis
 Fitting Coefficient : 0.1049

Element	(keV)	Mass%	Sigma	Atom%	Compound	Mass%	Cation	K
O K*	0.525	50.40	0.72	69.48				37.1182
Mg K*	1.253	1.06	0.09	0.96				1.0707
Al K*	1.486	1.85	0.12	1.51				2.0575
Si K*	1.739	8.49	0.24	6.67				10.4287
S K*	2.307	2.64	0.14	1.82				3.3858
Ca K*	3.690	35.55	0.72	19.56				45.9391
Total		100.00		100.00				

JED-2300 AnalysisStation

JEOL

(c)

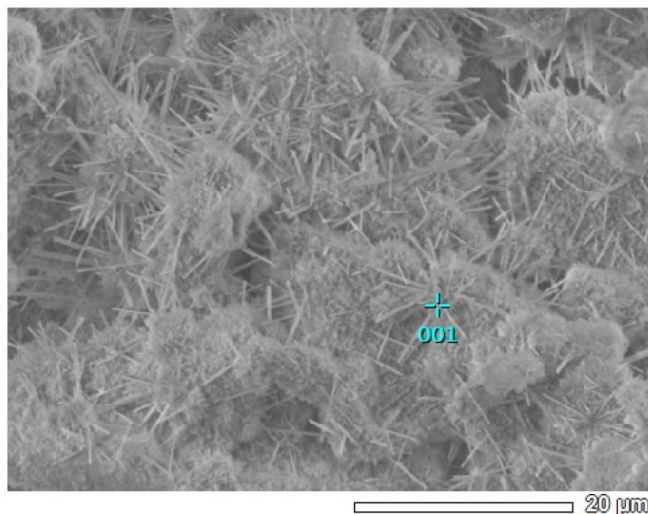
Figure C4: EDS Image of grouted three samples (2:1) after 90 days of curing
 (a) sample 1, (b) sample 2, (c) sample 3

Appendix D

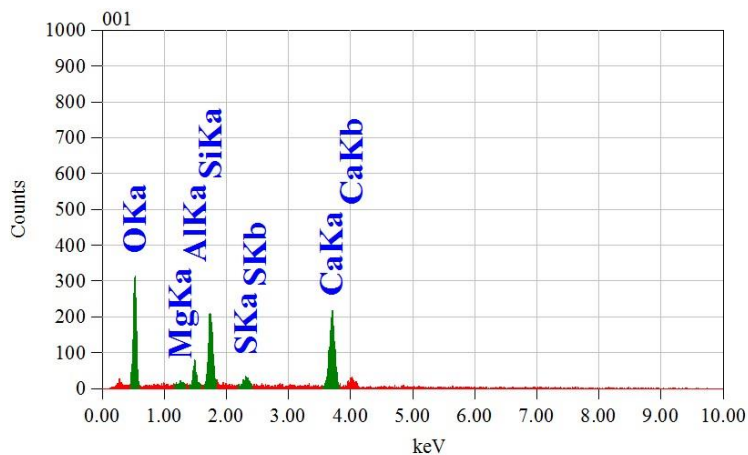
Energy Dispersive Spectroscopy Images of
Grouted Samples with W:C ratio 5:1,4:1,3:1 and
2:1 Cured for 90 days

View000

JEOLUSER 1/1



Title : IMG1
 Instrument : 7600F
 Volt : 5.00 kV
 Mag. : x 2,000
 Date : 2021/02/28
 Pixel : 512 x 384



Acquisition Parameter
 Instrument : 7600F
 Acc. Voltage : 10.0 kV
 Probe Current: 1.00000 nA
 PHA mode : T3
 Real Time : 30.10 sec
 Live Time : 30.00 sec
 Dead Time : 0 %
 Counting Rate: 348 cps
 Energy Range : 0 - 20 keV

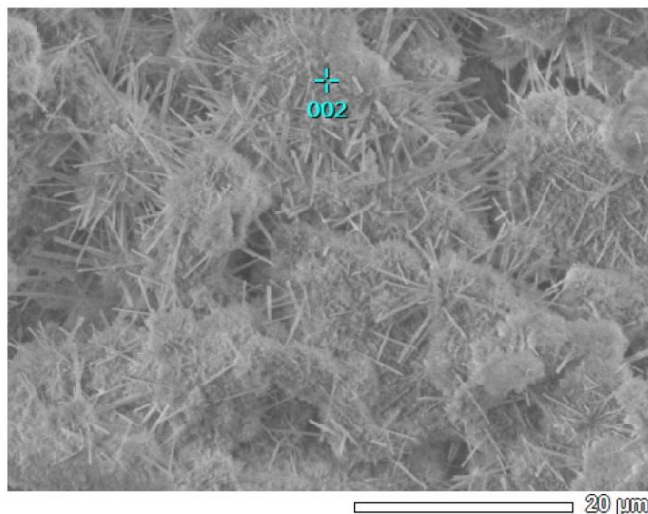
ZAF Method Standardless Quantitative Analysis
 Fitting Coefficient : 0.1203

Element	(keV)	Mass%	Sigma	Atom%	Compound	Mass%	Cation	K
O	0.525	46.80	0.97	66.18				32.9805
Mg	1.253	0.29	0.09	0.27				0.2898
Al	1.486	2.91	0.18	2.44				3.2416
Si	1.739	10.96	0.36	8.83				13.3934
S	2.307	1.71	0.16	1.21				2.1589
Ca	3.690	37.34	1.00	21.08				47.9357
Total		100.00		100.00				

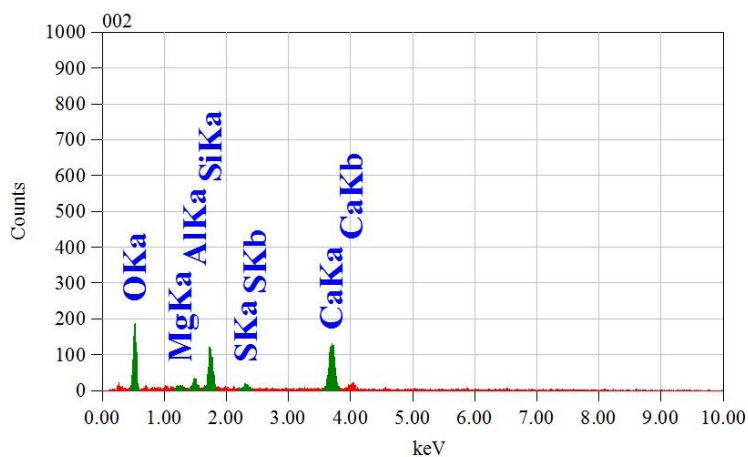
(a)

View000

JEOLUSER 1/1



Title : IMG1
 Instrument : 7600F
 Volt : 5.00 kV
 Mag. : x 2,000
 Date : 2021/02/28
 Pixel : 512 x 384



Acquisition Parameter
 Instrument : 7600F
 Acc. Voltage : 10.0 kV
 Probe Current: 1.00000 nA
 PHA mode : T3
 Real Time : 30.10 sec
 Live Time : 30.00 sec
 Dead Time : 0 %
 Counting Rate: 235 cps
 Energy Range : 0 - 20 keV

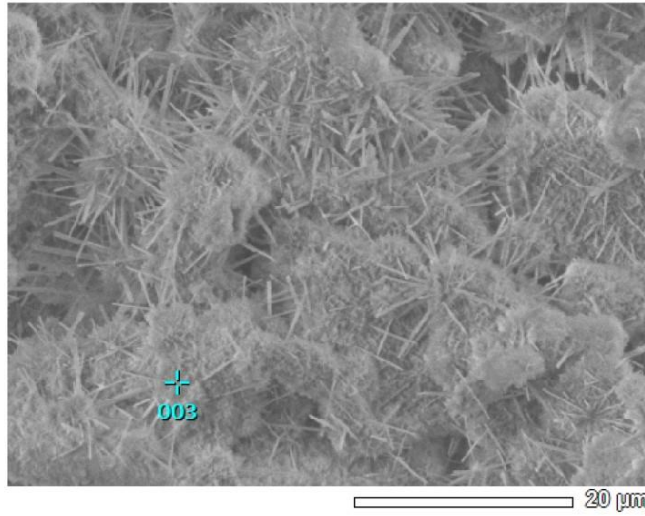
ZAF Method Standardless Quantitative Analysis
 Fitting Coefficient : 0.1579

Element	(keV)	Mass%	Sigma	Atom%	Compound	Mass%	Cation	K
O	0.525	46.47	1.24	66.23				31.8969
Mg	1.253	0.56	0.13	0.52				0.5623
Al	1.486	2.22	0.21	1.88				2.4738
Si	1.739	9.42	0.43	7.65				11.5846
S	2.307	1.44	0.18	1.03				1.8435
Ca	3.690	39.89	1.31	22.69				51.6387
Total		100.00		100.00				

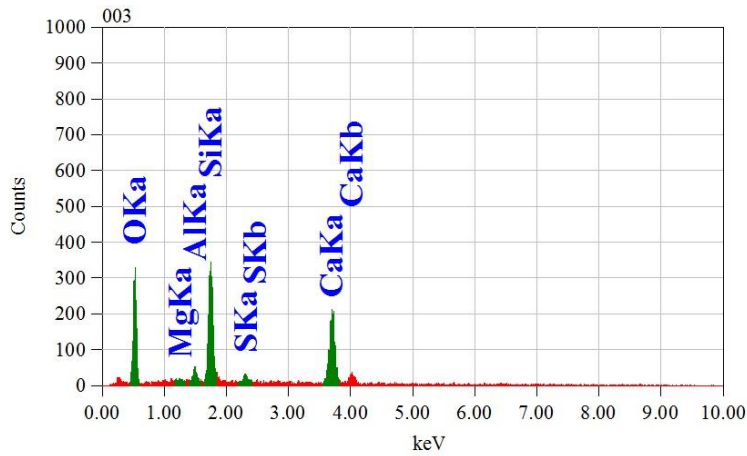
(b)

View000

JEOLUSER 1/1



Title : IMG1
 Instrument : 7600F
 Volt : 5.00 kV
 Mag. : x 2,000
 Date : 2021/02/28
 Pixel : 512 x 384



Acquisition Parameter
 Instrument : 7600F
 Acc. Voltage : 10.0 kV
 Probe Current: 1.00000 nA
 PHA mode : T3
 Real Time : 30.12 sec
 Live Time : 30.00 sec
 Dead Time : 0 %
 Counting Rate: 408 cps
 Energy Range : 0 - 20 keV

ZAF Method Standardless Quantitative Analysis
 Fitting Coefficient : 0.1119

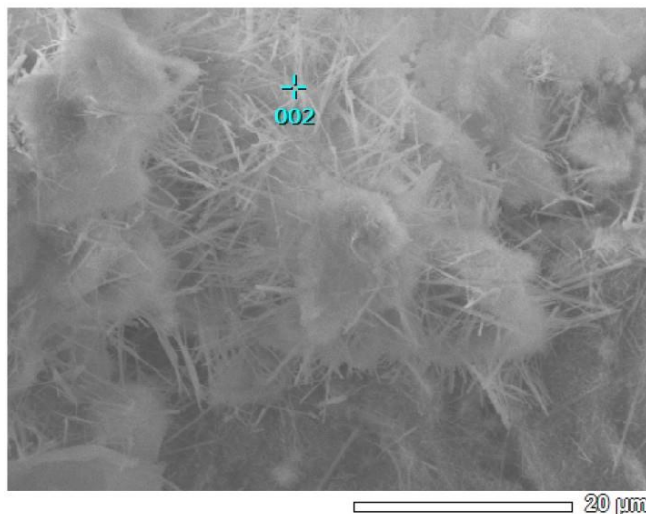
Element	(keV)	Mass%	Sigma	Atom%	Compound	Mass%	Cation	K
O	0.525	44.14	0.90	63.27				30.6601
Mg	1.253	0.27	0.08	0.25				0.2707
Al	1.486	1.37	0.13	1.17				1.5198
Si	1.739	16.62	0.42	13.57				20.2661
S	2.307	1.62	0.15	1.16				1.9858
Ca	3.690	35.98	0.95	20.59				45.2974
Total		100.00		100.00				

(c)

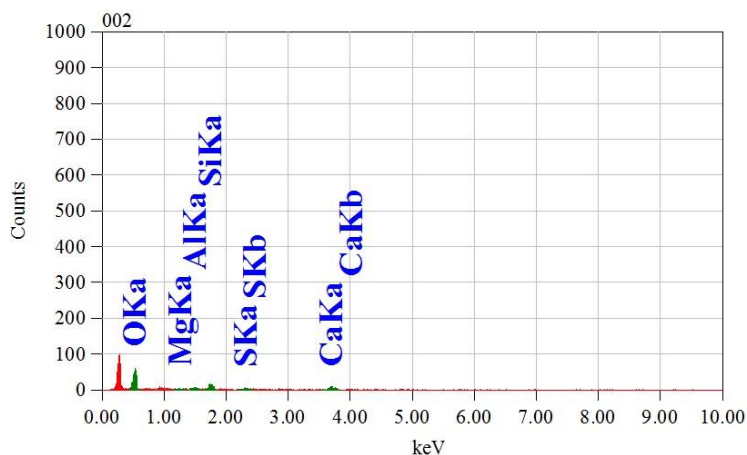
Figure D1: EDS Image of grouted three samples 5:1) after 28 days of curing (a) sample 1, (b) sample 2, (c) sample 3

View000

JEOLUSER 1/1



Title : IMG1
 Instrument : 7600F
 Volt : 15.00 kV
 Mag. : x 2,000
 Date : 2021/02/28 28
 Pixel : 512 x 384 1



Acquisition Parameter
 Instrument : 7600F
 Acc. Voltage : 10.0 kV
 Probe Current: 1.00000 nA 1A
 PHA mode : T3
 Real Time : 30.04 sec :
 Live Time : 30.00 sec :
 Dead Time : 0 %
 Counting Rate: 69 cps
 Energy Range : 0 - 20 keV keV

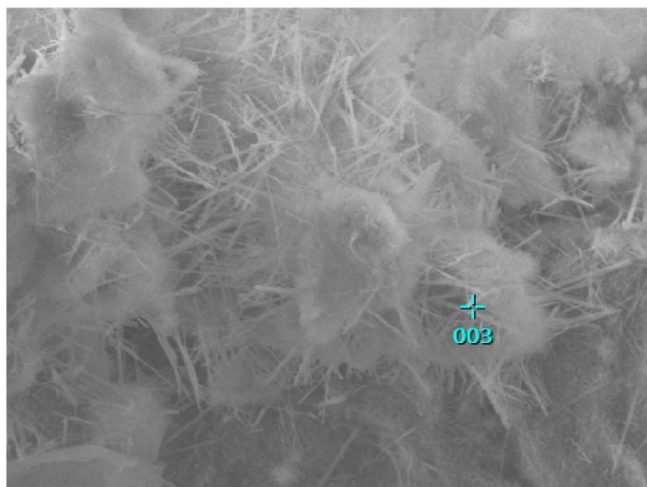
ZAF Method Standardless Quantitative Analysis
 Fitting Coefficient : 0.6858

Element	(keV)	Mass%	Sigma	Atom%	Compound	Mass%	Cation	K
O K	0.525	72.51	3.49	84.57				71.7019
Mg K*								4
Al K	1.486	2.41	0.73	1.67				2.2166
Si K	1.739	8.80	1.28	5.85				8.8976
S K*	2.307	2.91	0.75	1.69				3.0516
Ca K	3.690	13.36	2.40	6.22				14.1323
Total		100.00		100.00				

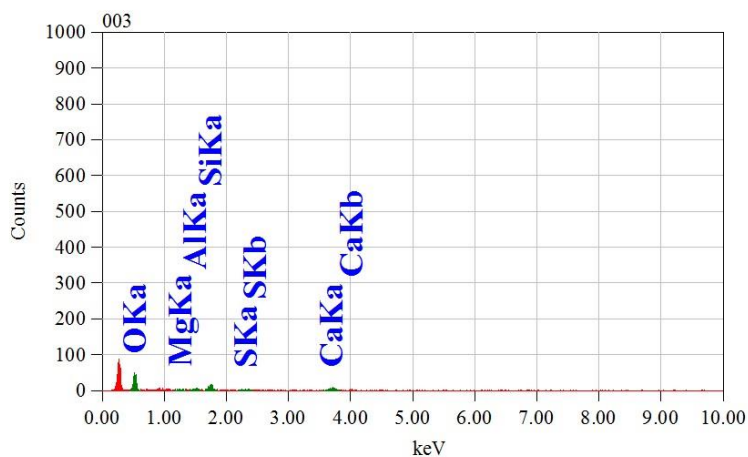
(a)

View000

JEOLUSER 1/1



Title : IMG1
 Instrument : 7600F
 Volt : 15.00 kV
 Mag. : x 2,000
 Date : 2021/02/28
 Pixel : 512 x 384



Acquisition Parameter
 Instrument : 7600F
 Acc. Voltage : 10.0 kV
 Probe Current: 1.00000 nA
 PHA mode : T3
 Real Time : 30.03 sec
 Live Time : 30.00 sec
 Dead Time : 0 %
 Counting Rate: 63 cps
 Energy Range : 0 - 20 keV

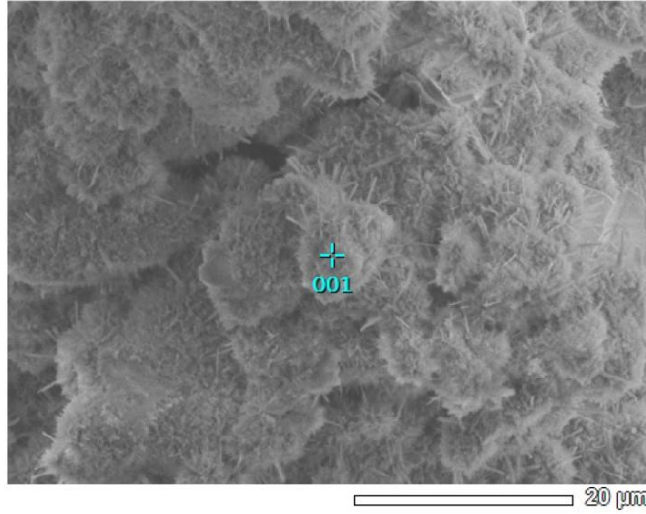
ZAF Method Standardless Quantitative Analysis
 Fitting Coefficient : 0.6980

Element	(keV)	Mass%	Sigma	Atom%	Compound	Mass%	Cation	K
O	0.525	69.54	3.65	82.29				68.1432
Mg	1.253	0.78	0.52	0.61				0.6638
Al	1.486	1.37	0.69	0.96				1.2854
Si	1.739	12.77	1.56	8.61				13.2202
S	2.307	1.66	0.68	0.98				1.7496
Ca	3.690	13.88	2.60	6.56				14.9379
Total		100.00		100.00				

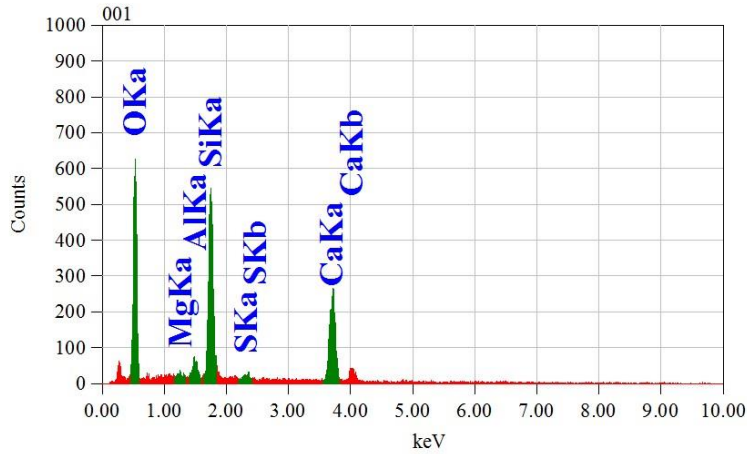
(b)

View000

JEOLUSER 1/1



Title : IMG1
 Instrument : 7600F
 Volt : 5.00 kV
 Mag. : x 2,000
 Date : 2021/02/28
 Pixel : 512 x 384



Acquisition Parameter
 Instrument : 7600F
 Acc. Voltage : 10.0 kV
 Probe Current: 1.00000 nA
 PHA mode : T3
 Real Time : 30.21 sec
 Live Time : 30.00 sec
 Dead Time : 0 %
 Counting Rate: 602 cps
 Energy Range : 0 - 20 keV

ZAF Method Standardless Quantitative Analysis
 Fitting Coefficient : 0.1124

Element	(keV)	Mass%	Sigma	Atom%	Compound	Mass%	Cation	K
O K	0.525	52.14	0.75	70.01				41.2512
Mg K*	1.253	0.27	0.07	0.24				0.2705
Al K	1.486	1.31	0.11	1.04				1.4310
Si K	1.739	16.75	0.35	12.81				20.2217
S K*	2.307	0.52	0.08	0.35				0.6364
Ca K	3.690	29.01	0.70	15.55				36.1891
Total		100.00		100.00				

JED-2300 AnalysisStation

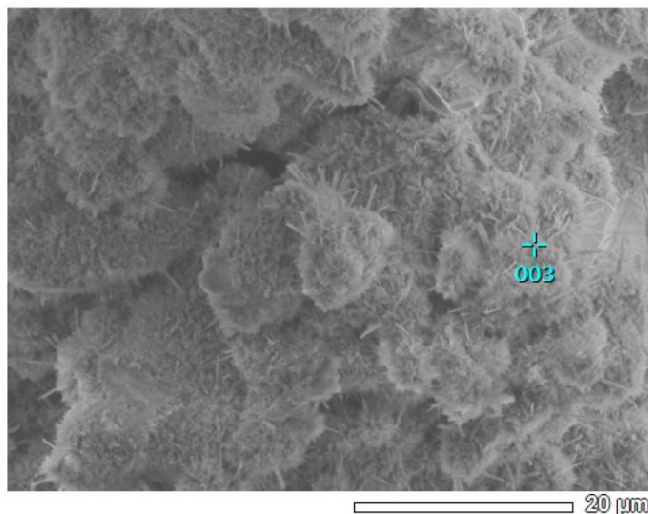
JEOL

(c)

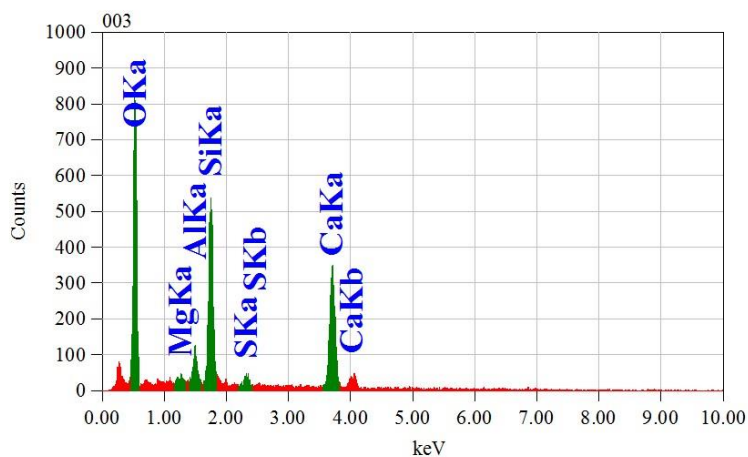
Figure D2: EDS Image of grouted three samples (4:1) after 28 days of curing
 (a) sample 1, (b) sample 2, (c) sample 3

View000

JEOLUSER 1/1



Title : IMG1
 Instrument : 7600F
 Volt : 5.00 kV
 Mag. : x 2,000
 Date : 2021/02/28
 Pixel : 512 x 384



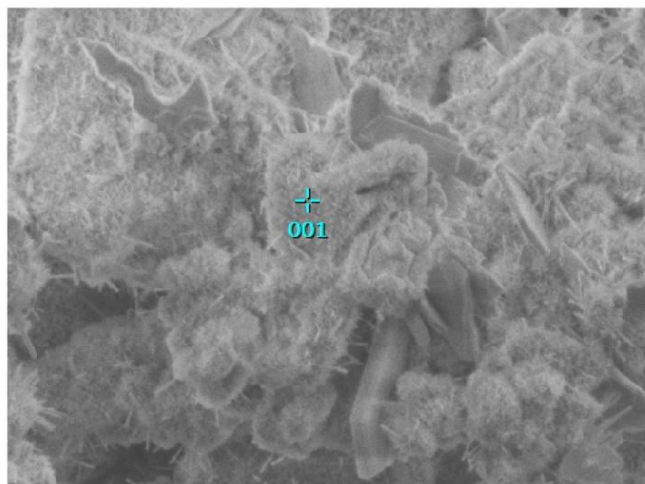
Acquisition Parameter
 Instrument : 7600F
 Acc. Voltage : 10.0 kV
 Probe Current: 1.00000 nA
 PHA mode : T3
 Real Time : 30.23 sec
 Live Time : 30.00 sec
 Dead Time : 0 %
 Counting Rate: 751 cps
 Energy Range : 0 - 20 keV

ZAF Method Standardless Quantitative Analysis
 Fitting Coefficient : 0.1076

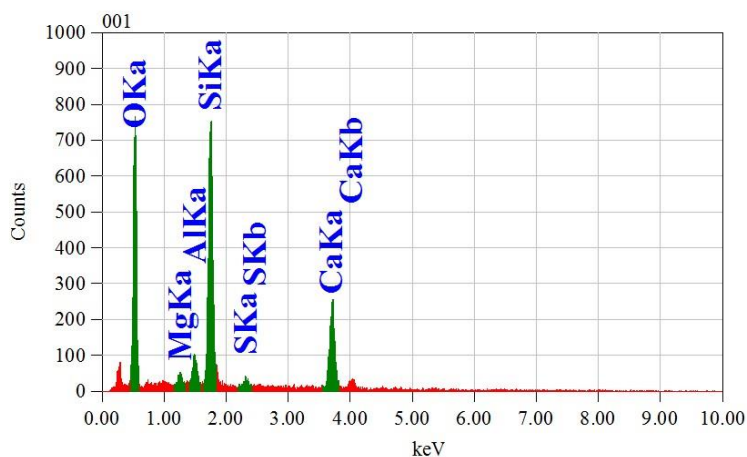
Element	(keV)	Mass%	Sigma	Atom%	Compound	Mass%	Cation	K
O	0.525	54.53	0.68	72.21				44.0277
Mg	1.253	0.23	0.06	0.20				0.2295
Al	1.486	2.02	0.11	1.59				2.2132
Si	1.739	13.37	0.28	10.09				16.0996
S	2.307	1.03	0.09	0.68				1.2615
Ca	3.690	28.82	0.62	15.24				36.1685
Total		100.00		100.00				

View000

JEOLUSER 1/1



Title : IMG1
 Instrument : 7600F
 Volt : 5.00 kV
 Mag. : x 2,000
 Date : 2021/02/28
 Pixel : 512 x 384



Acquisition Parameter
 Instrument : 7600F
 Acc. Voltage : 10.0 kV
 Probe Current: 1.00000 nA
 PHA mode : T3
 Real Time : 30.23 sec
 Live Time : 30.00 sec
 Dead Time : 0 %
 Counting Rate: 708 cps
 Energy Range : 0 - 20 keV

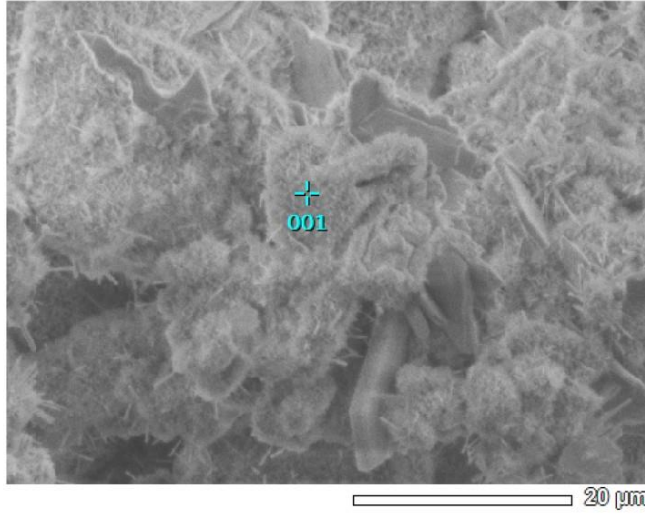
ZAF Method Standardless Quantitative Analysis
 Fitting Coefficient : 0.1093

Element	(keV)	Mass%	Sigma	Atom%	Compound	Mass%	Cation	K
O K	0.525	52.60	0.25	69.44				44.1756
Mg K*	1.253	0.57	0.06	0.50				0.5637
Al K	1.486	2.03	0.08	1.59				2.1684
Si K	1.739	21.14	0.23	15.89				24.7324
S K*	2.307	0.83	0.06	0.54				0.9543
Ca K	3.690	22.84	0.33	12.04				27.4056
Total		100.00		100.00				

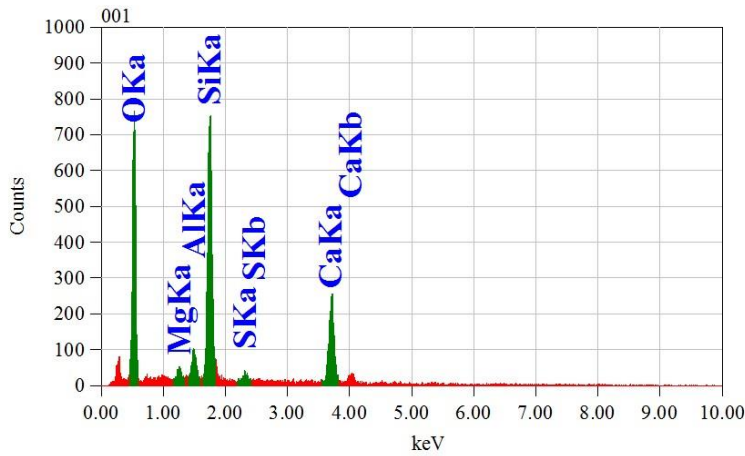
(b)

View000

JEOLUSER 1/1



Title : IMG1
 Instrument : 7600F
 Volt : 5.00 kV
 Mag. : x 2,000
 Date : 2021/02/28
 Pixel : 512 x 384



Acquisition Parameter
 Instrument : 7600F
 Acc. Voltage : 10.0 kV
 Probe Current: 1.00000 nA
 PHA mode : T3
 Real Time : 30.23 sec
 Live Time : 30.00 sec
 Dead Time : 0 %
 Counting Rate: 708 cps
 Energy Range : 0 - 20 keV

ZAF Method Standardless Quantitative Analysis
 Fitting Coefficient : 0.1093

Element	(keV)	Mass%	Sigma	Atom%	Compound	Mass%	Cation	K
O K	0.525	52.60	0.25	69.44				44.1756
Mg K*	1.253	0.57	0.06	0.50				0.5637
Al K	1.486	2.03	0.08	1.59				2.1684
Si K	1.739	21.14	0.23	15.89				24.7324
S K*	2.307	0.83	0.06	0.54				0.9543
Ca K	3.690	22.84	0.33	12.04				27.4056
Total		100.00		100.00				

JED-2300 AnalysisStation

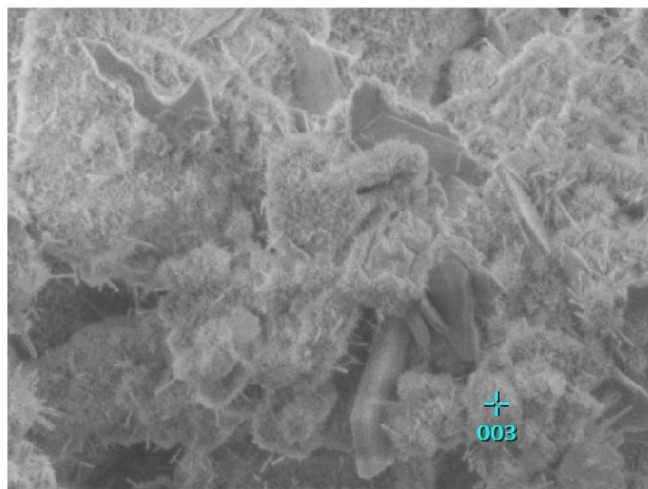
JEOL

(c)

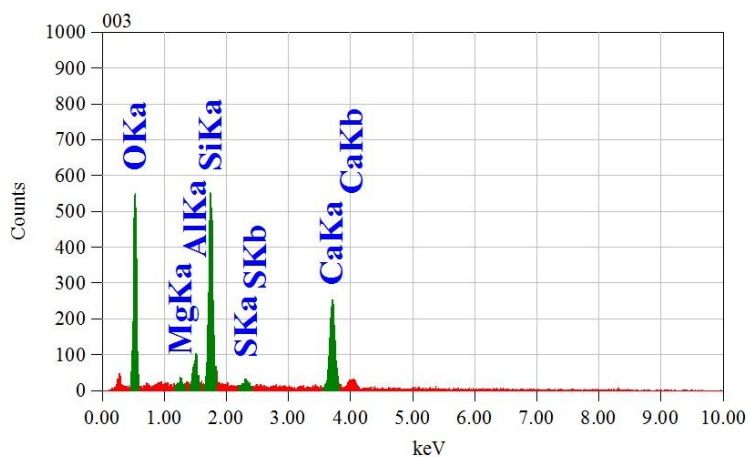
Figure D3: EDS Image of grouted three samples (3:1) after 28 days of curing
 (a) sample 1, (b) sample 2, (c) sample 3

View000

JEOLUSER 1/1



Title : IMG1
 Instrument : 7600F
 Volt : 5.00 kV
 Mag. : x 2,000
 Date : 2021/02/28
 Pixel : 512 x 384



Acquisition Parameter
 Instrument : 7600F
 Acc. Voltage : 10.0 kV
 Probe Current: 1.00000 nA
 PHA mode : T3
 Real Time : 30.16 sec
 Live Time : 30.00 sec
 Dead Time : 0 %
 Counting Rate: 604 cps
 Energy Range : 0 - 20 keV

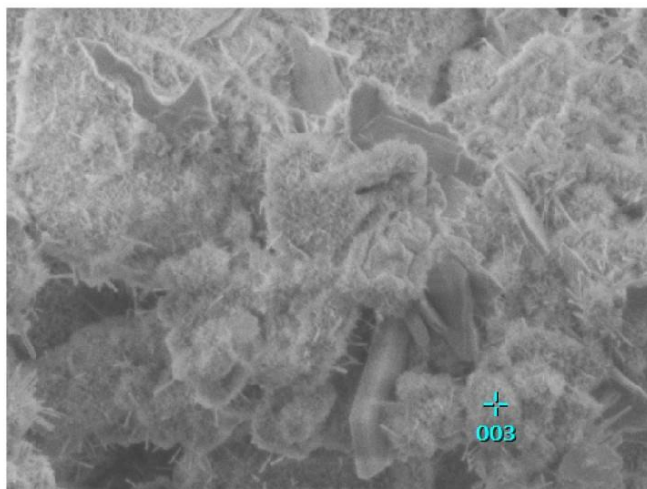
ZAF Method Standardless Quantitative Analysis
 Fitting Coefficient : 0.1094

Element	(keV)	Mass%	Sigma	Atom%	Compound	Mass%	Cation	K
O	0.525	49.76	0.74	67.65				38.9889
Mg	1.253	0.39	0.07	0.35				0.3937
Al	1.486	2.32	0.14	1.87				2.5425
Si	1.739	18.18	0.37	14.08				21.7857
S	2.307	0.97	0.10	0.66				1.1642
Ca	3.690	28.37	0.70	15.40				35.1250
Total		100.00		100.00				

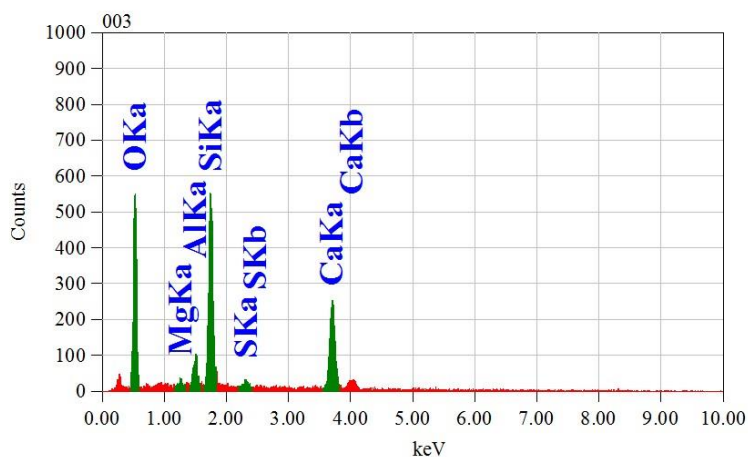
(a)

View000

JEOLUSER 1/1



Title : IMG1
 Instrument : 7600F
 Volt : 5.00 kV
 Mag. : x 2,000
 Date : 2021/02/28
 Pixel : 512 x 384



Acquisition Parameter
 Instrument : 7600F
 Acc. Voltage : 10.0 kV
 Probe Current: 1.00000 nA
 PHA mode : T3
 Real Time : 30.16 sec
 Live Time : 30.00 sec
 Dead Time : 0 %
 Counting Rate: 604 cps
 Energy Range : 0 - 20 keV

ZAF Method Standardless Quantitative Analysis

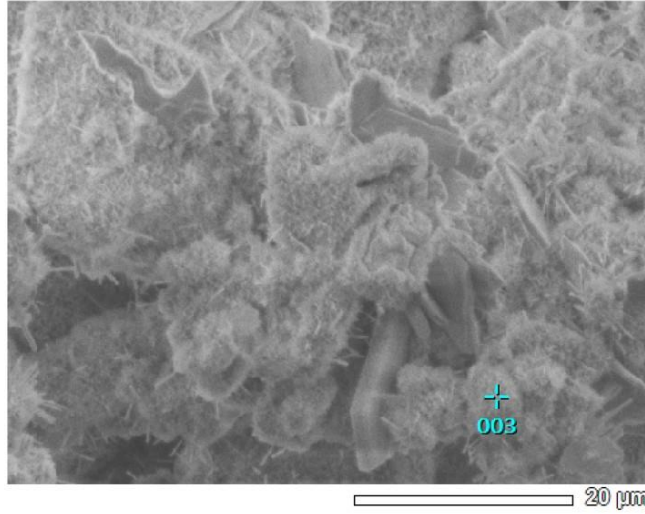
Fitting Coefficient : 0.1094

Element	(keV)	Mass%	Sigma	Atom%	Compound	Mass%	Cation	K
O K	0.525	49.76	0.74	67.65				38.9889
Mg K*	1.253	0.39	0.07	0.35				0.3937
Al K	1.486	2.32	0.14	1.87				2.5425
Si K	1.739	18.18	0.37	14.08				21.7857
S K*	2.307	0.97	0.10	0.66				1.1642
Ca K	3.690	28.37	0.70	15.40				35.1250
Total		100.00		100.00				

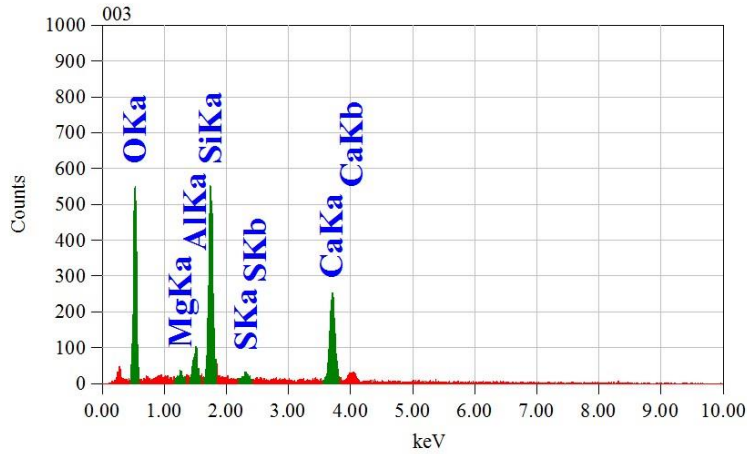
(b)

View000

JEOLUSER 1/1



Title : IMG1
 Instrument : 7600F
 Volt : 5.00 kV
 Mag. : x 2,000
 Date : 2021/02/28
 Pixel : 512 x 384



Acquisition Parameter
 Instrument : 7600F
 Acc. Voltage : 10.0 kV
 Probe Current: 1.00000 nA
 PHA mode : T3
 Real Time : 30.16 sec
 Live Time : 30.00 sec
 Dead Time : 0 %
 Counting Rate: 604 cps
 Energy Range : 0 - 20 keV

ZAF Method Standardless Quantitative Analysis
 Fitting Coefficient : 0.1094

Element	(keV)	Mass%	Sigma	Atom%	Compound	Mass%	Cation	K
O	0.525	49.76	0.74	67.65				38.9889
Mg	1.253	0.39	0.07	0.35				0.3937
Al	1.486	2.32	0.14	1.87				2.5425
Si	1.739	18.18	0.37	14.08				21.7857
S	2.307	0.97	0.10	0.66				1.1642
Ca	3.690	28.37	0.70	15.40				35.1250
Total		100.00		100.00				

JED-2300 AnalysisStation

JEOL

(c)

Figure D4: EDS Image of grouted three samples (2:1) after 28 days of curing
 (a) sample 1, (b) sample 2, (c) sample 3